# Cyanobacteria Based Photosynthetic Microbial Fuel Cell: Development and Application for Sensing Alcohol

A Thesis

submitted for the partial

fulfilment of the award of the degree of

**Doctor of Philosophy**

by

**SHARBANI KAUSHIK**
**(136151005)**


**Centre for Energy**

**Indian Institute of Technology Guwahati**

**Guwahati -781039, Assam (India)**

**October 2018**


Dedicated to my father (late)
"Pita swarga
Pita dharma
Pita hi Paramang Tapo
Pitori pritima pannay
Priyantay sarva devata"
When you bless the day, I get wings to fly!
Father is compared to Heaven & Religion. He is placed at a higher pedestal than all Gods combined

**INDIAN INSTITUTE OF TECHNOLOGY GUWAHATI**
**Centre for Energy**
**Guwahati – 781039**

# STATEMENT

I do hereby declare that the matter embodied in this thesis entitled "**Cyanobacteria Based Photosynthetic Microbial Fuel Cell: Development and Application for Sensing Alcohol**", is the result of investigations carried out by me in the Centre for Energy, Indian Institute of Technology Guwahati, Assam, India, under the guidance of Prof. Pranab Goswami.

In keeping with the general practice of reporting scientific observations, due acknowledgements have been made wherever the work described is based on the findings of other investigators.

October, 2018 Sharbani Kaushik

**INDIAN INSTITUTE OF TECHNOLOGY GUWAHATI**
**Centre for Energy**
**Guwahati – 781039**

# CERTIFICATE

It is certified that the work described in this thesis, entitled "**Cyanobacteria Based Photosynthetic Microbial Fuel Cell: Development and Application for Sensing Alcohol**", done by Ms. Sharbani Kaushik (Roll No. 136151005) for the award of degree of Doctor of Philosophy is an authentic record of the results obtained from the research work carried out under my supervision in the Centre for Energy, Indian Institute of Technology Guwahati, India.

The results embodied in this thesis have not been submitted to any other University or Institute for the award of any degree.

October, 2018

Prof. Pranab Goswami
(Supervisor)

# Acknowledgements

*Quoting a Shloka in Sanskrit: "Gurur Brahma Gurur Vishnu Gurur Devo Maheshwarah; Guru Saakshaat Parabrahma, Tasmai Shri Gurave Namah!" A guru is considered in the equal stature of the Tridev Lords (Brahma, Vishnu and Shiva). My supervisor* ***Prof. Pranab Goswami****, has inculcated the habit of acquiring knowledge and reasoning, destroyed the weed of impatience, and have crafted a fine human being and researcher out of me, giving an edge of rationality to my thoughts and actions. I bow down with my soul, to such a great "guru" (teacher), who is committed to academic excellence.*

*I will always be obliged to my doctoral committee members* ***Prof. G. Pukazhenthi****,* ***Prof. Aiyagari Ramesh*** *and* ***Dr. Ranjan Tamuli*** *for their suggestions and intensive assessment, that gave a proper direction to accomplish my research.*

*I would like to extend my appreciation towards to* ***Dr. Lepakshi Barbora*** *for her incessant motivation and all the staff members of Centre for Energy, CIF, CoE of Dept. of Biosciences and Bioengineering for their technical support,* ***Prof. Eduardo Corton*** *for his insightful active discussions during his visit as guest faculty to PG lab IITG, from Argentina, as well as* ***Dr. Sachin Mangale*** *from Wipro GE Healthcare, for providing Delta Vision Deconvoluted Microscope facility.*

*A well-equipped lab, resources and then crowned with dedicated and helpful* ***work group****- Mrinal, Priyanki, Babina, Priyamvada, Naveen, Dr. Lightson, Ankana, Seraj and Abdul for their professional support in smooth conduction of experiments. A vote of cheers to Santosh and Vinay for their partnerships in winning badminton leagues alongside the technical upkeep. My beloved* ***juniors****, Phurpa, Smita, Rupam, Caroline, Torsha, Ankit and Pooja for lifting the spirits with their inquisitive nature.*

*Aside academia, I would have a special mention in this place for my* ***badminton group*** *(Pugal Sir, Ram, Jiten, Rahul, Asha and Mrinmoy) for instigating in me the spirit of sportsmanship. Due to this group and the included early morning "chai" (tea-time), my days received the prompt activation for which I could reach lab early. Ajay Sir, Bhuyan Sir, Charu Sir, Khatiyar Sir, Nandi Sir, Sisir Sir for instigating in me the winning fortitude on and off the badminton court*

*and Khatiyar Sir especially, for the contact angle measurement facility in CoE-SusPol, in the work compiled in chapter II of this thesis.*

*My classical Sattriya dance guru,* ***Dr. Anwesha Mahanta*** *and all my* ***dance team****, for introducing me to a whole new world of creativity, team spirit and abating stage fear. Thank you guys for sharing my love for dance and being my stress buster.*

*My* ***friends****, Pranami, Dimple, Reshmi, Ram, Jiten, and Shasanka who have made my campus days memorable with their advice and deeds; Namami for sharing my love for animals; Garima and Ajeet for their wonderful company in outings; Dibyajyoti and Rahul for being the brothers I always wished, but never had; Garima for sharing my fondness for cooking.*

*If I could ever narrate a story untold of a great man, it would be of my revered (late) father* ***Dr. D. N. Sharma*** *who had a heart of gold! Along with it, all that I am or hope to be, I owe it to my angel mother* ***Mrs. Ranjita Sharma****. My parents' unconditional love and discipline urged me to develop a sense of love and sincerity towards my career. I am in debt to my doting husband* ***Dr. Babul Prasad*** *for his reassurance in my potential time and again, and standing by me with a cheerful positive attitude in all the circumstances.*

*A token of affectionate gratitude to my granduncle* ***Mr. Pankaj Thakur*** *for his sustained love, the never-ending kindness of* ***Dr. L. R. Bishnoi****, and optimistic care from* ***Dr. Anuj Kumar Baruah****, have added a delightful essence to this journey. A kind appreciation to all my family members, in-laws, and friends for their instrumental efforts in steering this phase of the journey.*

*Last but not the least, I express my tribute of praise to the helpers and the security personnel for their labour and sacrifices to keep up a healthy and safe work atmosphere.*

*I offer my gentle reverence to the almighty and feel blessed to have this opportunity of working in one of the esteemed institutes and to carry forward an assortment of beautiful memories that will build a stronger and better "****me****"-* ***Sharbani Kaushik****.*

# Table of Contents

# Abstract

The major objective of the present study is to develop an efficient photosynthetic microbial fuel cell (PMFC) using cyanobacteria as anodic catalyst with a further aim of utilizing this energy generating device for sensing applications. One of the key issues to make the bacterial catalysts effective for generating power in microbial fuel cell is the proper electrical communications between the bacterial cells and the conductive electrode of the fuel cell device. We proposed the direct electron transfer (DET) as the guiding principle for channelizing the cellular electrons to the anode for which, setting up of cyanobacteria biofilm on the anode was considered as a suitable strategy to comply the principle. We explored different synthetic and natural polymeric thin films for their rapid biofilm promoting abilities of cyanobacteria, *Synechococcus* sp. For a comparative analysis, the study was extended to two commonly available bacteria, namely, *Escherichia coli* and *Lactobacillus plantarum*. The activating role of different polymer thin films coated over polystyrene support on the *Synechococcus* sp. biofilm growth was examined concurrently by measuring biofilm florescence using a dye and by measuring cell density in the isolated biofilm. Compared to blank (no coating), the increase in biofilm formation (%) on silk, chitosan, silk-chitosan (3:2) blend, polyaniline, osmium, and Nafion films were 27.73 (31.16), 21.55 (23.74), 37.21 (38.34), 5.35 (8.96), 6.70 (6.55) and (nil), respectively with corresponding cell density (%) shown in the parentheses. This trend of biofilm formation on the films did not significantly vary for *E. coli* and *L. plantarum* strains. The films of 20 residues long each of glycine-alanine repeat peptide, which mimics a silk fibroin motif, and a hydrophobic glycine-valine repeat peptide, increased the biofilm growth by 13.53 % and 26.08 %, respectively. Silk and blend films exhibited highest adhesion unit (0.48 to 0.49), adhesion rate ((4.2 to 4.8) $\times 10^{-6}$, m $s^{-1}$) and Gibbs energy of adhesion (-8.5 to -8.6 kT) with *Synechococcus* sp. The results confirmed interplay of electrostatic and hydrophobic interaction between cell-surface and polymer films for promoting rapid biofilm growth. This study established that the thin films of silk and the blend (3:2) promoted rapid biofilm growth for all the tested micro-organisms. This positive trait of silk-film was then implemented to develop biofilm on the anodic surface of the PMFC where the silk fibroin

(SF) was rationally doped with CdTe quantum dots (QD) and graphene nanoplatelets (GNP) to enhance and stabilize the photocurrent in the PMFC. The nanocomposite matrix supported biofilm growth of the photo-catalyst *Synechococcus* sp., surged the bacterial photo systems (PS I and PS II) with appropriate light ($\lambda_{650 - 750\ nm}$) at a broad excitation spectrum ($\lambda_{350 - 644\ nm}$) through fluorescence resonance energy transfer (FRET) and facilitated the metabolic electron relay through DET to the anode during operation of the PMFC. The maximum current density of the PMFC obtained with the nanocomposite bioanode (1.89 A $m^{-2}$) was ~ 5.7 fold higher than the corresponding blank graphite anode. The positive effect of QD was further confirmed from the fading reversal of polarity during the circadian cycle leading to sustained current generation in the PMFC. The SF with the highest band gap of 4.09 eV and GNP with the lowest band gap of -3 eV, were finally compromised to a band gap energy of 2.9 eV in the nanocomposite matrix. The GNP decreased the charge transfer resistance by ~ 9 fold that facilitated DET as evident from the appearance of a pair of redox peak of the bioanode in the voltammogram with a formal potential of -156 mV. Structural studies demonstrated rational interactions of the hydrophobic $\beta$-sheet of the SF with the nanomaterials. An unprecedented light conversion efficiency of 4.01 % for the cyanobacteria was achieved with the nanocomposite bioanode based PMFC. The developed PMFC was then evaluated for its biosensing application using alcohol as target analyte. A novel signal in the form of potential burst against the substrate alcohol was identified. The origin of the potential burst was attributed to the bacterial membrane depolarization caused by the interaction with the substrate. The magnitude of the PMFC burst potentials was well correlated to the alcohol concentration with a dynamic range of 0.001 to 20 % and LOD of 0.13 % ($R^2$ = 0.96). The device exhibited higher selectivity towards ethanol than methanol as discerned from the corresponding cell-alcohol interaction constant ($K_i$) of 780 mM and 1250 mM. The concept when translated to a paper-based PMFC (p-PMFC) (size ~ 20 $cm^2$), the device exhibited shelf-life of ~ 3 months, detected ethanol within 10 s with a dynamic range of 0.005 to 10 % and LOD of 0.02 % ($R^2$ = 0.99). This novel approach with portable format has great application potential for selective, sensitive and rapid detection of alcohol.

# List of Abbreviations

| | |
|---|---|
| AA | Acetic acid |
| AFM | Atomic force microscope |
| ANOVA | Analysis of variance |
| ASN III | Artificial seawater medium |
| ATP | Adenosine triphosphate |
| Au | Adhesion unit |
| BES | Bioelectrochemical system |
| BOD | Biological oxygen demand |
| BPV | Bio-photovoltaic |
| BQ | 4-Benzoquinone |
| CA | Carbonic anhydrase |
| CD | Circular dichroism |
| CdTe | Cadmium Telluride |
| Chlorophyll a | Chl-*a* |
| CLSM | Confocal laser scanning microscope |
| CNT | Carbon nanotubes |
| CV | Cyclic voltammetry |
| CVS | Crystal violet solution |
| DET | Direct electron transfer |
| DMBQ | 6-dimethyl-1, 4-benzoquinone |
| DMSO | Dimethyl sulfoxide |
| $E_{cell}$ | Cell voltage |

| | |
|---|---|
| EIS | Electrochemical impedance spectroscopy |
| $E_{Ox}^{onset}$ | Onset oxidation potential |
| $E_{Red}^{onset}$ | Onset reduction potential |
| EPS | Exo-polysaccharides |
| ETC | Electron transport chain |
| ETM | Electron transfer mediator |
| EtOH | Ethanol |
| FACS | Fluorescence activated cell sorting |
| FESEM | Field emission scanning electron microscope |
| FRET | Fluorescence resonance energy transfer |
| GApep | GAGAGAAGAAGAAGAAGAAG |
| GNP | Graphene nanoplatelets |
| GE | Graphite electrode |
| GVpep | GVGVGVVGVVGVVGVVGVVG |
| HI | Hydrophobicity index |
| HNQ | 2-hydroxy-1, 4-naphthoquinone |
| HOMO | Highest occupied molecular orbital |
| IP | Isopropanol |
| ITO | Indium tin oxide |
| LB | Luria-Bertani |
| LCE | Light energy conversion efficiency |
| LED | Light emitting diode |
| LUMO | Lowest unoccupied molecular orbital |
| MeOH | Methanol |
| MET | Mediated electron transfer |

| | |
|---|---|
| MFC | Microbial fuel cell |
| MRS | de Man, Rogosa and Sharpe |
| MTT | 3-[4,5-dimethylthiazole-2-yl]-2,5-diphenyltetrazolium bromide |
| NADPH | Nicotinamide adenine dinucleotide phosphate |
| OCP | Open-circuit potential |
| OMC | Outer membrane cytochromes |
| OPP | Oxidative pentose phosphate |
| P-ETC | Photosynthetic electron transport chain |
| pmf | Proton motive force |
| PMFC | Photosynthetic microbial fuel cell technology |
| PS | Photosystem |
| p-PMFC | Paper-based photosynthetic microbial fuel cell |
| PBS | Phosphate buffer solution |
| PC | Plastocyanin |
| PDMS | Polydimethylsiloxane |
| PEDOT | Poly(3,4-ethylenedioxythiophene) |
| PEM | Proton exchange membrane |
| PMMA | Poly(methyl methacrylate) |
| POC | Point-of-care |
| PQ | Plastoquinone |
| PSS | Polystyrene |
| PTFE | Polytetrafluoroethylene |
| QD | Quantum dots |
| R-ETC | Respiratory electron transport chain |
| RSD | Relative standard deviation |

| | |
|---|---|
| RT | Room temperature |
| SF | Silk fibroin |
| TCA | Tricarboxylic acid |
| TRPL | Time resolved photoluminescence |
| TEM | Transmission electron microscope |
| UV | Ultraviolet |
| WHO | World Health Organization |
| WSxM | Windows-Scanning-x-Microscope |
| XRD | X-ray diffraction |

# List of Symbols

| | |
|---|---|
| % | Percent |
| ~ | Approximately |
| < | Lesser than |
| = | Equal to |
| > | Greater than |
| ≥ | Greater than equal to |
| -ve | Negative |
| +ve | Positive |
| °C | Degree Celsius |
| nF | Charge transferred in the reaction |
| n | Number of electrons per reaction mol |
| $E_{emf}$ | Electromotive force |
| $E_{cat}$ | Cathodic potential |
| $E_{an}$ | Anodic potential |
| $IR_{\Omega}$ | Ohmic over potential |
| $\eta_{con}$ | Concentration overpotential |
| I | Current |
| A | Electrode active surface area |
| $i_o$ | Exchange current density |
| b | Tafel slope |
| λ | Wavelength |
| $M_w$ | Molecular weight |
| ζ | Zeta potential |
| $\zeta_1$ | Surface potential of the cell surface |
| $\zeta_2$ | Surface potential of the polymers |
| $V_R$ | Electrostatic repulsion |
| k | Debye length |
| d | Minimum separation distance |
| E | Interaction energy |
| D | Separation distance |
| $A_{bws}$ | Hamaker constant between bacteria, water and solid surface |
| $\theta_w$ | Water contact angle |
| $H_{o/w}$ | Relative hydrophobicity between microbes and support surface |
| $H_m$ | Relative hydrophobicity of microbes |
| $H_p$ | Relative hydrophobicity of polymeric support |
| $C_0$ | Concentration of cell suspension initially |
| $t$ | Contact time |
| $C_t$ | Cell suspension concentration after contact time $t$ |
| $a$ | Adhesion rate constant |

| | |
|---|---|
| $V$ | Volume |
| $A$ | Area |
| $w$ | Width |
| $l$ | Length |
| $R_e$ | Effective radii |
| $D_e$ | Diffusion coefficient |
| $T$ | Absolute temperature |
| $k$ | Boltzmann constant |
| $\eta$ | Dynamic viscosity |
| $C_b$ | Concentration of cell suspension recorded after 12 h |
| $\tau$ | Adhered cells |
| $\pi$ | Pi |
| $\Delta G^{\neq}$ | Activation Gibbs energy of adhesion |
| $D$ | hickness of polymer film |
| $\mathbf{\Phi}_D$ | Fluorescence quantum yields |
| F | Integrated fluorescence intensity |
| $\eta$ | Refractive index of solvent |
| $\eta_R$ | Refractive index of reference |
| $f$ | Absorption factor |
| $A$ | Absorption |
| $R_0$ | Förster radius |
| $\kappa$ | Orientation factor between donor and acceptor molecules |
| $\varepsilon_A$ | Molar extinction coefficient of the acceptor |
| $F_D$ | Peak-normalized fluorescence intensity of the donor |
| $\chi$ | Value of fitting for fluorescence intensity decay profile with time |
| $\alpha$ | Optical absorption coefficient |
| $X$ | Sample thickness |
| $h\upsilon$ | Energy of the incident photons |
| $E_g$ | Value of the optical energy band gap |
| $r$ | Empirical exponent index |
| $I$ | Current |
| $P$ | Power |
| $U$ | Voltage |
| $R_{ex}$ | External load |
| $P_{cell}$ | Fuel cell power output |
| $F_f$ | Fill factor |
| $I_{sc}$ | Short circuit current |
| $V_{oc}$ | Open circuit potential |
| $\Gamma$ | Electron transfer rate |
| $e$ | Electron charge |
| Q | Charge |

| | |
|---|---|
| $S_e$ | Estimate surface coverage of the redox species |
| F | Faradays constant |
| D | Diffusion coefficient |
| $S_a$ | Electrochemical surface area |
| γ | Scan rate |
| $K_a$ | Binding constant |
| ΔH | Change in enthalpy |
| ΔS | Change in entropy |
| ΔG | Change in Gibb's free energy |
| h | Hour |
| $R_{ohm}$ | Ohmic resistance/solution resistance |
| $R_{ct}$ | Charge transfer resistance |
| W | Warburg's diffusion element |
| $C_{dl}$ | Double layer constant phase capacitance |
| $I_p$ | Peak current response |
| $K_i$ | Cell-alcohol interaction constant |
| $f_i$ | Fluorescence intensity before addition of solvent |
| $f_f$ | Fluorescence intensity after addition of solvent |
| $V_1$ | Base potential before addition of alcohol |
| $V_2$ | Potential amplitude from the base mid-point of the inflection peak to the peak point |
| $B_{max}$ | Maximum potential burst |
| X | Concentration of the alcohol |
| Y | Potential burst |
| *C* | Concentration of the probe in solution |
| L | Distance between the copper clips |
| $\lambda_{em}$ | Excitation wavelength |
| $\lambda_{ex}$ | Emission wavelength |
| $\epsilon_r$ | Dielectric constant |
| ρ | Resistivity |
| R | Resistance |
| σ | Conductivity |
| Ω | Ohm |
| V | Volt |
| mV | Milivolt |
| v/v | Volume/volume |
| w/v | Weight/volume |
| Wt | Weight |
| A | Ampere |
| J | Joules |
| Å | Angstrom |

| | | | |
|---|---|---|---|
| a.u. | Arbitrary units | m | Meter |
| µA | Microampere | mm | Milimeter |
| cal | Calorie | min | Minutes |
| µcal | Microcalorie | S | Siemens |
| µg | Micrograms | nm | Nanometer |
| µl | Microliter | L | Liter |
| µM | Micromolar | mL | Mililiter |
| mol | Mole | M | Molarity |
| µmole | Micromole | W | Watt |
| g | Gram | cm | Centimeter |
| mg | Miligram | Hz | Hertz |
| ng | Nanogram | MΩ | Mega ohm |
| nM | Nanomolar | eV | Electron volt |

# List of Figures

# List of Tables

# Introduction

# Introduction

Cyanobacteria are pioneer autotrophs that can grow in a self-sustainable manner and can fix carbon in globe into energy-dense biomass by capturing atmospheric $CO_2$ and solar energy. This route of massive solar energy transformation into microbiological energy medium opens the scope of harvesting various forms of eco-friendly energy, among which, the electrical energy through photosynthetic microbial fuel cell technology (PMFC) (Scheme I) has been an emerging subject in the frontier field of renewable energy research. One of the major driving forces for exploiting cyanobacteria as fuel cell catalyst is their flexible growth conditions since these bacteria grow well under phototrophic as well as heterotrophic conditions. Moreover, most of these photosynthetic microorganisms are tolerant to high salt concentrations and organic contaminants which are favorable features for their onsite applications particularly, for bioremediation and other environmental studies. Another interesting characteristic of cyanobacteria that has been discovered in the recent past from the intensive investigation on their metabolic network is the interlinking photosynthetic and respiratory pathways, which are housed together in their thylakoid assembly. It has been envisioned that this unique feature of interlinking these two energetically suppled electron shuttling pathways may play a critical role in harvesting the metabolic electrons for sustained current generation in PMFC devices. However, even though there are many positive traits as discussed above to ascribe cyanobacteria as potential fuel cell catalysts, the desired progress particularly, on the technological advancement of these biocatalysts-based PMFC devices is yet to be made. In order to develop an efficient PMFC of practical use, we feel that few critical issues need to be addressed, among which the approach for capturing the metabolic electrons efficiently on the electrode surface and the capability of PMFC to deliver adequate power even under low light conditions are to be reckoned first. It may be mentioned that the theoretical maximal light energy conversion efficiency (LCE) of photosynthesis in cyanobacteria is 11 %, as only 50 % of the incident solar energy can be accessed (Chen *et al*., 2015a; Tsujimura *et al*., 2001). Our effort in this direction would be to explore a suitable strategy to boost the photosystems (PS I and PS II) of the cyanobacterial cells considering the fact that this photosynthetic machinery is vital for

absorption of light energy in photosynthetic organisms at large. Two major mechanisms are frequently highlighted in the literature for capturing the cellular metabolic electrons on the microbial fuel cell electrode, namely, direct electron transfer (DET) and mediated electron transfer (MET) processes, while a third approach involving bacterial nanowires for transferring the metabolic electrons to the electrode is in a nascent stage.

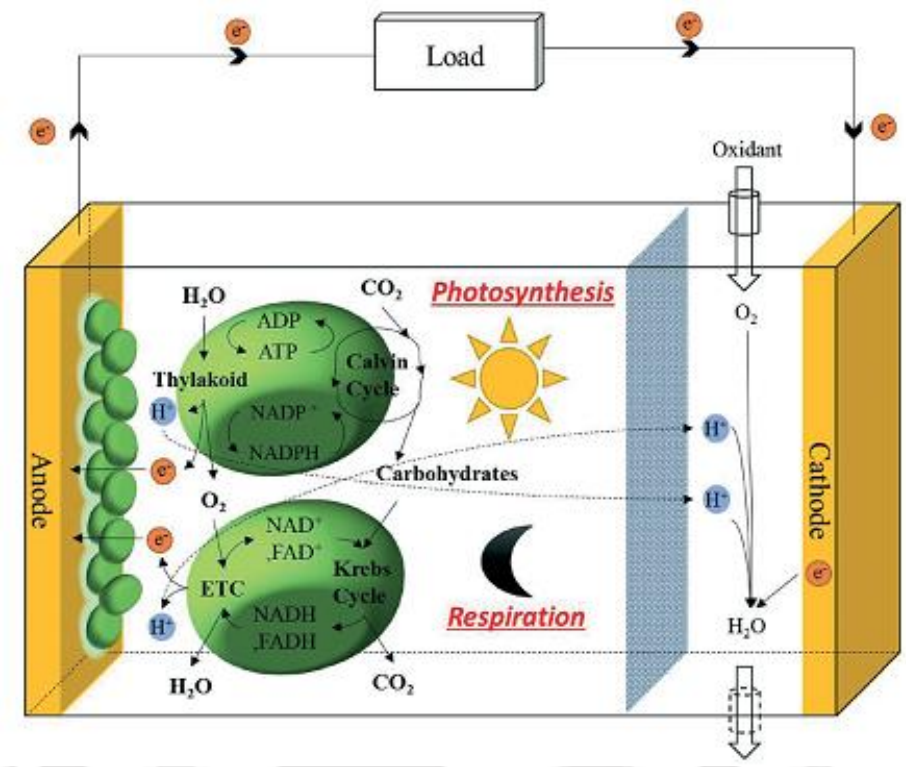


**Scheme I:** Schematic diagram of a photosynthetic microbial fuel cell (Lee and Choi, 2015).

If the PMFC is to develop for use in open environmental conditions, the design approach for developing the electrode may be focused on adopting the DET mechanism, as the complementary MET-based approach is often snagged with gradual leaching of the chemical mediators, which are largely hazardous in nature and are thus unwanted from the ecological perspective. To implement the concept of DET in a PMFC setup for steady generation of electric current, a naturally sustained close contact between the bacterial cells and the conductive electrode is a desired condition. To meet this condition, the creation of a natural bacterial biofilm over the electrode surface has been evolved as the method of choice for generating stable current from the cellular electrons in the biofuel cell setup. However, the

biofilms are usually formed slowly and their formation is governed by the nature of the support medium being used. Moreover, most of the electrode materials, such as graphite and conductive metals, commonly used in the fuel cell applications are either unreceptive or non-conducive to the bacterial growth to yield biofilm. Hence, the rapid development of biofilm on the electrode surface has been subsumed as an important domain in the microbial fuel cell research. The study, however, should take into account the electron transfer distance as guided by the modern Marcus Electron Transfer Theory, for seamless hopping of the metabolic electrons to the conductive electrode across the bacterial cell wall of microscale dimension. A feasible approach to overcome this hurdle is to employ highly conductive advance nanomaterials in the interface of the electrode and the biofilm to enhance the electron transfer kinetics following the DET mechanism.

The phototrophic growth characteristic of cyanobacteria may be an attractive feature for developing small scale PMFCs. The condition may support the organism to sustain growth on small scale electrode surface without entailing much complexity in supplying and adjusting the carbon substrates in the microbial fuel cell (MFC) devices with the tailored scope of developing small scale PMFC design. A potential application area for such small scale PMFC devices is biosensor. As per the definition, a biosensor is an analytical tool consisting of biologically active material used in close conjunction with a device that converts a biochemical signal into a quantifiable electrical signal (IUPAC definition)**.** A biosensor consists of a bio-receptor (enzymes, antibodies, whole cells, proteins etc.) for the specific detection of the respective analyte in spatial contact to a transducer for converting the signal into an electrically manageable format and a signal processing unit (Scheme II ) (Andrade *et al*., 2011).

One of the critical performance factors for a biosensor is the sensitivity of the signal. A small scale PMFC that cannot afford to deliver high power (current or potential) due to obvious reason may be thus, developed as a suitable biosensor device if it can produce the power signal sensitively and selectively against the target compound of interest. In the present study, we propose to develop a suitable PMFC biosensor for alcohol. The importance of rapid, selective and portable alcohol detection systems is sharply increasing not only in traditional brewing, pharmaceutical, food, and clinical industries but also in

rapidly growing alcohol-based fuel industries (Thungon *et al*., 2017). Surprisingly, there is no suitable portable low-cost system for selective, sensitive and quantitative detection of alcohol for commercial applications.

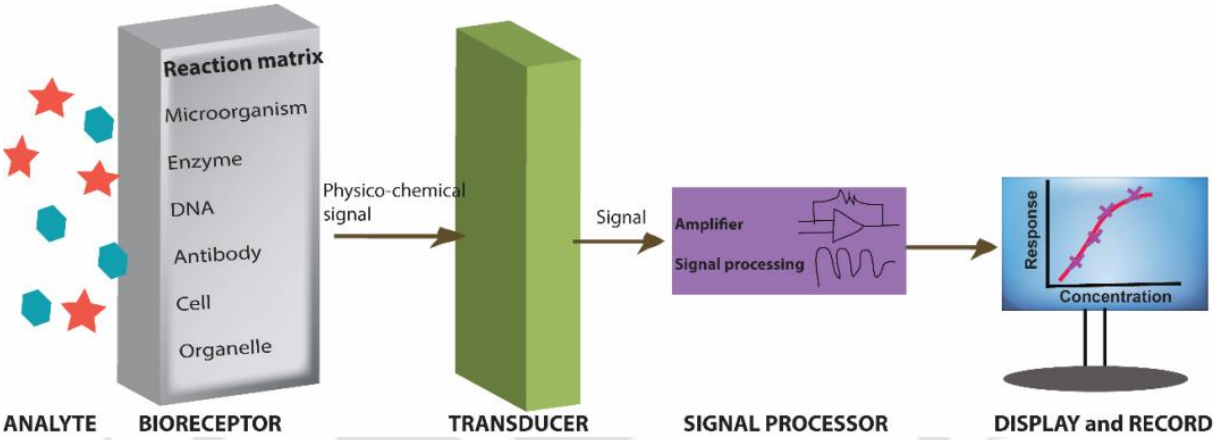


**Scheme II:** General configuration of typical biosensors.

Considering the enormous potential of cyanobacteria as PMFC catalyst, and the gaps and challenges to develop such PMFC as briefly discussed above, the following objectives have been set for the present investigation embodied in this thesis.

- Studies on support material for rapid cyanobacterial biofilm growth on the solid surface.
- Development of a nano-biocomposite based anode material to enhance and stabilize current in PMFC.
- Fabrication of a small scale PMFC for selective alcohol detection using a suitable support platform

The entire thesis has been delineated into four chapters as described below, followed by a short section covering the overall conclusion on the present work and the scope for future research.

**Chapter I: Review of literature**

A summary on the current status and progress in the area of MFC with cyanobacteria as the anodic catalyst has been presented. It highlights the basic concept of the MFC,

underlying molecular electron transport systems in cyanobacteria, the electrode materials used in MFC, and a brief review on the alcohol detection systems with a special focus on MFC-based sensors.

**Chapter II: Studies on support materials for growth of cyanobacterial biofilm**

Various chemical and biological materials such as silk, chitosan, silk-chitosan blend, polyaniline, osmium, and Nafion films were investigated for their capability to induce rapid biofilm formation. Based on this study, the physico-chemical parameters responsible for the biofilm growth has been investigated and a comprehensive concept has been forwarded under this chapter.

**Chapter III: Development of nano-biocomposite material based bioanode to enhance and stabilize current in PMFC**

The study in this chapter included the development of a nano-biocomposite matrix consisting of silk fibroin, quantum dots and graphene nanoplatelets for bioanode fabrication. The developed bioanode was characterized and then assembled in a PMFC setup. The performance of the PMFC was evaluated.

**Chapter IV: Fabrication of a small scale PMFC for selective detection of alcohol**

This chapter describes a detection principle for alcohol following a novel signal form in a lab scale PMFC device. The proof-of-concept was then successfully translated into a paper-based photosynthetic microbial fuel cell (p-PMFC) in a small scale design. Additionally, the probable mechanism involved in the detection has been illustrated.

**Conclusion and scope for future research**

This section recounts the significant conclusions on the present work. Furthermore, a brief critical evaluation of the work and the future scope to advance the work for a technologically viable device has been projected.

# Chapter I

## Review of literature

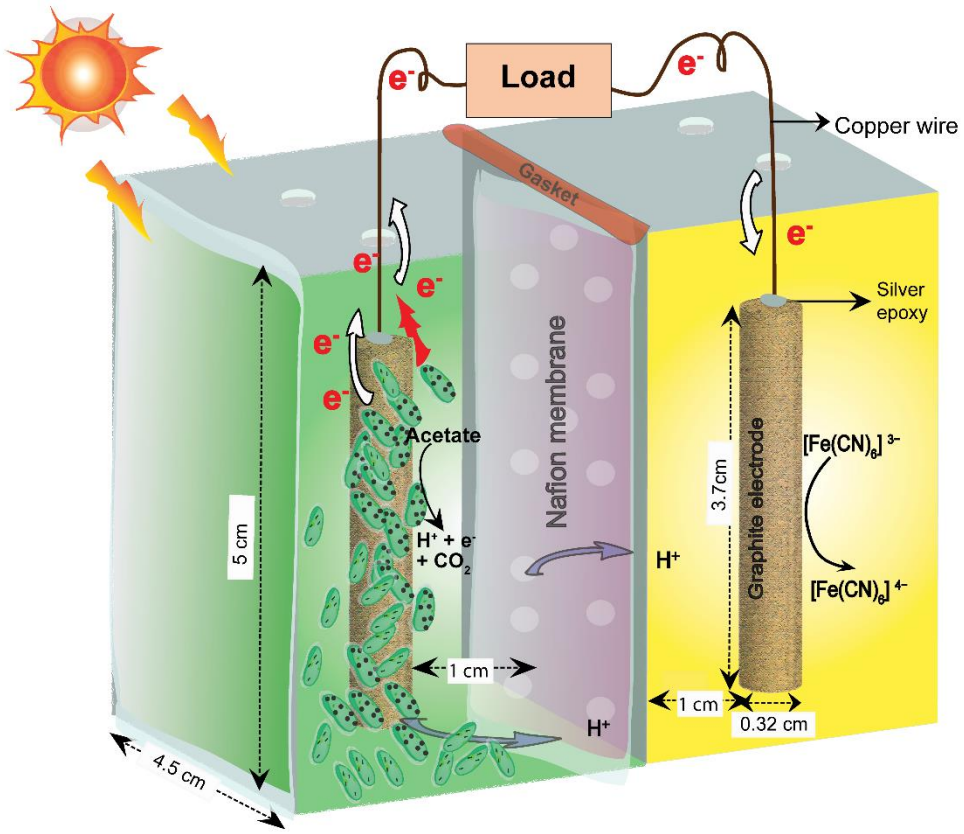


*Graphical abstract on PMFC with an abiotic cathode*

# Chapter I

## Review of Literature

Cyanobacteria are primitive prokaryotes performing oxygenic photosynthesis for their growth and survival. It can fix an estimated 25Gt $a^{-1}$ (Pisciotta *et al*., 2010) of carbon in the globe from atmospheric $CO_2$ by capturing the solar energy into energy-dense biomass. Cyanobacteria have emerged as a potential source of various compounds of industrial importance such as biodiesel, ethanol, vitamins, proteins, and many other products of pharmaceutical sectors (Hall *et al*., 1995; Paumann *et al*., 2005). These photosynthetic microorganisms have recently attracted wide interest as catalysts in microbial fuel cell (MFC) devices. The progress on the development of these photosynthetic MFCs (PMFCs) using cyanobacteria as fuel cell catalysts is central to the literature described in this chapter. An initial description of the photosynthesis and the linked metabolic pathways in cyanobacteria would be useful to understand the concept of using this microorganism as fuel cell catalyst.

### 1.1 Photosynthesis and respiration in cyanobacteria

The photosynthetic apparatus in cyanobacteria is present in the thylakoid membranes corresponding to that found in the chloroplast of plants. Phycobilisome is a group of pigmented proteins (phycobiliproteins) present as an ordered array of closely spaced granular structures in the thylakoid membrane. Its function is to trap the light and transfer the captured photon energy into the photosynthetic reaction centers. Hemidiscoidal phycobilisomes are the most commonly found light-harvesting complexes in cyanobacteria. It is composed of two subdomains, the core, and the peripheral rods. The core consists of three cylinders composed of allophycocyanin. Six peripheral rods extend from this core constituting the second sub domain of phycobilisome. The chromophores phycoerythrin and phycocyanin constitute the peripheral rods that trap light. The light energy absorbed by the peripheral rod proteins is transferred in a cascading way to allophycocyanin and then to photosystem I (PS I) or photosystem II (PS II) reaction centers (Walter, 2004) which further

collaborate to transfer electrons from water to $NADP^+$. The reaction centers consist of chlorophyll which is the epicenter of actual charge separation when the light is absorbed. Eventually, the electron is transferred to a $P_{680}$ pheophytin complex which reduces $Q_A$, the bound plastoquinone molecule. $Q_A$ reduces a secondary quinone $Q_B$ (semiquinone) leading to the formation of plastoquinol. On the luminal side of PS II, the light-induced chlorophyll cation radical $P_{680}^+$, oxidizes a tyrosine residue, which in turn oxidizes a cluster of four manganese atoms. Splitting of water occurs at this metal center, and the metal cluster is capable of assembling four oxidizing equivalents that act as a hinge to release $O_2$ from two molecules of water. The five successive oxidized forms are termed as S states. The reaction center also contains a non-heme iron atom and a stable tyrosine radical (Walter, 2004). The intermediary S states may act as a regulatory mechanism and a link between the S states and the tyrosine radical. PS II is made up of both integral membrane proteins and extrinsic proteins. It is susceptible to damage by sunlight under electron limiting conditions. However, a repair cycle operating within PS II aids in sustaining the PS II activity (Komenda *et al*., 2012). The proton gradient generated as a result of this flux is used for the synthesis of adenosine triphosphate (ATP).

The excited electron from PS II travels down to the cytochrome $b_6f$ complex in the z- scheme. The rate-limiting step of quinol oxidation in aerobic photosynthesis is catalyzed by plastoquinol-cytochrome $c_{553}$/plastocyanin oxidoreductase (Cyt$b_6f$ complex) enzyme. Electrons released from plastoquinol oxidation are accepted by the cytochrome $b_6$f complex, which provides electrical connection between the PS II and PS I photochemical reaction centers (Walter, 2004; Gabdulkhakov and Dontsova, 2013). This complex is coded by *pet* (photosynthetic electron transport) genes that contain Cyt$b_6$ – a low potential protein, subunit IV, a high energy *Rieske* iron sulphur protein [2Fe-2S] center, Cyt f protein, two *b* and a c-heme moiety. The proton-pumping cytochrome $b_6f$ complex is a dimer and contains eight firmly bound subunits in the cyanobacterium *M. laminosus* (Whitelegge *et al*., 2002). The respiratory and photosynthetic pathway in cyanobacteria requires oxidation of the quinone pool by the Cyt $b_6$f complex and ultimately by molecular oxygen at a terminal cytochrome $aa_3$ type oxidase (Nicholls *et al*., 1992) while, the obligate role of the later is yet to be clearly elucidated. Thus, the cytochrome $b_6f$ complex appears to be a part of the

common set of elements essential for the growth of cyanobacteria by photosynthesis or respiration.

The PS I complex in cyanobacteria uses all of its biochemical machinery to oxidize plastocyanin or other electron carriers and reduce ferredoxin across a wide thermodynamic gradient. The membrane-bound components of the complex comprise of the reaction center P700, a chlorophyll *a* dimer and the primary donor absorbs light energy releasing electron that is captured by $A_0$, the primary electron acceptor and a chlorophyll *a* (Chl *a*) monomer. This electron is then transferred to the secondary electron acceptor molecule $A_1$, a phylloquinone which acts to stabilize the rapid transient charge separation (Golbeck, 1994). The *psa* genes codes for PS I multimeric protein complex and consists of eleven discrete proteins as reported from various cyanobacterial strains. Both monomeric and trimeric cyanobacterial PS I forms have been elucidated. The trimeric form is the prominent oligomeric state at low light intensity, which is the natural habitat of cyanobacteria. An enormous antenna complex that consists of 90 antenna chlorophyll and 22 carotenoids captures the light. The electron transport chain (ETC) in PS I comprises of two phylloquinone, six chlorophylls, and three iron sulphur [4Fe-4S] clusters (Tsiotis *et al*., 1993). Cofactors of the ETC in PS I from cyanobacteria and higher taxon like plants are identical. PsaM and PsaX are the proteins found exclusively in cyanobacteria. Rest of the main proteins with all the cofactors are well conserved between plants and cyanobacteria. The electron from secondary electron acceptor $A_1$, i.e. phylloquinone is transferred to the three iron-sulphur clusters [4Fe-4S] designated as $F_X$, $F_A$, $F_B$ in a cascading manner rendering P700 to an oxidized state. From $F_B$ the electron travels to ferredoxin located on the stromal side of PS I. Ferredoxin leaves its docking site after reduction to transfer the electron to ferredoxin-$NADP^+$ reductase that produces the end product nicotinamide adenine dinucleotide phosphate (NADPH) to be used for $CO_2$ assimilation. The soluble electron donors located on the luminal side- the plastocyanin and cytochrome $C_6$ of PS I, receives the electron along the z -scheme and reduces P700 which stabilizes the loss of energy due to charge recombination (Sommer *et al*., 2004). The changes in copper and iron concentration, however, do not lead to any known alterations in the polypeptide composition of the membrane-bound PS I complex.

The understanding of the cyanobacterial F-ATPases is limited. The $F_1$ portion purified from cyanobacterial sources to reconstitute photophosphorylation (Hicks and Yocum, 1986; Lubberding *et al*., 1983) showed the same five subunits (α, β, γ, δ, and ε) with molecular masses similar to those of other F-ATPases (Lubberding *et al*., 1983). The integral membrane protein complex, i.e. the $F_0$ portion, comprises of single copies of subunits a, b and b' and about ten copies of subunit c. The extrinsic protein complex attached to the $F_0$ portion has 3α, 3β, 1γ, 1δ, and 1ε subunits (Süss and Schmidt, 1982). ATPase enzyme comprises of a total of six sites, of which three are catalytic to which metal and nucleotides bind forming complexes. ATP synthesis occurs in conformity with the transfer of phosphoric acid residue between ADP and water when all the phosphate groups are synchronized to the catalytic sites in the active state.

Cyanobacteria have a plant-type ferredoxin — ferredoxin I that transfer electrons from the membrane-bound, iron-sulfur centers in PS I to FNR (Ferredoxin-NADP oxidoreductase). It is a strong acidic protein with a [2Fe-2S] center that transfers one electron. Ferredoxin- I is evolved from a single gene as evident from the conserved gene clusters. It is replaced in the situation of iron deficiency by the non-iron containing flavoprotein, the flavodoxin. Ferredoxin is loosely held in the thylakoid membranes making it easier to serve other electron acceptors, e.g. nitrite reductase, thioredoxin reductase etc. (Plas *et al*., 1988). Flavodoxin is also an acidic protein resembling ferredoxin in net charge and redox properties.

Plastocyanin is a protein of approximately 100 amino acid residues. It acts as an electron carrier and contains a single atom of copper in its redox-active center. This protein transfers the electron from cytochrome *f* to P700 of PS I in the electron transfer chain of photosynthesis. Experiments indicate that the 'east-face acid patch' of plastocyanin is the site for receiving electrons from cytochrome *f* and the 'north-face hydrophobic patch' of plastocyanin is the site for donating electrons to PS I (Morand *et al*., 1989).

Cytochrome $c_6$ is another soluble electron carrier protein that replaces plastocyanin in some cyanobacteria and algae experiencing copper exhaustion. It permanently replaces plastocyanin in some species. Several isoforms of this protein have been reported along with variations under different growth conditions indicating involvement in various physiological

roles. This particular protein is functional during both photosynthesis and respiration. It is distributed uniformly in the cytoplasm. Another low potential cytochrome, $c_{549}$ is found in many cyanobacteria that support the structural stability of PS II.

Cyanobacteria have an efficient $CO_2$ uptake and concentrating mechanism. Central to the mechanism is the carboxysome, an icosahedral or quasi-icosahedral protein micro-compartment within the cell whose outer shell holds the Rubisco together with a carboxysomal carbonic anhydrase (CA) (Badger, 2003). The CA converts the accumulated $HCO_3^-$ anion to $CO_2$ within the cabroxysome. The protein shell of the carboxysome possibly prohibits the efflux of elevated levels of $CO_2$ from itself thereby making it accessible to Rubisco enzyme within the organelle. Active $CO_2$ and $HCO_3^-$ transporters operate to bring in the substrate. They are present in the plasma membrane as well as thylakoid membrane, both in high and low affinity forms (Kaplan and Reinhold, 1999).

A unique feature of the cyanobacteria is the intersecting photosynthesis and respiratory pathways that allow for a continuous relay of electrons inside the thylakoid membrane. The oxygenic photosynthesis and aerobic respiration occur in the same compartment in cyanobacteria (Kaplan and Reinhold, 1999). Some of the membrane proteins are common to both the pathways (Vermaas, 2001) (Figure 1.1). Some cyanobacterial cells contain two distinct respiratory chains, one in the thylakoid and the other in the cell membrane. The photosynthetic apparatus is exclusively present in the thylakoids. Components like NADPH, plastoquinone, and a chloroplast type cytochrome $b_6f$ complex which are not involved in the respiratory system of other organism are also a part of the respiratory chain of cyanobacteria (Kraushaar *et al*., 1990). There is significant evidence that the respiratory chain in cyanobacteria is branched and may turn out no chemical reaction is common to all respiratory electron transport pathways. Therefore, no specific sequence of reactions can be said to make up the respiratory electron transport chain as is found in mitochondria of eukaryotic organisms. The lack of complete information on respiration of cyanobacteria is a major roadblock in defining it in a complete manner.

Some cyanobacterial species have developed the ability to extract energy heterotrophically in response to challenging environmental conditions along with its photosynthetic capability (Gill *et al*., 2002). They catabolize glucose pathway, the glycolytic

pathway, and a type IV tricarboxylic acid (TCA) cycle and oxidative pentose phosphate (OPP) to produce ATP, NADPH and carbon anabolic precursors for further cellular processes (Takahashi *et al*., 2008). All of the above mentioned metabolic pathways, $CO_2$ fixation, gluconeogenesis, and glycolysis, are performed in the carboxysome and cytoplasm where different enzymes of both photosynthetic and respiratory pathways exist.

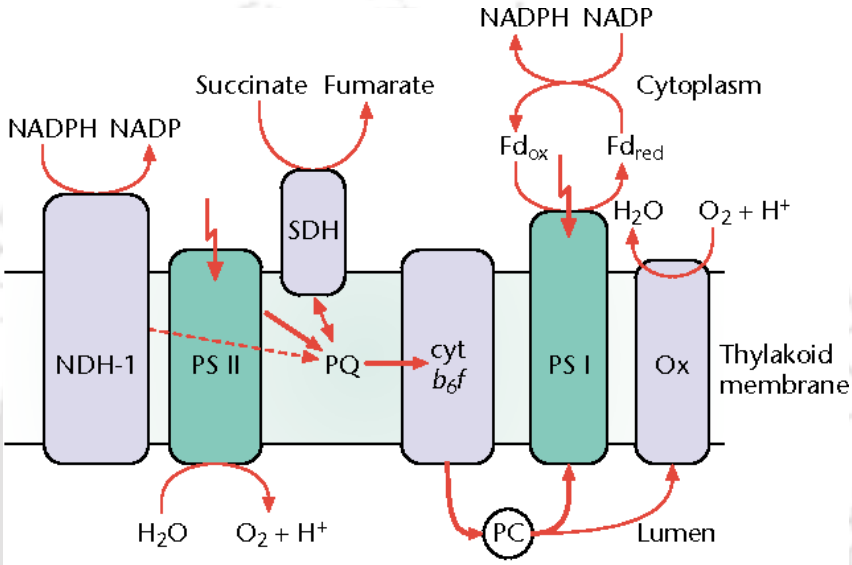


**Figure 1.1:** Intersecting photosynthetic and respiratory electron transport pathways in the thylakoid membrane of the cyanobacterium *Synechocystis* sp. PCC 6803 (Vermaas, 2001).

## 1.2 Cyanobacteria biofilm

Biofilms are microbial communities growing on solid surfaces and frequently embedded in a matrix of extracellular polymeric substances, mostly composed of proteins, polysaccharides, nucleic acids and other bio-molecular components (Flemming and Wingender, 2010). The life cycle of biofilm formation consists of several steps (Figure 1.2). The basic steps include surface conditioning and attachment (reversible and irreversible attachment), maturation and dispersion (Baranitharan *et al*., 2015; Toyofuku *et al*., 2016). The surface attachment signifies an important transition from planktonic to biofilm mode. This is preceded by surface conditioning by adsorption of various macromolecules to the surface, which is a time-consuming process (Svensater and Bergenholtz, 2004). Cell division, proliferation, and exo-polymeric substance secretion lead to the creation of a

complex architecture. This matured biofilm intensifies the social networking activities like nutrient exchange and quorum sensing. Finally, the dispersion of cells from biofilm to planktonic mode indicates the start of another cycle (Toyofuku *et al*., 2016). The major driving forces for biofilm research are their clinical insinuation and detrimental effect on human comfort which incited to delve into the intensive investigation of their disruption and prevention (Bazaka *et al*., 2012). Consequently, the biofilm research largely dealt with the pathogenic microorganisms (Hancock *et al*., 2011), sulphate reducing bacteria (Enning and Garrelfs, 2014), microbial fouling on structural setups (Diaz-Herraiz *et al*., 2013) etc. while, the same with beneficial microorganisms focusing on their formation and linked applications is meager (Nguyen *et al*., 2014). The beneficial effects of biofilm are being increasingly identified in areas such as bioremediation, pharmaceuticals, bioenergy, biosensors, and microbial fuel cells (Kalathil *et al*., 2013; Karatan and Watnick, 2009; Yang *et al*., 2015). Under certain circumstances, most of the bacteria produce biofilms for their growth and survival. The biofilm of some of the bacteria, such as *Staphylococcus* spp, *Listeria monocytogenes*, *Bacillus* spp, lactic acid bacteria, *Pseudomonas aeruginosa*, *Escherichia coli* etc. have been studied to a greater extent owing to their industrial, environmental or clinical implications (Karatan and Watnick, 2009).

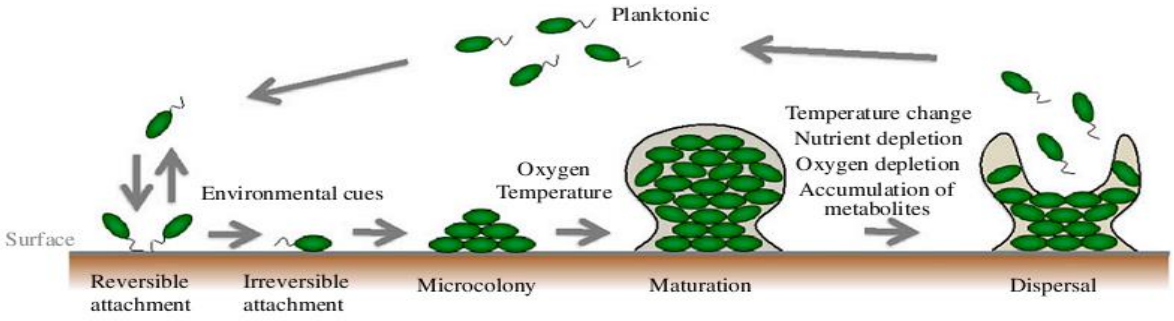


**Figure 1.2:** The life cycle of biofilm and some environmental factors that have an influence on its development (Toyofuku *et al*., 2016).

The biofilm produced by the phototrophic microorganisms under the natural environment has been studied to a limited extent (Bruno *et al*., 2012). One of the major components of the cyanobacteria biofilm is the exo-polysaccharides (EPS) that constitute ~ 60 % of their dry biomass. In addition to EPS, a small amount of fatty acids and peptides were also detected in the biofilm matrix of cyanobacteria. The composition of EPS is

however, species-specific that might enable them to endure adverse environmental conditions. Genomes of diverse cyanobacteria encode GG-containing small proteins that are crucial for biofilm development (Parnasa *et al*., 2016). The detailed genetic information on the EPS is however, yet to be elucidated (Rossi and De Philippis, 2015). The cyanobacterial species are known to produce a large number of secondary metabolites. Some of these metabolites deter the development of biofilm by other paralleled competing microbial life forms and protozoan predation (Gademann, 2007). The cyanobacterial EPS have found applications as antibacterial, antifungal and antifouling agents (Gademann, 2007).

Microbial biofilm is usually preferred over suspended growth for various applications such as wastewater treatment, bioremediation, as it facilitates to reduce water and energy consumption in the processes (Bombelli *et al*., 2015; Safi *et al*., 2014; Vijayakumar, 2012). In the case of wastewater treatment plants, thick biofilms and biofilm support can aid to counteract peak loading fluctuations and keep the effluent concentration from exceeding set discharge levels (Wilderer *et al*., 2000). There are limited reports on the application of cyanobacteria in bioremediation and wastewater treatment. The importance of biofilm of the catalytic cells over MFC electrode has been greatly recognized as the higher cell density in biofilm promotes cell-to-cell contact aiding in electron transfer kinetics and operational stability of this power generating device (Ozkan and Berberoglu, 2013a; Mohan *et al*., 2008). The economic viability of the production of various microbial compounds of industrial importance relies on the efficient cultivation and harvesting of the bacterial cell mass, which in turn depends on the cell to cell and cell to surface interaction (Ozkan and Berberoglu, 2013a). Similarly, for developing biosensors using cyanobacteria as biorecognition system, the microorganism needs to be coupled to a transducer for rapid screening of the targets (Shao *et al*., 2002). Microbial biofilm on the surface of the transducer may fulfill the condition for facilitating the transduction of the biochemical signal. The biofilm may bring the reaction site closer to the transducer for generating the signal efficiently. Further, it will increase the operational stability of the developed sensor (Wong *et al*., 2013). In regards to the microbial fuel cells (MFCs), the creation of anodic biofilm may be an effective strategy to reduce start-up time and electrochemical potential loss (ElMekawy *et al*., 2014; McCormick *et al*., 2011). A sustained electrically close contact between the biofilm on the anode is a prerequisite for the practical implementation of MFC

as energy converting devices, environment monitoring or as MFC biosensors (You *et al*., 2015). However, the knowledge on the support materials which induce and accelerate the cyanobacterial biofilm formation is not yet adequately elucidated (Matsumoto *et al*., 2012; Ursell *et al*., 2013).

## 1.3 Microbial fuel cell: A highlight on the basic principles and operation

MFC is a device that converts biochemical energy into electrical energy through microbial oxidative catalysis at the anode and parallel reductive catalysis using an electron acceptor, such as oxygen, at the cathode (Du *et al*., 2007). Like chemical fuel cells, two compartments - the anode and cathode half-cells – are usually separated by a proton exchange membrane in the MFC (Figure 1.3). The research on membrane-less BFC has also been pursued to simplify the design, technical complexity, and to reduce the cost of the devices (Sekretaryova *et al*., 2016). The electrons generated from the oxidation of fuel substrates at the anode are directed to the cathode via an external circuit, and the associated protons are transported across the membrane to the cathodic chamber for sustaining the current generation (Logan and Regan, 2006).

The electrons generated from the oxidation of organic substrates are transferred by the bacteria to the anode (Figure 1.3) using either or a combination of the following mechanisms: (i) direct electron transfer (DET) (Bond and Lovley, 2003), (ii) 'nanowires' (Reguera *et al*., 2006), and (iii) mediating electron transfer (MET) using chemical mediators/ shuttling agents (Rabaey *et al*., 2004).

The fundamentals of the fuel cell can be extended to MFC to evaluate its performance. When the overall reaction of a MFC is thermodynamically favourable, electricity is generated (Logan *et al*., 2006). The concept may be defined by the following equation:

$$\Delta G_r = - E_{emf} \times nF \quad \text{.....(1.1)}$$

Where, $\Delta G_r$ (J) is the Gibbs free energy, nF is the charge transferred in the reaction with n representing the number of electrons per reaction mol, and F is Faraday's constant (9.64853 × 104 C/mol). The electromotive force (emf) generated in the fuel cell is due to the

difference between the cathodic ($E_{cat}$) and anodic ($E_{an}$) potential as shown below (Logan *et al*., 2006) and can be calculated from the Gibbs free energy change for the anodic and cathodic reactions (Osman *et al*., 2011).

$$E_{emf} = E_{cat} - E_{an} \quad \text{.....(1.2)}$$

Ideally, the cell voltage should be independent of the current drawn. But in practice, this reversible cell voltage ($E_{cell}$) is not realized even under infinite load (zero current) conditions due to internal losses and fuel crossover, when the cell is operated. The cell voltage at zero current is termed as open-circuit potential (OCP). As current is drawn from the fuel cell (at varying load), the $E_{cell}$ deviates from OCP as a result of various losses which are known as overpotential as depicted by the following equation (Logan *et al*., 2006).

$$E_{cell} = E_{emf} - (\sum\eta_{act} + \sum\eta_{conc} + IR_{\Omega}) \quad \text{.....(1.3)}$$

Where, $\eta_{act}$ is the activation overpotential, $\eta_{conc}$ is concentration overpotential; I and $R_{\Omega}$ represent current and resistance (load), respectively. The current discharge pattern with respect to the external resistance can be illustrated by the polarization curve, which is plotted by considering the change in current density versus voltage (Mohan *et al*., 2014). The influence of external and internal resistances can be understood by such polarization graphs. There are three distinct regions at different current ranges (Figure 1.4):

a) At low currents, activation (charge transfer) overpotential ($\eta_{act}$) dominates. They arise from the energy barrier to charge transfer, from the mediator or bacteria/enzyme to the electrodes. The charge transfer overpotentials depend on the nature of the electrode materials, catalysts, reactant activities, electrochemical mediators, biofilm, electrode microstructure, microbial species and their metabolism, and operational conditions (Zhao *et al*., 2009b).
b) The ohmic overpotential ($IR_{\Omega}$) is observed at the intermediate current regions. Ohmic losses are due to the resistance to charge transport both ionic and electronic resistances through the current collectors, electrolytes, biofilm, membrane, and electrodes, as well as the interfaces between these components (Osman *et al*., 2011). These overpotentials

(separate for the two electrodes) can be approximated if expressions for the reaction rates are known, e.g. a Tafel's or Butler–Volmer's relation.

c) Concentration overpotential ($\eta_{con}$) manifests itself due to mass transport limitations at the interface between electrode surface region and bulk electrolyte prevalent at high current densities. It can be avoided by proper reactor design, mixing/aeration and thus eliminating diffusion gradients.

d) Additionally, MFCs suffer from bacterial metabolic losses as well. Some of the electrons are also lost to sustain the various metabolic activities necessary for the growth of the bacteria (Logan *et al*., 2006).

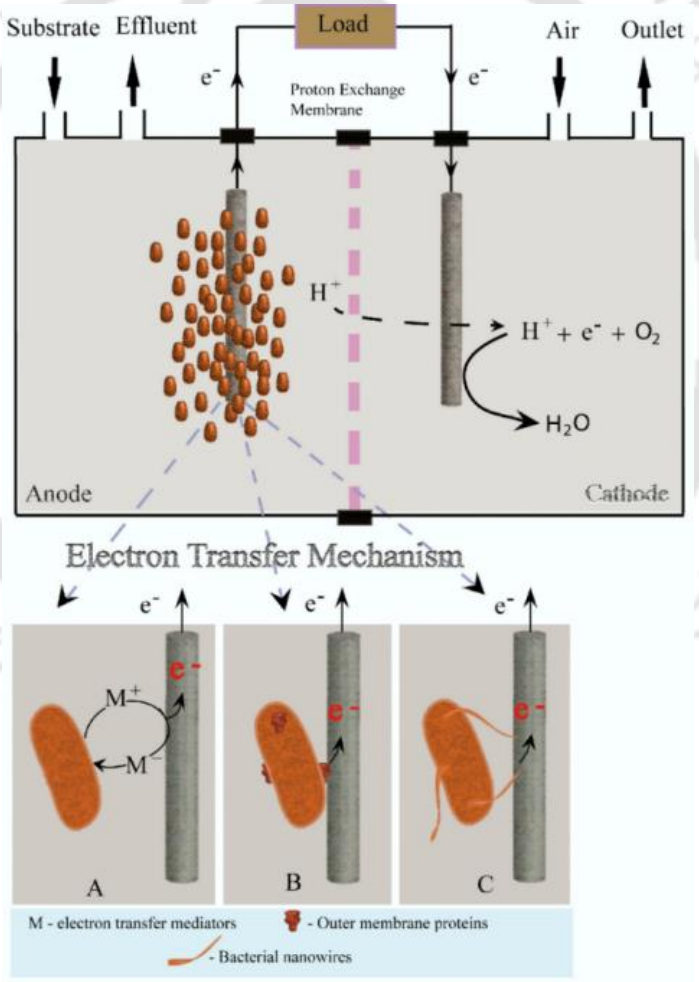


**Figure 1.3:** Electron transfer mechanisms from microorganisms to electrode: (A) mediated electron transfer (MET) by using electron transfer mediator (M), (B) direct electron transfer (DET) through the intimate contact between the outer membrane redox proteins and electrode or (C) by means of 'nanowires'.

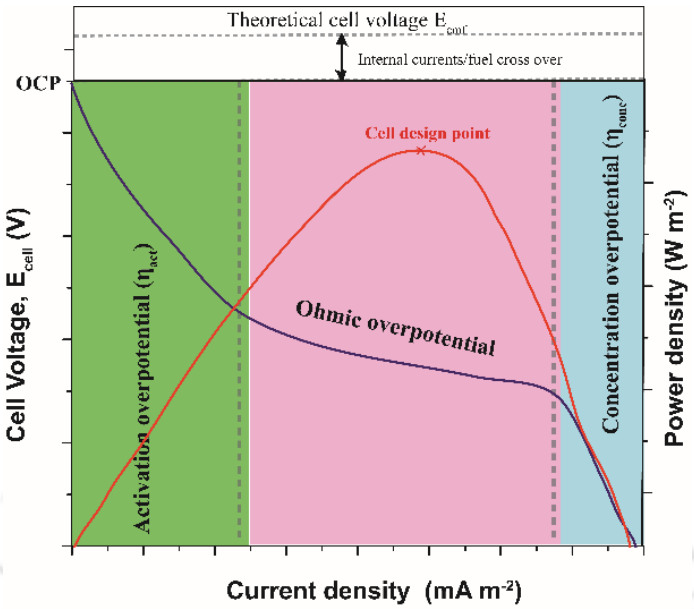


**Figure 1.4:** Polarization and power curves of a typical MFC depicting the possible losses incurred during the transfer of the electrons from microbe to the anode.

The power generated by a MFC is quantified in terms of power output, $P = V_{cell}$ (V) × I (A). The power density can be calculated by normalizing the power with respect to the electrode cross-sectional area, electrode volume or the working volume of the anodic chamber. The resistance at which both the current and voltage are optimum for highest power output is called the cell design point (Mohan *et al*., 2014).

The overpotentials as discussed above can be analyzed separately for the two electrodes if the expressions for the reaction rates are known with the help of Butler–Volmer's and Tafel's relation. The charge transfer overpotentials are controlled by the rate of heterogeneous electron transfer, and the kinetics of this process are described by the Butler–Volmer equation *(*Zhao *et al*., 2009b) when the reactants are abundant and the current is small enough that the ohmic and concentration overpotentials are negligible:

$$I = Ai_o \{e^{\left(\frac{\alpha nF\eta_{act,c}}{RT}\right)} - e^{\left(\frac{(1-\alpha)nF\eta_{act,a}}{RT}\right)}\} \quad \text{.....(1.4)}$$

where I is the current, A is the electrode active surface area, $i_o$ is the exchange current density, *a* is the charge transfer barrier (symmetry coefficient), n is the number of electrons involved in the electrode reaction, and $\eta_{act}$ is the charge transfer overpotential (Zhao *et al*.,

2009b). The Butler–Volmer equation can be simplified in the high overpotential region (>118/n mV), yielding the Tafel equation (Zhao *et al*., 2009b):

$$\eta_{act} = b \log_{10}(\frac{i}{i_o}) \quad \text{.....(1.5)}$$

Where i is the current density and b is Tafel slope, which is an important experimental parameter commonly used to probe the mechanism of an electrode reaction. Plots of overpotential against $\log_{10} i$ are known as Tafel Plots (Figure 1.5); $i_o$ and b are obtained by extrapolation of the linear region of the curve to $\eta_{act}$ =0 (Zhao *et al*., 2009b). The activation overpotential can be reduced by facilitating direct electron transfer through biofilm formation on the anode, increasing the reaction sites by increasing the surface area, improving the biocatalyst acclimatization and beneficial gene expression analysis (Zhao *et al*., 2009b).

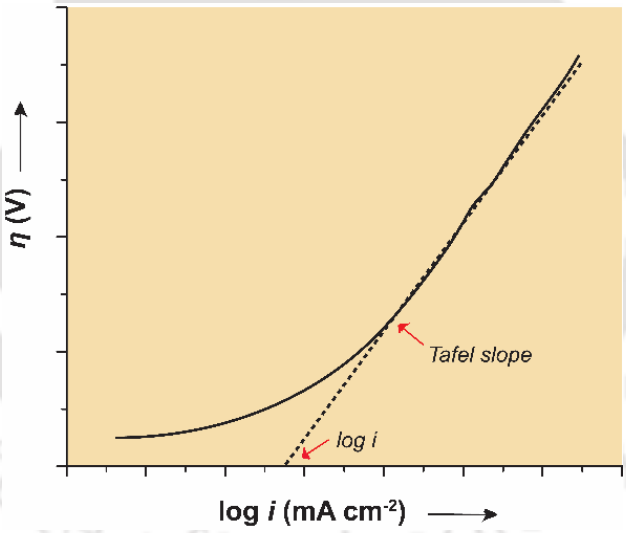


**Figure 1.5:** Tafel plot for calculation of current density.

## 1.4 Photosynthetic microbial fuel cell (PMFC)

The ability of cyanobacteria to grow phototrophically has appeared to be one of the major driving forces for using these bacteria as fuel cell catalysts to generate electric power from sunlight in a self-sustainable manner. The potential application of these light

harvesting organisms for integrated waste treatment and power generation through MFC technology is huge due to their usual tolerance to high salt concentration and organic contaminants, survival under adverse environmental conditions (such as, high temperature, low and high pH), and their ability to form stable biofilms and grow symbiotically with a wide range of organisms on earth (Sekar *et al*., 2014). However, among the known microbial strains or their consortium reported so far as catalysts in MFCs, the work on cyanobacteria is quite less (Logan, 2009). Amongst the total publications on microbial catalysts in MFCs (in open access and SCI journals), only ~ 6.5 % has been reported on cyanobacteria as compared to ~ 39.7 %, ~ 31.5 %, ~ 12.1 %, and ~ 10.2 % for *Shewanella sp., Geobacter sp.,* algae and *E. coli sp*., respectively.

### 1.4.1 Electrogenic property of cyanobacteria

Fuel cells utilizing electrogenic cyanobacteria or other photosynthetic microorganisms are also enlisted under bio-photovoltaic device (BPV) or microbial bio-solar cells where the light-harvesting apparatus of these organisms transduce photonic energy into electrical energy without metabolizing organic fuels (McCormick *et al*., 2011). The electrogenic behaviour of cyanobacteria is well documented. However, how the electrons generated in the cellular process are channelized across the electrogenic metabolic pathways (photosynthetic/respiration) to the external environment are not yet clearly known. Nevertheless, the presence of the intersecting photosynthetic electron transport chain (P-ETC) and respiratory electron transport chain (R-ETC) in the thylakoid membranes (Vermaas, 2001) may additionally support the electrogenicity of these micro-organisms. In a study, a conserved light-dependent (in the absence of any exogenous organic fuel) electrogenic activity of diverse genera of cyanobacterial strains was demonstrated (Pisciotta *et al*., 2010). The diverse genera including *Anabaena*, *Calothrix*, *Pseudanabaena*, *Nostoc, Synechococcus, Synechocystis* PCC6803 and *Lyngbya* exhibited preserved electrogenic activity originating from the P-ETC (Pisciotta *et al*., 2010). Using site-specific inhibitors, the P-ETC was confirmed as the source of electrons. Treatment with PS II inhibitors [3-(3,4-dichloro-phenyl)-1,1-dimethylurea (DCMU) and carbonyl cyanide m-chlorophenyl hydrazone (CCCP)] and PS I inhibitor [phenylmercuric acetate (PMA)] led to decrease in electrogenic responses of two cyanobacterial species (*Lyngbya* and *Nostoc*) under

illumination. Additionally, Duroquinone that competes with DCMU for binding to the $Q_B$ site on PS II was used to confirm the origin of electrons from PS II. Notably, Duroquinone mimics the activity of PQ by shuttling electrons between PS II to PS I (Pisciotta *et al*., 2010) (Figure 1.6). The finding was fundamentally different from those reported on anaerobic MFCs, or sediment MFCs, where the electrons for current were ascribed to be generated from R-ETC (Zou *et al*., 2009).

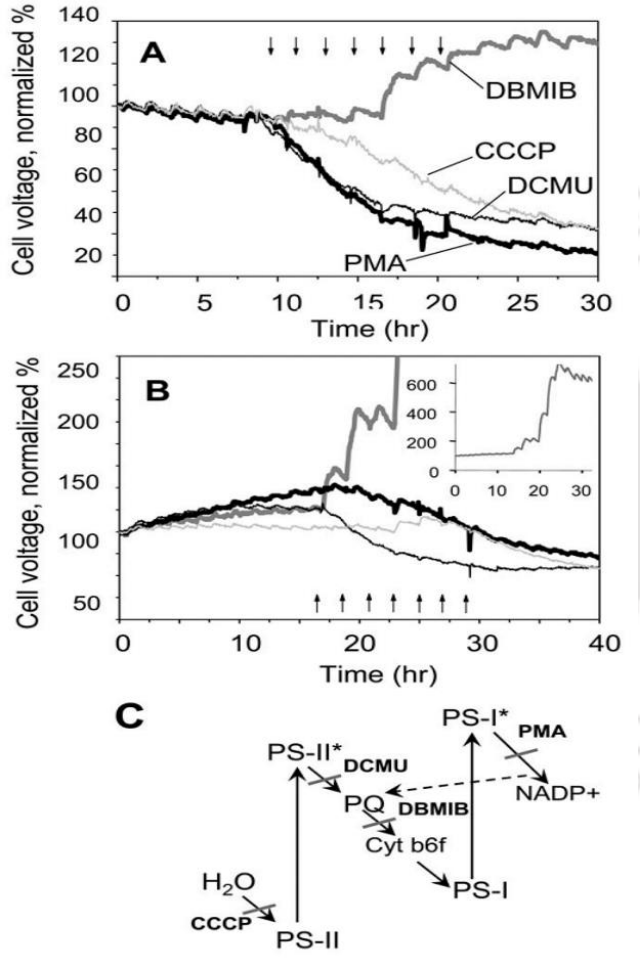


**Figure 1.6:** Effect of P-ETC site-specific inhibitors on the electrogenic activity of (A) *Lyngbya* or (B) *Nostoc* monitored under constant illumination and at 1 kV fixed external resistance. Inhibitors were added with cumulatively increasing concentrations (at two hours' interval): 1, 5, 10, 25, 50, 75 and 100 mM for DCMU (thin black lines), DBMIB (thick gray lines) and PMA (thick black lines); or 5, 10, 25, 50, 100, 150 and 200 mM for CCCP (thin gray lines) as indicated by arrows. (C) Schematic diagram showing P-ETC and sites targeted by inhibitors. Cyclic electron transfer (Q-cycle) is indicated by the dashed line (Pisciotta *et al*., 2010).

As discussed elsewhere, photosynthetic and respiratory chains share several redox active compounds in thylakoid membrane namely the plastoquinone (PQ) pool, plastocyanin (PC) and cytochrome $b_6f$ (Cyt $b_6f$). Hence, the study on electrons flux through these shared points may enrich our knowledge on the electrogenic metabolic channels precisely involved in these photosynthetic organisms for discharging the electrons into the environment. From an investigation in *Synechocystis* sp. PCC 6803 using the metabolic inhibitor DCMU and methyl viologen (a competitor of $NADP^+$ for capturing photosynthetic electrons), it was inferred that the residual photocurrent produced in the presence of DCMU may come from electrons that were initially introduced into the PQ pool from the respiratory chain and later on, used to reduce ferredoxin via PS I. Notably, the photosynthetic and respiratory chains in the thylakoid membrane in this organism share the PQ pool. This suggested that the electrons responsible for generating the current, leave the P-ETC at the reductive side of PS I (Bombelli *et al*., 2011). Most of the photocurrent is contributed by PS II. This was also demonstrated for other organisms like, *Nostoc* sp. by using the inhibitors such as, DCMU. Further, chlorophyll-*a* followed by phycocyanin was reported to be the major contributor to light capture that resulted in the increased generation of photocurrent (Sekar *et al*., 2014). The mutant strain of *Synechocystis* sp. PCC6803 lacking chlorophyll binding CP47 protein losses significant (81 – 84 %) reduction in photocurrent production capability (Cereda *et al*., 2014).

In order to transduce the light energy directly and efficiently to electrical power, the metabolism of the cyanobacterial cells (*Synechocystis* sp. PCC 6803) was manipulated rationally by deleting the terminal oxidase complexes and thus, eliminating the possible function of molecular oxygen as the electron sink. It is likely that the reducing power of cyanobacteria can be dissipated to oxygen through the terminal oxidases during respiration or at times of excess electron production. The result showed higher ferricyanide (a membrane-impermeable soluble electron acceptor) reduction rates as a consequence of creating an excess of reducing power. The gain was higher in dark conditions, especially from the triple deletion (bd-quinol oxidase, cytochrome c oxidase, and alternative respiratory terminal oxidase) strains where the mutant transferred the equivalent of 10 % of its aerobic respiratory electron flux to ferricyanide, causing a 23-fold increase in ferricyanide reduction rate compared to the wild-type (Bradley *et al*., 2013). To track the

source of reductive equivalent that is eventually utilized to generate the transmembrane electron flow and proton motive force (pmf) responsible for the electrogenicity of the cells and generation of ATP, respectively, the understanding of TCA cycle is also important. The primary function of TCA cycle is to produce NADPH/NADH in addition to provide essential precursor metabolites that are required for the biosynthesis of cellular components, such as fatty acids. Interestingly, the cyanobacteria have a variant of common TCA cycle as they lack 2-oxoglutarate dehydrogenase and succinyl CoA synthetase. The enzymes, 2-oxoglutarate decarboxylase and succinic semialdehyde dehydrogenase encoded by their genes, as studied in *Synechococcus sp*. PCC7002, convert 2-oxoglutarate to succinate, and thereby these organisms use this shunt pathway to regulate the production of reducing equivalents (NADPH) in addition to other functions most of which are not yet known (Steinhauser *et al*., 2012; Zhang and Bryant, 2011).

### 1.4.2 Electron transfer mediator (ETM)-based PMFC

As early as 1985, Tanaka *et al*. (1985a) investigated a bioelectrochemical system (BES) employing cyanobacteria, *Anabaena variabilis* as biocatalyst and 2-hydroxy-1, 4-naphthoquinone (HNQ) as artificial redox mediator operated under anaerobic conditions and confirmed current output from the cell. Later on, when *Synechococcus sp*. was used as the catalyst in PMFC using HNQ as a mediator, an increase in cell voltage upon illuminating with light was observed. When glucose was added to the anode solutions after a discharge of 13 h upon illumination, a current output of 230 µA was obtained. However, this resulted in low coulombic yield (30 %) from glucose due to its incomplete oxidation of all the carbon in the chain (Yagishita *et al*., 2007). A photosynthetic BES was also developed that utilizes *Synechococcus sp*. PCC7942 and bilirubin oxidase as anodic and cathodic biocatalysts, respectively in H-type cell. The device generated power (maximum 300 – 400 mW $m^{-2}$) without using any special chemical fuel. In another study, the photo-anodic current density increased linearly with increasing concentration of cyanobacterial cells in a quinonoid mediator bound MFC. However, the further increase in current was limited by light scattering and large thermodynamic losses in the electron transfer from the photosystem to the mediator (Tsujimura *et al*., 2001). The electron transfer efficiency of *Synechococcus* sp. PCC7942 into exogenous electron acceptors 1, 4-Benzoquinone (BQ) and 2, 6-dimethyl-1,

4-benzoquinone (DMBQ) from the photosynthetic system by entrapping the cells on the surface of the DMBQ- embedded carbon paste electrode was examined and a current density of 10 μA $cm^{-2}$ was achieved (Torimura *et al*., 2001). In order to boost up the photocurrent generation, two mediators, one soluble (ferricyanide) and one osmium-based polymeric mediator were used with *Lyptolyngbia* sp. (CYN82) immobilized on graphite electrodes that resulted in a maximum current density of 48.2 μA $cm^{-2}$ (Hasan *et al*., 2014).

In another study, phycobiliprotein was extracted from *Spirulina* sp. to composite with squaraine dye to sensitize nanocrystalline $TiO_2$ photoanode for building dye sensitized solar cell, and the photoelectric properties of the cell were also investigated (Wang *et al*., 2014a). The photo-electrochemistry of PS II *in vivo* was compared to PS II *in vitro* to probe into the electron transfer mechanism. The light-triggered release of intracellular redox species was responsible for electron relay in absence of the mediator. Improving the anode architecture to enable higher cell loading will support in enhancing the power improvement (Zhang *et al*., 2018).

### 1.4.3 DET-based PMFC

Cyanobacteria also generate current in photo BES via DET mechanism. From power generation point of view, DET from the bacteria to the electrode is more desirable than MET, as the overpotential losses could be minimized and design, as well as the operation of the electrochemical cell, could be simplified in the former case (Rosenbaum *et al*., 2010). A rudimentary design of electrochemical cell was reported where the cyanobacteria (*Nostoc* sp.) /carbon nanotubes (CNT) on the anode and *laccase*/CNT on the cathode as catalysts were used. The cell produced a maximum current density of 250 mA $m^{-2}$ and a peak power density of 35 mW $m^{-2}$ without any mediator. The electricity generation capacity of the cell was however, significantly improved upon addition of BQ as a redox mediator, with a current density of 2300 mA $m^{-2}$ and a power density of 100 mW $m^{-2}$ (Sekar *et al*., 2014). A mediator-less flexible direct photosynthetic/metabolic biofuel cell, using purple photosynthetic bacteria (*Rhodopesudomonas palustris*) as a fuel source, was also developed that generated a maximum power density of 5.26 μW $cm^{-2}$ with an OCP of 0.089 V (Moriuchi *et al*., 2009). A mediator-free and membrane-less PMFC was constructed where a thin biofilm of *Spirulina platensis* on the gilding gold mesh was used as the anode. The

PMFC produced a maximum power density of 10 mW $m^{-2}$ (Lin *et al*., 2013). The organism (*Spirulina platensis*) was further investigated in a membrane and mediator-less system, to assess the feasibility of using these PMFCs as instant-use and portable devices and observed that once the organism was attached to the anode, the voltage was instantly generated. When two PMFCs were connected, a maximum OCV of 450 mV and 310 mV were obtained for serial and parallel connections, respectively (Fu *et al*., 2010). Native cyanobacteria (*Nostoc* sp.) when illuminated with monochromatic light of different wavelengths, the power density of 100 mW $m^{-2}$ and 35 mW $m^{-2}$ were achieved with and without addition of redox mediator, respectively (Sekar *et al*., 2014). The strain *Synechocystis* sp. PCC 6803 was also reported to produce nanowires in response to the electron-acceptor limitation (Gorby *et al*., 2006).

Photo-electrochemical cells have also been developed by using isolated photosynthetic reaction centres (Trammell *et al*., 2004), thylakoids (Lam *et al*., 2006; Rasmussen *et al*., 2013) or PS II (Yehezkeli *et al*., 2012) and PS I (Faulkner *et al*., 2008) in the anode and PS I in the biocathode (Kothe et al., 2014). The constructs however suffer from drawbacks like labour-intensive procedures for isolation, complex immobilization strategies, expensive metals as immobilization supports and stability (Sekar *et al*., 2014). The key issues like stability, DET-based photocurrent production and electrode surface area needs to be addressed to make photo bioelectro-catalytic devices practical for real-life applications (Rasmussen and Minteer, 2014). Seven different configurations of PMFCs were explored stressing on the fact that much scale up might not be necessary to provide enough current to power environmental sensors if excreted organic matter from cyanobacteria or plants are used as feedstock in sediment-based MFCs (Rosenbaum *et al*., 2010).

### 1.4.4 Performance and application potential of PMFC

The performance of PMFC depends on various environmental factors such as light intensity, temperature, pH etc. The response of a PMFC with *Arthrospira maxima* as catalyst exhibited sensitive response towards temperature and light perturbations. Upon doubling light intensity from 10 $Wm^{-2}$ to 20 $Wm^{-2}$, the power densities were increased from 6.7 μW $m^{-2}$ to 9.9 μW $m^{-2}$ at 25 ° C and 11.2 μW $m^{-2}$ to 24.8 μW $m^{-2}$ at 35 ° C. *Arthrospira maxima* was susceptible to photo-inhibition with an increase in the light intensity (Inglesby *et al*., 2013). When the strain itself was used as a carbon substrate for growth of purple non-sulfur

bacterium *Rhodopseudomonas palustris* in MFC, a power generation of 10.4 mW $m^{-3}$ was achieved which was higher than the power density obtained by using glycerol and acetate substrates (Inglesby *et al*., 2012).

Synergistic interaction between photosynthetic microorganisms and heterotrophic bacteria (exist in places, such as lagoon, coastal area, and microbial mat) was exploited in a sediment-type self-sustained PMFC to generate electricity. Both the sediment and the air-cathode PMFCs showed an increased current in the dark (54 ± 2 µA) and a decreased current in the light. The accumulation of organic compounds led to the observed increase in current in the dark following the light reactions. The current was decreased following prolong illumination as dissolved oxygen evolved during photosynthesis, acted as the electron scavenger. There is feasibility to power remote sensors for monitoring environmental conditions by converting solar energy into electricity through the PMFC with an apt design strategy (He *et al*., 2009).

In a study, four categories of microbial biocatalysts (*S. cerevisiae, C. reinhardtii, G. sulphur reducens* and *Synechocystis* sp. PCC 6803) were studied for *in-silico* modeling of MFCs (Mao and Verwoerd, 2013). Biofilms of green algae (*D. tertiolecta and C. vulgaris*) and cyanobacteria (*Synechococcus* sp. WH 5701 and *Synechocystis* sp. PCC 6803) were developed on Indium tin oxide (ITO) coated polyethylene terephthalate in a Bio-photovoltaic (BPV) single chamber system that produced a power density of 10.3 mW $m^{-2}$. The four BPVs (each 110 $cm^2$) in series connection generated power sufficient to run a commercial digital clock (McCormick *et al*., 2011). A variety of different anodic conductive materials: stainless steel, ITO, carbon paper and glass coated with a conductive polymer polyaniline were used to develop multi-channel BPV device to conduct photosynthetic biofilm studies on filamentous cyanobacterium, *Pseudanabaena limnetica*. ITO offered the largest photo responses with power output 134 ± 18 pW $nmol^{-1}$ chl and 472 ± 80 pW $nmol^{-1}$ chl during the dark and light cycles respectively, whereas carbon paper showed the lowest power outputs of 22 ± 4 pW $nmol^{-1}$ chl and 41 ± 4 pW $nmol^{-1}$ chl under corresponding conditions (Bombelli *et al*., 2012).

MFCs can also serve a two-fold purpose of producing electrical power and degrading effluents from agricultural, industrial and municipal wastewater. The use of cyanobacteria as

photo bioelectrocatalysts to generate electrical power represents a simple and sustainable system lacking any significant negative impact on the environment (Rasmussen and Minteer, 2014). Production of electricity from *Synechocystis* PCC 6803 results in no net $CO_2$ production. Under high intensity of light, the optimum removal of $CO_2$ was 625 mmol $m^{-3}$ over 20 h (Madiraju *et al*., 2012). In another study, a low-cost oxy-hydrogen biofuel cell for generation of electricity using *Nostoc* as a source of hydrogen was investigated where 1 L free cell algal reactor was attached to the anode end of the fuel cell for hydrogen gas input. The cell generated about 300 mV of voltage and 100 mA of current (Dawar *et al*., 1998). The studies on the production of hydrogen using *Spirulina plantesis* and *Spirulina maxima* were also conducted for supply to a low-temperature alkaline fuel cell (Behera *et al*., 2007).

The self-sustainable, environment friendly phototrophic growth characteristic of cyanobacteria is an attractive feature for their potential applications in developing small scale MFCs as compared to other small scale energy sources (Wei *et al*., 2016). The condition may support the organism to sustain growth on small scale electrode surface without much intricacies being involved in supplying and adjusting the carbon substrates in MFC, with the tailored scope of developing miniaturized MFC design. Miniaturized designs will improve the efficiencies by not only overcoming the charge transport limitations but also reducing the cost. Remarkably high power density (> 100 mW $m^{-2}$) was achieved by using membrane-free, mediator free microfluidics-based BPV device using *Synechocystis* sp. PCC 6803 biofilm as catalyst fabricated by using soft lithography technique with a low melting alloy InBiSn. The approach is suggested to be applicable to any photosynthetic biofilm forming organism (Bombelli *et al*., 2015). In order to scale up the limited performance, an attempt was made by connecting multiple (nine) miniaturized bio-solar cells in an array with *Synechocystis* sp. as the anodic catalyst. A maximum power of 5.59 µW and voltage 1.28 V was retrieved under a 200 kΩ external resistor by exploiting both the photosynthetic and respiratory transport chains of electrons. At the application of 150 kΩ external resistor, polarity reversal was observed due to a disparity in the performance of the individual cell units (Wei *et al*., 2016). Micro solar cells constructed of Poly(methyl methacrylate) (PMMA) with a volume of 300 µl generated a maximum power density of 0.9 mW $m^{-2}$ with the help of face-up anode configuration (Lee and Choi, 2015). A 90-µl single

chambered microfluidic biological solar cell was designed that sustained power production of ~18.6 μW $cm^{-2}$ during the day and ~11.4 μW $cm^{-2}$ at night for 20 days. A polydimethylsiloxane (PDMS) gas permeable layer, a PMMA reservoir layer, air cathode (Pt as the catalyst) and a Nafion membrane were used in the micro device construction. The device architecture and incorporation of 3D porous Poly(3,4-ethylenedioxythiophene): polystyrene (PEDOT: PSS) polymeric anodic structure was attributed to the high power density and sustained operations. The findings indicate that anode surface chemistry and topography plays a crucial role in bacterial adhesion and electron transmission (Liu and Choi, 2017a). For powering point-of-care (POC) diagnostics, flexible, portable systems are required that may ignite a minimal burst of potential for a short period. This can be fulfilled by BPVs. The paper owing to its microporous structure, high water retention, thus avoiding accessory pumps can prove to be a desired support platform. A digitally zigzag pattern was printed onto the paper with cyanobacteria as anodic catalyst over CNT–based conductive ink that had the potential for powering a digital clock and a light emitting diode (LED) (Sawa *et al*., 2017). Hence, there is an enormous possibility to explore cyanobacteria for developing small scale MFC sensors for potential applications in many emerging areas as described above.

The maximum OCP reported for MFCs is 500 – 800 mV and that for light-dependent BES is 500 – 700 mV (McCormick *et al*., 2015). Bio-solar cells are MFCs that produce bioelectric power based on exploitation of the biocatalytic reactions of photosynthetic microorganisms such as, cyanobacteria or microalgae (Wei *et al*., 2016). A direct methanol fuel cell (single chambered), operated at an atmospheric pressure below 60 °C can deliver a power of 800 $Wm^{-2}$ (Qiao *et al*., 2010). Whereas, a maximum of 3.9 $Wm^{-2}$ power density was recorded for the MFC with *Geobacter* sp. (Yi *et al*., 2009), which was higher as compared to 100 mW $m^{-2}$, the maximum achieved with *Synechocystis* sp. in absence of a mediator (Bombelli *et al*., 2015). Liu and Choi compared the performance of *Shewanella oneidensis* and *Synechocystis* sp. PCC 6803 in a micro sized MFC and found that the current generation of the later was much lower. Non-formation of multiple layers of biofilm on the anode was suggested as the possible reason and advocated on formulating a specific strategy to promote anodic biofilm of photosynthetic microbes (Liu and Choi, 2017b). The electrocatalysis process in MFC comprises of multiple biocatalytic redox reactions. One of

the primary reasons recognized for low power output is the comparatively longer doubling time (~ 24 h) and biofilm development on anodic surface as compared to that of heterotrophic bacteria (*Shewanella* and *Geobacter* sp. doubling time ~ 40 min) (Liu and Choi, 2017a; Liu and Choi, 2017b). Additionally, the metal reducing model organisms *Geobacter* and *Shewanella* have the superior capability of electron flux owing to the presence of outer membrane cytochromes (OMC) (Sekar and Ramasamy, 2015) or conductive pili network within the biofilm (McCormick *et al*., 2015) as compared to photosynthetic microbes.

**Table 1.1:** A comparative account on the functional characteristics of some prominent PMFCs reported in the literature.

| Cyanobacteria strains | $P_{out}$ / $I_{out}$ / $V_{out}$ | Anode/Cathode | Electron transfer mechanism | Reference |
|---|---|---|---|---|
| ***Anabaena variabilis* M-2** | < 0.2 mA | NA | MET (HNQ) | Tanaka *et al*., (1985b) |
| ***Synechocystis sp.* PCC6714** | 0.2 mA | Carbon cloth/ potassium ferricyanide | MET (HNQ) | Yagishita *et al*., (1999) |
| ***Synechococcus sp.* PCC7942** | 0.3 – 0.4 $Wm^{-2}$ | carbon felt sheet /bilirubin oxidase | MET (DMBQ)/diaminodurene | Tsujimura *et al*., (2001) |
| ***Synechococcus sp.* PPC7942** | 10 µA $cm^{-2}$ | Carbon paste electrodes | MET (BQ/ DMBQ) | Torimura *et al*., (2001) |
| ***Synechococcus* sp.** | 0.5 mW $m^{-2}$ | Carbon cloth/ potassium ferricyanide | MET (2-hydroxy-1, 4-napththoquinone) | Yagishita *et al*., (2007) |
| ***Synechocystis* PCC-6803** | 1.3 mW $m^{-2}$ | Carbon cloth coated with polyaniline/ Carbon cloth with Pt catalyst | DET | Zou *et al*., (2009) |

| | | | | |
|---|---|---|---|---|
| **Cyanobacteria and heterotrophic bacteria** | 0.078 mA | Graphite felt/graphite plate | DET | He *et al.*, (2009) |
| ***Synechococcus* sp. WH5701** | 10.3 mW $m^{-2}$ | ITO-PET/ Carbon paper coated with Pt | DET | McCormick *et al.*, (2011) |
| ***A. maxima* used as carbon source for *R. palustris*** | 10.4 mW $m^{-3}$ | Stainless steel/ potassium ferricyanide | DET | Inglesby *et al.*, (2012) |
| ***Pseudanabaena limnetica*** | 472 ± 80 pW (nmol chl)$^{-1}$ | ITO-PET/ CP coated with Pt | DET | Bombelli *et al.*, (2012) |
| ***Synechocystis* sp. PCC6803** | 6.7 mW $m^{-3}$ | Carbon fiber | DET | Madiraju *et al.*, (2012) |
| ***Synechocystis* sp. PCC 6803 mutant with three terminal oxidases removed** | 64 ± 11 µA (nmol chl)$^{-1}$ $m^{-2}$ | ITO-PET/ carbon coated with Pt | MET (ferricyanide) | Bradley *et al.*, (2013) |
| ***Spirulina platensis*** | 10 mW $m^{-2}$ | Gold mesh/ graphite carbon cloth | DET | Lin *et al.*, (2013) |
| ***Arthrospira maxima*** | 24.8 µW $m^{-2}$ | (ITO)-coated glass /Pt coated CP | DET | Inglesby *et al.*, (2013) |
| ***Lyptolyngbia* sp. CYN82** | 48.2 µA $cm^{-2}$ | Graphite | MET (Osmium and ferricyanide) | Hasan *et al.*, (2014) |
| ***Nostoc sp.* ATCC 27893** | 100 mW $m^{-2}$ | CP/ laccase-CNT | MET (BQ) | Sekar *et al.*, (2014) |
| ***Synechocystis*** | 0.4 mA | Woven carbon | DET | Cereda *et* |

| | | | | |
|---|---|---|---|---|
| **sp. PCC6803** | $cm^{-2}$ | fabric | | *al*., (2014b) |
| ***Synechocystis* sp. PCC 6803** | 100 mW $m^{-2}$ | InSnBi alloy/Pt | DET | Bombelli *et al*., (2015) |
| ***Synechocystis* sp. PCC 6803** | 0.8 µW $cm^{-2}$ | carbon powder and 30 wt % PTFE solution onto the carbon cloth containing Pt as catalyst | DET | Wei *et al*., (2016) |
| ***Synechocystis* sp. PCC 6803 and *Shewanella oneidensis* MR-1** | ~ 7 µA $cm^{-2}$ | Gold coated on PMMA substrates | DET | Liu and Choi, (2017b) |
| ***Synechocystis* sp. PCC 6803** | 43.8 µW $cm^{-2}$ | Carbon cloth modified with PEDOT: PSS/ Carbon cloth coated with carbon powder in PTFE solution and 10 % Pt | DET | Liu and Choi, (2017c) |
| ***Synechocystis* sp. PCC 6803** | 4 mA $m^{-2}$ | Paper printed with CNT-based conductive ink | DET | Sawa *et al*., (2017) |

* NA- not available, HNQ–2-hydroxy-1, 4-naphthoquinone, DMBQ–6-dimethyl-1, 4-benzoquinone, BQ–4-benzoquinone, DET– Direct electron transfer

The prospect of PMFCs as a source of clean energy is quite high but the current efficiency is comparatively lower than the other MFCs. Notably, only ~ 50 % of the solar energy can be accessed by the cyanobacteria (Blankenship *et al*., 2011). With increased cell biomass at the electrode, mutual shading and light scattering lead to the saturation of the current (Rasmussen and Minteer, 2014). The light to current conversion efficiency achieved in BES with oxygenic photosynthetic organisms is 0.05 - 0.3 %. Conventional non-microbial

solar cells/photovoltaic cells are often compared to PMFCs or microbial bio-solar cells (McCormick *et al*., 2011). Difficulty in the recycling of the constituted materials of solar cells and inefficient operation during night makes the PMFCs as feasible alternate technology (ElMekawy *et al*., 2014). The lower efficiency of PMFC can be balanced by the self-sustaining, high shelf-life and inexpensive nature of the biocatalysts.

## 1.5 Electrode materials used in MFCs

The efficacy of a MFC device is governed by the electrode-microbe interaction which again depends on the configuration and physicochemical properties of electrode materials that decides the electron transfer kinetics and cell viability on the surface. The electrode can also act as the terminal electron acceptor even under aerobic condition (Fraiwan and Choi, 2014). Ideally, an electrode should be highly conductive, biocompatible, low cost as well as chemically and mechanically stable (Wei *et al*., 2011). The most common carbon/graphite-based electrodes like felt, cloth, paper, foils, rods, plates etc. have been used in the anode as these are porous, stable and provides a high surface area (Santoro *et al*., 2017). Carbon fiber offers high adhesion rate for bacterial colonization (Matsumoto *et al*., 2012). Modification of the anode by surface treatment/deposition can be adopted to alter the surface charge and hydrophobicity to influence the development of biofilm (Guo *et al*., 2013; Krishnaraj *et al*., 2013; Li *et al*., 2014; Zhou *et al*., 2011). Smooth surfaces and corrosive nature of the metals do not make them a popular choice for MFC electrode material. However, copper and stainless steel displayed potential as anode materials due to low specific resistivity and cost as well as the absence of oxidative dissolution potential within the studied anode potential range (Baudler *et al*., 2015). Micro and nano-structured electrodes in a miniaturized MFC established a linear relationship between the current production and effective surface area of the electrodes (Inoue *et al*., 2012). Though power output can be improved by connecting multiple electrodes in a single MFC or connecting individual MFCs together and operational mode conditions (fed-batch/continuous), care should be taken to avoid the parasitic current that may arise due to variation in the individual electromotive forces (emf) (Ren *et al*., 2014). Excellent conductivity, mechanical strength and physical properties led graphene and graphene-modified materials without and with conducting polymers (polyaniline and polypyrrole) were used as electrode materials in

different configurations that increased active sites for interaction (Yu *et al*., 2018, 2016). Various nanomaterials and their composites have been incorporated in electrode fabrication to improve the electroactive surface area. The close proximity of the nanostructured materials with the bacterial cell wall leads to credible improvement in the electron transfer kinetics permitting direct electron relay (Qiao *et al*., 2010).

However, in PMFC additional requirement in the cell system makes the task of choosing the appropriate electrode quite challenging. The device should permit perfusion of light to run the photosynthetic apparatus of the cells and promote rapid biofilm of the otherwise dispersed photosynthetic cells (Schneider *et al*., 2016b). The electrogenic activity of the photosynthetic organisms is an overflow mechanism which protects the plastoquinone pools from over-reduction at high light intensities (Pisciotta *et al*., 2011). A reasonable light-induced stress is obligatory to influence the maximum power output but without compromising the cell viability. Hence the PMFC anode and reactor design still remain a thrust area of research. ITO has been considered widely for applications in PMFCs as it is transparent (Bombelli *et al*., 2011; McCormick *et al*., 2011). Opaque materials such as carbon paper have higher electron transfer efficiency and biofilm development. A "face-up" configuration of the carbon paper electrode in a micro-sized cell ensured optimum light exposure and dense biofilm formation (Lee and Choi, 2015). The inclusion of CNTs onto carbon paper enabled DET for photocurrent generation (Sekar *et al*., 2014). However, clogging issues and high cost limits the use of CNTs (Zhou *et al*., 2011). The wiring of redox polymers like osmium to the graphite electrode enabled extracellular electron transfer to boost the photocurrent (Darus *et al*., 2017; Hasan *et al*., 2014). Highly porous and mechanical strength, carbon cloth treated with polytetrafluoroethylene (PTFE) and PEDOT: PSS have shown promise as it can provide a high surface area with increased affinity for biological components (Liu and Choi, 2017a). Porous ceramic anodes displayed enhanced biofilm formation leading to high power generation in absence of mediators (Schneider *et al*., 2016b).

Incorporation of nanomaterials can be used to increase the anodic surface area however, the biocompatible nature needs to be analyzed for promoting biofilm formation (Mustakeem, 2015; Rasmussen and Minteer, 2014). Efforts directed towards the study of

mechanism of microbial interactions with abiotic support, electron transfer mechanisms and optimization of the reactor design can further be effective in lowering the cost allowing a competitive edge over conventional technologies (ElMekawy *et al*., 2014). Understanding the molecular electron transport systems, augmentation of total light absorption, genetic tools can aid in enhancing the electron flux (McCormick *et al*., 2015). Material science contributes to solve the challenges of advanced electrode material design for enhancing the electrochemical communication between the biocatalysts and electrode (Pankratova and Gorton, 2017).

## 1.6 Applications of MFC for sensing alcohol

Microbial biosensors with different transduction principles have been explored among which, MFC sensors have received increasing attention over the last few years due to their fabrication simplicity, feasibility to operate in external environments in a self-sustained manner, low cost of operation and sensitive signal transduction mechanism (Dávila *et al*., 2011). However, most of these MFC-based biosensors are snagged with long response time as the response acquired from the interaction of the target species with the catalytic cells in the MFC is usually governed by the metabolism and growth of the organisms on the electrode surface (Abrevaya *et al*., 2015). Majority of the MFC sensors developed so far are targeted for monitoring onsite water quality by measuring biochemical oxygen demand (BOD). This BOD sensor was one of the first projected biosensor applications of MFC (ElMekawy *et al*., 2018). In this case, lack of sensitivity and long detection time limited their commercialization. MFCs could also detect low levels (1 mg $L^{-1}$) of heavy metals and pesticides but these studies did not document concentration-response relationship for these targets. Further, the enrichment of such devices including inoculation, immobilization, and stabilization took a long time with a reported time of minimum 10 min (Kim *et al*., 2007). A miniaturized MFC with *G. sulfurreducens* as a biocatalyst could detect formaldehyde (detection limit 0.1 %) within 3 min but the calibration and the upper limit of detection were not clearly recorded (Dávila *et al*., 2011). MFCs have also been proposed for the detection of microbial activity in the extra-terrestrial zone with a measurement time of 72 h (Abrevaya *et al*., 2015).

The importance of rapid, selective and portable alcohol detection systems is sharply increasing not only in traditional brewing, pharmaceutical, food, and clinical industries but also in rapidly growing alcohol-based fuel industries (Thungon *et al*., 2017). However, there is no suitable portable low-cost system for selective and quantitative detection of alcohol for commercial applications (Azevedo *et al*., 2005). Different alcohol sensors and biosensors reported so far have their own set of advantages (Thungon *et al*., 2017). The widely acknowledged conventional laboratory techniques are though sensitive and accurate, they require long time as well as expensive and elaborate instruments rendering them undesirable for on-site applications. Some biosensors were explored based on colorimetric and microfluidic techniques but are yet to be confirmed on their commercial potential (Churski *et al*., 2015; Paul, 2012). Different enzyme-based alcohol biosensors fabricated by using advance materials such as nanoparticles and conductive polymers following electrochemical principles, have been reported (Chinnadayyala *et al*., 2014; Gómez-Anquela *et al*., 2015). Although these enzyme-based biosensors offer high selectivity, they suffer from short shelf-life, as the stability of the enzymes is often deteriorated under high temperature and altered pH condition. Though efforts have been directed towards enzyme function and stability improvement, a majority of the reported sensors and biosensors including the enzyme-based biofuel cell devices (Das *et al*., 2014) failed to meet the demand while setting fast response time, selectivity, portability and simple instrumentation as the collective performance factors for detection of alcohol. The low selectivity and sensitivity of the microbial biosensors are often pacified by their considerable low analysis cost, long shelf-life and robust nature to endure environmental conditions as compared to that of other molecular biorecognition systems such as, enzymes and antibodies (Lim *et al*., 2015).

Alcohol biosensors using microorganism as biorecognition system have been also reported (Table 1.2). Low cost for mass production, ease of manipulation and longer shelf-life have made microbe-based sensors as emerging victors in the quest for new analytical systems (Su *et al*., 2011). The methylotrophic yeast *Pichia angusta* was explored for ethanol detection due to the presence of high content of intracellular alcohol oxidase (Voronova *et al*., 2008).

**Table 1.2:** Some of the key performance factors documented by using microbial biosensors for alcohol detection.

| Microorganism as bio-receptor | Transducer | Response time | LOD | Linear range | Reference |
|---|---|---|---|---|---|
| ***Hansenula polymorpha* and *Pichia pinus*** | Potentiometric (Field effect transistor) | 1500 s | 0.5 mM | 5 – 100 mM | Korpan *et al*., (1993) |
| ***Acetobacteraceti*** | Amperometric | 120 s | | 0 – 1 mM | Ikeda *et al*., (1997) |
| ***Aspergillus niger*** | Amperometric | | 35.3 ppm | 1 – 32 ppm | Subrahmanyam *et al*., (2001) |
| ***Glucono bacteroxydans* and *Pichia methanolica*** | Amperometric | | 0.05 mM | 0.05 – 10 mM | Reshetilov *et al*., (2001) |
| ***Glucono bacteroxydans*** | Amperometric | 12.6 s | 0.85 µM | 2 – 270 µM | Tkac *et al*., (2003) |
| ***Saccharomyces ellipsoideus*** | Potentiometric | 420 s | | 0.05 – 5 mM | Rotariu and Bala, (2003) |
| **Recombinant *E.coli*** | Optical (Bioluminescence) | | | 5 – 200 µM 1-decanol and n-decanal | Minak-Bernero *et al*., (2004) |
| ***Candida tropicalis*** | Amperometric | 120 s | 0.5 mM | 0.5 – 7.5 mM | Akyilmaz and Dinckaya, (2005) |
| ***Saccharomyces ellipsoideus*** | Amperometric | 300 s | 6 µM | 0.01 – 0.8 mM | Rotariu *et al*., (2004) |
| ***Pichia angusta*** | Amperometric | – | 0.012 mM | – | Voronova *et al*., (2008a) |
| ***Methylobacterium organophilium*** | Amperometric | 1200 s | 0.27 mg/L | 1.6 – 4800 mg/L | Zhao *et al*., (2009a) |
| ***Glucono bacteroxydans*** | Amperometric | 180 s | 3.3 µM | 10 µM – 1.5 mM | Valach *et al*., (2009) |
| ***Methylobacterium organophilium*** | Amperometric | < 60 s | 0.047 mM | 0.050 – 2.5 mM | Wen *et al*., (2014a) |

The cell-electrode interaction or electrical communication between these two entities is important for channelizing electrical response signal through the electrode in electrochemical microbial biosensor or biofuel cells. Immobilization procedures were adopted to meet the requirement for generating a sensitive response towards alcohol (Wen *et al*., 2014). However, a majority of these electrochemical microbial sensors are based on microbial respiration and is often limited by selectivity. To overcome these limitations, an alternative strategy with a suitable detection principle is highly encouraged. The integration of both the biocatalyst and transduction principle being available in the same system, MFC sensors offer ease of construction and operation as compared to other microbial biosensors. The surge in the number of granted US patents on MFC devices is another indication of these versatile devices for sensor applications (Yang *et al*., 2011). Adaptation of micro MFC systems, redox mediators and a technique to allow fast colonization of the electrode material are suggested as feasible routes to overcome stability, reproducibility and start-up time of MFC biosensors (Abrevaya *et al*., 2015).

# Chapter II

## Studies on support materials for growth of cyanobacterial biofilm

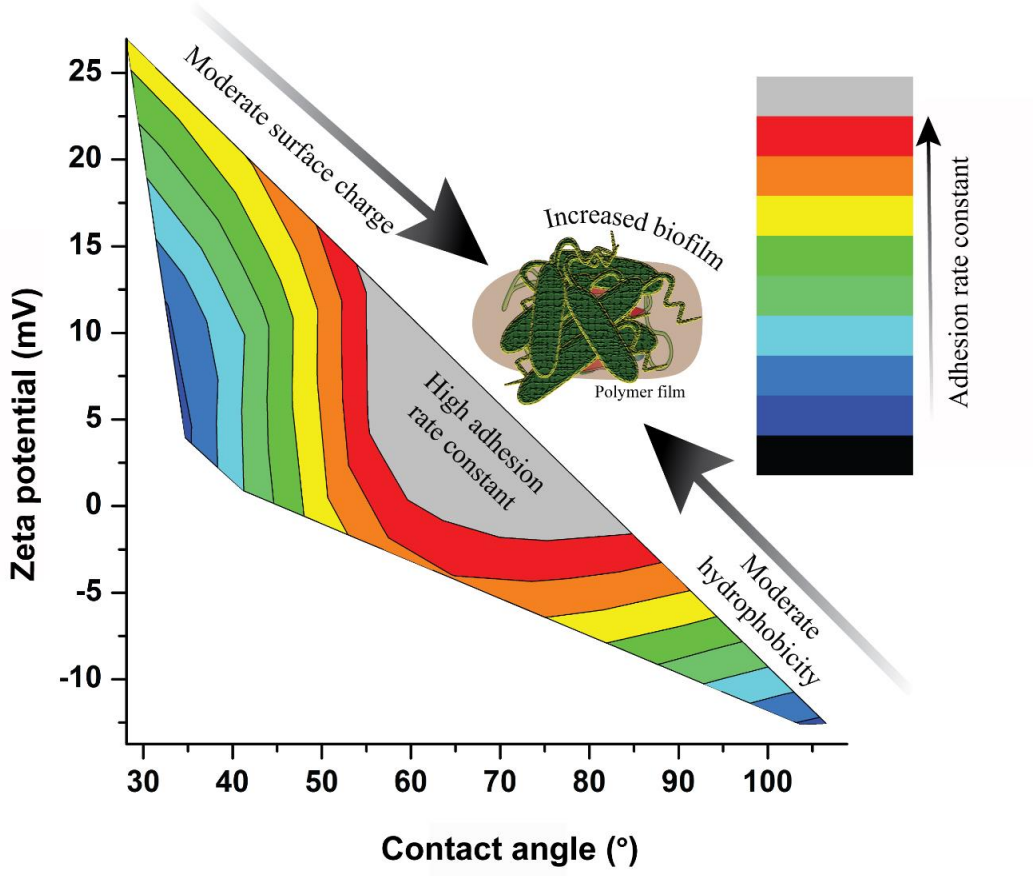


*Graphical abstract on physico-chemical factors influencing biofilm growth*

# Chapter II

# Studies on Support Materials for Growth of Cyanobacterial Biofilm

## 2.1 Overview

The microbial biofilm on anode usually promotes current density in the microbial fuel cells (Ozkan and Berberoglu, 2013a; Mohan *et al*., 2008). However, the growth of the biofilm is usually a slow process and depends upon the type of support being used (Matsumoto *et al*., 2012). The knowledge on the support materials for cyanobacterial biofilm growth is yet to be adequately elucidated (Ursell *et al*., 2013). Herein, we explored the biopolymers- silk and chitosan for developing bacterial biofilm rapidly on the solid surface. The study was inspired by the fact that these biomaterials could induce rapid growth of mammalian cells (Croisier and Jérôme, 2013; Rockwood *et al*., 2011). For a comparative account, we also included some widely available synthetic polymers (cationic- polyaniline, osmium and anionic- Nafion) in the list to study the induction and propagation of biofilm of the cyanobacterial strain, *Synechococcus* sp. Results imply that silk fibroin and chitosan blended silk thin films are better biofilm-inducing materials as reflected from the biofilm thickness and propagation. High biofilm inducing activity of these biomaterials was also demonstrated for the strains, *Escherichia coli* and *Lactobacillus plantarum*. Through this work, an effort was also made to understand the physico-chemical factors responsible for the rapid growth of the cyanobacterial biofilm on the thin films of the tested biomaterials.

## 2.2 Experimental approaches

### 2.2.1 Materials

Chitosan from crab's shells ($M_w$ ~ 150000, degree of deacetylation > 75 %), polyaniline, osmium tetraoxide on poly (4-vinylpyridine) (osmium), Nafion, Crystal violet solution (CVS) and Gram's Iodine solution were procured from Sigma Aldrich (USA). Chitosan was dissolved in 0.1 M acetic acid by ultra-sonication at 15 Hz for 1 h. Osmium

and polyaniline were dissolved in ethyl benzene and methanol, respectively by ultra-sonication at 15 Hz for 45 min each. Biofilm stain,

FilmTracer™ FM® 1-43 was from Invitrogen (USA). Nanopure water (18.2 MΩ) (Milipore Co.) and 0.1 M potassium phosphate buffer saline (PBS) of pH 7.5 were used throughout the experiment. Luria-Bertani (LB) and de Man, Rogosa and Sharpe (MRS) broth were obtained from HiMedia (India). All other reagents were of analytical grade. Graphite rod (0.318 cm dia x 30.48 cm length) was purchased from GraphiteStore.com. Peptides GAGAGAAGAAGAAGAAGAAG (GApep) > 90 % purity and GVGVGVVGVVGVVGVVGVVG (GVpep) > 80 % purity were synthesized by GenScript (USA).

### 2.2.2 Silk fibroin extraction

Cocoons of *Bombyx mori* used for the extraction of silk fibroin (silk) (Rockwood *et al*., 2011) were cut and boiled for 30 min, in 0.02 M of sodium carbonate to remove sericin. After a thorough rinse with water, the fibroin was removed, squeezed and placed on aluminium foil to dry in the laminar hood overnight. 9.3 M of LiBr was used for dissolving the silk for 4 h at 60 ° C. The amber coloured silk solution was dialyzed against water until $AgNO_3$ test detects no bromide ion in the silk solution. The final solution with the silk concentration of 5 - 6 % (w/v) was stored at 4 °C until use.

### 2.2.3 Microorganisms and cultivation

The cyanobacterial strain *Synechococcus* sp. BDU 140432 (*Synechococcus* sp.) used in this thesis work was procured from National Facility for Marine Cyanobacteria at Bharathidasan University (India). *Escherichia coli* DH5α (*E. coli*), *Lactobacillus plantarum* MTCC 1746 (*L. plantarum*) were procured from MTCC (India). The growth of *Synechococcus* sp. (2500 lux, 28 ± 2 °C, in light-dark cycles of 16: 8 h) was maintained in artificial seawater (ASN III) medium (Raghukumar *et al*., 2001) and was monitored at optical density (OD) $OD_{750}$. *E. coli* was routinely maintained in LB medium whereas, *L. plantarum* was maintained in MRS medium at 37 °C in dark, without shaking and their growths were monitored at $OD_{600}$.

### 2.2.4 Analysis of biofilm growth

The biofilm growth on polymer thin films was studied on polystyrene 24-well (5 mL capacity) plates (NEST, USA) as support and analyzed by: (1) Biofilm and (2) cell density assays. 20 µL of the polymers (3 mg $mL^{-1}$) were drop cast coated on 24-well plates, each covering 5 ± 3 mm dia (as shown in Figure 2.1). The drops in plates were dried properly in a laminar hood for 5 h, prior to their use as support films. The as-prepared films had negligible dissolution effect under the conditions used in this study. For composite film study, 3 mg $mL^{-1}$ (0.3 % w/v) of each silk and chitosan were mixed in varying ratio of 95:5, 80:20, and 60:40 by vortex mixing for 1 min and were used for the coating. Three mg $mL^{-1}$ of each of the peptides GApep and GVpep in aqueous solutions were used for the coating on the support materials.

The bacterial strains were cultivated (O'Toole, 2011) with some modifications for generating the biofilm. One mL of sterile media was added into the wells of 24-well plates previously coated with the test polymers as described above and then inoculated with 200 µL of cell suspension ($OD_{750/600}$ ~ 0.29 – 0.32). After incubation for 72 h, the biofilm formed in the wells were rinsed thrice with water to remove planktonic cells and media components and then used for biofilm and cell density assays. The readings were taken in a multiwell plate reader (Infinite M200, TECAN, Switzerland).

*(a) Biofilm assay*:

Biofilm formation was probed by using biofilm stain (FilmTracer™ FM® 1-43) as per the technical specification of Invitrogen. The biofilm in the wells was treated with the staining solutions (1 µg $mL^{-1}$ in aqueous solutions) and then incubated for 30 min at room temperature (RT) under dark. Afterward, the excess stain was removed gently with water and the fluorescence intensity (counts) of the wells was recorded immediately at $\lambda_{580\ nm}$ emission (excitation at $\lambda_{472\ nm}$).

*(b) Cell density assay:*

The assay was performed (O'Toole, 2011) with slight modification. 1.2 mL of 0.1 % CVS in water was added to each of the wells and incubated for 15 min at RT. The plates

were rinsed thrice with water by submerging and shaking in water and then kept in the laminar hood for 5 h. Once dried, 1.2 mL of 30 % acetic acid in water was added and incubated at RT for 15 min to solubilize the CVS. 200 µL of the solubilized CVS was transferred to a new multiwell plate and absorbance was recorded at $OD_{590}$ using 30 % acetic acid in water as the blank. Adhesion unit (Au) offers semi-quantitative information on the surface affinity and the extent of biofilm formation of the bacterial strains on the test polymer films as compared to control (with no coating). It was calculated after 72 h till which microbial adhesion took place, by normalizing the optical density (OD) of the solubilized CVS by the corresponding grown cell density ($OD_{750/600}$) (Nucleo *et al*., 2009). Hence concentration change derived from cell growth will be less significant. For growth studies on polymeric supports, the 24-well plates coated and inoculated as above were used, and the growth was monitored at $OD_{750}$ for *Synechococcus* sp. and at $OD_{600}$ for *E. coli* and *L. plantarum*. Control without polymer coatings was invariably run at all stages using the same growth media and conditions to nullify any influence of media ingredients and cell growth on the biofilm formation.

### 2.2.5 Microscopic studies on biofilm of different polymers

A total 50 µL of polymers in aqueous solutions (3 mg $mL^{-1}$) were drop cast on glass slides (75 mm × 25 mm) each covering 15 ± 2 mm dia were dried in the laminar hood for 5 h. The thickness (*D*) of the polymer film so formed was measured by a litematic thickness gauge (Mitutoyo, VL-50; Measuring pressure, 0.15 N; Japan). For morphological studies of the biofilms, the polymer coated glass slides were immersed vertically in actively growing *Synechococcus* sp. culture medium ($OD_{750}$ ~ 0.8 – 0.9). The glass slides, taken out at different time intervals were rinsed with water to remove non-adhered bacterial cells. The stable biofilm retained on these surfaces was then analyzed by microscopic techniques.

*(a) Deconvolution microscopy analyses*

200 µL of prepared biofilm stain in aqueous solution (1 µg $mL^{-1}$) (Kost *et al*., 2005) was added to seven days grown biofilm on glass slides. The samples were incubated for 30 min at RT under dark. The excess stain was removed gently with water and observed immediately under deconvolution microscopy (Delta Vision Elite, GE Healthcare Life

Sciences) at $\lambda_{580\ nm}$ (excitation at $\lambda_{472\ nm}$). The thickness of the biofilm was analyzed using DECON3D software.

*(b) Fluorescence measurements*

The images were recorded after excitation through blue light and observed under green light at 20X resolution under a fluorescence microscope (Eclipse Ti-U, Nikon, USA) exploring the autofluorescence property of *Synechococcus* sp. The area coverage with time was calculated using the software NIS, Elements AR provided with the instrument.

*(c) Field emission scanning electron microscope (FESEM) based analysis*

The graphite rods were cleaned ultra-sonically using acetone, 70 % methanol and water for 15 min each, consecutively. After proper drying, these were coated with the test polymers, dried in the laminar hood for 5 h and were then immersed vertically in actively growing *Synechococcus* sp. culture medium ($OD_{750}$ ~ 0.8 – 0.9). The rods were taken out after seven days, a 3 mm piece was cut and rinsed with PBS and then fixed in 2.5 % aqueous glutaraldehyde (v/v) at 4 ° C for 8 h. The rods were then withdrawn, washed with PBS and subsequently dehydrated in a graded series of ethanol concentration (50 – 100 %) for 10 min each and then dried in vacuum desiccator overnight. The specimens were mounted on aluminium stubs with carbon tape, sputtered with gold and then examined under a FESEM (Zeiss, Model Sigma) at 2 – 3 kV.

### 2.2.6 Circular dichroism (CD) analyses

A total of 0.2 mg $mL^{-1}$ of the samples was analyzed by CD instrument (Jasco J-815, Japan) by purging with $N_2$ gas at a flow rate of 3 – 5 mL $min^{-1}$. The spectra were recorded in the far UV region ($\lambda_{240\ -\ 190\ nm}$) at a scan rate of 100 nm $min^{-1}$, a time constant of 1s, 1 nm intervals, in 0.1 cm path length suprasil quartz cuvette, and an average of 3 - 4 scans at 18 °C. A blank solution as measured under the similar experimental conditions was deducted from the data and the resultant spectra were smoothed by Savitsky-Golay filter using Jasco spectral analysis. The content of secondary structure was estimated with the help of the estimation program supplied with the instrument (Jasco SSE-protein secondary structure) (Yang *et al*., 1986).

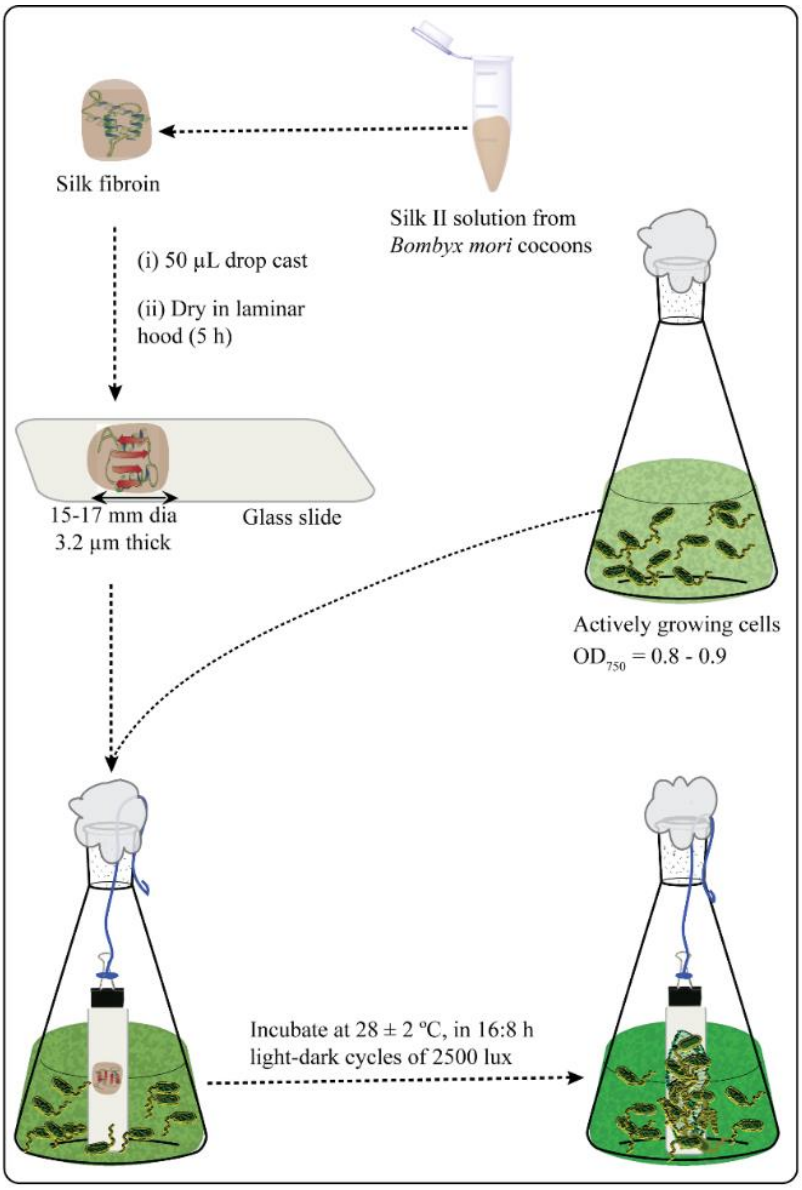


**Figure 2.1:** Steps showing the preparation of *Synechococcus* sp. biofilm on the solid surface (graphite and glass) using silk thin film as the inducer.

### 2.2.7 Zeta (ζ) potential measurements

Bacterial suspension harvested at late exponential phase by 8000g for 5 min at 4 °C, was washed thrice and then diluted in PBS, pH 7.5 to $OD_{600}$ of 0.32 - 0.42. The cell culture, equilibrated without settling the cells for 3 h was taken to measure the ζ potential in a folded capillary cell. For ζ potential measurements of the polymers, 0.2 mg $mL^{-1}$ of each polymer in

PBS at their physiological pH were used. The mobility of the bacteria/particles under the applied voltage was converted to apparent ζ potentials using the Helmholtz–Smoluchowski equation by Malvern Zetasizer (ZEN3690). The ζ potential correlates well with the surface charge of the cells (Zhang *et al*., 2014) and polymers (Chu *et al*., 2009). ζ potential was calculated as the average of three replicates. The electrostatic repulsion, $V_R$ can be related to the surface potential (ζ) of cells and polymers and the Debye length (k) via the following equation (Chu *et al*., 2009):

$$V_R = \zeta_1 \zeta_2 e^{-kd} \quad \text{.....(2.1)}$$

Where $\zeta_1$ and $\zeta_2$ are the surface potential of the cell surface and polymers used in this study and d is taken as the minimum separation distance $1.57 \times 10^{-10}$ m between the cell and the surface (Ozkan and Berberoglu, 2013b). Here kd is assumed to be less than 1.

### 2.2.8 Evaluation of hydrophobicity index (HI) of bacterial cells

The surface hydrophobicity of the microbial cells was measured as reported (Serebryakova *et al*., 2002). The cells suspended in 0.85 % NaCl, were set to an $OD_{540}$ ($E_o$) of 0.45 – 0.5. The cell suspension was then mixed with chloroform at a ratio of 5:1 (v/v) in a 10 mm dia tube for 1 min using vortex mixture followed by a 5 min standing to allow phase separation. The upper aqueous phase with cells was transferred into a cuvette to measure the decrease in $OD_{540}$ (E) of the cell suspension due to the partition of cells between the aqueous (hydrophilic) and chloroform (hydrophobic) phases. HI was calculated as:

$$HI = 100 - \left[\frac{(E \times 100)}{E_o}\right] \quad \text{.....(2.2)}$$

### 2.2.9 Calculation of interaction energy profile

The relative strength of the van der Waals interaction between a sphere and plane, and the surface separation dependence of this interaction is given by (Notley *et al*., 2004)

$$E = -A/6D^2 \quad \text{.....(2.3)}$$

Where E is the interaction energy (*kT*), D is the separation distance (nm), and *A* is the Hamaker constant (J). The Hamaker constant for two materials separated by water can be

calculated as a function of the constants of the individual materials in their condensed state. For a system where a bacterium is interacting with a solid surface in water, the Hamaker constant ($A_{bws}$) can be defined in the following way (Matsumoto *et al*., 2012)

$$A_{\mathrm{bws}} = (A_{\mathrm{bb}}^{1/2} - A_{\mathrm{ww}}^{1/2})\,(A_{\mathrm{ss}}^{1/2} - A_{\mathrm{ww}}^{1/2}) \quad \text{.....(2.4)}$$

Where $A_{ij}$ is the Hamaker constant between materials *i* and *j* (*j* = b, w, s) and subscripts b, w, and s represent bacteria, water and the solid surface, respectively.

### 2.2.10 Contact angle measurements

Uniform drops (4 ± 0.5 µL) of water (18.2 MΩ) were carefully dropped onto the polymer thin films coated on glass slides and on dried bacterial lawns (van der Mei *et al*., 2003) by sessile drop method, using a micrometer syringe assembled with the instrument. As a measurement of surface hydrophobicity (Farris *et al*., 2011), water contact angles, ($\theta_{w,}$°) were measured at RT after 120 s, using a Krüss Drop Shape Analyzer – DSA25 (Germany) equipped with a recording system and a camera at three different spots on the same sample and averaged. The relative hydrophobicity ($H_{o/w}$) between microbes and support surface can be written as (Liu *et al*., 2004):

$$H_{o/w} = \frac{overall\ hydrophobicity\ of\ the\ cell\ and\ support}{overall\ hydrophilicity\ of\ the\ cell\ and\ support}$$

$$H_{o/w} = \frac{H_m + H_p}{(1-H_m) + (1-H_p)} \quad \text{.....(2.5)}$$

in which $H_m$ and $H_p$ are the relative hydrophobicity (%) of microbes and polymeric support, respectively; which are predicted in terms of their respective $\theta_w$ (converted to %); the terms (1 – $H_m$) and (1 – $H_p$) represent respective relative hydrophilicity of microbial cell and polymer support.

### 2.2.11 Calculation of adhesion rate constant and activation Gibbs energy of adhesion

Cover slips (18 × 18 mm) sterilized as in (Azeredo *et al*., 1999) were dipped in polymers (3 mg $mL^{-1}$) and dried in the laminar hood for 5 h. The bacterial suspension was

harvested at late exponential phase by 8000g for 5 min at 4 °C and diluted in PBS to an $OD_{750/600}$ of 0.32 – 0.42 which was noted as $C_0$.

*(a) Adhesion rate constant*

The prepared cover slips were inserted in 6 mL bacterial suspensions in a 10 mL beaker and gently agitated at 100 rpm. The microbial concentration in the suspension decreased following first-order model (till contact time, $t \leq 72$ h). The adhesion rate constant of the microbes to each polymeric support was calculated (assuming no transport limitations) during this time from the decrease in OD ($OD_{750}$ for *Synechococcus* sp. and $OD_{600}$ for other bacteria) of each cell suspension ($C_t$). Experiments were repeated with renewed cell suspension. The adhesion rate constant, $a$ (m $s^{-1}$) is defined as (Matsumoto *et al*., 2012)

$$a = -\left(\frac{V}{A}\right)\left(\frac{1}{t}\right)\ln\left(\frac{C_t}{C_0}\right) \quad \text{.....(2.6)}$$

Where $V$ and $A$ are the volumes of the cell suspension and the area of the polymer coated cover slip.

*(b) Gibbs energy of adhesion*

The effective radii, $R_e$ (m) of the microbes were calculated from the average cell width ($w$) and length ($1$) determined from FESEM images.

$$R_e = 0.5\,(wl)^{1/2} \quad \text{.....(2.7)}$$

The diffusion coefficient, $D_e$ ($m^2/s$) was calculated using Stokes-Einstein equation *(Rijnaarts et al*., 1993)

$$D_e = \frac{kT}{6\pi\eta Re} \quad \text{.....(2.8)}$$

Where $T$ is the absolute temperature, $k$ is the Boltzmann constant and η is the dynamic viscosity. The prepared cover slips were dipped in 6 mL bacterial suspensions in a 10 mL beaker. The decrease in $OD_{700/600}$ of each cell suspension was recorded ($C_b$) after 12 h incubation under static conditions. Activation Gibbs energy of adhesion, $\Delta G^{\neq}$ ($kT$) is related to the adhesion efficiency, i.e. the probability for a (bacterial) particle to adhere upon arrival

at a substratum surface. This transport is controlled by diffusion in absence of convection. For the given incubation time, $\Delta G^{\neq}$ can be estimated from the adhered cells ($\tau = c_0 - c_b$) (Rijnaarts *et al*., 1999)

$$\frac{\Delta G}{kT} = \ln\left[\frac{2C_0\left(\frac{tD_e}{\pi}\right)^{\frac{1}{2}}}{\tau}\right] \quad \text{.....(2.9)}$$

in which *k*, *T*, $C_0$ and $D_e$ are as described above.

### 2.2.12 Statistical analysis and graphics program:

All the experiments and assays were carried out in triplicate, mean centred and scaled-up to variance using Origin 8.0 software. Statistical analysis was performed using analysis of variance (ANOVA). Adobe Illustrator CS6 was used for graphic artwork.

## 2.3 Results and discussion

### 2.3.1 Biofilm growth on polymer films

*Synechococcus* sp. is a gram-negative bacterium of marine origin. We investigated this cyanobacterium for its ability to form biofilm on different polymer thin films coated on solid support materials (glass or polystyrene). Polymer film materials from natural origins- silk and chitosan, as well as synthetic origins -osmium, polyaniline, and Nafion were examined for their biofilm inducing capabilities. A preliminary study was also extended to *E. coli* (gram-negative) and *L. plantarum,* (gram-positive) to understand the efficacy of the polymer materials in promoting biofilm of these widely used non-photosynthetic bacteria. The biofilm formation was examined by a combination of two methods: one involves the measurement of fluorescence intensity generated after staining the film with a specific dye and the other method measures the cells density in the biofilm as mentioned in the methodology section.

On the blank polystyrene support (control), the magnitude of *Synechococcus* sp. biofilm and cell density accumulated in it, following 72 h incubation were 154 ± 15 (counts) and 0.24 ± 0.01 ($OD_{590}$), respectively. As compared to the control, the increase in biofilm formation (%) of *Synechococcus* sp. in silk, chitosan, polyaniline, osmium films, and Nafion

were 27.73 ± 4.21 (31.16 ± 2.48), 21.55 ± 5.61 (23.74 ± 1.69), 5.35 ± 3.43 (8.96 ± 3.11), 6.70 ± 1.41 (6.55 ± 2.750), and nil, respectively with the corresponding increase in cell density (%) values are shown in the parentheses (Figure 2.2 A-B). Thus the trends of biofilm formation on the tested polymer films revealed from the biofilm (fluorescence) and cell density assays (Figure 2.2 A-B) are comparable with a minor deviation observed for polyaniline film on biofilm fluorescence intensity. Unlike the trend observed with cell density assay, the fluorescence intensity with polyaniline film was less than that of osmium film. This discrepancy has been attributed to the marginal fluorescence quenching property of polyaniline (Serban *et al*., 2012). Interestingly, this trend of formation of *Synechococcus* sp. biofilm and cell density on the tested polymer films did not significantly vary for *E. coli* and *L. plantarum*. The *Synechococcus* sp. cell adhesion unit to coated film was- silk: 0.48 ± 0.16, chitosan: 0.39 ± 0.07, polyaniline: 0.30 ± 0.06, osmium: 0.25 ± 0.03, Nafion: 0.19 ± 0.02, and control: 0.18 ± 0.10. As evident from the results, the formation of biofilm and cell density was highest on silk followed by chitosan films ($p < 0.05$).

The formation of *Synechococcus* sp. biofilm was investigated under deconvolution microscope to understand the biofilm thickness morphology using the better biofilm inducing materials, silk ($D = 3.2 \pm 0.2$ μm) and chitosan ($D = 2.8 \pm 0.3$ μm) films. Notably, deconvolution microscopy can provide image of specimens at very low light levels enabling multiple-focal-plane imaging of light-sensitive living specimens over long time periods, hence proposed to be suitable for analyzing cyanobacteria. The entire series of optical sections were analyzed to create a 3D montage without bleaching the dye and compromising in the bacterial cell viability (McNally *et al*., 1999). The biofilm thickness of *Synechococcus* sp. on silk was found to be the highest (16.20 μm) followed by chitosan (11.35 μm) and control (blank glass surface) (2.3 μm) (Figure 2.3 a-c).

The biofilm thickness of *E. coli* and *L. Plantarum* on silk film obtained after a similar incubation period of seven days were 8.3 μm and 5.6 μm, respectively (Figure 2.4 A-B, Video E1 a-c for e-version of this thesis). The rate of propagation of *Synechococcus* sp. biofilm on silk and chitosan films were $13 \times 10^3$ μm$^2$ day$^{-1}$ and $9 \times 10^3$ μm$^2$ day$^{-1}$, respectively, as discerned from the real time fluorescence images and its derived graph (Figure 2.5 A-B). *Synechococcus* sp. could also produce a high level of biofilm on graphite

substrate with silk and chitosan as coating films as revealed in the FESEM images (Figure 2.6 a-c). Bacterial cells with EPS formation on chitosan and silk films are clearly visible in the image. The extent of the cyanobacterial colonization on silk film coated graphite was higher than the chitosan film coated one.

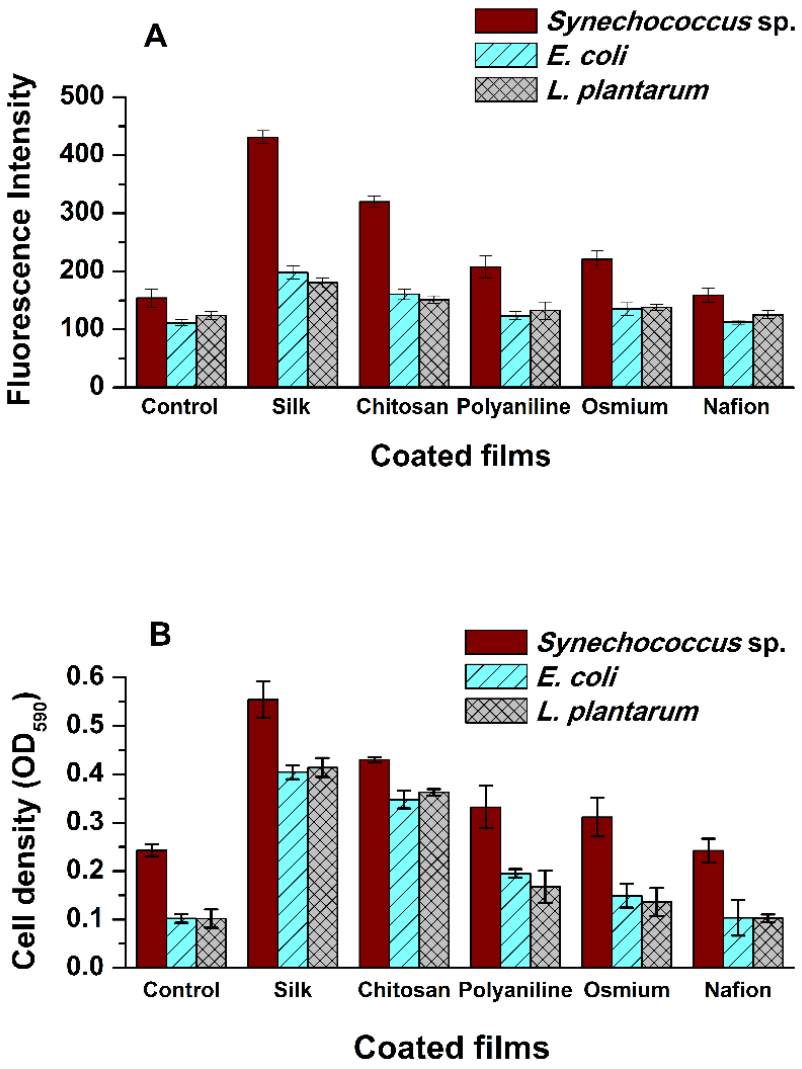


**Figure 2.2:** Formation of (A) biofilm and (B) cell density by the tested bacteria on control and various polymer films.

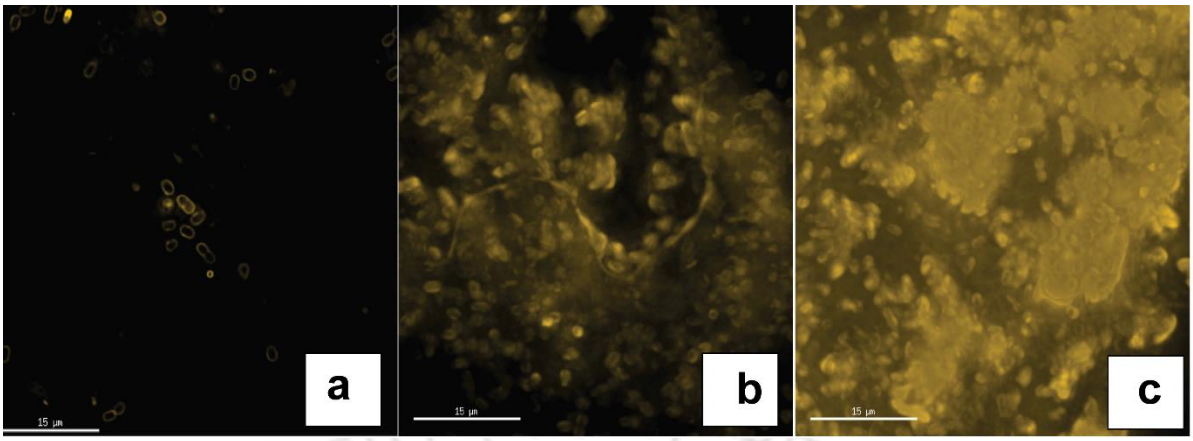


**Figure 2.3:** Deconvolution microscopy analyses of biofilm of *Synechococcus* sp. grown for seven days on (a) control, (b) chitosan and (c) silk films.

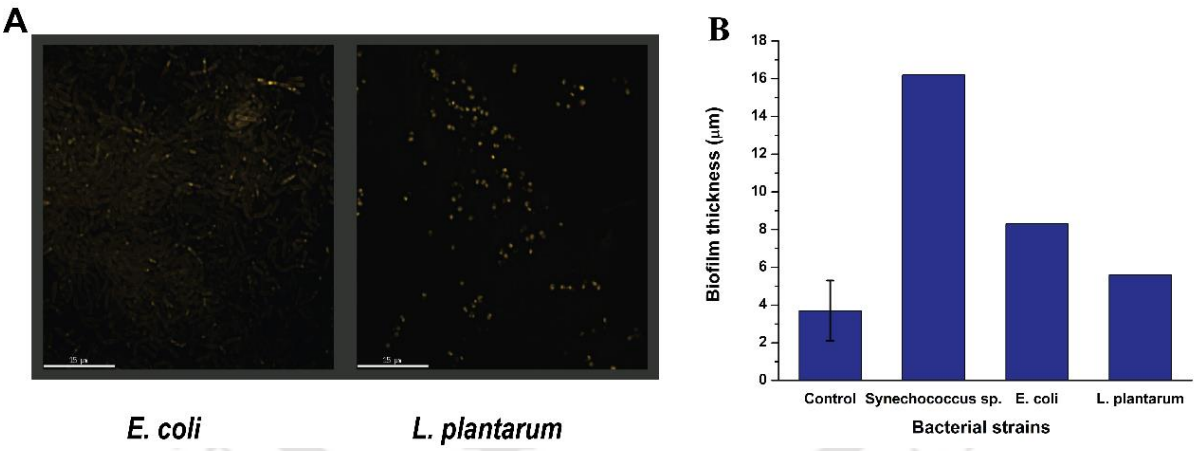


**Figure 2.4:** (A) Biofilm formation on silk by *E. coli* and *L. plantarum* analyzed by deconvolution microscopy. (B) Biofilm thickness of the bacterial strains grown on silk film calculated through the DECON3D software with the standard deviation of control representing the biofilm thickness of all the bacterial strains on glass slide without any coating.

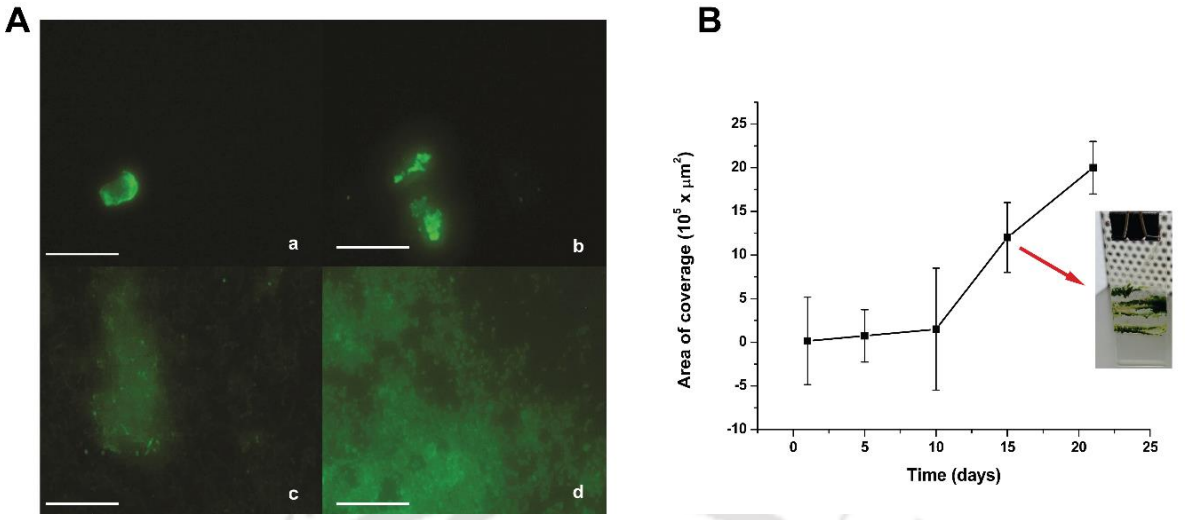


**Figure 2.5:** (A) Fluorescent microscope analyses (observed at 20X) of *Synechococcus* sp. on silk film with time (a) 1 day (b) 5 days (c) 10 days (d) 21 days. The inset bars represent 300 µm. (B) The area of coverage on silk film by *Synechococcus* sp. calculated from the captured fluorescent images and the software mentioned. The inset figure shows *Synechococcus* biofilm on silk film.

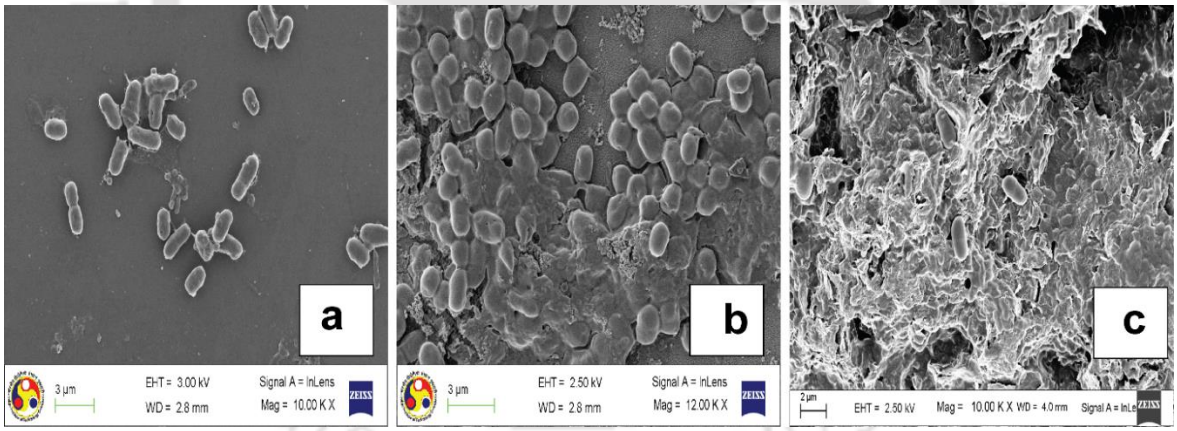


**Figure 2.6:** FESEM images of biofilm of S*ynechococcus* sp. on (a) control, (b) chitosan film and (c) silk film.

There was no colonization of bacterial strains on the blank graphite substrate. Notably, graphite is negatively charged and hence, it's surface charges likely to counteract the adherence of negatively charged bacterial cells (ζ potential value in Table 2.1). The formation of *Synechococcus* sp. biofilm on graphite surface is encouraging as this

photosynthetic microorganism has been increasingly used as the anodic catalyst with various graphite materials as base electrodes in a fuel cell setup due to its many benefits (Hasan *et al*., 2014).

The film of chitosan at ~ 0.3 % (w/v) ($D$ = 2.8 ± 0.3 µm) on the surface drastically increases the cell density and biofilm formation (Figure 2.7 A-B). The biofilm growth, however, was declined drastically beyond this chitosan concentration. When a blend of silk and chitosan at a ratio of 3:2 was used, the cell density of *Synechococcus* sp. on the composite film was increased by 12.13 ± 2.02 % and 26.58 ± 3.95 % than the corresponding pure silk and chitosan films (Figure 2.8 A). Interestingly, in the blended condition, the secondary structure of silk fibroin was marginally altered leading to an increase in the random coil by ~ 8.20 % (Figure 2.8 B). The exact role of the changed structural content in the silk fibroin on the adhesion of bacterial cell and biofilm formation is not known.

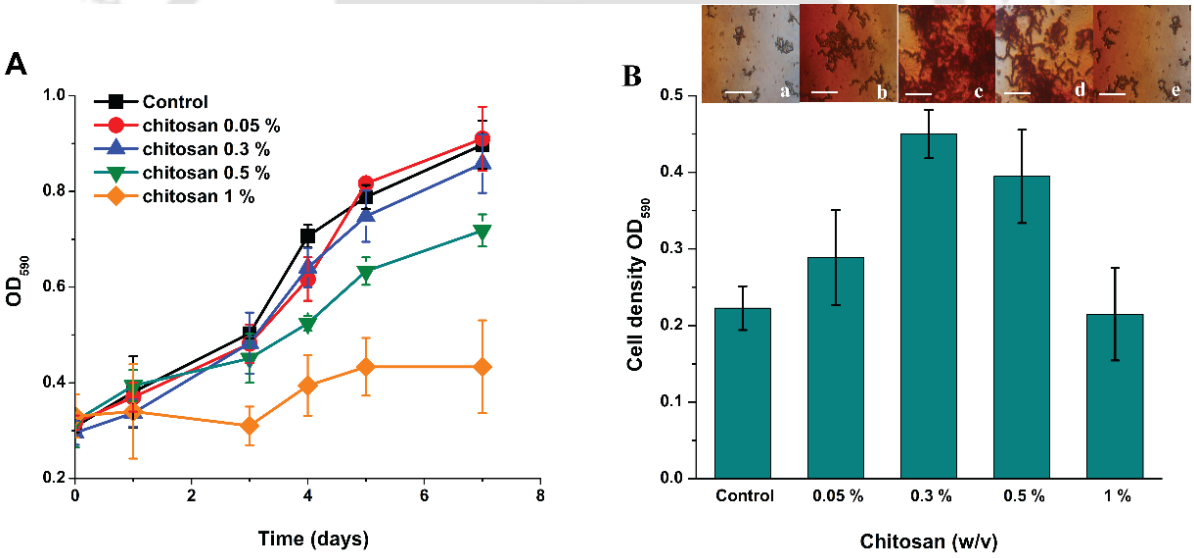


**Figure 2.7:** (A) Growth of *Synechococcus* sp. on control and chitosan film with varying chitosan concentrations (w/v). (B) Cell density assay of *Synechococcus* sp. and inset figures observed under bright field at 40 X resolution after gram staining, on control and chitosan film with varying concentrations of chitosan (a) control, (b) 0.05 %, (c) 0.3 %, (d) 0.5 % and (e) 1% (w/v) Inset bars represent 100 µm. The results are average of five independent experiments ± standard deviation.

**Table 2.1:** Physico-chemical properties of the bacterial cells.

| Bacterial strains | ζ (mV) at pH 7.5 | $R_e$ (µm) | $D_e$ ($m^2/s$) | $\theta_w$ (°) | $H_m$ (%) | HI |
|---|---|---|---|---|---|---|
| ***Synechococcus* sp.** | -20.47 ± 0.97 | 0.91 | $2.32 \times 10^{-13}$ | 67.8  | 0.68 | 8.36 ± 0.33 |
| ***E. coli*** | -12.83 ± 1.66 | 0.89 | $2.44 \times 10^{-13}$ | 20.7  | 0.20 | 1.63 ± 0.89 |
| ***L. plantarum*** | -10.13 ± 1.33 | 0.68 | $3.20 \times 10^{-13}$ | 19.1  | 0.19 | 0.17 ± 0.06 |

*ζ- surface potential, $R_e$- effective radii, $D_e$- diffusion coefficient, $\theta_w$- water contact angle, $H_m$- relative hydrophobicity of microbes, HI- hydrophobic index.

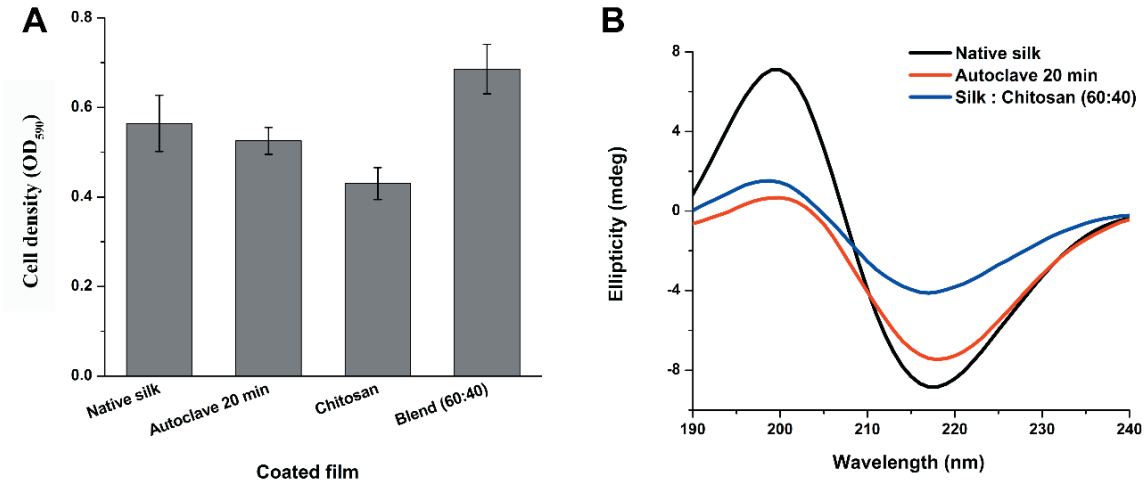


**Figure 2.8:** (A) Cell density assay of *Synechococcus* sp. on coated films namely, native silk, autoclaved silk, pure chitosan and blend of silk and chitosan (3:2). The results are average of five independent experiments ± SE. (B) CD analyses of native silk, autoclaved silk and the blend of silk and chitosan (3:2).

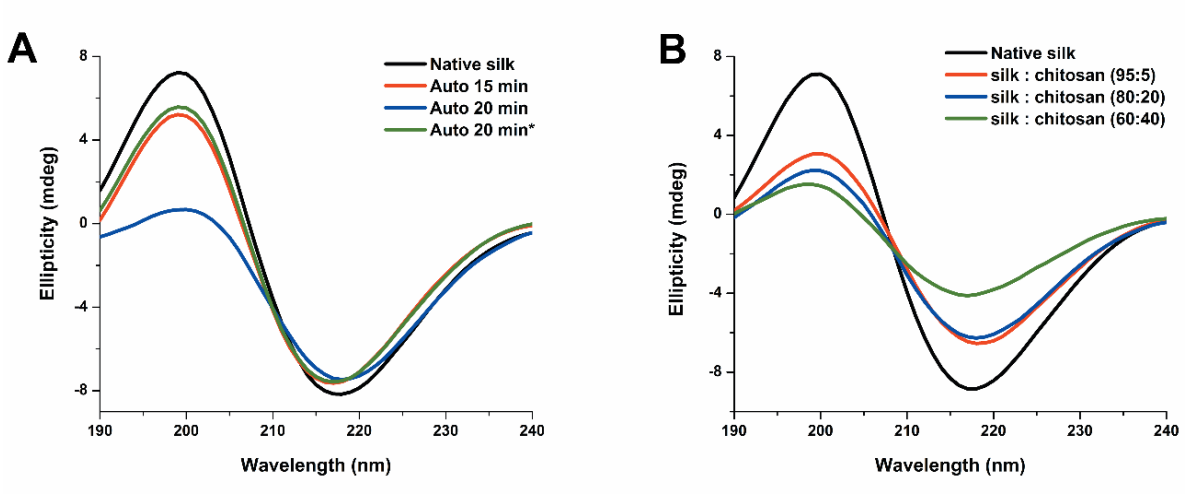


**Figure 2.9:** (A) CD analyses of steam autoclave treatment on silk for 15 min (Auto 15), 20 min (Auto 20) and *Auto 20 min kept overnight as compared to native silk. (B) CD analyses of the blend of silk and chitosan in the ratio 95:5, 80:20 and 60:40 as compared to native silk.

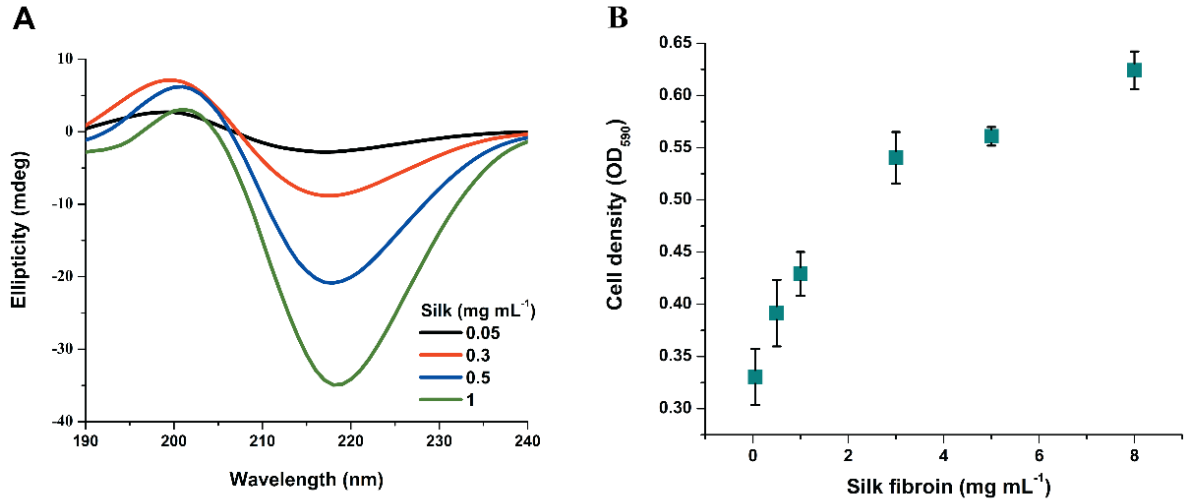


**Figure 2.10:** (A) CD analyses of various concentrations of silk in aqueous solution. (B) The cell density of *Synechococcus* sp. versus concentration of silk. The silk used for the rest of the experiments is 3 mg $mL^{-1}$ in order to have a uniform comparison to chitosan whose optimum concentration that supported cyanobacterium growth was found to be 3 mg $mL^{-1}$. The results are average of five independent experiments ± standard deviation.

The silk fibroin from *Bombyx mori* is composed of two major proteins- the heavy chain ($M_w$ of ~ 350 kDa) and the light chain ($M_w$ ~ 26 kDa) linked by a disulfide bond. The

central region of the fibroin is mostly hydrophobic (Liu and Zhang, 2014). The heavy chain with dominating *β*-sheet is composed of 45.9 % Gly, 30.3 % Ala, 12.1 % Ser, 5.3 % Tyr, 1.8 % Val and 0.25 % Try (Yang *et al*., 2004). Val is more hydrophobic than Ala (Matthews, 2001). Silk fibroin has two types of molecular conformation of the secondary structure, called silk I and silk II. Silk I is a metastable form of silk fibroin, soluble in water, with non-crystalline random coil containing *α*-helix conformations. On the other hand, silk II is a highly stable organized structure with *β*-sheet conformation and insoluble in water. Generally, both silk I and silk II are present in the silk fibroin products, but it is their relative proportions that define the final properties (Moraes *et al*., 2010). The silk fibroin is in soluble form when extracted. Once it is cast and dried to form the film, it becomes insoluble in water as the *β*-sheet content increases. The silk fibroin (0.2 mg/ mL in water) when treated at 15 lb and 121 $^{o}$C for 20 min, the *β*-sheet content of this protein was decreased by 7.80 % and there was a corresponding decrease in the cell density by 4.39 ± 1.40 % (compared to untreated native silk) (Figure 2.9). The decrease in *β*-sheet content during the steam autoclave can be attributed to the pressure factor since the mere effect of heat has been ascribed to increase the *β*-sheet content of silk (Yang *et al*., 2004). Increase in cell density was observed when silk of higher concentration was used (Figure 2.10). Notably, the *β*-sheet content in the silk protein increases by increasing the concentration of silk in aqueous solution (Li *et a*l., 2008).

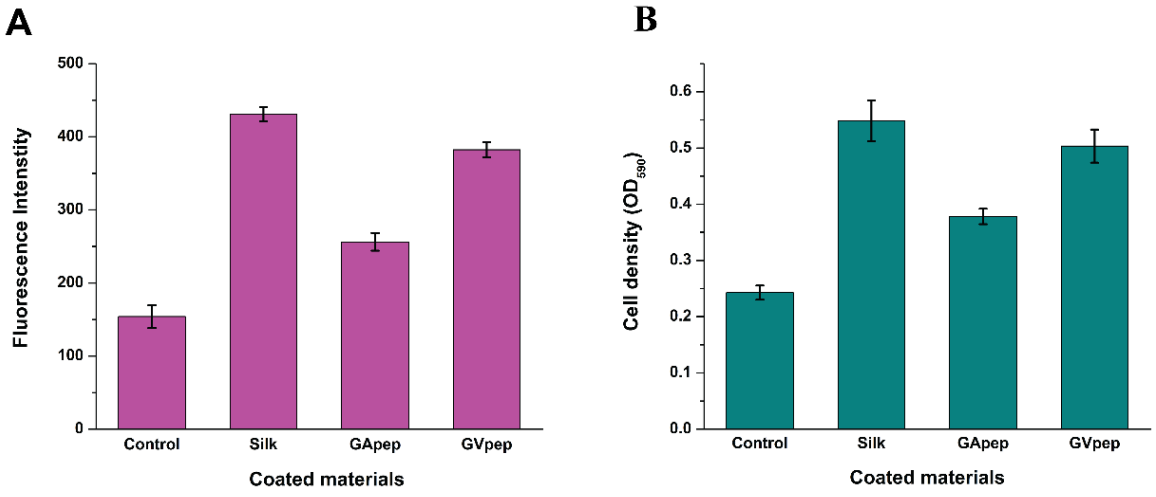


**Figure 2.11:** Biofilm formation of *Synechococcus* sp. on GApep and GVpep by using (A) biofilm assay and (B) cell density. The results are average of five independent experiments ± standard deviation.

The GAGAGS motif of the silk fibroin is known to form pleated *β*-sheet (Liu and Zhang, 2014). To examine the role of the hydrophobic motif on triggering biofilm formation, the peptides GApep that mimic the above motif of silk and GVpep with higher hydrophobicity were investigated. The study showed GApep, GVpep and silk promoted 10.23 ± 3.44 %, 22.83 ± 5.43 % and 27.73 ± 4.21 % increase in biofilm and 13.53 ± 1 %, 26.08 ± 1.69 % and 30.58 ± 2.40 % increase in cell density, respectively, as compared to control (Figure 2.11 A-B). The GVpep promoted higher cell density and biofilm formation than GApep. This is an indication of the important role of the hydrophobicity of the substrate on the biofilm formation. However, the biofilm growth on native silk film was still marginally higher than the GVpep film. This may be attributed to the additional structural properties of the silk such as *β*-sheet and porosity, which is known to support biofilm formation (Matsumoto *et al*., 2012).

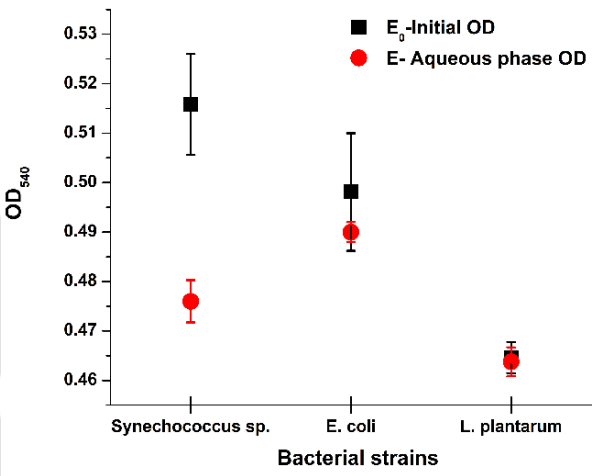


**Figure 2.12:** Initial ($E_o$) and aqueous phase (E) OD at $\lambda_{540\ nm}$ recorded for calculation of HI of the tested bacterial strains.

### 2.3.2 Physico-chemical factors influencing the biofilm growth

To understand the conditions for the observed rapid biofilm formation of the *Synechococcus* sp., a range of physic-chemical parameters were investigated for the tested bacterial strains (Table 2.1), the polymers and their interactions with the bacterial strains (Table 2.2). *Synechococcus* sp. exhibits higher values of negative ζ potential, HI, and $\theta_w$ as compared to *E. coli* and *L. plantarum*. These data imply that the cell surface of the

cyanobacterial strain is covered with a very high level of negative charge and hydrophobic entities. The HI of the tested bacterial strains were calculated by using the equation 2.2, with the data input from the Figure 2.12.

**Table 2.2:** Physico-chemical properties of the polymer supports and the interaction properties between *Synechococcus* sp. and polymer films for induction of biofilm.

| **Physico-chemical properties of polymers** | | | | **Interaction properties between *Synechococcus* sp. and polymer films** | | | | |
|---|---|---|---|---|---|---|---|---|
| **Polymers** | $\zeta$ (mV) | $\theta_w$ (°) | $H_p$ (%) | $V_R$ (mJ m $^{-2}$) | $H_{o/w}$ | Au | $a$ ($10^{-6}$, m $s^{-1}$) | $\Delta G^{\neq}$ ($kT$) |
| **Nafion** | -13.73 ± 2.01 | 108.9  | 1.08 | 281.05 | 7.33 | 0.19 ± 0.02 | 0.23 ± 0.17 | 1.21 |
| **Silk fibroin** | -2.95 ± 1.35 | 59.2  | 0.59 | 60.39 | 1.74 | 0.48 ± 0.16 | 4.21 ± 0.13 | -8.57 |
| **Blend (60:40)** | 4.17 ± 2.32 | 52.9  | 0.53 | -146.77 | 1.53 | 0.49 ± 0.17 | 4.85 ± 0.12 | -8.66 |
| **Polyaniline** | 6.68 ± 1.50 | 38.1  | 0.38 | -136.74 | 1.12 | 0.30 ± 0.06 | 2.00 ± 0.10 | -7.42 |
| **Osmium** | 2.18 ± 1.01 | 35.2  | 0.35 | -44.62 | 1.06 | 0.25 ± 0.03 | 1.60 ± 0.14 | -7.27 |
| **Chitosan** | 26.96 ± 1.62 | 28.1  | 0.28 | -551.87 | 0.92 | 0.39 ± 0.07 | 3.62 ± 0.16 | -8.44 |

*****$\zeta$- surface potential, $\theta_w$- water contact angle, $H_p$- relative hydrophobicity of polymer support, $V_R$- electrostatic repulsion $H_{o/w}$ - relative hydrophobicity between microbes and support surface, Au- adhesion unit, $a$- adhesion rate constant, $\Delta G^{\neq}$- activation Gibbs energy of adhesion.

The presence of hydrophobic proteins on the outer membrane of *Synechococcus* sp. has been reported (Umeda *et al*., 1996). Additionally, the obtained value of $\theta_w$ (67.8°) corroborates to the presence of hydrophobic polysaccharides on the cell surface (Rijnaarts *et al*., 1999). The information on physico-chemical properties such as hydrophobicity and surface charge of cyanobacteria are not adequately known previously.

Much higher hydrophobicity and negative surface charge value of the cyanobacteria as compared to the commonly available strains considered here are interesting. In natural habitat these properties of the marine cyanobacterium likely to play important roles in facilitating various physical interaction of the cells leading to symbiosis, mat formation and uptake of substrate and nutrient (Dittrich and Sibler, 2005; Fattom and Shilo, 1984).

The silk fibroin exhibits ζ potential of -2.95 ± 1.35 mV, which is of similar charge type with the test bacterial cells (Table 2.2). Theoretically, similar charge types develop the repulsive force that prevents the microbial cells from adhering to the material (Chu *et al*., 2009). The estimated electrostatic repulsion ($V_R$) between the cyanobacterial cell and silk was 60.39 mJ $m^{-2}$, which is, though positive, not as high as the repulsion level exhibited by the interaction of the cell with Nafion polymers (281.05 mJ $m^{-2}$). However, even though moderate, the positive $V_R$ value does not qualify to support a conducive interaction between silk and the cells for validating the formation of the observed colossal biofilms. An attempt has been made to explain the high cyanobacterial biofilm promoting nature of the silk fibroin exclusively based on the relative strength of the Van der Waals interaction between the entities that could be best described by the Hamaker approach. The reported Hamaker constant of a bacteria/water/silica interaction (equation 2.3) is $8.0 \times 10^{-22}$ J (Matsumoto *et al*., 2012). Taking into consideration the respective Hamaker constants of silica, water, chitosan and silk to be $15 \times 10^{-20}$ J, $4.0 \times 10^{-20}$ J (Matsumoto *et al*., 2012), $2.15 \times 10^{-21}$ J (Chern *et al*., 1999) and $45 \times 10^{-21}$ J (Asakura and Miller, 2013), the constants for bacteria/water/chitosan ($A_{bwch}$) and bacteria/water/silk ($A_{bwsf}$) interactions were discerned as $1.59 \times 10^{-21}$ J and $-1.25 \times 10^{-22}$ J, respectively (Figure 2.13). However, the negative Hamaker constant implies repulsion between silk and bacterial cells, hence, this parameter cannot be considered to explain the observed fact of bacterial adhesion for biofilm growth. Contrary to the aforementioned physico-chemical properties, the $H_p$ and $\theta_w$ levels of silk are

very high and second highest among the listed materials (Table 2.2). All these values are closer to those of chitosan blended silk. Further, in regards to the interaction, silk and silk-blend chitosan showed highest Adhesion unit (Au) (0.48 – 0.49), adhesion rate constant (*a*) [(4.2 – 4.8) × $10^{-6}$, m $s^{-1}$)] and Activation Gibbs energy of adhesion ($\Delta G^{\neq}$) (-8.5 – -8.6 *kT*) with the *Synechococcus* sp. The $H_{o/w}$ values of silk and silk-blend chitosan occupy the 2nd and 3rd rank in the list.

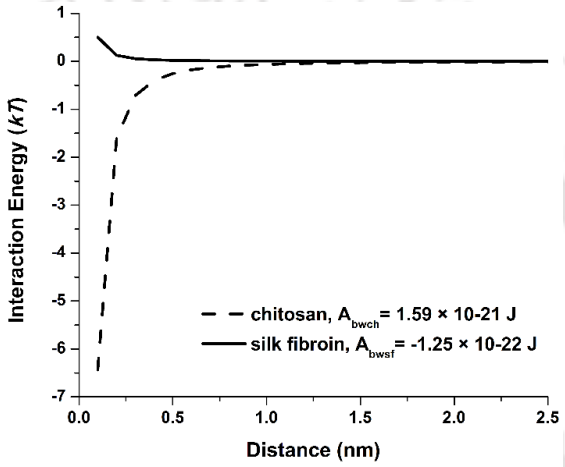


**Figure 2.13:** Interaction energy between bacteria-chitosan and bacteria-silk as a function of distance.

From the above results, it can be concluded that hydrophobic interaction between the cells and the supporting polymer film is an important factor leading to a facile adherence of bacterial cell on the film as validated by the values of Au, *a*, and $\Delta G^{\neq}$. The conclusion is also endorsed by our results on the biofilm promoting nature of the hydrophobic peptides GApep, GVpep films. These peptides do not have electrostatic interaction with the bacterial cells due to lack of their significant charge at the selected growth pH of the microorganisms. The high negative charge of the supporting film may be counterproductive for biofilm formation as evident from the results with Nafion. In comparison to other polymers, Nafion though exhibits the highest $H_p$ (1.08 %) and highest $H_{o/w}$ (7.33) with the cyanobacterial cells, the extremely high magnitude of $\zeta$ potential (-13.73 ± 2.01 mV) and $V_R$ (281.05 mJ $m^{-2}$) counterbalanced the hydrophobic force for adherence of bacterial cells onto its surface as indicated by the lowest values of Au (0.19 ± 0.02) and *a* (0.23 × $10^{-6}$ m $s^{-1}$) and highest

positive value of $\Delta G^{\neq}$ (1.21 *kT*). Except for Nafion, the activation energy values for the rest of the polymer films are negative with varying magnitude and corresponding biofilm promoting ability. Nafion failed to induce microbial adhesion for significant biofilm growth.

Again, the high positive surface charge of the film as exemplified with chitosan (ζ = + 26.96 mV) may strongly immobilize the negatively charged bacterial cells on the 3D film matrix that may suppress microbial growth (Zhang *et al*., 2013) as observed in the case of chitosan film > 0.3 % w/v (Figure 2.7). This is indirectly supported by the fact that in a blended film, the charges of both the silk fibroin and chitosan were significantly compensated leading to a ζ potential value of + 4.17 mV, where high biofilm growth was realized. Notably, all the tested bacterial strains displayed the highest adhesion rate to the blended film (Figure 2.14 and 2.15) which also coincided with the increase in negative $\Delta G^{\neq}$ values.

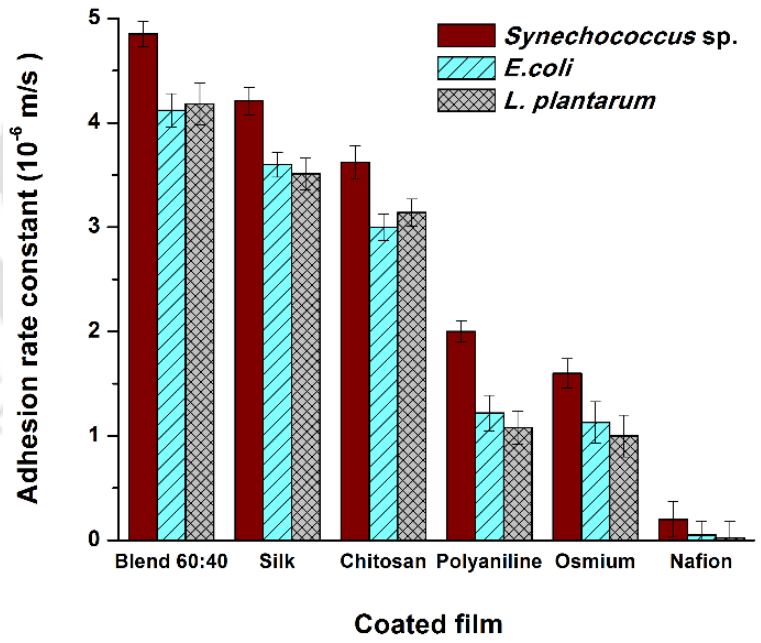


**Figure 2.14:** Adhesion rate constants of bacterial strains to polymeric films. The results are average of three independent experiments ± standard deviation.

The above results thus prompted us to conclude that very high surface charge (positive/negative) on the polymer film is not conducive for cell adhesion and biofilm formation. The interplay of surface charge (in terms of ζ potential) and hydrophobicity (in terms of $\theta_w$) of the polymer film and the generated adhesion rate constant of the cells of *Synechococcus* sp. could be reasonably explained through a contour plot (Figure 2.16). As evident from the plot, high hydrophobicity and moderate surface charge (~ -3 to +15 mV) augment facile adherence of microbes onto the polymer support. If the surface charge is highly negative, the adherence is not supported even at very high $\theta_w$ value. Similar is the case for hydrophilic support with high positive surface charge.

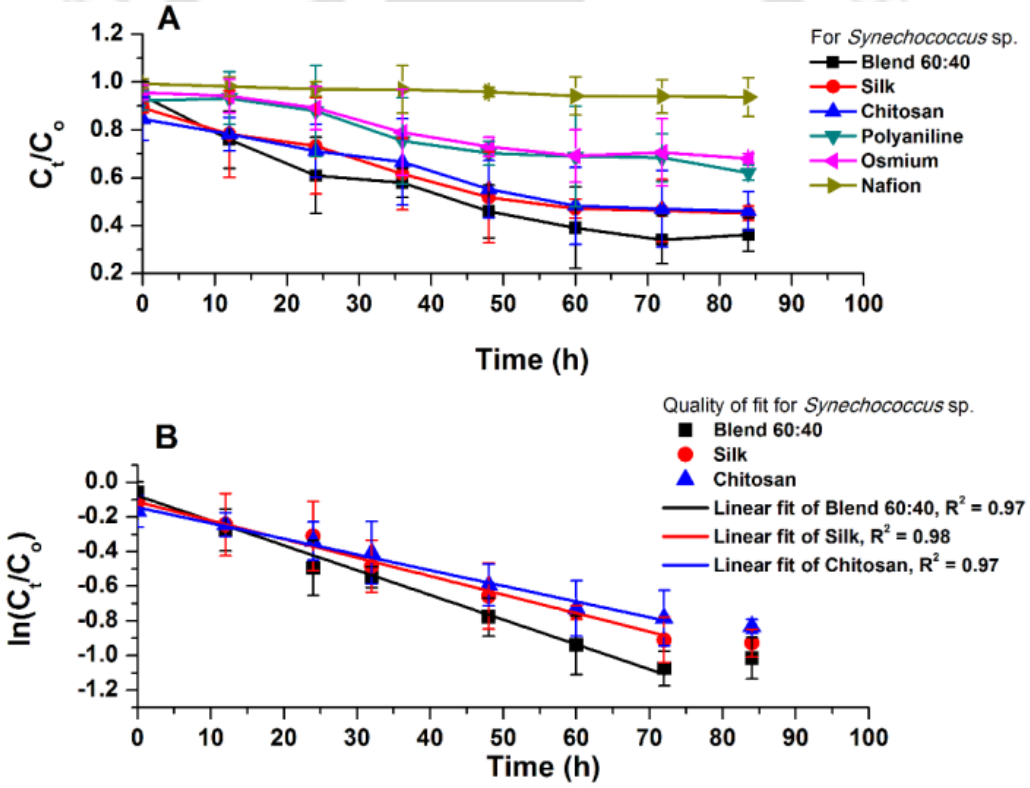


**Figure 2.15:** Time-courses of normalized *Synechococcus* sp. concentrations in suspension during adsorption tests to cover slips coated with polymers under study. (A) $C_t/C_0$ vs time, and (B) ln ($C_t/C_0$) vs time. Adhesion rate constants were calculated at 72 h when first-order kinetics was obeyed. The results are average of three independent experiments ± standard deviation.

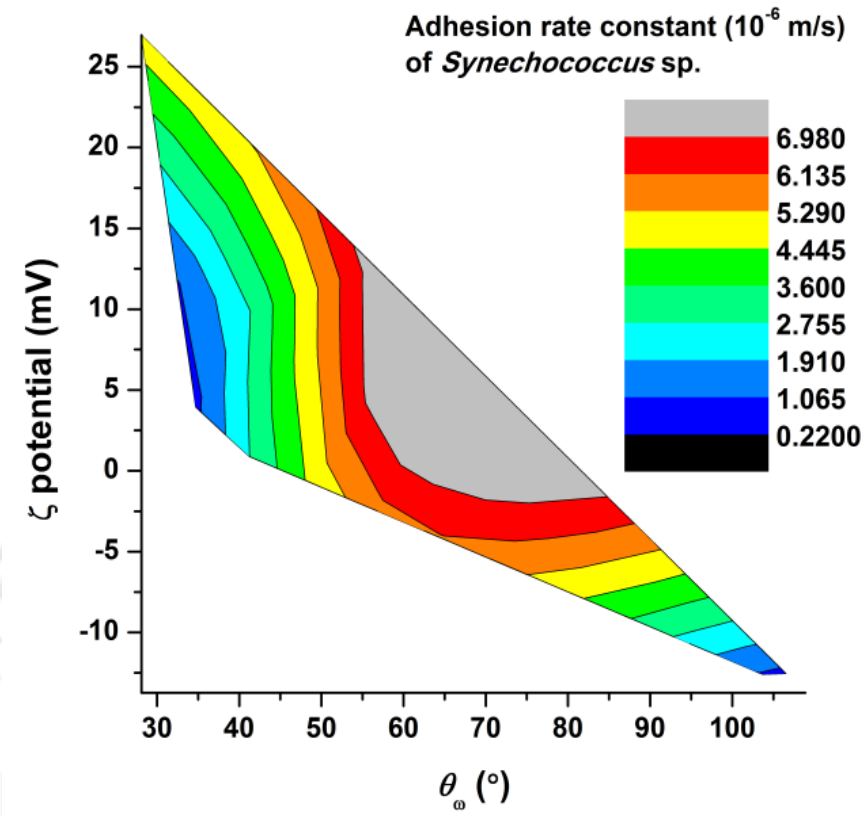


**Figure 2.16:** Contour plot representing the role of hydrophobicity ($\theta_w$) and surface charge (ζ potential) in microbial adhesion. The colour gradient represents the adhesion rate constants of *Synechococcus* sp. to polymeric supports.

## 2.4 Conclusion

The study aimed at investigating polymer thin-films that supported rapid biofilm growth for three different bacterial strains with a major focus on a marine cyanobacterial strain, *Synechococcus* sp. due to its emerging applications in various industrial niches. Biofilm specific fluorescent dye and cell density assay using crystal violet solution were used for analysing the biofilm growth on the polymeric test supports along with the advance microscopic techniques. This is the first report on the demonstration of silk fibroin and its blend with chitosan as the most effective candidates for inciting high bacterial cell adhesion and biofilm on all the solid supports including graphite, for all the bacterial strains under study. Further, two synthetic peptides GApep, that mimics a motif of silk-fibroin, and

another peptide GVpep with high hydrophobicity, when investigated for their efficacy in promoting biofilm. This established the fact that the hydrophobic property of the silk fibroin plays a key role in accelerating the biofilm growth. This was followed by a detailed study on the prerequisite interfacial physico-chemical phenomena between the bacterial cells and supporting polymeric films. This investigation also highlights the findings that surface charge (in terms of $\zeta$ potential) and hydrophobicity (in terms of $\theta_w$) of the support and bacteria exert combinatorial influence on the biofilm formation and propagation. The results embodied here advances the concept that the biofilm growth may be accelerated by using thin films of the tested biomaterials. The concept forwarded through this investigation on preparing microbial biofilm in a short timescale will have great application potentials in the fields such as, biofuel, microbial fuel cell, and other bioprocesses, where biofilms are growingly acclaimed as appropriate reusable bio-catalytic conduits owing to their aid in economic and environmentally friendly processes.

# Chapter III

## Development of nano-biocomposite material based bioanode to enhance and stabilize current in PMFC

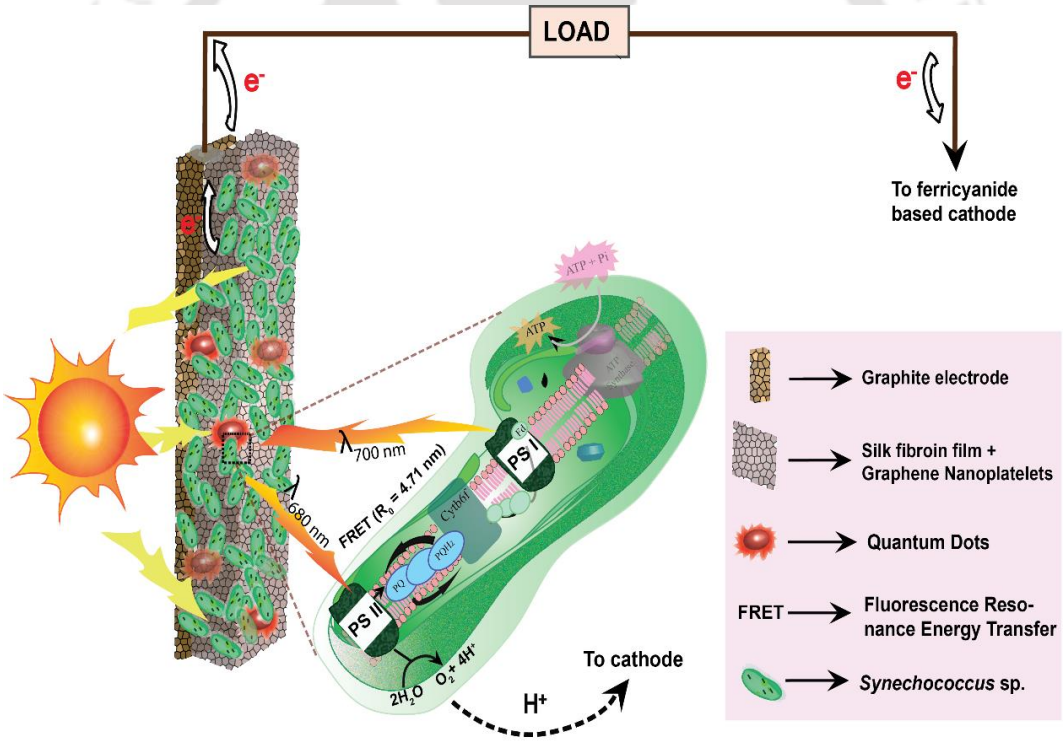


*Graphical abstract on FRET-based surging of cyanobacterial photosystems for enhancing and stabilizing the current of PMFC*

# Chapter III

## Development of Nano-biocomposite Material Based Bioanode to Enhance and Stabilize Current in PMFC

### 3.1 Overview

The interest on cyanobacteria as fuel cell catalysts is sharply growing owing to many advantages being identified by their use in these electrical power generating devices. These photosynthetic microorganisms are widespread in nature and can grow in heterotrophically as well as photo-autotrophically in a self-sustainable manner following a carbon concentrating mechanism. The application potential of these microorganisms for combined power generation and waste treatment through PMFC technology is vast due to their inherent survival capacity in adverse environmental conditions. However, to develop an efficient PMFC of practical essence few critical issues need to be addressed, among which the harvesting of adequate light energy to boost the photosynthetic machinery of the cells under low light conditions and the approach for capturing the metabolic electrons efficiently on the electrode surface are to be reckoned first. The mechanisms which are relied upon capturing the metabolic electrons are mostly limited to DET and MET processes, while a third approach involving bacterial nanowire for transferring the metabolic electrons to the electrode is in a nascent stage (McCormick *et al*., 2015). We propose to explore here DET as the guiding principle for capturing the cellular electrons on the electrode due to its certain stark advantages that have already been described in a previous chapter. To implement the concept of DET in a MFC for steady generation of electric current, a naturally sustained close contact between the bacterial cells and the conductive electrode is a desired condition. To meet this condition, the creation of a natural bacterial biofilm over the electrode surface has been evolved as a method of choice for generating stable current from the cellular electrons in the fuel cell setup (Chen *et al*., 2015b). However, a systematic investigation of the preparation of cyanobacterial biofilm for fuel cell application is yet to be witnessed. Our studies as described in chapter II established that the silk fibroin (SF) promotes rapid biofilm growth of *Synechococcus* sp. Here, we utilized this biopolymer to induce the biofilm growth

of *Synechococcus* sp. on graphite electrode for developing PMFC bioanode. However, while complying with the biofilm growth requirement on these biopolymers on the electrode surface to address the issue of DET approach, an associated obstacle of poor electrical conduction of the underneath semiconducting silk-film needs to be overcome. Furthermore, to increase the photosynthetic metabolic activity of the cells beyond the basal level in the complex milieu of biofilm, appropriate photon energy needs to be delivered to the underneath cells that warrants additional strategy in designing the electrodes. Notably, the design of microbial photo-bioreactor is a critical issue as the light scattering and mutual shading caused by the increased biomass and other materials in the reactor challenges the performance of the reactors (Antal *et al*., 2016; Bombelli *et al*., 2011). To circumvent these problems for generating current efficiently in PMFC, we adopt here a three-step strategy: (i) induction of biofilm formation directly on the graphite anode with the help of biocompatible SF film, (ii) exploiting the Fluorescence resonance energy transfer (FRET) principle to transfer appropriate photon energy to the photosystems of the cyanobacteria with the aid of a suitable quantum dot (QD) and (iii) incorporation of highly conductive graphene nanoplatelets (GNP) to provide an electroactive biofilm surface for facilitating the relay of cellular electrons to the electrode across the semiconducting SF film. To materialize these strategies, a novel nanocomposite matrix has been developed by incorporating Cadmium Telluride (CdTe) QD and GNP in the SF film and this nanocomposite matrix was employed over the graphite electrode to develop the anode for the PMFC. Notably, QDs are semiconducting nanomaterials with remarkable properties such as light absorption at wide spectra, sharp and tunable emission as well as photo-stability (Poderys *et al*., 2010). These nanocrystals have been extensively used in biological labelling, solar cells, etc. (Rajbanshi *et al*., 2014). A detailed account on the development of the QD-based nano-biocomposite matrix to implement the above mentioned strategies for improving the power generation in a PMFC has been reported in this chapter.

## 3.2 Experimental approaches

### 3.2.1 Materials

Mercaptocarboxylic acid coated CdTe QD (3.8 nm in size, 146000 g/mol, 40 % quantum yield and absorption maximum at $\lambda_{644\ nm}$ and fluorescence maximum at $\lambda_{680 \pm 5\ nm}$) and GNP (3 nm in size) were procured from M K Impex Corp. (Canada) and Graphene Laboratories Inc. (New York), respectively. Isomolded graphite electrode (GE) (0.318 cm dia × 30.48 cm length) was purchased from GraphiteStore.com (USA). Nafion 117™ was procured from Sigma Aldrich (USA). SF (375 kDa) was extracted from *Bombyx mori* cocoons with a yield 5 – 7 % (w/v) as described in chapter II. The growth of *Synechococcus* sp. was maintained in ASN III medium under the condition of 15 W $m^{-2}$ of white light in circadian cycle of 12 h light/12 h dark and 28 ± 2 °C (Table 3.1). All solutions were prepared in ultrapure water with resistivity > 18 MΩ cm. The experiments were performed at RT unless stated otherwise. Rest of the reagents were of analytical grade.

**Table 3.1:** Artificial seawater (ASN III) medium with pH adjusted to 7.4.

| | |
|---|---|
| **NaCl** | 25.0 g $L^{-1}$ |
| **$MgSO_4 \cdot 7H_2O$** | 3.5 g $L^{-1}$ |
| **$MgCl_2 \cdot 6H_2O$** | 2.0 g $L^{-1}$ |
| **$NaNO_3$** | 0.75 g $L^{-1}$ |
| **$K_2HPO_4 \cdot 3H_2O$** | 0.75 g $L^{-1}$ |
| **$CaCl_2 \cdot 2H_2O$** | 0.5 g $L^{-1}$ |
| **KCl** | 0.5 g $L^{-1}$ |
| **$NaCO_3$** | 0.02 g $L^{-1}$ |
| **Citric acid** | 3.0 mg $L^{-1}$ |
| **Ferric ammonium citrate** | 3.0 mg $L^{-1}$ |
| **EDTA** | 0.5 mg $L^{-1}$ |
| **Trace element solution** | 1 mL $L^{-1}$ |

**Trace elements**

| | |
|---|---|
| **$H_3BO_3$** | 2.86 g $L^{-1}$ |
| **$MnCl_2 \cdot 4H_2O$** | 1.81 $gL^{-1}$ |
| **$ZnSO_4 \cdot 7H_2O$** | 0.222 $gL^{-1}$ |
| **$NaMoO_4 \cdot 2H_2O$** | 0.39 $gL^{-1}$ |
| **$CuSO_4 \cdot 5H_2O$** | 0.079 g $L^{-1}$ |
| **$Co(NO_3)_2 \cdot 6H_2O$** | 49.4 mg $L^{-1}$ |

### 3.2.2 Cell density assay

The cell density assay for *Synechococcus* sp. was done following the method as described in section 2.2.4 under chapter II. Here, the assay was mainly performed to understand the effect of SF doped QD on the bacterial cells. Briefly, SF (3 % w/v in water) and QD (0.1 % w/v in water) were mixed in different ratio. A total of 20 µL mixture of SF and QD was drop-cast on 24-well plate (NEST, USA) and dried inside a laminar hood. One mL of sterile ASN III media inoculated with 200 µL of active cells ($OD_{750}$ = 0.29 – 0.32) was added to the SF/QD coated wells. After 72 h of incubation, the wells were rinsed with water and then submerged under 1.2 mL of 0.1 % aqueous CVS for 15 min. The plates were again rinsed thoroughly with water and then dried under a laminar hood for 5 h. Once dried, 1.2 mL of 30 % acetic acid was added and incubated for 15 min to solubilize the CVS. 200 µL of the solubilized CVS was transferred to a new multiwell plate and absorbance was recorded at $OD_{590}$ in a microtiter plate reader (TECAN M200 Pro, Switzerland). The mean of three independent measurements are plotted, while the error bars represent the relative standard deviation.

### 3.2.3 Interaction study between SF and QD

#### *3.2.3.1 Circular dichroism (CD) analysis*

QD in a range of 0 – 4 µM prepared in freshly extracted SF solution (0.5 mg $mL^{-1}$) was subjected to CD analysis in a Jasco J-815 spectropolarimeter (Japan). The spectra were recorded from $\lambda_{240-190\ nm}$, in a 0.1 cm path length suprasil quartz cuvette at 18 °C, at a scan

rate of 100 nm $min^{-1}$. The baseline corrected spectra were analyzed for secondary structures using DICHROWEB (Whitmore and Wallace, 2008).

#### *3.2.3.2 Isothermal titration calorimetry (ITC) analysis*

The calorimetry experiments were performed in a Microcal ITC200 micro-calorimeter (G.E. Healthcare, UK), at 298 K. A total of 60 μL of SF (170 μM) in the syringe was reverse titrated into 300 μL of QD solution (1 μM) in the sample cell holder with stirring speed fixed at 250 rpm. The first drop was set to 0.4 μL followed by 16 subsequent 2.5 μL injections. To achieve complete equilibration, the spacing time of 120 s between each injection was set. Blank ITC experiment was performed to correct for the heat of dilution. Analysis of ITC data was performed by Origin v 7.0 (OriginLab, USA). The binding affinity and thermodynamic parameters of the binding process were obtained by fitting the integrated heats of binding the isotherm to the one site binding model.

### 3.2.4 Determination of FRET

The absorbance spectra of the acceptor, *Synechococcus* sp. ($OD_{750}$ ~ 0.3) was recorded in a UV/Vis spectrophotometer (Cary 100 Bio, Varian). Aqueous SF (3 % w/v) and QD (0.1 % w/v) were mixed in the ratio of 2.4:0.02 (wt/wt) to make the SF decorated quantum dots (SF/QD) solution. 1 mg of GNP was mixed with 1 mL of SF/QD solution to make SF doped with QD and GNP (SF/QD/GNP). The fluorescence spectra of the donors QD, SF/QD and SF/QD/GNP solutions were recorded by an LS-55 spectrofluorometer (Perkin-Elmer, USA), equipped with a quartz cuvette (1.0 cm × 1.0 cm) using 5 nm slit widths.

The fluorescence quantum yields ($\mathbf{\Phi}_D$) of the various nanocomposite materials were calculated according to the following equation:

$$\Phi_D = \Phi_R \frac{F}{F_R} \frac{f_R}{f} \frac{\eta^2}{\eta_R^2} \quad \text{.....(3.1)}$$

Where, $F$ is the integrated fluorescence intensity, η is the refractive index of solvent (1.33 for water), and $f$ is the absorption factor calculated from the measured absorption ($A$) at the excitation of $\lambda_{644\ nm}$ using $f = 1 - 10^{-A}$. The subscript $R$ refers to the standard fluorophore. Rhodamine 6G (in ethanol solvent, $\eta_R$ = 1.36) of known quantum yield, $\mathbf{\Phi}_R$ = 0.95 (Grabolle

*et al*., 2009) has been used here as standard. Förster radius ($R_0$) is defined as the distance at which the efficiency of energy transfer is 50 %.

$$R_0 = 8.785 \times 10^{-5} \kappa^2 \Phi_D J / \eta^4 \text{.....(3.2)}$$

$R_0$ depends on the $\mathbf{\Phi}_D$ of the donor in the absence of the acceptor, η, and orientation factor between donor and the acceptor molecules ($\kappa^2$) (Hink *et al*., 2003). For randomly oriented dipoles $\kappa^2$ = 0.66 (Clapp *et al*., 2004). *J* is the overlap integral between the fluorescence spectrum of the donor and the molar absorption spectrum of the acceptor.

$$J = \int F_D(\lambda) \varepsilon_A(\lambda) \lambda^4 \, d\lambda \text{ .....(3.3)}$$

Where, $F_D$ is the peak-normalized fluorescence intensity of the donor and $\varepsilon_A$ is the molar extinction coefficient of the acceptor. The $\varepsilon_A$ for chlorophyll *a* (Chl-*a*) has been used as $70.02 \times 10^{-3}$ $M^{-1}$ $cm^{-1}$ (Li *et al*., 2012).

TRPL studies of the nanocomposite with and without *Synechococcus* sp. were carried out on a picosecond time-resolved cum steady state luminescence spectrometer (Edinburgh Instruments, UK, Model FSP920) using an LED source, at an excitation wavelength of $\lambda_{635\ nm}$ and emission wavelength of $\lambda_{680\ nm}$.

### 3.2.5 Preparation and characterization of nanocomposite films

The size of the QD was determined under a JEOL 2100 transmission electron microscope (TEM) (Japan) operated at 150 kV. The presence of QD in SF/QD matrix was also examined under a confocal laser scanning microscope (CLSM) (Zeiss LSM 880) with excitation at $\lambda_{644\ nm}$ and the red emission filter.

A total of 50 µL of SF, SF/QD and SF/QD/GNP solutions were drop cast on microscopic glass slides and allowed to dry under a laminar hood overnight. The dried films were then subjected to the following characterizations. The UV–Visible absorption characteristics in the range $\lambda_{200\ -\ 800\ nm}$ were measured using a UV-VIS-NIR spectrophotometer (Shimadzu UV-2101/3101PC) with reference to air. The optical absorption coefficient ($\alpha$) was calculated from the sample thickness (*X*) and optical absorbance (*A*), by using relation:

$$\alpha(h\upsilon) = 2.303\, A/X \text{ .....(3.4)}$$

The optical absorption coefficient for non-crystalline materials has the following frequency dependence:

$$\alpha(h\upsilon) = B(h\upsilon - E_g)^r / h\upsilon \ldots\ldots\ldots\ldots\ldots\ldots\ldots\ldots\ldots\ldots (3.5)$$

Here $h\upsilon$ is the energy of the incident photons, $E_g$ is the value of the optical energy band gap and $r$ is an empirical exponent index that determines the type of optical transition. In the present case, r = 1/2 which means an allowed direct transition (Asha *et al*., 2016). Extrapolation of the linear part of the curve [plotting $(\alpha h\upsilon)^{1/2}$ against $(h\upsilon)$] to intersect the x-axis at zero absorption gives the corresponding $E_g$ values.

Raman spectra were recorded on a Horiba Jobin Yvon, LabRam HR (Japan). X-ray diffraction (XRD) patterns were recorded on a Rigaku X-ray diffractometer (model TTRAX III, Japan) using Cu-Kα radiation (λ = 1.5406 Å).

### 3.2.6 Construction and operation of PMFC

#### *3.2.6.1 Construction of PMFC*

A two-chambered PMFC was fabricated using light transparent Plexiglas glass material. The anodic and cathodic chambers, each with an effective volume of 100 mL, were separated by a proton exchange membrane (PEM) (Nafion 117). The PEM was pretreated at 80 °C for 1 h in 3 % $H_2O_2$, followed by washing with distilled water and 0.5 M sulfuric acid sequentially to increase the porosity (Yang *et al*., 2015). The membrane was then fixed between gaskets with the help of clamps. Each chamber was provided with sample inlets and wire point inputs at the top which were sealed later on to perform the operation. The cathode chamber was fed with PBS (0.1 M, pH 7.0) containing 80 mM of $K_3[Fe(CN)_6]$ (ferricyanide) as the electron acceptor. This hexacyanoferrate is a suitable redox material for fundamental laboratory studies of fuel cell owing to its facile reaction rate, low overpotential and ease of handling (Lv *et al*., 2013). The anolyte contained ASN III media with 750 mg $L^{-1}$ of acetate. The anode chamber was inoculated with *Synechococcus* sp. ($OD_{750}$ ~ 0.4) acclimatized in an anaerobic environment. The chamber was purged with argon gas to remove oxygen and stirred periodically to avoid diffusion limitation.

Two graphite electrodes (GEs) (3.7 cm × 0.32 cm) were positioned at a distance of 1 cm on either side of PEM, to serve as the anode and cathode. Prior to use, the electrodes were rinsed with acetone, methanol and water. Alligator copper clips (Mouser Electronics, USA) were used as the contact with electrodes. A total of 100 μL for each of SF, SF/QD and SF/QD/GNP solutions were drop cast on the anode and dried under a laminar hood for 5 h to fabricate modified graphite anodes SF/GE, SF/QD/GE and SF/QD/GNP/GE, respectively.

### *3.2.6.2 Operation of PMFC*

The PMFC was operated in a batch mode at RT with a white light intensity of 15 W $m^{-2}$ and in a 12 h: 12 h light - dark cycle. A data acquisition system (Agilent 34972A LXI, USA) was used to continuously record the voltage outputs of the PMFCs. For generating the polarization curve, loading a range of 10 x $10^6$ - 1.6 Ω with a stabilization of 20 min at each load was employed. The current ($I$) and power ($P$) were calculated using Ohm's Law ($I = U/R_{ex}$, where $U$ (V) is the voltage, $I$ (A) is the current, and $R_{ex}$ (Ω) is the external load) and normalized to the projected surface area of anode (3.84 $cm^2$). All the experiments were performed in triplicates and the average is reported.

The light energy conversion efficiency (LCE) was calculated by dividing the maximum measured electrical power output ($P_{cell}$) divided by incident solar irradiance (15 W $m^{-2}$) (Blankenship *et al*., 2011).

The fill factor ($F_f$) of the PMFC was calculated from

$$F_f = P_{cell}/(I_{sc} \times V_{oc}) \quad \text{.....(3.6)}$$

Where, $V_{oc}$ is the open circuit potential (OCP) and $I_{sc}$ is the short circuit current obtained from the polarization curve.

From the slope of the polarization curve, the internal resistance and the activation overpotential were calculated (Das *et al*., 2014). The electron transfer rate ($\Gamma$) was computed using the relation

$$\Gamma = I/e \quad \text{.....(3.7)}$$

where $I$ is the measured current and $e$ is the electron charge (Malvankar *et al*., 2012).

### 3.2.7 Characterization of PMFC electrodes

#### *3.2.7.1 Electrochemical characterizations of electrodes*

All electrochemical measurements were performed in a potentiostat (Autolab, PGSTAT 302N, Netherland) using a three-electrode system with the anode as the working electrode, Ag/AgCl (saturated KCl) as the reference electrode and platinum as the counter electrode. The electrochemical interaction between the cells of *Synechococcus* sp. and electrodes and the interfacial kinetics were probed by using cyclic voltammetry (CV) and electrochemical impedance spectroscopy (EIS).

For non-turnover CV analysis of the bioanode, the culture broth from the anodic chamber of the PMFC was drained off and filled with fresh buffer (PBS, pH 7). The biofilm on the anode was then allowed to starve for two days in that same buffer to deplete any residual acetate from the bacterial cells. The acetate free bioanode was then subjected to CV analysis in a potential window of -1.0 V to +1.0 V (vs Ag/AgCl) at a scan rate of 1 mV $s^{-1}$. Integration of the anodic peak area in the CV provides an estimate of the charge passed upon electrolysis of the redox species within the biofilm (Katuri *et al*., 2012). This charge (Q in coulombs) was used to estimate surface coverage of the redox species ($S_e$, in mol $cm^{-2}$) within the biofilm per geometric projected electrode area ($A$ = 3.84 $cm^2$) via $S_e = {}^{Q}/_{nFA}$, where $n$ is the number of electrons and F is Faradays constant.

The electrochemical surface area of the GE and modified GEs were measured in an electrolyte solution containing 0.1M KCl and 1mM $K_3FeCN_6$. The Randles–Sevcik equation (which assumes mass transport occurs only by diffusion),

$$I_P = 2.69 \times 10^5 \times S_a \text{ x } D^{1/2} \times n^{3/2} \times \gamma^{1/2} \times C \qquad \text{.....(3.8)}$$

was employed to measure the electrochemical surface area ($S_a$) using D, the diffusion coefficient of $K_3FeCN_6$ in solution ($6.70 \times 10^{-6}$cm $s^{-1}$), $n$, the number of electrons ($n$ = 1), $\gamma$, the scan rate (100 mV $s^{-1}$), $C$, the concentration of the probe in solution and $I_p$, the peak current response (Santhosh *et al*., 2016).

The EIS measurements were performed in a background solution of 5 mM $K_3Fe(CN)_6$/ $K_4Fe(CN)_6$ (1:1) and 0.1 M KCl in PBS. The frequency range was $10^6$ – 0.1 Hz

with a potential perturbation signal of 10 mV amplitude at open circuit potential. The Randles circuit was chosen to fit the impedance outputs (Parlak *et al*., 2014).

#### *3.2.7.2 Characterization of electrodes by FESEM*

The morphological characterizations of the biofilm on anodes were performed by a FESEM (Zeiss, Model Sigma) at 3 kV. The samples were fixed with 2 % glutaraldehyde and then dehydrated by treating the samples with increasing alcohol concentration (40 – 100 %). Gold coating on the sample was done prior to imaging.

## 3.3 Results and discussion

### 3.3.1 Development of biofilm on nanocomposite casted anode

The *Synechococcus* sp. biofilm propagates rapidly on SF film. The reason has been ascribed to the interplay of electrostatic and hydrophobic interaction between the bacterial cells and SF film as described in chapter II. This concept has been extended here to develop biofilm on GE for using it as the anodic catalyst in a PMFC. However, to efficiently harvest the catalytic power of these photosynthetic microorganisms, the LCE of the bacterial photosystems in this complex biofilm conduit needs to be increased. Additionally, the flow of electrons from the cells in the biofilm to the anode has to circumvent the barrier caused by the semiconducting SF film for generating current in the PMFC. We attempt to address these issues by incorporating QD and highly conductive GNP (Yong *et al*., 2014) in the SF film to prepare the nanocomposite matrix. The QD is visible in the TEM image (Figure 3.1 A) and the presence of QD in the SF/QD matrix was detectable under CLSM (Figure 3.1 B).

The QD alone though inhibited the bacterial growth, it increased the biofilm cell density by ~ 8 % at an optimum SF: QD doping ratio of 2.4:0.02 than the SF (Figure 3.2). Notably, the SF film enhances the cell density of *Synechococcus sp.* in the biofilm by 31 ± 1.6 % than the blank GE. The $Cd^{2+}$ ions are known to be toxic to the cells (Poderys *et al*., 2010) and hence, would prevent the biofilm formation if released from the QD. The result suggests that the SF stabilized the QD from degrading to ions when mixed at the said ratio. There was however, no significant influence of GNP on the cell density with the above ratio (2.4:0.02) of SF/QD hybrid at its working dispersion loading of 10 % in the SF film. The

biofilm growth on SF/GE and SF/QD/GNP/GE are clearly visible in FESEM images (Figure 3.3 a-b).

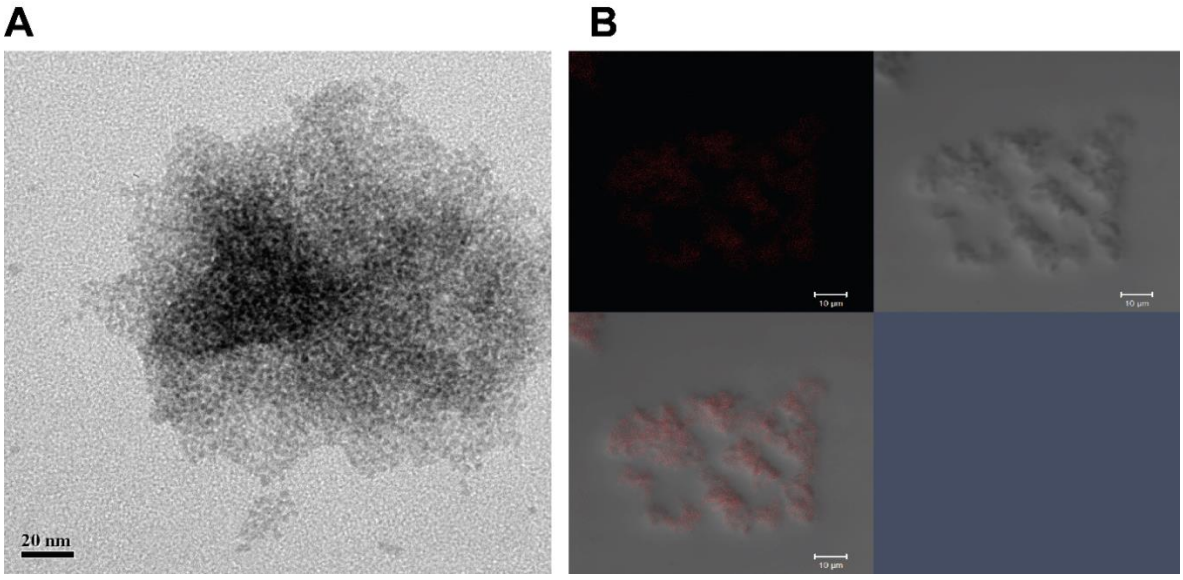


**Figure 3.1:** (A) TEM image of the CdTe QD. (B)The presence of QD in SF/QD matrix examined under CLSM with excitation at $\lambda_{644\ nm}$ and the red emission filter.

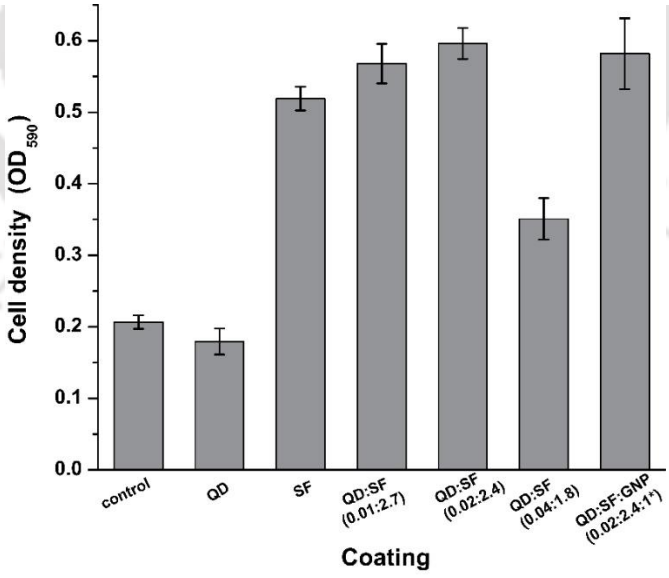


**Figure 3.2:** Cell density assay of *Synechococcus* sp. on the solid support coated with different concentrations of QD in SF film. *Concentration of GNP with respect to SF.

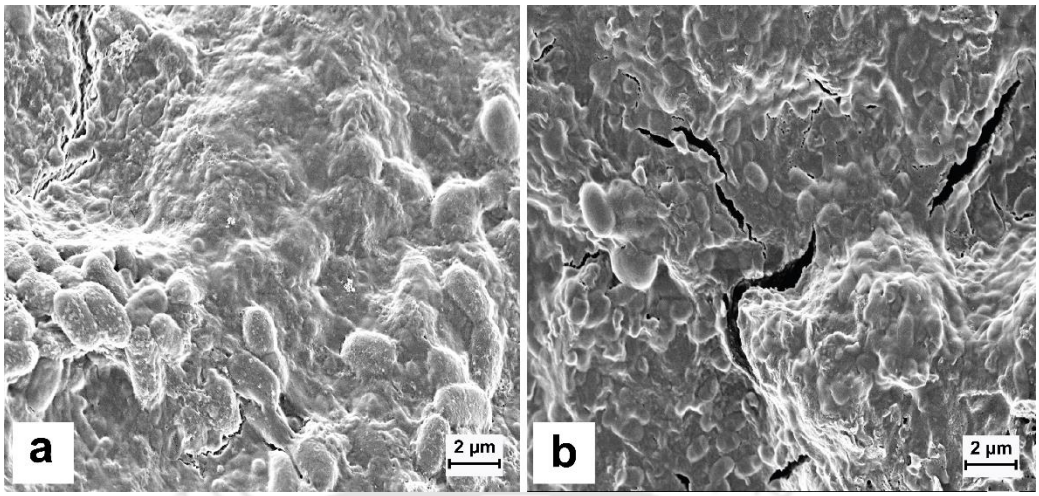


**Figure 3.3:** FESEM images of biofilm formation on (a) SF/GE (b) SF/QD/GNP/GE following 280 h run of the PMFC.

### 3.3.2 Interactions among the nanocomposite materials and bacterial cells

XRD analysis (Figure 3.4 A) indicated that the intensity of diffraction peak at 26.2° , which is ascribed to the (002) reflection of a hexagonal graphite structure and signature peak of pure graphite powder (GNP) (Fan *et al*., 2012), was decreased by ~ 60 % in the hybrid nanocomposite. This is because of the attachment of SF on the surface of GNP reduced stacking of the graphene sheets to some extent (Wang *et al*., 2014b). The Raman spectra (Figure 3.4 B) of the pristine graphite is dominated by the G band (1576 $cm^{-1}$) and a D band (1324 $cm^{-1}$) complying to a previous report (Fan *et al*., 2012). The G band is related to graphitic carbon and the D band is associated with the structural defects or partially disordered structures of graphitic domains (Huang *et al*., 2013). The intensity ratio of the D and G band ($I_D/I_G$) reflects the structural defects and disorder (Fan *et al*., 2012). No shift in the position of the D and G bands is observed in the composite matrix. The $I_D/I_G$ ratio for GNP and SF/QD/GNP were 0.35 and 0.34 respectively, signifying a marginal decrease in the defects (Choi *et al*., 2015).

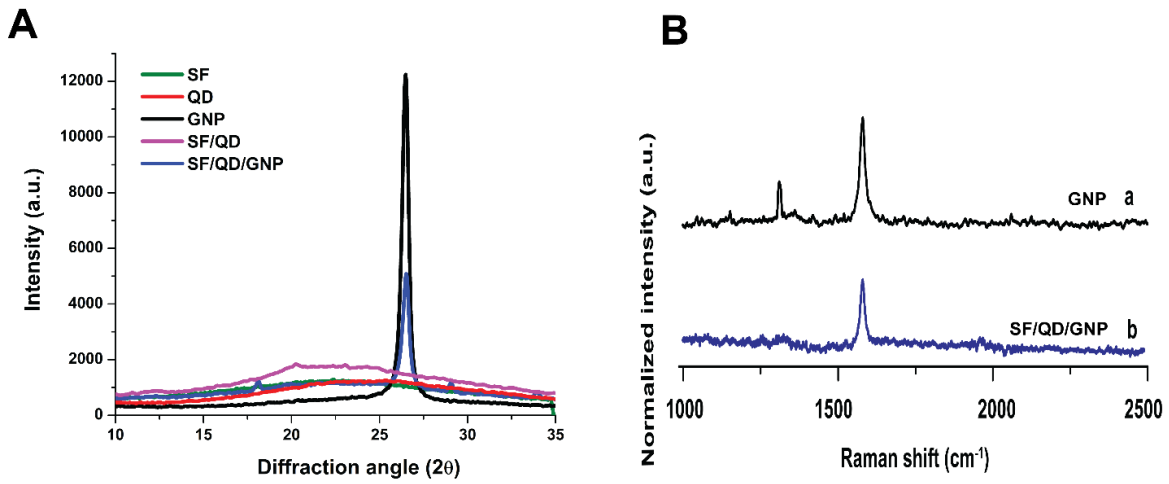


**Figure 3.4:** (A) XRD patterns of the nanocomposite films. (B) Normalized Raman spectra of the films (a) GNP and (b) SF/QD/GNP.

The absorption spectrum of *Synechococcus* sp. revealed prominent peaks in $\lambda_{440-460\ nm}$ and $\lambda_{600-700\ nm}$ corresponding to phycobilisome and chlorophyll a (Chl-*a*) (Figure 3.5 A). Chl-*a* is associated with both PS I and PS II contributing towards the light energy capture and photocurrent generation (Sekar *et al*., 2014). The excitation of the QD at $\lambda_{350\ nm}$, $\lambda_{550\ nm}$ and $\lambda_{644\ nm}$ generates overlapping fluorescence spectra in the range of $\lambda_{600-800\ nm}$, that endorses suitability of the QD for the present study due to its broad spectral excitation range and matching fluorescence spectrum with the absorption spectrum of the bacterial photosystems (Figure 3.5 B-C).

The fluorescence peak position of the QD did not significantly shift when it was doped in SF/GNP composite (Figure 3.6 A). The fluorescence intensity of SF/QD/GNP (donor) (at $\lambda_{ex\ 550\ nm}$) in presence of *Synechococcus* sp. (acceptor) was reduced to a sizeable level (~ 22 %). The peak located at $\lambda_{650-700\ nm}$ corresponds to the auto-fluorescence property of photosynthetic pigments present in cyanobacteria (Sekar *et al*., 2014) . The intensity however, was not quenched in presence of a non-photosynthetic microbe, *E. coli* at similar conditions and cell concentrations ($OD_{600}$ = 0.3), due to the absence of photosynthetic pigments. The normalized absorbance spectra of cyanobacteria (Figure 3.6 B) displays peak centered at $\lambda_{625-650\ nm}$, which is the characteristic absorbance caused by the cyanobacterial photosynthetic pigments (Sekar *et al*., 2014). The quantum yields, integral overlap and Förster radius were calculated from the spectral overlap with *Synechococcus* sp. as the

acceptor (Figure 3.6 B and Table 3.2) and observed that in the nanocomposite, even as the quantum yield of the QD was decreased by 45 %, the Förster radius was also significantly decreased (~ 12 %) in SF/QD/GNP as donor.

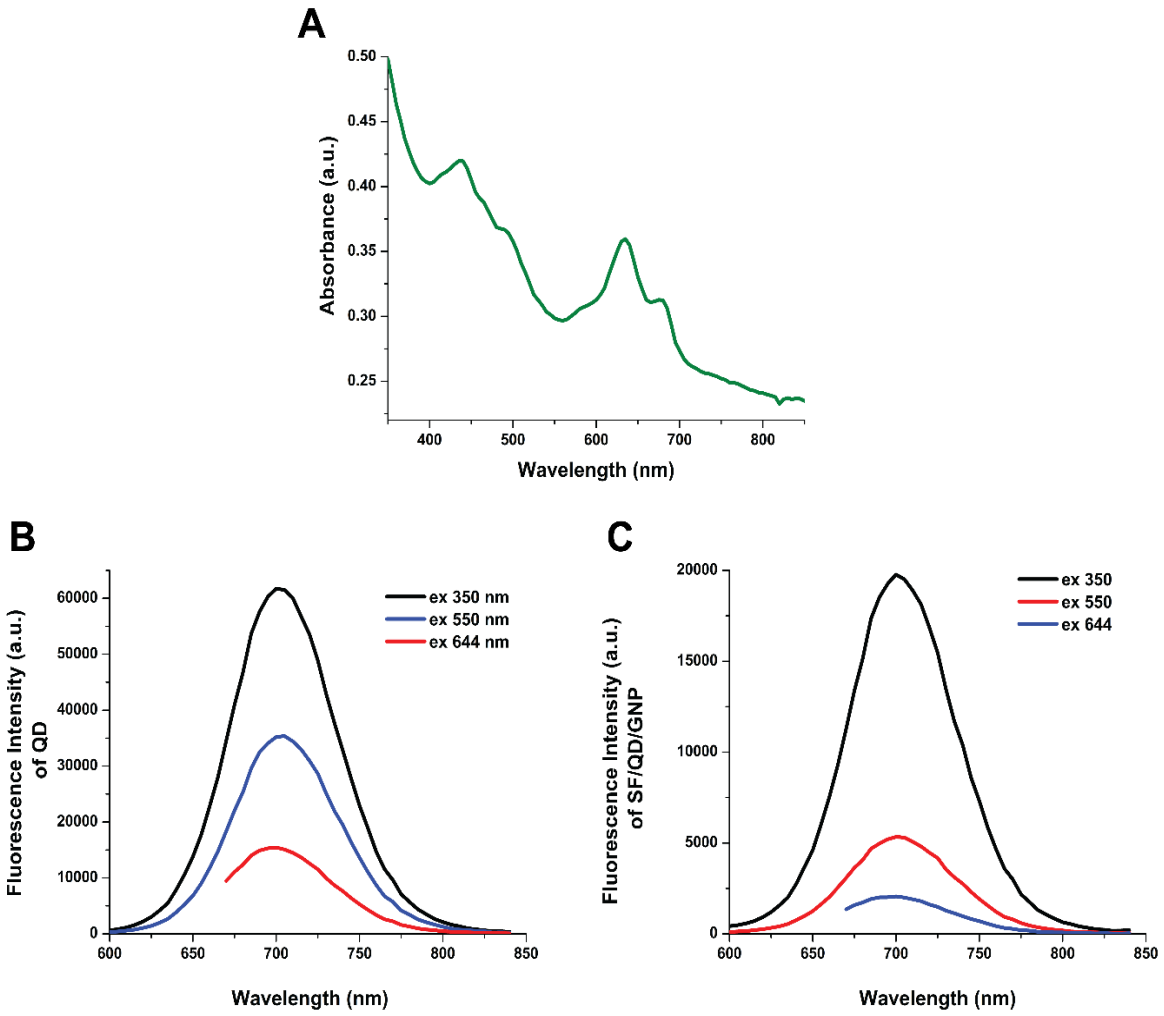


**Figure 3.5:** (A) Absorbance spectra of *Synechococcus* sp. and fluorescence emission spectra at the different excitation wavelength of (B) QD and (C) SF/QD/GNP solutions.

The band gap data were discerned from the band structure plot (Figure 3.7 A). The SF with the highest band gap of 4.09 eV and GNP with the lowest band gap of -3 eV are finally compromised to a band gap energy of 2.9 eV in the nanocomposite matrix, which is in a desirable range of 1 – 3 eV for electronic and photonic application (Rajbanshi *et al*., 2014). Markedly, graphene can act as an excellent relay material for the generated electrons due to its unique linear electronic dispersion capability. The decrease in the band gap of the

SF hybrid nanocomposite indicates an interaction of the QD with crystalline graphene in the composite system (Asha *et al*., 2016). The reduced band gap could also be correlated with the redshift (~ 4 nm) of the absorption spectra of the nanocomposite system after doping with GNP (Figure 3.7 B). These data have confirmed a rational interaction to yield the optoelectronic hybrid nanocomposite and the establishment of FRET between QD and *Synechococcus* sp. cells.

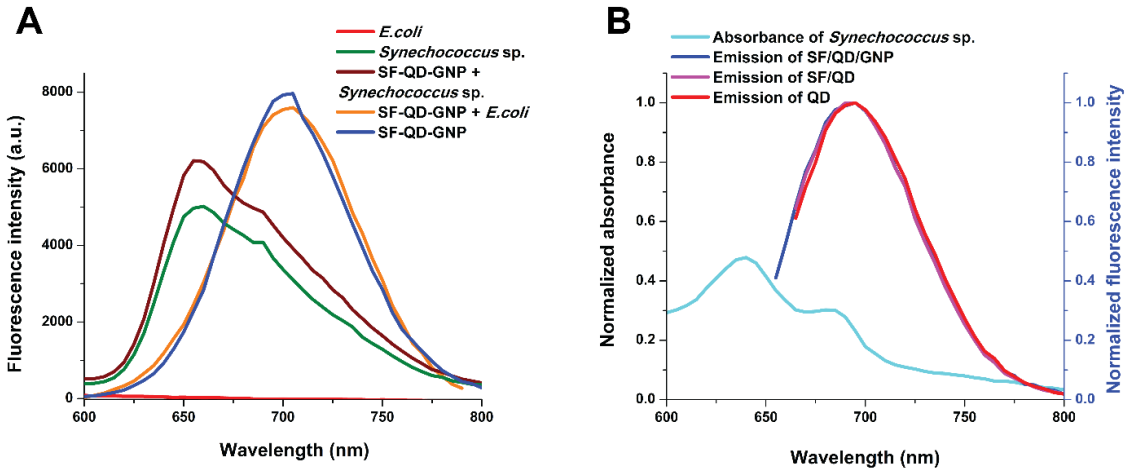


**Figure 3.6:** (A) Fluorescence intensity of *Synechococcus* sp. and SF/QD/GNP (donor) (at $\lambda_{ex\ 550\ nm}$) in absence and presence of *Synechococcus* sp. (acceptor). Fluorescence intensity of SF/QD/GNP in presence of *E. coli* as acceptor has also been recorded as the control. (B) Normalized absorption spectra of *Synechococcus* sp. and photoemission spectra of QD, SF/QD and SF/QD/GNP at $\lambda_{ex\ 644\ nm}$. The mean of three independent experiments has been plotted.

**Table 3.2:** Quantum yields of donors, overlap integrals and Förster distances calculated for donor-acceptor pairs using *Synechococcus* sp. as the common acceptor.

| Donors | Quantum yield<br>**Φ** | Integral overlap<br>**J ($cm^3 M^{-1}$)** | Förster radius<br>**$R_0$ (Å)** |
|---|---|---|---|
| **QD** | 0.40 | $3.2 \times 10^{15}$ | 53.74 |
| **SF/QD** | 0.24 | $2.93 \times 10^{15}$ | 48.59 |
| **SF/QD/GNP** | 0.18 | $3.25 \times 10^{15}$ | 47.12 |

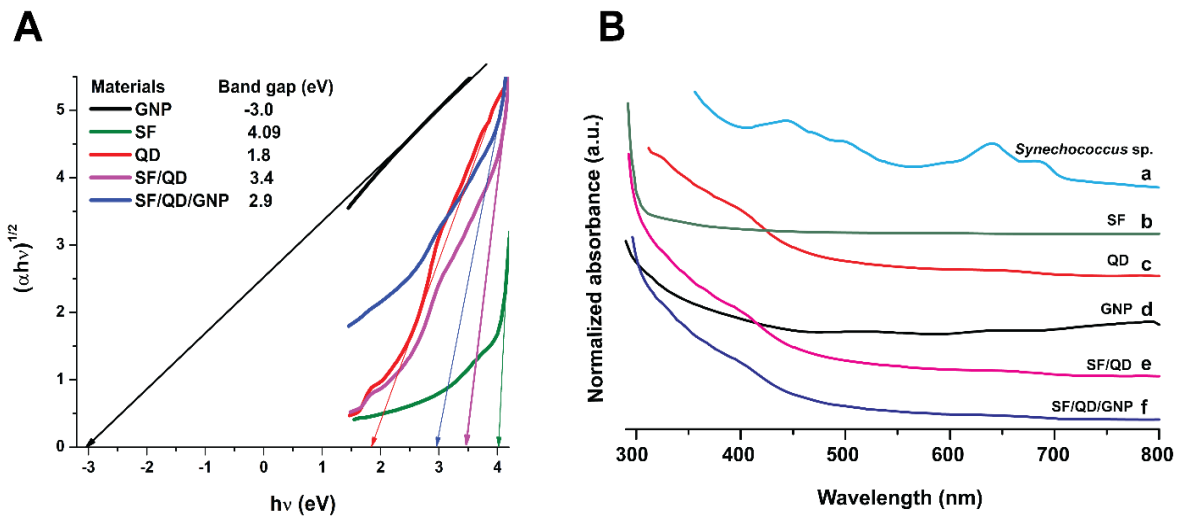


**Figure 3.7:** (A) Variation of $(\alpha h\nu)^{1/2}$ as a function of the photon energy h$\nu$. (B) Absorbance spectra of (a) *Synechococcus* sp. (b) SF (c) QD (d) GNP (e) SF/QD and (f) SF/QD/GNP.

FRET is extremely sensitive to the separation distance between the donor and acceptor and their extent of spectral overlap. Non-radiative exciton transfer is expected to substantially truncate the exciton lifetime of the donor (Clapp *et al*., 2004). The fluorescence intensity decay profile with time was measured for the interaction between the nanocomposite with the *Synechococcus* sp. cells. Shortening of the fluorescence lifetime of QD (as the donor) was detected in presence of *Synechococcus* sp. (as the acceptor) (Figure 3.8). These observations confirmed the successful FRET between the SF/QD/GNP nanocomposite and the cyanobacterial cells.

To understand the interaction between QD and SF, CD analysis of SF with and without doping with QD was performed. Freshly extracted native SF solution (0.5 mg $mL^{-1}$) exhibited $\alpha$-helix 11.8 %, $\beta$-sheet 16.7 %, $\beta$-turn 20.2 % and random coil 51.3 % which nearly conformed to a previous report (Li *et al*., 2008). When QD with increasing concentration was doped on SF, the $\beta$-sheet content of SF was consistently increased up to 14.6 % and $\alpha$-helix and random coil were decreased by 12 % and 3 % respectively (Figure 3.9). The results clearly indicate reorientation of the secondary structure of the SF protein upon its interaction with the QD, shifting towards a hydrophobic $\beta$-sheet dominant architecture.

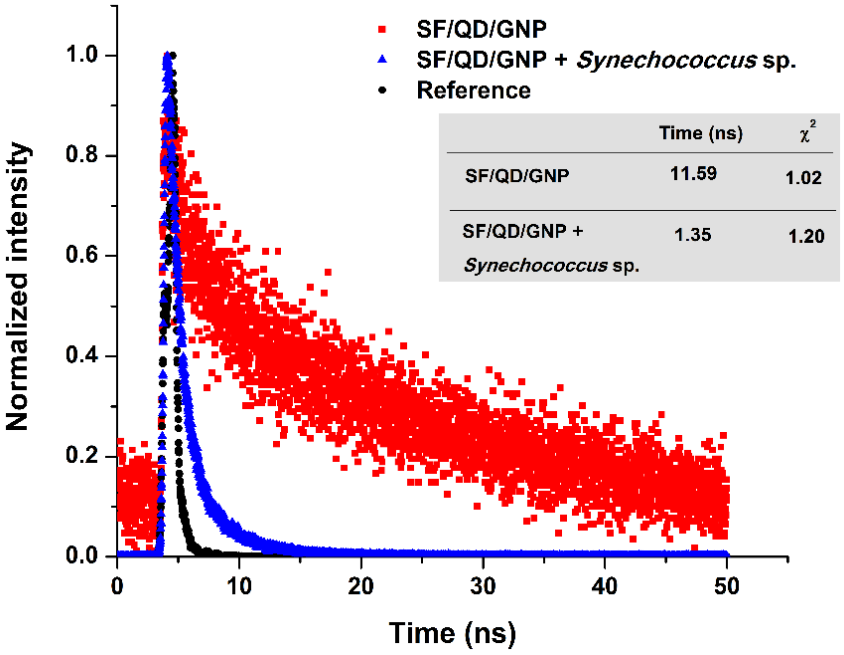


| | Time (ns) | $\chi^2$ |
|---|---|---|
| SF/QD/GNP | 11.59 | 1.02 |
| SF/QD/GNP + *Synechococcus* sp. | 1.35 | 1.20 |

**Figure 3.8:** TRPL profile of SF/QD/GNP, SF/QD/GNP + *Synechococcus* sp. and (inset table) fluorescence lifetimes (t) and $\chi^2$ value of fitting for fluorescence intensity decay profile with time.

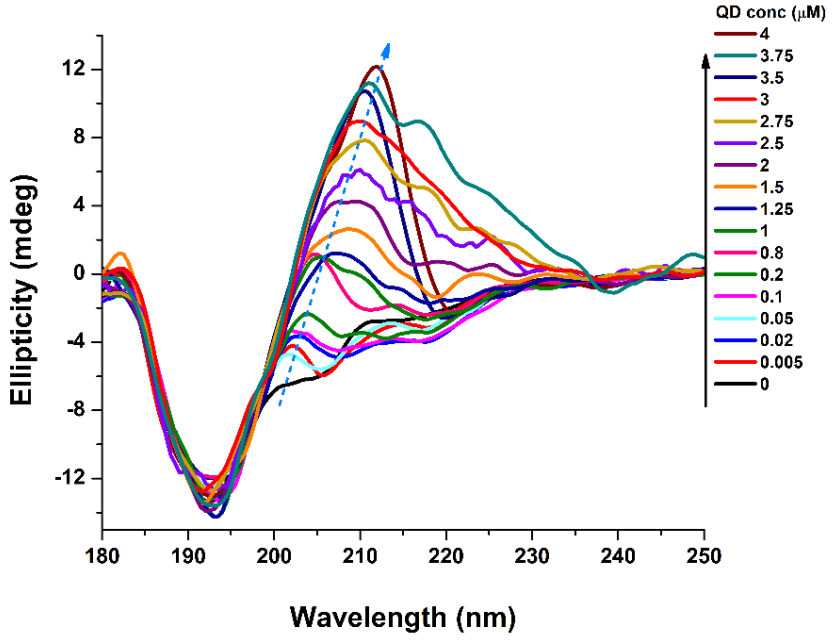


**Figure 3.9:** CD spectroscopy of SF (0.5 mg $mL^{-1}$) with varying concentration of QD (0 - 4 μM).

From the ITC analysis (Figure 3.10), the binding constant, $K_a$ ($LM^{-1}$) and the number of binding sites, *n*, between QD and SF were determined to be $1.56 \times 10^4 \pm 4.46 \times 10^2$ and 0.93 respectively. The ITC analysis provides further the thermodynamic parameters, change in enthalpy ΔH (cal $mol^{-1}$) of $-6.43 \times 10^4 \pm 416$, change in entropy, ΔS (cal $mol^{-1}$ $K^{-1}$) of -190 and change in Gibb's free energy, ΔG (cal $mol^{-1}$) of -7680 on the interaction between QD and SF. The negative ΔG indicates that the interaction process is spontaneous (Perozzo *et al*., 2004). These parameters denote favorable interactions leading to a rational binding between these two entities with a moderate binding affinity that helped in retaining photoemission and stability of QD.

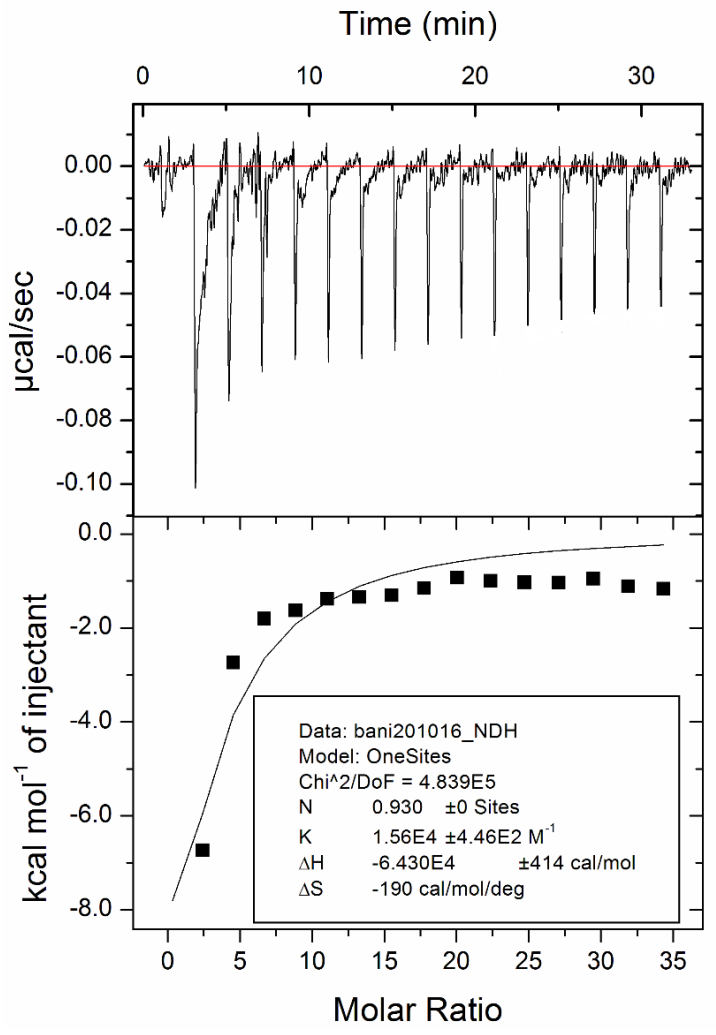


**Figure 3.10:** ITC isotherms of SF interactions with QD. The top panel represents the raw heats of binding obtained by titrating SF to QD. The lower panel is the binding isotherm fitted to the raw data. The solid line represents the nonlinear best fit to the data assuming a single-site binding model.

### 3.3.3 Performance of the nanocomposite anode in PMFC setup

The SF/QD/GNP based nanocomposite on GE as anode with *Synechococcus* sp. as biocatalyst and ferricyanide based abiotic cathode were assembled in a dual chambered PMFC setup (Figure 3.11 A). The PMFC was operated under photoheterotrophic condition using a circadian cycle of 12 h light: 12 h dark at 25 °C, without using an electron transfer mediator. The OCP of the PMFC with different anodes were continuously measured and observed its attainment to a steady state in all cases except for GE, before reaching 90 h of operation. The OCP of the GE was low and fluctuating (0.05 – 0.2 V) within that period. A clear effect of inclusion of SF in the GE was visible on the OCP as the steady state potential was increased to ~ 0.55 V. Furthermore, when QD was included in the SF/GE to make SF/QD/GE, the steady state potential was marginally declined (~ 16 %) to 0.46 V. However, with the inclusion of GNP to make SF/QD/GNP/GE, the OCP was substantially increased and reached a stable state of ~ 0.66 V. This revealed the effect of highly conductive GNP on the enhancement of the bacterial metabolic charge on the electrode surface.

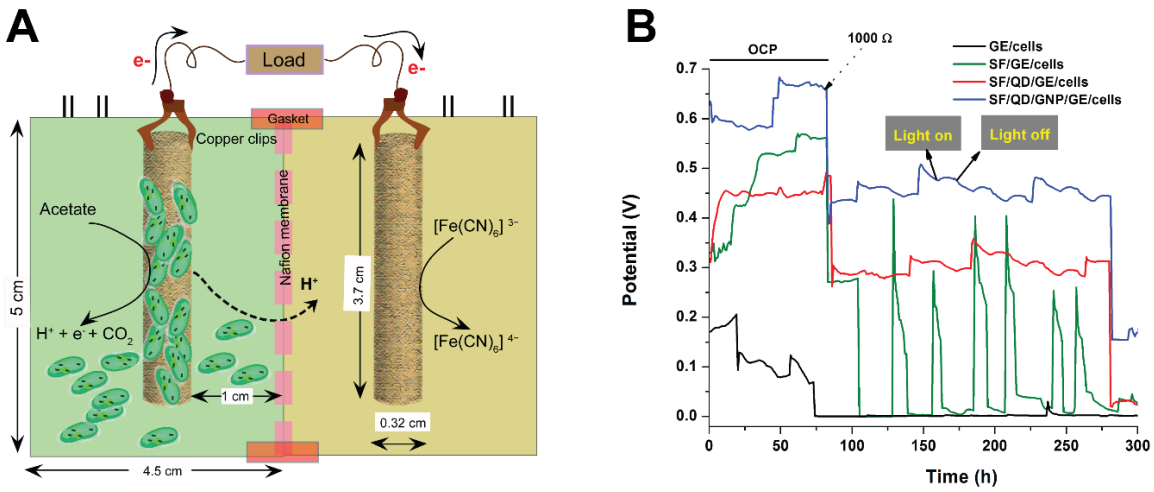


**Figure 3.11:** (A) Schematic of the two-chambered PMFC used in the present investigation. (B) Steady state OCP and potential discharge profiles (V vs time) under a load (1000 Ω) for GE, SF/GE, SF/QD/GE and SF/QD/GNP/GE anodes in PMFC. At the onset of all the cases, an active bacterial cell density of $OD_{750}$ ~ 0.4 was used in the anodic chambers.

The OCP of the PMFCs with different anodes namely, GE, SF/GE, SF/QD/GE and SF/QD/GNP/GE was reduced by (%), ~ 99, 50, 37, 32 respectively following the steady state level at 92 h of operation when a load (1000 Ω) was connected to the PMFC.

Interestingly, there was a stark difference in the captured potential pattern of the PMFC between the anodes with and without QD. In absence of QD, the potential oscillate drastically with the varying light intensities as per the light-dark cycle (Figure 3.11 B). The cyanobacteria showed positive photo-response. During the light-cycle, the electrons generated from the photosynthesis aid in up-surging the potential. Whereas, in the dark-phase, the lack of photosynthesis as well as increasing catabolic processes succumb to metabolic electron loss with the linked potential drop in the PMFC (Bombelli *et al*., 2012). Whereas, with the anodes containing QD, a nearly steady state potential was generated till 280 h run time of the PMFC, due to surging of the cyanobacterial photosystems with appropriate light energy even in low light conditions. Moreover, the SF/QD/GNP/GE anode delivered the highest potential; hence this anode was utilized for further study on the PMFC.

The power curves for the PMFC were generated with SF/QD/GNP/GE as the anode (Figure 3.12 C). Experiments with the control (bare GE) (Figure 3.12 A) and SF/GE (Figure 3.12 B) were run for comparison to understand the role of QD and GNP composites. The maximum current and power densities of the PMFC with SF/QD/GNP/GE were 1.89 A $m^{-2}$ and 0.61 W $m^{-2}$, respectively which were corresponding ~ 5.7 and ~ 50.8 times higher than the values (0.33 A $m^{-2}$, 0.012 W $m^{-2}$) obtained with the bare GE and ~ 1.7 and ~ 2.8 times higher than the values (~ 1.1 A $m^{-2}$, 0.22 W $m^{-2}$) obtained with the SF/GE. The positive impact of QD on the differently fabricated anodes was revealed from the fading of the current reversal post illumination cycle of PMFC operation with the load connected. The currents (A) in the light: dark phases for SF/GE ($3.7 \times 10^{-4}$: $1.88 \times 10^{-4}$), SF/QD/GE ($3.26 \times 10^{-4}$: $2.95 \times 10^{-4}$) and SF/QD/GNP/GE ($4.83 \times 10^{-4}$: $4.43 \times 10^{-4}$) are shown in the parentheses and the corresponding current differences were 1.82, 0.31, and 0.4.

The results clearly demonstrated the facilitating role of QD that helped to establish FRET with the photosystems of the bacteria enabling the underlying cells in the biofilm to harvest photon even at a low light condition in the dark phase to generate photocurrent. The electronically coupled GNP in the nanocomposite matrix facilitated the relay of the metabolic electrons to the electrode owing to its exceptional high charge storage and electrical properties (Yong *et al*., 2014).

There was a substantial improvement of potential output from the control experiment to the SF/QD/GNP/GE through SF/GE based runs in the PMFC as evident from the polarization curves. The improvement was particularly visible in the section dealing with the activation and ohmic overpotentials, which implied the fact that the nanocomposite anode promotes harvesting charge as well as facilitates charge transfer both on the anode (for the electron) and through the electrolytes (for the proton). The activation polarization is mostly influenced by the processes involving adsorption of reactant species, desorption of product species, transfer of electrons across the double layer cell membrane, and the physical nature of the electrode surface (Du *et al*., 2007). The fill factor ($F_f$) is a significant factor that characterizes the fuel cell performance (an ideal case pertains to $F_f$ = 1). The superior performance of the nanocomposite anode was evident with higher $F_f$ = 0.48 compared to SF/GE (0.31) and GE (0.24). Based on the energy of the input light and output power generation in the PMFC, the LCE (%) was calculated to be 0.08 ± 0.01, 1.46 ± 0.32 and 4.01 ± 0.68 for GE, SF/GE and SF/QD/GNP/GE anodes, respectively. A maximum LCE from solar energy to bioenergy and electric power attained previously were 3.79 ± 0.76 % and 2 – 2.5 % respectively (Chen *et al*., 2015a; Tsujimura *et al*., 2001).

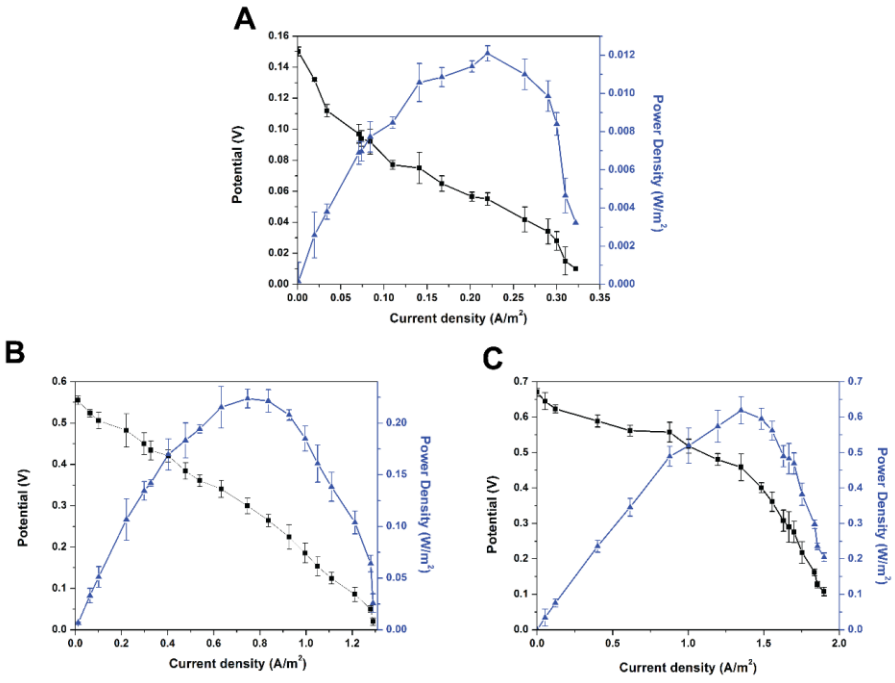


**Figure 3.12:** Polarization and power density graphs of the PMFCs with anodes as (A) GE (control), (B) SF/GE and (C) SF/QD/GNP/GE.

### 3.3.4 Characterization of anodes and electron transfer mechanism

Various parameters involved in the PMFC, pertaining to the anode electrochemistry and kinetics that influence the performance of a fuel cell were deduced. Initially, the charge transfer behaviors of the differently fabricated anodes were examined by CV analysis using $FeCN_6^{-3}$ as redox indicator (Figure 3.13). A pair of quasi-reversible peaks for $Fe^{-2}/Fe^{-3}$ system at 0.43 V and 0.010 V was detected. In SF/GE and QD/SF/GE, the redox peak current was decreased by ~ 33 % and ~ 23 %, respectively. The marginal gaining of the current response upon inclusion of QD in SF/GE may be due to the ionic coating material (mercaptocarboxylic acid) on QD that likely to increase the charge on the electrode surface at the operating pH value. Addition of GNP on the QD/SF/GE had drastically increased the current by ~ 55 %. The properties of graphene material, such as high electronic conductivity (7200 S $m^{-1}$) and large specific surface area (up to 2600 $m^2$ $g^{-1}$) expected to contributes to the current increase (Lv *et al*., 2013).

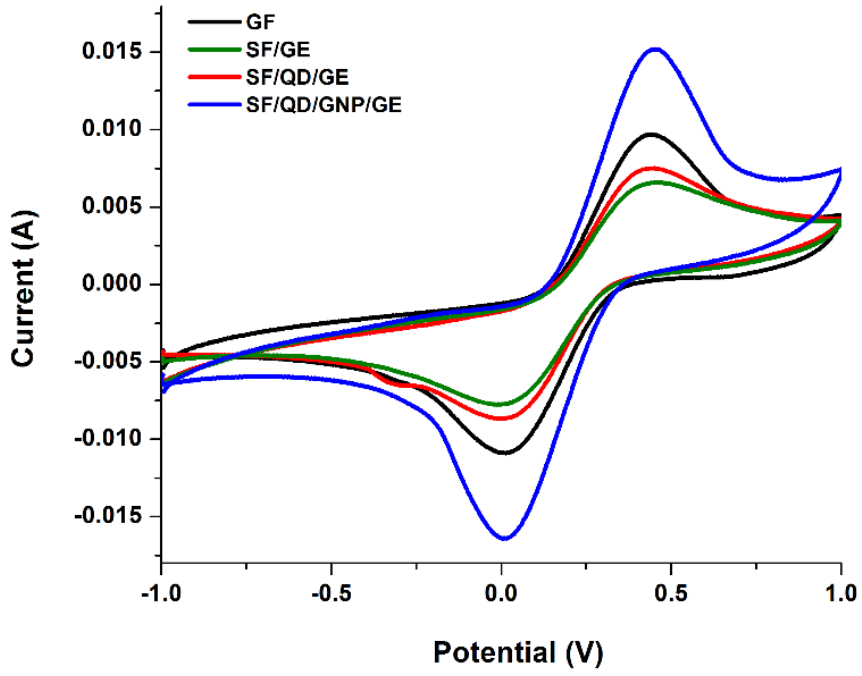


**Figure 3.13:** CV profiles (100 mV $s^{-1}$) of bare and different modified anodes in 5 mM $K_3FeCN_6$ and 0.1 M KCl solution in PBS buffer (pH 7).

EIS was performed to understand the internal resistance for which the Randles circuit was chosen to fit the impedance outputs. On the Nyquist plots (Figure 3.14 a-d), the ohmic resistance/solution resistance ($R_{ohm}$) is indicated by the high frequency intercept with the x-axis and the charge transfer resistance ($R_{ct}$) is indicated by the diameter of the semicircle (Lv *et al*., 2013). The relevant equivalent circuit (inset Figure 3.15) consists of a $R_{ohm}$, connected in series with a parallel combination of an electrochemical $R_{ct}$ and a Warburg's diffusion element (W) with a double layer constant phase capacitance ($C_{dl}$). With SF coating, $R_{ct}$ increased and electroactive surface area ($S_a$) decreased due to insulating properties of the biopolymer (band gap 4.09 eV). Whereas, QD and GNP imparted a positive effect on decreasing $R_{ct}$ and increasing $S_a$ (Table 3.3). As compared to the control (GE without biofilm), almost nine-fold decrease in $R_{ct}$ was observed in case of the GNP embedded hybrid nanostructure without biofilm. The formation of biofilm on SF/QD/GNP/GE is conspicuous from FESEM analysis (Figure 3.3 b). The extent of biofilm coverage on the anodic surface showed a direct influence on the power improvement of the PMFC. A marginally higher $R_{ct}$ (with biofilm) for SF/QD/GE than SF/QD/GNP/GE may be attributed to the lack of GNP in the matrix. The imaginary impedance mainly originates from the $C_{dl}$, reflecting the changes at the electrode interface as well as the adsorption/adhesion process on the electrode surface (Bayoudh *et al*., 2008). GNP appended hybrid nanocomposite displayed the highest $C_{dl}$ owing to its much more accessible surface area for charge storage (Sullivan *et al*., 2014). The solution resistance had minor change indicating that it was not intensely affected by the chemical transformations occurring on the electrode surface. The lowest $R_{ct}$ of the operated nanocomposite anode manifested the underlying electroactive nature of the biofilm formed.

The CV analyses (under non-turnover conditions) of the differently fabricated anodes withdrawn from the PMFC after 280 h of run time, revealed the presence of two redox species. The corresponding formal potentials of the redox couples [($E_{pa}$ + $E_{pc}$)/2] were -156 mV and + 225 mV (Figure 3.16 a-d). These quasi-reversible peaks (> 59/n mV) were absent in the pristine nanocomposite electrode (not run in PMFC) (Figure 3.17). The potentials at ~ -156 mV coincides well with the free flavin, while + 225 mV is closer to multi-heme cytochromes (*cyt*) (Larom *et al*., 2015; Xu *et al*., 2016). Cyanobacterial strains contain 1 – 4 paralogs of cytochrome $c_6$ (*cyt* $c_6$), which is a small heme protein that can act

as electron transfer agent and possess lower midpoint potential (< 300 mV) in *Synechococcus* sp. (Bell *et al*., 2009; Bernroitner *et al*., 2009). The surface coverage by the redox species present in the biofilms followed the order GE < SF/GE < SF/QD/GE < SF/QD/GNP/GE which is consistent with the order of electron transfer rate (considering both light and dark phases) by different biofilms. These differences are signposts of the amount of biomass associated with different biofilms (Guo *et al*., 2013).

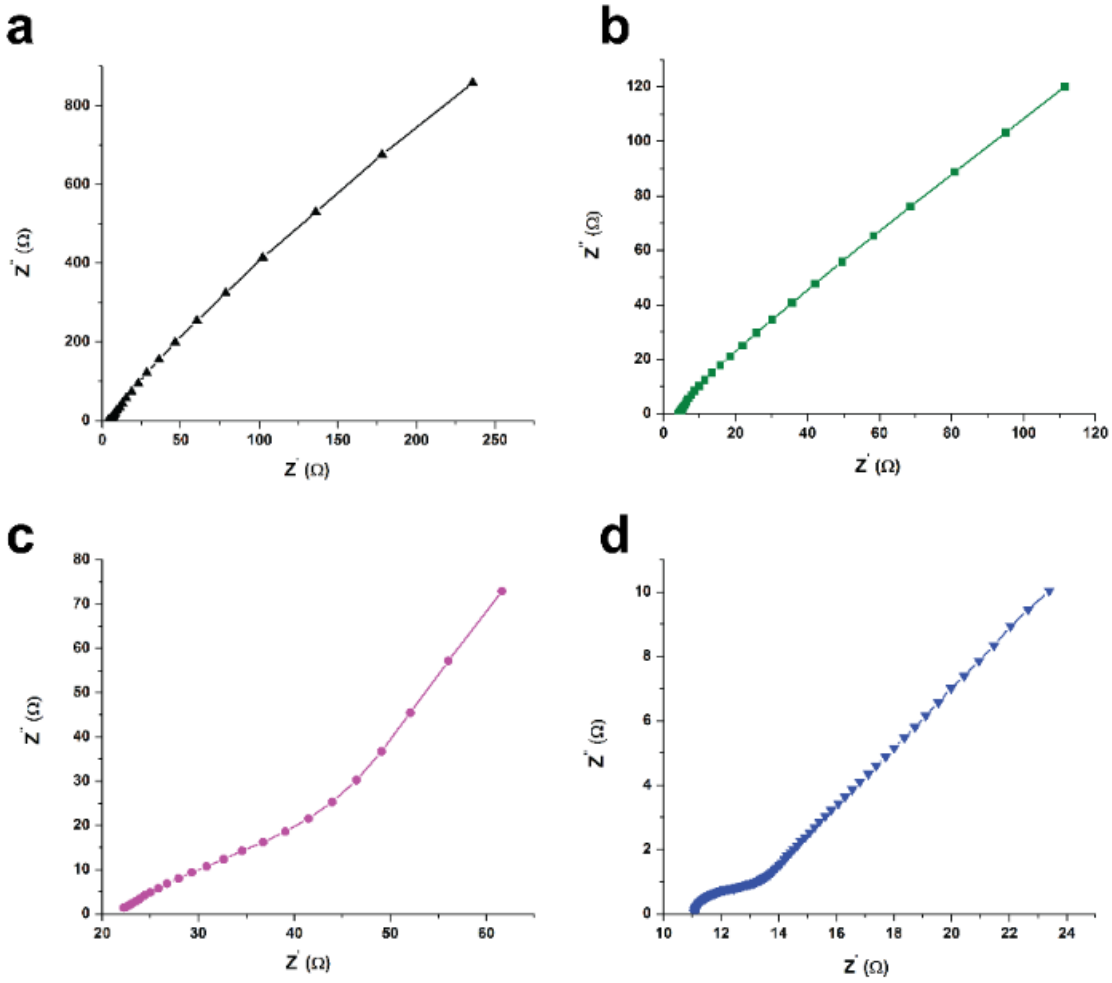


**Figure 3.14:** Nyquist plots of anodes (a) blank GE and with different modifications, (b) SF/GE, (c) SF/QD/GE and (d) SF/QD/GNP/GE.

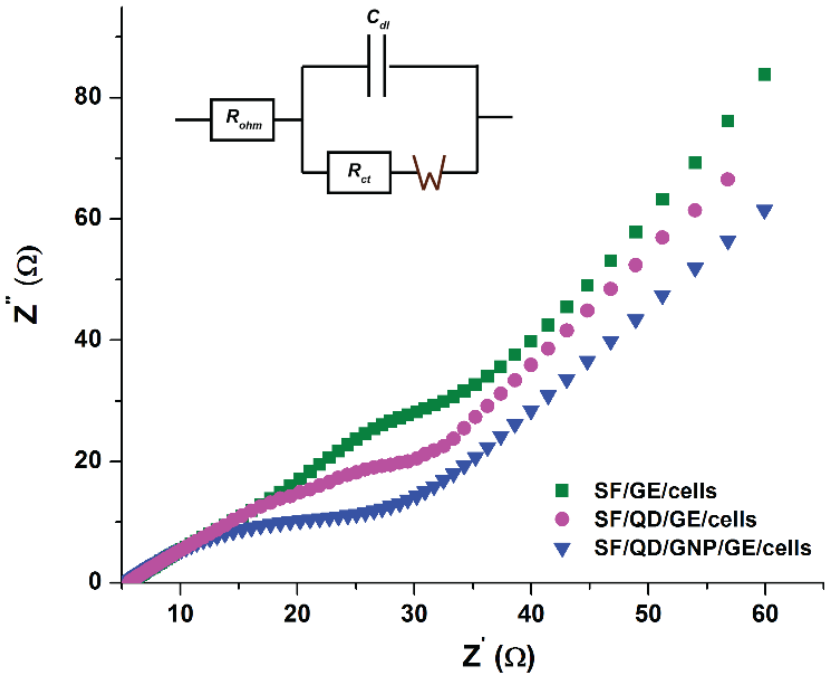


**Figure 3.15:** Impedance profile of different anodes with bacterial cells after PMFC run (inset Randles circuit).

The absorbance spectrum of the bacterial cells was examined to understand the presence of *cyt* (Figure 3.18 A). Under aerobic condition when the *cyt* is in the reduced state, the culture broth displayed the characteristic soret peak at ~ $\lambda_{415\ nm}$. Nevertheless, under the anoxic state in the PMFC, when the *cyt* was in the oxidized condition, the intensity of the soret peak was decreased with a shift to ~ $\lambda_{409\ nm}$ (Bell *et al*., 2009). In the reduced state when the *cyt* were excited at $\lambda_{350\ nm}$, they fluoresced with maxima at $\lambda_{402-437\ nm}$ (Figure 3.18 B). The fluorescence intensity was reduced by 1.6 fold when the culture from PMFC was transformed to an oxidized state (Esteve-Núñez *et al*., 2008). The aerobic culture when treated with $K_3Fe(CN)_6$ (2mM), analogous drop in the fluorescence intensity was perceived (Figure 3.18 B). Overall, the above results suggest the presence of two electroactive compounds in the biofilm that could electronically contact with the hybrid nanocomposite anode. These compounds are tentatively, assigned as flavins and *cyt*. Flavins like luteolin, has been reported to increase the photon transfer and trapping capacity in the photosynthetic system in cyanobacteria (Huang *et al*., 2015). In the present case, the flavin-like compound with low potential of ~ -156 mV can be safely attributed to the role for directly channelizing

the biocatalytic electrons to the electrode that generates the current in the PMFC. However, further investigation is warranted to understand the exact chemical nature of these compounds.

**Table 3.3:** Various parameters pertaining to the anode electrochemistry and kinetics estimated for the different fabricated anodes.

| Anode | GE | SF/GE | SF/QD/GE | SF/QD/GNP/GE |
|---|---|---|---|---|
| **Electron transfer rate, $\Gamma$ ($e^-$ per second) (light/dark)** | $3.125 \times 10^{13}$/ $1.44 \times 10^{13}$ | $2.31 \times 10^{15}$/ $1.18 \times 10^{15}$ | $2.04 \times 10^{15}$/ $1.84 \times 10^{15}$ | $3.02 \times 10^{15}$/ $2.77 \times 10^{15}$ |
| **Solution resistance, $R_{ohm}$ (Ω)** | 5.52 | 2.91 | 2.74 | 3.2 |
| **Charge transfer resistance, $R_{ct}$ (Ω)** | 50.3 (32.6)* | 84.0 (42.5)* | 44.72 (37.7)* | 37.8 (3.6)* |
| **Capacitance, $C_{dl}$ (mF)** | 2.62 | 3.69 | 4.38 | 10.4 |
| **Surface coverage by redox species, $S_e$ (pM cm$^{-2}$)** | $0.220 \times 10^{-12}$ $(3.37 \pm 0.06)$** | $0.785 \times 10^{-12}$ $(2.72 \pm 0.03)$** | $10.2 \times 10^{-12}$ $(3.01 \pm 0.08)$** | $11.2 \times 10^{-12}$ $(5.73 \pm 0.12)$** |
| *without biofilm, ** Electroactive surface area, $S_a$ (cm$^2$) without biofilm. | | | | |

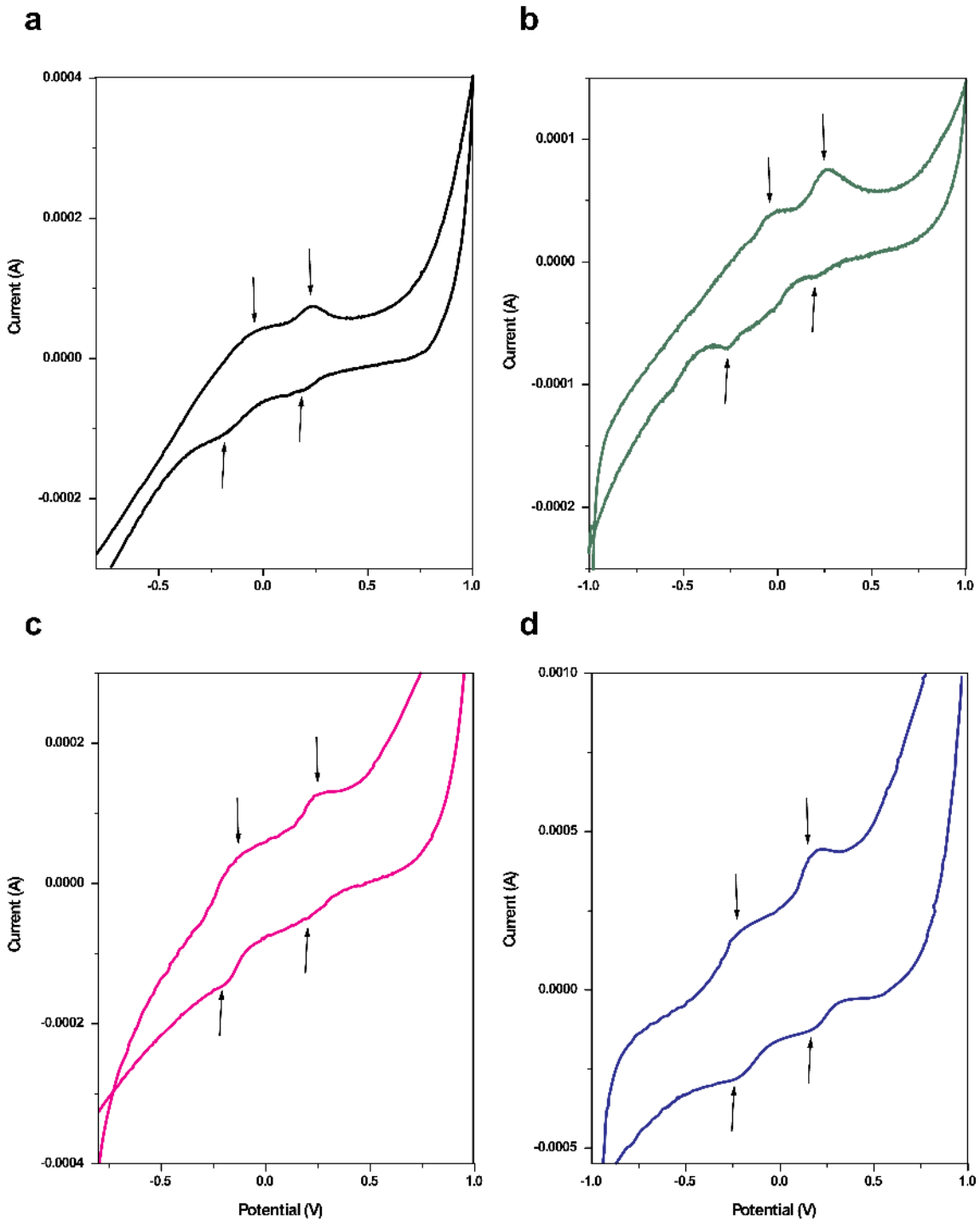


**Figure 3.16:** Non-turnover CV analyses (scan rate: 1 mV/s, vs Ag/AgCl) of different modified anode surfaces (a) GE, (b) GE/SF, (c) GE/SF/QD and (d) GE/SF/QD/GNP anodes with biofilm. The inset arrows indicate the redox peaks.

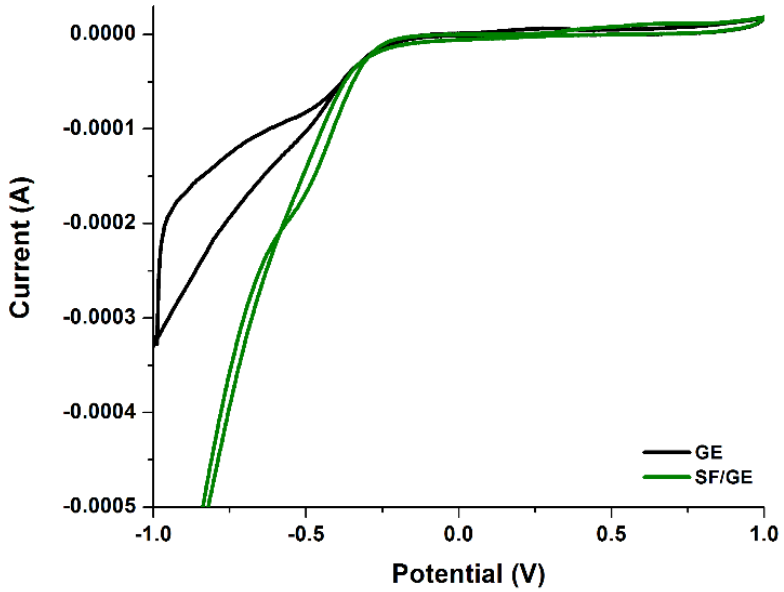


**Figure 3.17:** CV of blank GE and SF/GE in PBS buffer (pH 7) at a scan rate of 1 mV/s.

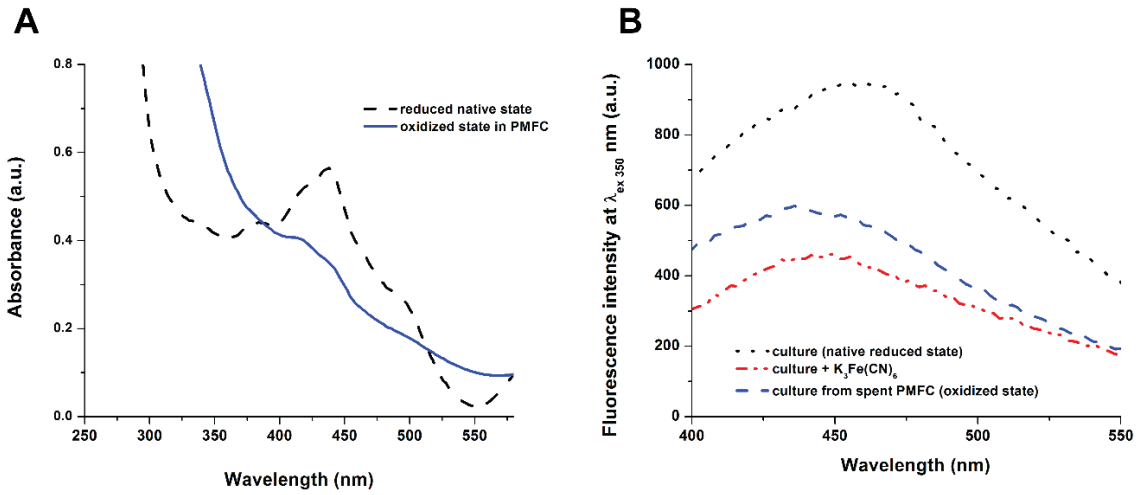


**Figure 3.18:** Harvested cells in PBS (pH 7), $OD_{750}$ ~ 0.2 from PMFC were subjected to (A) Absorbance spectra and (B) Fluorescence spectra under different conditions at $\lambda_{ex\ 350\ nm}$.

## 3.4 Conclusion

This chapter elaborates the development of a novel silk-based nanocomposite matrix endowed with biocompatible, optoelectronic and electroactive properties suitable for bioanode fabrication for a PMFC, by rationally doping QD and GNP in the silk fibroin. The nanocomposite matrix when, cast on graphite anode promoted rapid biofilm growth of *Synechococcus* sp., supported FRET to surge the photosystems of the underneath bacteria in the biofilm and provide an electroactive surface for relaying metabolic electrons from the cells to the electrode through DET during operation of the PMFC. The cumulative action of these properties not only enhanced the power density but also stabilizes the power during the dark phase of the PMFC operation. Each of these functions of the nanocomposite matrix has been adequately evaluated in the light of their evolved properties in the hybrid state to validate the results. SF also interactively retained the significant activity of the QD in its matrix as evident from the remolded $\beta$-structure of the protein and residual fluorescence activity of the QD in the nanocomposite matrix. From the high integral spectral overlap and Förster radius, a significant FRET from the QD in the nanocomposite to the photosystems of *Synechococcus* sp. has been confirmed. The highly conductive property of the GNP made it possible to transform the nanocomposite matrix to a highly electroactive surface (band gap of 2.9 eV) surpassing the semiconducting behavior (band gap of 4.09 eV) of the silk film thus, facilitating the direct flow of cellular electrons from the biofilm to the graphite electrode. A seamless transfer of biocatalytic electrons is demonstrated from the clear redox peaks obtained from the bioelectrode in a non-turnover study. The involvement of DET mechanism in generating current in this PMFC is further validated by the fact that no electron transfer mediator was used to operate the system. We envision that our approach will be a big step forward not only to improve the overall current density in a PMFC but also to sustain its power at low light operating conditions due to FRET guided surging of the photosystems of the cyanobacteria.

# Chapter IV

## Fabrication of a small scale PMFC for detection of alcohol

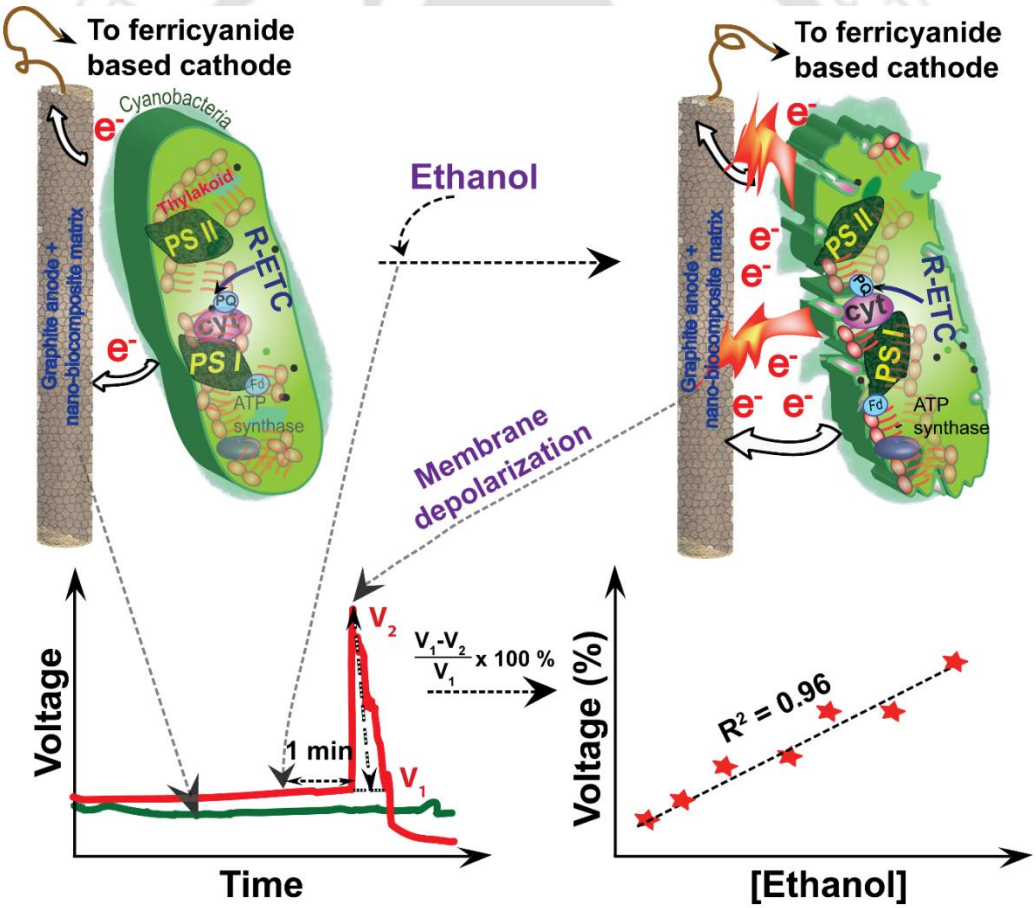


*Graphical abstract on bacterial membrane depolarization-linked fuel cell potential burst as signal for selective detection of alcohol*

# Chapter IV

## Fabrication of a Small Scale PMFC for Detection of Alcohol

### 4.1 Overview

The search for novel bio-sensing techniques is becoming an integral R&D activity in various sectors including environmental monitoring, diagnostics, fuel, food and pharmaceutical industries. This is owing to certain distinct advantages of biosensors such as, higher selectivity, sensitivity, and better scope for improving the properties of the biorecognition elements over the conventional chemical and physical recognition based sensors (Su *et al*., 2011). Among the different biorecognition elements used in biosensor applications, whole cell-based recognition elements find special interest in the fields where information related to toxicology, pharmacology, and cell physiology of a sample is to be gathered which is normally difficult to achieve by using the molecule-based recognition elements in the biosensor platforms. Additionally, the whole cell-based recognition systems offer better stability under the ambient conditions as compared to their free bio-molecular counterparts. The low selectivity and sensitivity of the microbial biosensors are often pacified by their considerable low analysis cost, long shelf life, and robust nature to endure environmental conditions (Lim *et al*., 2015). Microbial biosensors with different transduction principles have been explored among which, MFC sensors have received increasing attention over the last few years due to their fabrication simplicity, feasibility to operate in external environments in a self-sustained manner, low cost of operation and sensitive signal transduction mechanism (Dávila *et al*., 2011). However, most of these MFC-based biosensors are snagged with long response time as the response acquired from the interaction of the target species with the catalytic cells in the MFC is usually governed by the metabolism and growth of the organisms on the electrode surface. The long response time and poor selectivity of the MFC-based biosensors discourage their applications in the fields where rapid and specific detection of the targets is an important task. The requirement of cellular growth of the biocatalysts in the MFC-based sensors is another constraint that

impedes the development of small scale and chip-based-MFC biosensors. Hence, a strategy to impasse the aforesaid challenges is explored in this work to develop MFC based biosensors with fast response time, selective detection capability, low cost and portable design for extending their applications to emerging areas, such as healthcare, clinical, and fermentation industries.

There is a plethora of reports on the applications of various pure or consortium bacteria as catalysts for MFC (Abrevaya *et al*., 2015; Li *et al*., 2016). Among these reports, only a limited work has been directed towards exploring cyanobacteria PMFC. These studies are mostly confined to unearth the basic information on the suitability of the cyanobacteria as MFC catalysts for their potential applications in power generation and wastewater treatment. Certain interesting traits that have been widely cited to endorse the application potential of cyanobacteria in the fields of energy and environment are their flexible growth conditions, tolerance to high salt concentrations and organic contaminants, and their ability to form stable biofilms. These photosynthetic microbes can grow well under phototrophic and heterotrophic conditions. Moreover, the existence of interlinking photosynthetic and respiratory pathways in cyanobacteria has been acclaimed as an interesting trait for facilitating metabolic electron flux for a sustained current generation in PMFC during both the day and night (Choi, 2015). The cyanobacterial phototrophic nature obviates the need of providing carbon source that can simplify growth sustenance on small scale electrode surfaces for developing miniaturized PMFCs for powering microscale device and sensor applications. Notably, the efforts towards miniaturization of PMFCs are limited in-spite of the fact that small scale PMFCs improve mass transport and reduce internal resistance (Fraiwan *et al*., 2016; Lee and Choi, 2015).

The importance of a portable low cost device for rapid and selective determination of alcohol is sharply increasing for various applications. However, such an efficient portable low-cost alcohol detection system is not widely available in the global market. Alcohol sensor for selective detection of methanol and ethanol has vast importance because of the fact that methanol is toxic in alcoholic beverages, and a less efficient blend than ethanol in fuel. Different alcohol sensors and biosensors reported so far have their own set of advantages (Thungon *et al*., 2017). However, a majority of these reported sensors including

the enzyme-based biofuel cell devices failed to meet the demand while setting fast response time (in seconds), selectivity (no cross-reactivity to other compounds), portability and simple instrumentation as the collective performance factors for detection of alcohol.

In this chapter, the application of cyanobacteria based PMFC to detect ethanol selectively in a short response time has been reported which is based on a novel recognition technique that generates the potential signal instantaneously upon addition of alcohols. This concept was further translated successfully into a chromatographic paper-based PMFC (p-PMFC) platform to detect ethanol. The paper as the sensor platform is known to offer many advantages among which low-cost, portability, disposability, biocompatibility, ease of storage, and liquid wicking property that eliminates the need of external pumps are relevant for the present PMFC work (Kakoti *et al*., 2015; Martinez *et al*., 2010).

## 4.2 Experimental approaches

### 4.2.1 Materials

SF was extracted from *Bombyx mori* cocoons following the protocol in our work described in chapter III. The growth of *Synechococcus* sp. was maintained in ASN III medium at 28 ± 2 ºC with a cycled photoperiod of 12 h of 15 W $m^{-2}$ of white light: 12 h dark. Bis-(1,3-dibutylbarbituric acid) trimethine Oxonol ($DiBAC_4(3)$, $\lambda_{ex\ 490\ nm}$ and $\lambda_{em\ 516\ nm}$) was obtained from Invitrogen™. Graphene nanoplatelets (GNP) and CdTe quantum dots (QD) were acquired from Graphene Laboratories Inc. (New York) and MK Impex Corp. (Canada), respectively. Isomolded graphite electrode (GE) (0.318 cm diameter x 30.48 cm length) was purchased from GraphiteStore.com (USA). 3-[4,5-dimethylthiazole-2-yl]-2,5-diphenyltetrazolium bromide (MTT) and potassium ferricyanide ($K_3[Fe(CN)_6]$) were bought from HiMedia®. Nafion 117™ membrane and Nafion solution (~ 5 % purum) were purchased from Sigma Aldrich (USA). Whatman® Chromatography Paper No. 1 (20 × 20 cm) was obtained from GE Lifesciences. Ethanol (EtOH), methanol (MeOH), acetic acid (AA), butanol, dimethyl sulfoxide (DMSO), isopropanol (IP) and sodium succinate were purchased from Merck. All solutions were prepared in ultrapure water with resistivity >18 MΩ cm. The experiments were performed at RT unless stated otherwise. The rest of the reagents were of analytical grade.

### 4.2.2 Analysis of spectral properties of cyanobacteria

Bacterial suspension ($OD_{750}$ ~ 0.15 – 0.2) was harvested by centrifugation at 8000g for 5 min and 4 ºC. The cell pellet was washed thrice in 0.1 M PBS pH 7.5. Cells were treated with varying concentrations of alcohols in water. Absorbance was taken at $\lambda_{565\ nm}$ and $\lambda_{635\ nm}$ in a flat black round bottom 96-well microtiter plates (Corning®) in a plate reader (TECANM200 Pro, Switzerland). Graphs were plotted and analyzed using Origin 8.0 software.

### 4.2.3 MTT assay

MTT assay was performed to measure the bacterial cell viability. The viable respiring cells can reduce tetrazolium dyes to their respective purple formazan products. The stock of MTT was prepared in PBS (pH 6.8) at a concentration of 0.5 mg $ml^{-1}$ with 0.1 mol $L^{-1}$sodium succinate. One mL of cell suspension ($OD_{750}$ ~ 0.15) in an Eppendorf tube was centrifuged at 8000g for 8 min at 4 ºC. The cell pellets were washed with PBS (pH 6.8). Then, 250 µL of ASN III media was added to the washed pellets. To this, MTT was added to provide a final concentration of 0.1 mg $mL^{-1}$. The cell suspensions were incubated at 28 ºC inside an illuminating incubator for 1 h (Li and Song, 2007). After the incubation, the dye solution was removed by centrifugation at 8228g for 3 min. The cell pellets were then suspended in one mL of DMSO to dissolve the formazan crystals and incubated for 10 min in dark. The suspension was subjected to 8000g for 8 min at 4 ºC and the supernatant was collected to measure the absorbance at $\lambda_{556\ nm}$ by a UV-Vis spectrophotometer (Cary 100 Bio, Varian).

### 4.2.4 Measurement of membrane potential

The membrane integrity of the cyanobacterial cells was monitored using an anionic membrane potential sensitive fluorescent probe $DiBAC_4(3)$ (Huang *et al*., 2015). A stock of 50 µM of $DiBAC_4(3)$ was prepared in DMSO. Cell suspension ($OD_{750}$ ~ 0.5 - 0.6) was combined with filtered (through a 0.45 µm filter, MICRO-POR®, Genetix Biotech) 50 mM of sodium succinate prepared in water and incubated for 15 min to provide energy for all ATP-dependent membrane channels and cellular components (Clementi *et al*., 2014). The

assay was performed in a flat black clear bottom 96-well plate (Corning®) in a microtiter plate reader (TECAN M200 Pro, Switzerland), to detect fluorescence intensity of the bacterial suspensions in a format over time. This enabled to conduct several experiments at various time points with greater simplicity and to continuously monitor the fluorescence kinetics of the entire population for extended periods of time, which is difficult to achieve using flow cytometry (Clementi *et al*., 2014). The cell suspensions taken in the 96-well plate were mixed with the membrane potential probe (final 500 nM). The fluorescence ($\lambda_{ex\ 490\ nm}$ and $\lambda_{em\ 516\ nm}$) was then concurrently monitored following every five min until the reading was stabilized. After 45 min of stabilization period, the plate was ejected, the alcohols under study were added, and the plate was inserted immediately to continue the monitoring of the fluorescence deviations. The fluorescence intensities over the time period were plotted to evaluate the membrane depolarization. The depolarized cell population (%) was calculated as ($f_i - f_f/f_i$), where $f_i$ and $f_f$ are the fluorescence intensities before and after the addition of solvent (control subtracted), respectively.

### 4.2.5 Microscopic imaging

The structural integrity of the cyanobacterial cells untreated (control) as well as treated with 10 % of alcohols and dried overnight in the laminar hood, were visualized using atomic force microscope (AFM) (Innova, Bruker) and TEM, using operating voltage of 100 kV (JEOL MODEL: 2100F). AFM was performed in tapping mode at a scan rate 0.7 Hz. The height profiling was conducted using Windows-Scanning-x-Microscope (WSxM) software (Horcas *et al*., 2007).

### 4.2.6 Fluorescence activated cell sorting (FACS)

The culture broth of cyanobacterial cells ($OD_{750}$ ~ 0.3) was centrifuged at 8000g for 5 min at 4 ºC and washed in 0.1 M PBS (pH 7.5). The harvested cells were then treated for 10 min with 10 % concentration of alcohols. FACS was then conducted for 10000 events using CYTOFLEX Beckman Coulter, Life Sciences. The viability was checked using excitation at $\lambda_{496\ nm}$ and emission at $\lambda_{667\ nm}$ using the auto-fluorescence property of cyanobacteria.

### 4.2.7 Preparation of working electrode

Graphite electrodes were fabricated following the procedure described previously (chapter III). Briefly, aqueous SF (3 % w/v) and QD (0.1 % w/v) were mixed in the ratio of 2.4:0.02 (wt/wt) to make SF decorated quantum dots (SF/QD) solution. 1 mg of GNP was mixed with 1 mL of SF/QD solution to make SF doped with QD and GNP (SF/QD/GNP). A total of 100 µL of SF/QD/GNP solution was drop cast on the anode and dried in the laminar hood for 5 h to fabricate the modified graphite electrodes. This was used immediately as the anode in the subsequent PMFC studies.

### 4.2.8 Construction of PMFC and potential measurement

The PMFC was constructed following the work described in chapter III. Briefly, the anodic and cathodic chambers (made of Plexiglas), each with a working volume of 100 mL, were separated by Nafion membrane. The anode (3.7 cm × 0.32 cm) was fed with ASN III media (pH 7.4) containing *Synechococcus* sp. ($OD_{750}$ ~ 0.4) and 750 mg $L^{-1}$ of acetate. The cathode chamber contained 80 mM of ferricyanide in 0.1 M PBS, pH 7. The PMFC was operated at RT under white light illumination of 15 W $m^{-2}$. The PMFC was initially allowed to stabilize for 48 h. The cathode reaction was provided by the well-established ferricyanide reduction (Lv *et al*., 2013). Ferricyanide in cathode presents a stable and fast cathodic reaction, allowing only the changes in the anode chamber to reflect the MFC performance (Abrevaya *et al*., 2015). The bacterial suspension in the anode chamber was exposed to increasing concentrations of alcohols without media replacement and the voltage outputs at a load of 1000 Ω were monitored continuously by a data acquisition system (Agilent 34972A LXI, U.S.A) through copper clip connections (Mouser Electronics, U.S.A.). A positive control experiment with biofilm anode but without alcohol addition and a negative control experiment with anode filled with media but void of biofilm were also performed. Response curve was generated as an increase in the potential burst (%) vs. concentration of alcohols. The potential burst (%) was discerned from the following relation:

$$\frac{V_1 - V_2}{V_1} \times 100\ \% \quad \text{.....(4.1)}$$

where $V_1$ is the base potential before addition of alcohol, $V_2$ is the potential amplitude from the base mid-point of the inflection peak to the peak point.

The cell-alcohol interaction constant ($K_i$) was discerned from the equation using Sigma plot following one site binding saturation:

$$Y = \frac{B_{max}\, X}{K_i + X} \quad \text{.....(4.2)}$$

where, $B_{max}$ is the maximum potential (%) burst, X is the concentration of the alcohol, and Y is the potential burst (%).

### 4.2.9 Bacterial cell-electrode interaction analysis

The microbe-electrode interaction was investigated using CV performed in Autolab PGSTAT 302N (Netherlands), using the conventional three-electrode system, under non-turnover conditions. The CV profiles (scan rate of 10 mV $s^{-1}$) were generated in the absence (control) and presence (1 %) of alcohols from the anode, where the biofilm deprived of the substrate, was retained. Ferrocene value of - 4.4 eV has been used as the reference to calculate the energy of the highest occupied molecular orbital (HOMO) and lowest unoccupied molecular orbital (LUMO) levels. The band gap ($E_g$) energy levels of redox species were calculated from the onset oxidation ($E_{Ox}^{onset}$) and reduction ($E_{Red}^{onset}$) potential as mentioned: (Leonat *et al*., 2013; Ye *et al*., 2012)

$$HOMO = -e\,[E_{Ox}^{onset} + 4.4] \quad \text{.....(4.3)}$$

$$LUMO = -e\,[E_{Red}^{onset} + 4.4] \quad \text{.....(4.4)}$$

$$E_g = LUMO - HOMO \quad \text{.....(4.5)}$$

### 4.2.10 Fabrication of p-PFMC system

The p-PMFC for selective detection of alcohol was integrated onto the Whatman® chromatography paper. The design was primed onto the paper using Adobe Illustrator CS. A total of 100 mg of GNP was dispersed in 6 mL of Nafion solution by ultrasonication for 20 min. This was used as electrode base paint (loading of ~ 4 mg $cm^{-2}$) for the anode and for the connections to the data logger. The electrochemical surface area of the paper coated with

GNP ink was measured in an electrolyte solution containing 0.1 M KCl and 80 mM ferricyanide. The Randles–Sevcik equation 4.6 (which assumes mass transport occurs only by diffusion):

$$I_P = 2.69 \times 10^5 \times S_a \times D^{1/2} \times n^{3/2} \times \gamma^{1/2} \times C \text{.....(4.6)}$$

was employed to measure the electrochemical surface area ($S_a$) using $D$, the diffusion coefficient of ferricyanide in solution ($6.70 \times 10^{-6}$cm $s^{-1}$), $n$, the number of electrons ($n$ = 1), $\gamma$, the scan rate (100 mV $s^{-1}$), $C$, the concentration of the probe in solution and $I_p$, the current response.

Ferricyanide powder was added to the mixture of GNP and Nafion and used as cathode coating at a final concentration of 100 mM. The 4 mm separation between the cathode and anode circles was loaded with 60 µL of Nafion solution and served as the module for proton exchange. The paper substrate was then dried in an oven at 60 °C for 4 h. The anode was then layered with 40 µL of SF/QD/GNP, and placed inside a laminar hood for 30 min. Once semi-dried, a total of 40 µL of the harvested cells ($OD_{750}$ ~ 0.4, 8000g for 5 min at 4 ºC) suspended in ASN III media was coated on top of the SF/QD/GNP layered anode. This was then left for drying inside the laminar overnight at RT. The as-prepared p-PMFC was then stored at 4 ºC under the airtight condition for further use.

The resistivity (ρ, Ωm) was calculated from ρ = R A/l, where R is the resistance measured using the data logger, A is the area of the electrode and l is the distance between the copper clips. The conductivity (σ, $Sm^{-1}$) was derived as the inverse of resistivity. The prepared p-PFMC was activated by loading 40 µL (optimized volume capacity) of ASN III media in the anode, 60 µL of PBS (0.1 M, pH 7) in the cathode and 60 µL of PBS (0.1 M, pH 7) onto the proton exchange area. The buffer reserve zone held 120 µL of PBS (0.1 M, pH 7). The potential response of the p-PFMC was monitored in the presence of varying concentrations of alcohols with the help of a data logger. The results represent the average of three independent experiments conducted at RT under a light intensity of 15 W $m^{-2}$. The potential response of the p-PFMC against some potential interfering solvents was measured following the similar procedure.

### 4.2.11 Characterization of p-PFMC

The fabricated p-PFMC was characterized by FESEM (Zeiss, Model Sigma) at 3 kV. The cells layered over the anode were fixed with 2 % glutaraldehyde, rinsed with PBS (0.1 M, pH 7) and subsequently treated with serial transfers through 30, 50, 70, 80, 90, 95, and 100 % ethanol to dehydrate. The samples were sputtered with gold and fixed onto carbon tape prior to imaging. Uniform drops of 2 μL of the solvents were dropped onto the cell surface and the contact angles were measured by sessile drop technique at RT after 60 s using a Holmarc Model No. HO-1AD-CAM-018.

## 4.3 Results and discussion

### 4.3.1 Sensing of alcohols using PMFC potential burst signal

The cyanobacterial biofilm with the underneath nano-biocomposite matrix comprising of quantum dots, graphene nanoplatelets and silk fibroin is known to transfer cellular electrons to the base graphite anode of the PMFC through a mediator-less direct electron transfer mechanism as confirmed previously in chapter III. The effect of ethanol and methanol on the cyanobacteria-based anode was investigated by monitoring the potential changes in the two-chambered PMFC (Figure 4.1). With the injection of alcohol, a potential burst was observed within 60 s. The burst potential intensity was increased with the increasing concentration of alcohols in the dosages. Alcohol dose was injected sequentially keeping a recovery time for the stable baseline before next dose being injected which helped to rescind the cascading effect of the preceding alcohol doses on the burst signals. The base potential of the PMFC however, gradually declined and discharged down to less than 0.1 V at 40 % of alcohols (Figure 4.2 A) where a major inactivation of the biofilm cells has been presumed. A variation in the base potential within ~ 0.1 V among positive control, ethanol and methanol experiments has been ascribed to a minor variation of the anodic biofilm growth. The control experiments validated the role of biofilm cells in generating the signal. The direct oxidation of alcohols over the electrode surface may also be nullified by the fact that the experimental pH maintained in the anodic chamber does not promote ethanol oxidation (Akhairi and Kamarudin, 2016). Interestingly, the burst potential intensity obtained with ethanol was significantly higher than methanol (Figure 4.2 B). For instance, at

10 % of the respective concentrations, the burst potential detected for ethanol was ~ 1.4 fold higher than methanol. The recovery time of the base potential for ethanol was also relatively longer than the methanol for each dosage (Figure 4.2 B). From the plot, a dynamic range of 0.001 - 20 % for ethanol and 0.01 – 20 % for methanol and limit of detection (LOD, 3 × SD/slope) of 0.13 % (2.82 mM, $R^2$ = 0.96) and 0.20 % (6.24 mM, $R^2$ = 0.93) for ethanol and methanol, respectively, were discerned with a relative standard deviation (RSD) of 4.02 %. The cell-alcohol interaction constant ($K_i$) of 780 mM for ethanol and 1250 mM for methanol was deduced (Figure 4.3 A-B), which indicates ethanol has significantly higher interaction efficacy with the cyanobacterial cells than methanol to generate the potential burst. To understand the phenomena of potential burst, we investigated the effect of alcohols on the morphological, electrochemical and relevant spectroscopic properties of the cells as discussed in the next section.

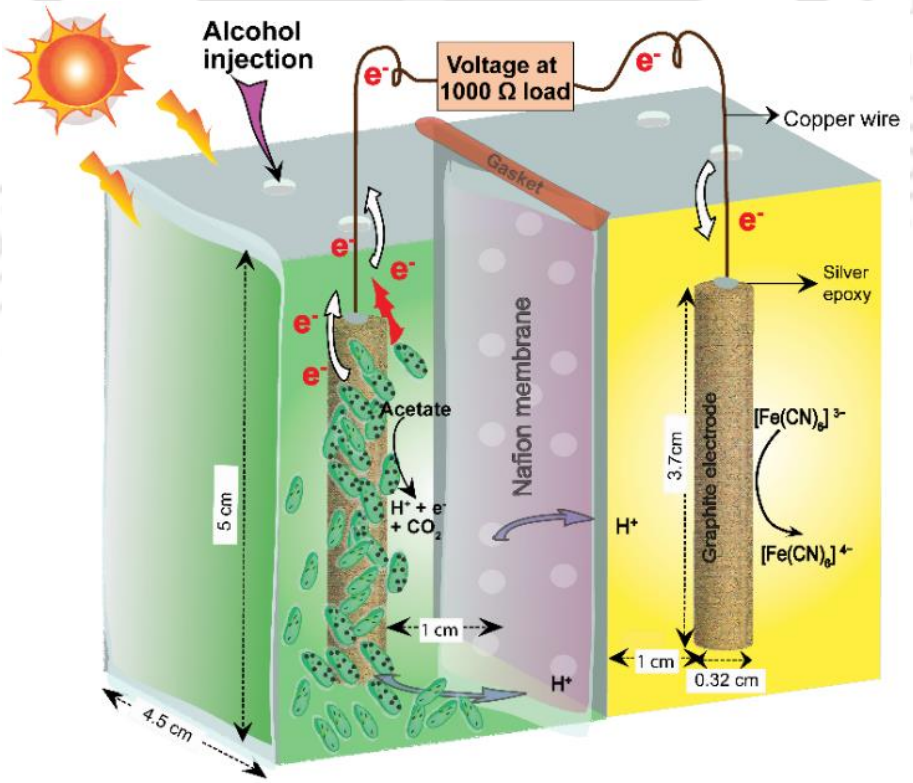


**Figure 4.1:** Schematic of the photosynthetic microbial fuel cell system used for alcohol detection.

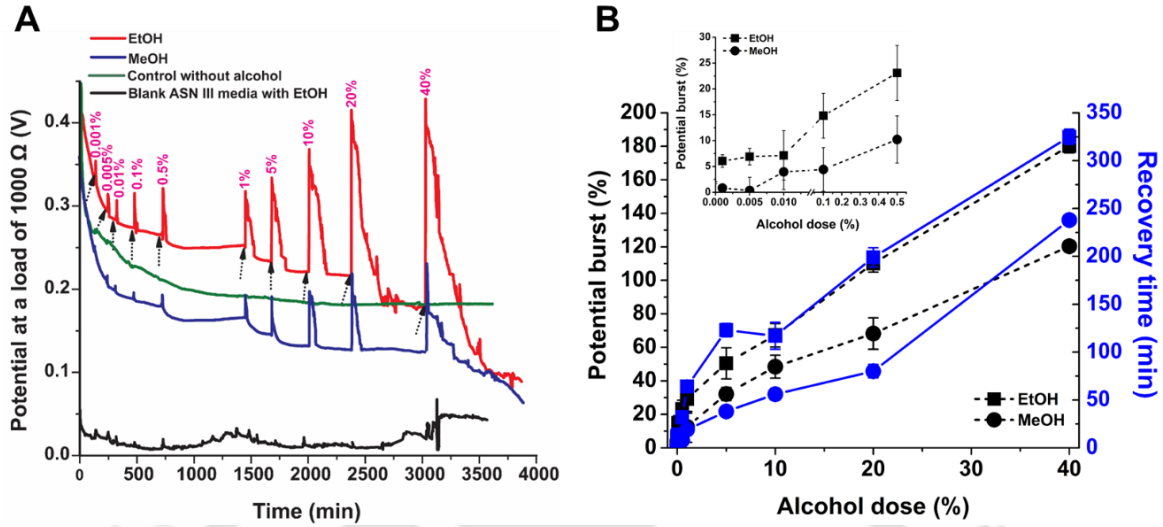


**Figure 4.2:** (A) Effect of sequential alcohol dose with increasing concentration on the PMFC potential over a time scale (depicted directly extracted graphs). The PMFC was operated at a load of 1000 Ω. (B) The plot of potential burst (%) and recovery time of the base potential vs concentration of alcohol dose (%). Inset graph is an enlarged view of the lower concentration (< 0.5 %) range of alcohols. Each datum is the mean (N = 3) ± SD.

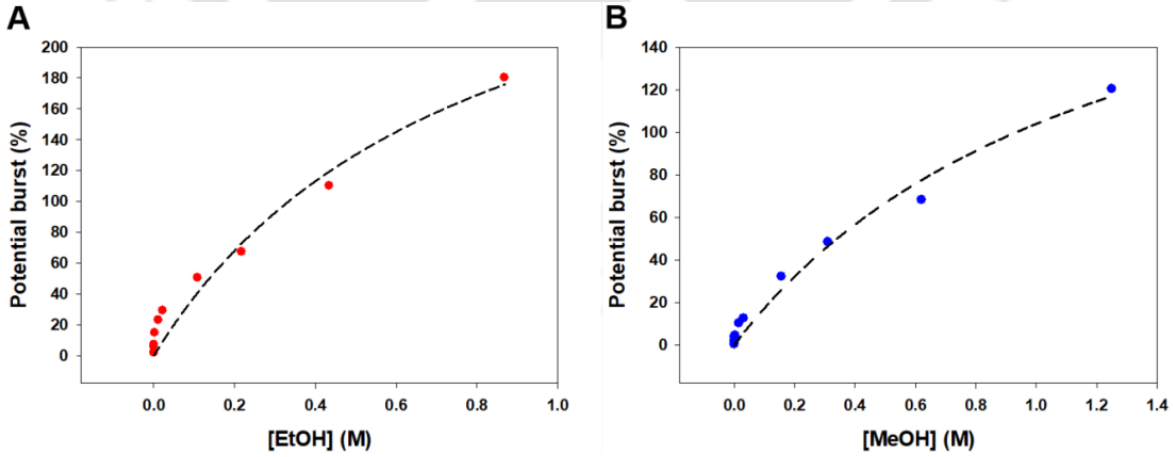


**Figure 4.3:** Plot of potential increase (%) vs concentration (M) with curve fitting to equation 4.2 (A) EtOH and (B) MeOH.

### 4.3.2 Effect of alcohols on the integrity of cyanobacterial cells

#### *4.3.2.1 Effect of alcohols on the cellular morphology*

Bacteria are known to maintain their cellular integrity through the strength of cell wall and cell membrane, while the former grants rigidity and the latter empowers the cells for selective exchange of nutrients, ions and other molecules with its immediate environment (Matos and Lopes, 2013). When treated with alcohol (10 %), the membrane of the cyanobacteria cells was extensively damaged by ethanol as evident from the severe membrane disintegrations, some of which are shown by the arrows in FETEM image (Figure 4.4 A a). The effect however, was less pronounced in the methanol treated cells (Figure 4.4 A b). The effect of alcohols on the cell morphology was further probed by AFM (Figure 4.4 B). The elevated and smooth height profile of the untreated cells (control) ascertain undulated membrane indicating intact cell structure (Figure 4.4 B a and 4.5 a). Conversely, the topography of the ethanol treated cells was significantly distorted as revealed from the reduced height profile with uneven surface structures of the cells (Figure 4.4 B b and 4.5 b-c). However, the methanol treatment did not furnish extensive cell damage which is evident from the marginally lower height profile than the control experiment (Figure 4.4 B c and 4.5 b-c). Thus the results of AFM supported the FETEM findings.

The size and granularity of the alcohol treated cells were examined by FACS (Figure 4.6 a-c). The morphology ($p > 0.05$) of ~ 5.6 % of the cell population changed when treated with ethanol (Figure 4.7 A). The fluorescence intensity of the ethanol treated cells was also decreased by 15.5 % (Figure 4.7 B). The morphological structure and the fluorescence intensity of the methanol treated cells did not deviate significantly from the control. The data support the fact that ethanol treatment induces higher stress in cyanobacteria, as compared to that of methanol. This corroborates to the earlier microscopic findings.

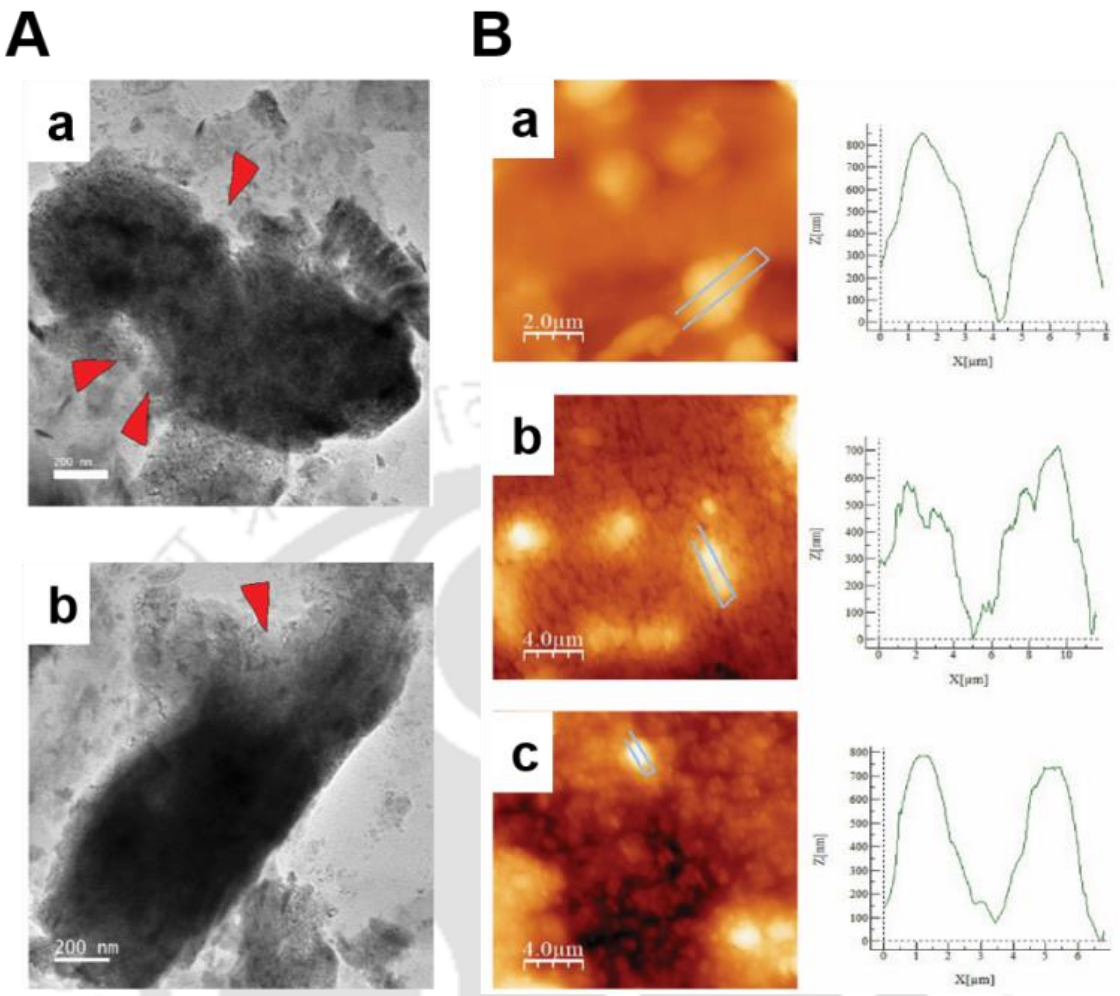


**Figure 4.4:** (A) FETEM studies on the effect of alcohols on the cell membrane structures: (a) ethanol and (b) methanol. (B) AFM studies on the topography including height profiling: (a) control (b) EtOH and (c) MeOH. The cyanobacterial cells were treated with 10 % alcohols.

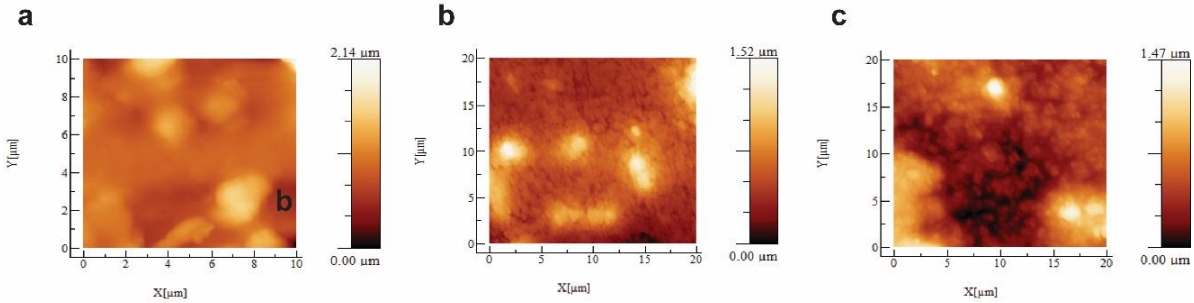


**Figure 4.5:** AFM images with z-axis on the effect of alcohols (10 % concentration) on cell membrane structures (a) control, (b) EtOH and (c) MeOH.

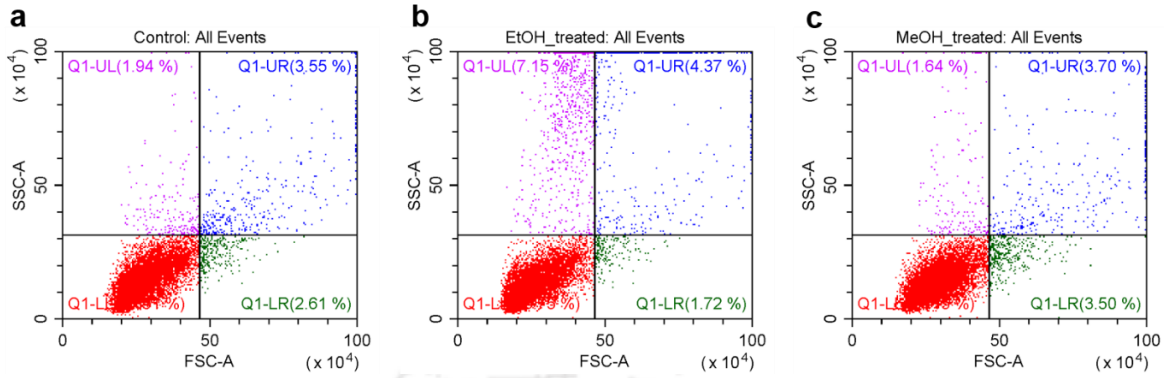


**Figure 4.6:** (A) Representative FACS analysis of cyanobacteria cells (a) control, (b) EtOH treated and (c) MeOH treated. The cells were treated with 10 % alcohols.

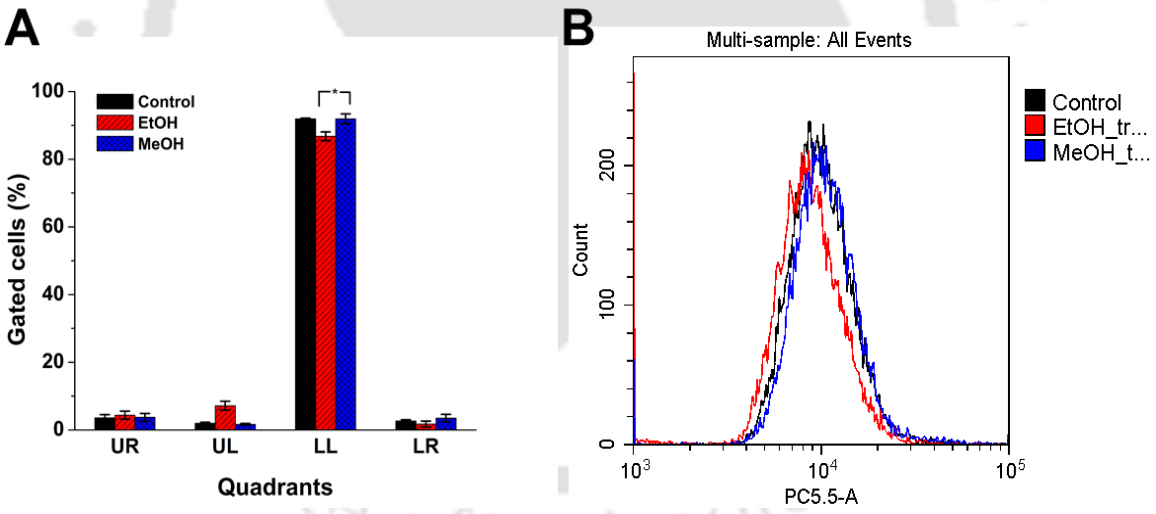


**Figure 4.7:** (A) Gated cells (%) in each quadrant (*p > 0.05) from FACS analysis of cyanobacterial cells treated with 10 % alcohols. (B) Viability check through auto-fluorescence of control and 10 % alcohol treated cells.

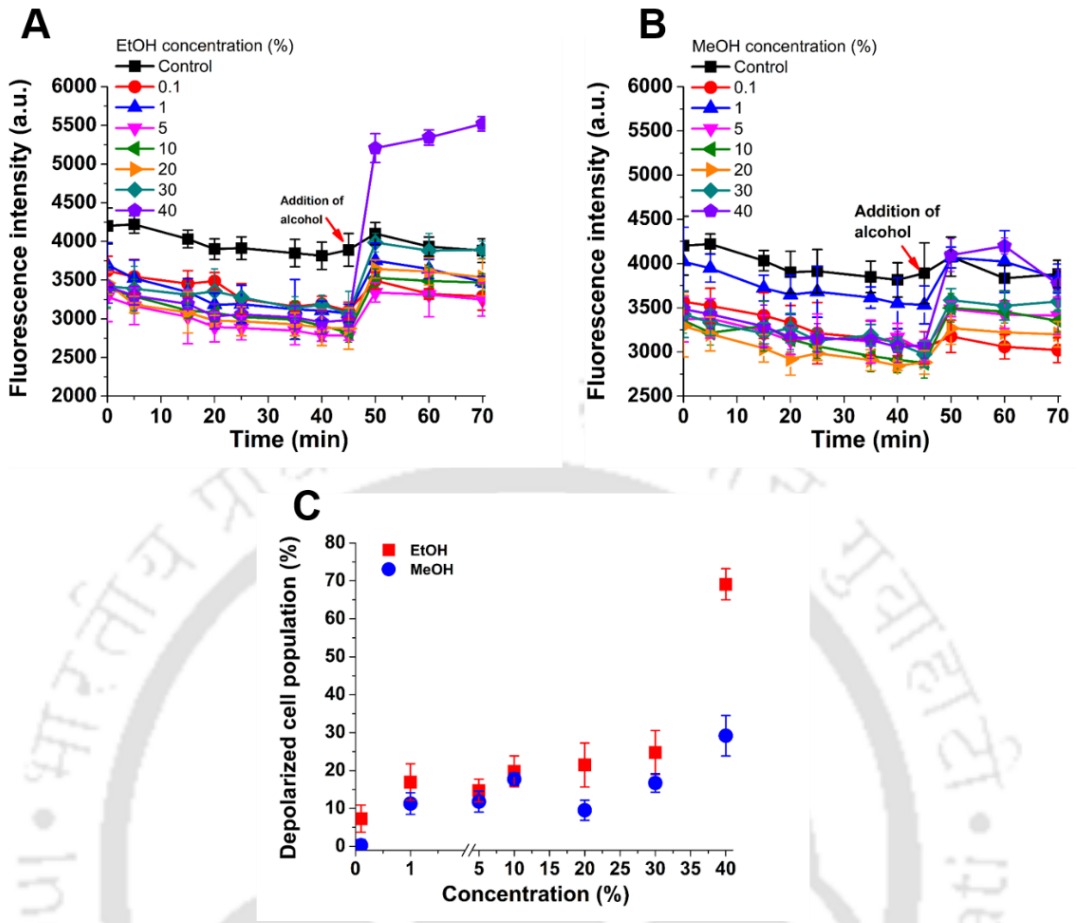


**Figure 4.8:** Fluorescence intensity of the cyanobacterial cells recorded over time at varying concentrations of (A) EtOH and (B) MeOH treatment. (C) Depolarized cell population (%) recorded over varying concentrations of alcohols. The data are background subtracted and each datum is the mean (N = 6) ± SD.

### *4.3.2.2 Effect of alcohols on the cell-membrane polarity*

The selective properties of cell membrane create the concentration gradients of ions and molecules across the membrane, thus maintaining the cells in a polarized state. The change in membrane polarity is usually probed by using membrane potential sensitive oxonol dye. The accumulation of lipophilic anionic oxonol dyes within the bacterial cells is favored by a reduction in the magnitude of the membrane potential which enables the dye molecules to concentrate within the cell through association with the intracellular macromolecules that amplify the fluorescence intensity (Deere, 1995). $DiBAC_4(3)$ ($\lambda_{em\ 525\ nm}$) oxonol dye is widely used to assess the membrane polarity (Huang *et al.*, 2015). The cells treated with increasing concentration of alcohols were stained with the dye and then the

fluorescence intensity was monitored (Figure 4.8 A-B). Both the alcohols triggered depolarization of the cell membrane, as evident from the elevated fluorescence intensity from the point of treatment (45 min). A background increase in the intensity following the ejection of the microtiter plate (after 45 min) in the control (without alcohol) was developed owing to the recovery of the dye from the photo bleaching. However, the magnitude of depolarization by ethanol was much higher than methanol. Ethanol caused a 7.7 ± 2.84 % higher depolarization of the cells than methanol at a concentration of 0.1 % for each (Figure 4.8 C).

Ethanol trespasses the bilayer much more easily than methanol (Patra *et al*., 2006). This can be explained by the hydrophobic nature of the carbon tail of ethanol, which facilitated higher ethanol density at the interface region between lipids and the surrounding water, as compared to methanol. Ethanol also interacts with the lipid membrane through hydrogen bonding and destabilizes the chain order, eventually causing disorientation of the trans-membrane proteins and dissipation of the pmf (Cartwright *et al*., 1986; Dombek and Ingram, 1984). The combination of all these effects results in a higher detrimental effect of ethanol on the cell membrane that eventually alters the electrostatic potential across the membrane.

#### *4.3.2.3 Effect of alcohol on microbial respiration and photosynthetic reaction center*

The effect of alcohols on the cyanobacterial respiration was investigated by MTT assay, which is a relatively reliable, accurate and reproducible method to assess the viability of cyanobacteria cells (Li and Song, 2007). Respiration was increased following the addition of alcohols (Figure 4.9 A). Beyond the concentration of 30 % of ethanol and 40 % of methanol, the respiration steeply decreased as evident from the downtrend of the absorbance intensities. The increase in respiration of the alcohol treated cells was not growth-related as revealed from the Figure 4.9 B. A decrease in the $OD_{750}$ following alcohol injection was likely to be caused by some cellular degradation which was more prominent with ethanol than methanol. The observed increase in respiratory activity may be a reflection of a cellular attempt to repair the damage or compensate for some modification of cell envelope structures caused by the alcohols. A similar increase in oxygen uptake rate was reported for marine *Pseudomonas* sp. in the presence of alcohol (Fletcher, 1983).

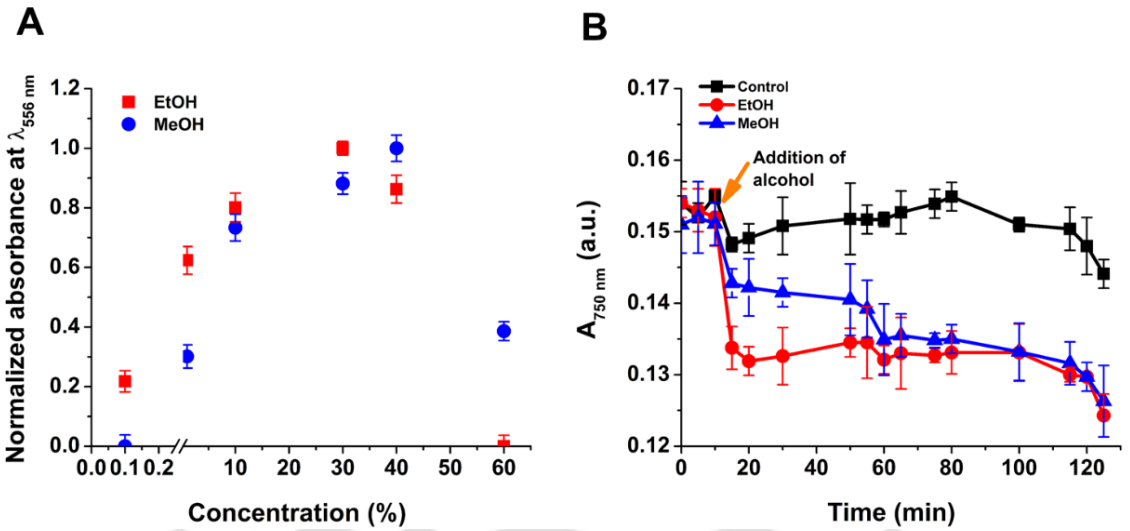


**Figure 4.9:** (A) MTT assay of cyanobacterial cells treated with increasing concentration of alcohols (control subtracted and normalized). (B) The growth of cyanobacterial cells under normal and alcohol treated (final concentration 10 %) conditions. Each datum is the mean (N = 3) ± SD.

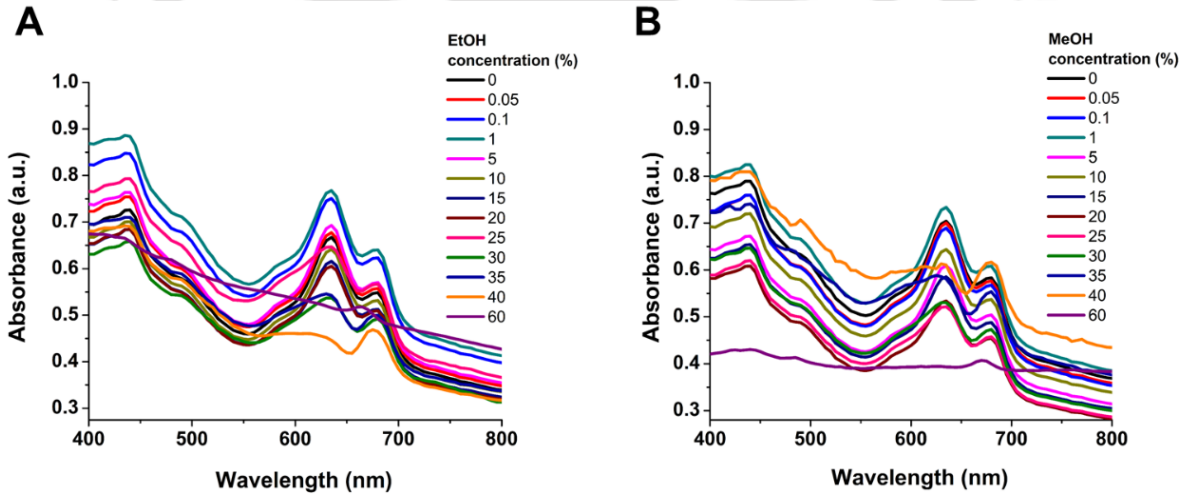


**Figure 4.10:** Effect of (A) EtOH and (B) MeOH on the spectral properties of cyanobacterial cells.

The bacterial photosynthetic reaction center consisting of chlorophyll and phycocyanin represent ideal photonic components to probe the fluctuation of its local

environment and cellular processes (Checchetto *et al*., 2012; Schulze *et al*., 2011). The photosynthetic reaction center is present in the innermost thylakoid membrane of cyanobacteria. The absorbance spectra revealed the presence of various photosynthetic pigments including chlorophyll *a* (abs maxima $\lambda_{440\ nm}$ and $\lambda_{680\ nm}$), phycocyanin (abs maxima $\lambda_{595\ -\ 640\ nm}$) and allophycocyanin (abs maxima $\lambda_{650\ -\ 655\ nm}$) (Figure 4.10 A). However, treatment of the cells with alcohol at a concentration of less than 30 % of ethanol or 40 % of methanol did not shift the spectral properties of the pigments (Figure 4.10 A-B). The dense packing of proteins in cyanobacterial thylakoids restrict the mobility of membrane-integral proteins (Mullineaux, 2014) and hence the embedded pigments were not considerably affected by the alcohols treatments. The spectral pattern was, however distorted by ethanol (≥ 30 %) and methanol (≥ 40 %) treatment at their respective concentrations as shown in the parentheses. The results revealed extensive damage to the cells beyond this level of alcohol concentrations. The results corroborated to the data from the Figure 4.2 A where beyond these limits of alcohol concentrations the base potential was extensively reduced.

#### *4.3.2.4 Analysis of redox potentials involved in cell–electrode interaction*

The characteristics of CV spectra provide vital information, such as, the mechanism of electron transfer between electrode and biocatalysts, the nature of the redox species involved in transferring the electrons, and the concentration of electroactive species (Zhao *et al*., 2009b). The effect of the alcohols at their moderate concentration (1 %) and at low scan rate (10 mV/s) on the bioanodes under non-turnover condition was examined by CV (Figure 4.11). A redox couple with formal potentials ($E_{pa}$+$E_{pc}$/2) at ~ -194 mV and ~ +280mV corresponding to flavin (redox species 1) and cytochrome (redox species 2) (Please see chapter III) was detected in the control (no alcohols) experiment. Following the injection of alcohols, the number of redox peaks of the bioelectrode was not altered. However, ethanol significantly increased the anodic peak current of the bioelectrode for both flavin (8.72 %) and cytochrome (35.48 %), the magnitude of which has been shown in the parentheses. Notably, ethanol is a non-ionic substrate and is electro-inactive within the potential window considered in this investigation as evident from the lack of redox features in the CV spectrum of the blank electrode. Moreover, ethanol is not a catalytic substrate for the redox couple involved here in the electron transfer process. The role of membrane-bound

cytochromes of cyanobacteria on the extracellular electron transfer process is known (Sekar *et al*., 2014). Additionally, the membrane permeability promotes the release of cytochrome-c (cyt *c*) (Manzo-Avalos and Saavedra-Molina, 2010). The CV results in conjunction with the above background information have suggested that the alcohol-mediated disruption of the cell membrane allows rapid interaction of this electron transporting redox couple with the anode promoting transiently a higher –ve potential in the anode as manifested from the potential burst in the PMFC. Ethanol had significant perturbation on both the cathodic peak potentials and marginally shifted these towards the lower potential range as evident from the magnitude of respective formal potentials (Table 4.1). The ethanol-induced cathodic peak current was though not much altered for flavin, a drastic decrease in the current intensity for cytochrome (37.72 % from control) was evident. It is likely that ethanol significantly affected the redox function of this protein-based electron shuttling agent. The reduction of the base potential (compared to control) of the PMFC has been attributed as the possible consequence of the successive injection of alcohol as observed in Figure 4.2 A. The CV pattern of the methanol-treated bioanode also followed the nearly similar trend with a bit lower magnitude of current.

The potential burst of PMFC upon addition of alcohols could also be explained on the basis of band gap change of the redox entities in the bioelectrode. CV is one of the most sensitive tools to interrogate the band gap energy profile. HOMO represents the energy required to extract an electron from a molecule, which is an oxidation process, and LUMO is the energy necessary to inject an electron to a molecule, thus implying a reduction process (Leonat *et al*., 2013). The highly conductive nature of the bioelectrode interface was validated by the discerned -ve values of the band gaps (Figure 4.11 and Table 4.1). The band gaps of the bioelectrode for both the redox couples were significantly decreased with the addition of alcohols indicating that the conductive redox process on the bioelectrode was further invigorated with the alcohol injection that manifested in the form of potential burst. The magnitude for flavin was more intense than the cytochrome based redox process (Table 4.1). However, a clear mechanism on the molecular electrochemistry is to be elucidated to understand the specific and combined role of these two cell membrane-associated redox entities in channelizing the metabolic electrons and developing the observed potential burst. In microbial cells, the electron transfer systems are composed of a series of electron carriers,

which are usually membrane-bound, such as flavoproteins, cytochromes and quinones that can accept electrons from an electron donor and can transfer them to an electron acceptor, which is anode in the present case. The energy released during this process is used to extrude protons to the external environment. Ethanol led disruption of the membrane structure causes passive diffusion of $H^+$ (Madeira *et al*., 2010) and decreases the magnitude of pmf (Cartwright *et al*., 1986). This was also confirmed by a decrease in the pH value of the anode chamber detected after 10 % ethanol treatment (pH 6.40) or methanol (pH 6.58) as compared to that of control (pH 6.82). The flushed out $H^+$ migrates to the cathode chamber across the membrane to combine with $O_2$ resulting in the formation of water.

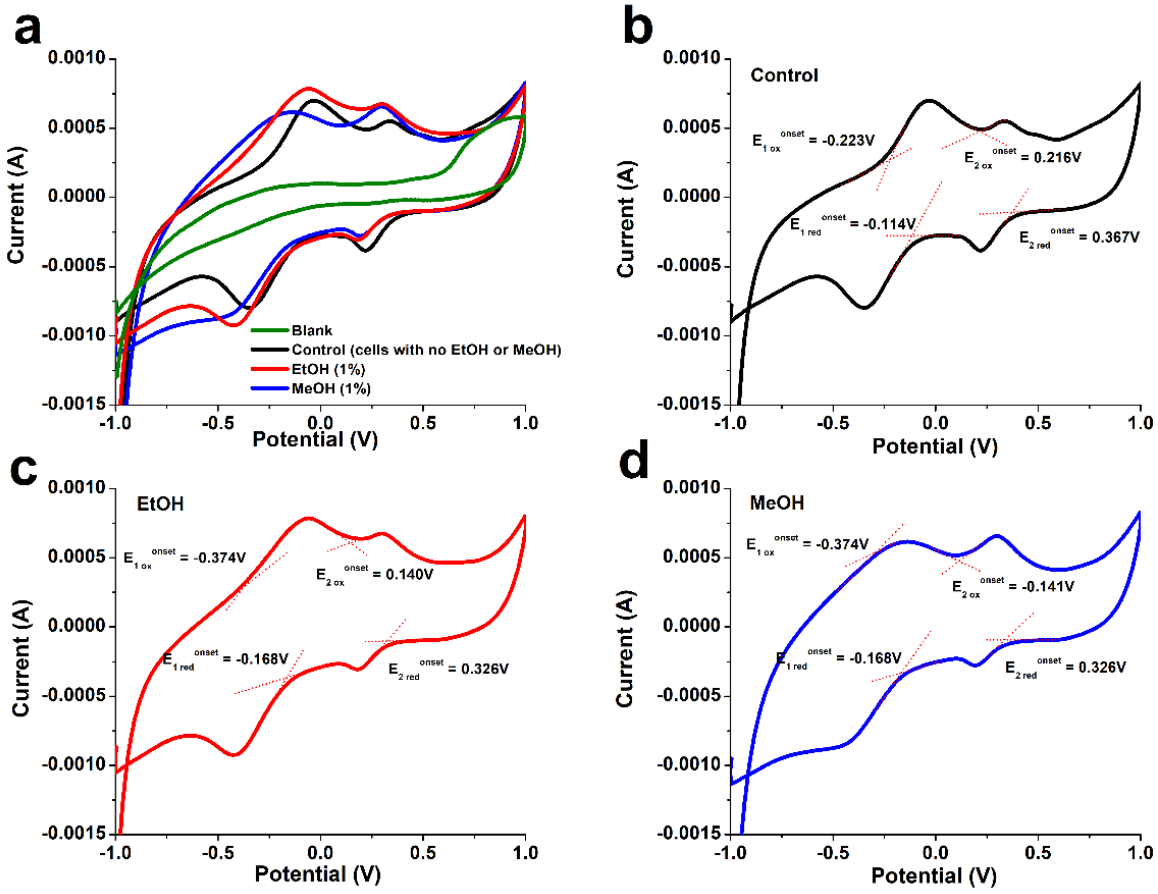


**Figure 4.11:** (a) Non-turnover CV analyses of anodes under different conditions. The blank voids biofilm. The $E_{Red}^{onset}$ and $E_{Ox}^{onset}$ traced for the CV profiles for (b) control electrode, (c) EtOH and (d) MeOH treated bioanodes. A scan rate of 10 mV $s^{-1}$ vs. Ag/AgCl was applied.

**Table 4.1:** The HUMO, LUMO and band gap energy levels discerned for the two redox species in control and in presence of 1 % each for EtOH and MeOH.

| | **$HOMO_1$** | **$LUMO_1$** | **Band $gap_1$ ($E_g^1$, eV)** | **Formal potential (flavin, mV)** | **$HOMO_2$** | **$LUMO_2$** | **Band $gap_2$ ( $E_g^2$, eV)** | **Formal potential (cyt, mV)** |
|---|---|---|---|---|---|---|---|---|
| **Control** | -4.177 | -4.286 | -0.109 | -194 | -4.616 | -4.767 | -0.151 | +280 |
| **EtOH** | -4.026 | -4.237 | -0.211 | -240 | -4.540 | -4.726 | -0.186 | +249 |
| **MeOH** | -4.104 | -4.232 | -0.128 | -295 | -4.511 | -4.726 | -0.215 | +242 |

### 4.3.3 Development of p-PMFC for sensing alcohol

The proof of concept of alcohol detection using the voltage burst signal in PMFC was translated to a paper-based platform considering the various advantages of using this emerging platform as discussed previously. These miniaturized MFCs also have the potential to overcome long start up time for bacterial acclimatization and complicated design with integrated multifunctional parts and to obviate auxiliary power devices for fuel injection (Fraiwan *et al*., 2016). A p-PMFC was designed, fabricated (Figure 4.12) and characterized by FESEM, contact angle, and CV analyses. The FESEM images revealed a porous morphology of the blank paper (Figure 4.13 a). The electrodes and current collection zones when coated with GNP based paint, the porosity of the zones was reduced (Figure 4.13 b) with the concomitant increase in the conductivity to 0.02 $Sm^{-1}$. The anodic zone was further layered with the nano-biocomposite matrix (SF/QD/GNP) which completely transformed the surface to a non-porous coarse structure (Figure 4.13 c). The active bacterial cells were then immobilized over the nano-biocomposite matrix as visible from the exploded view in the bottom inset of Figure 4.13 d.

The contact angles with water of the modified paper surfaces were recorded as 108°, 21° and 60.6°, for GNP based paint coating, nano-biocomposite layer and immobilized bacterial cells, respectively (upper insets of Figure 4.13 b-d). The electroactive anodic surface area of the GNP based paint coated surface discerned from the CV (Figure 4.14) and equation 4.6 was found to be 0.05 $mm^2$.

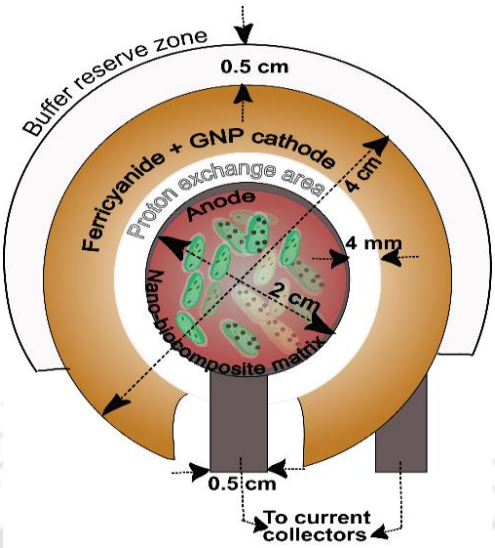


**Figure 4.12:** Schematic of the photosynthetic microbial fuel cell system used for alcohol detection.

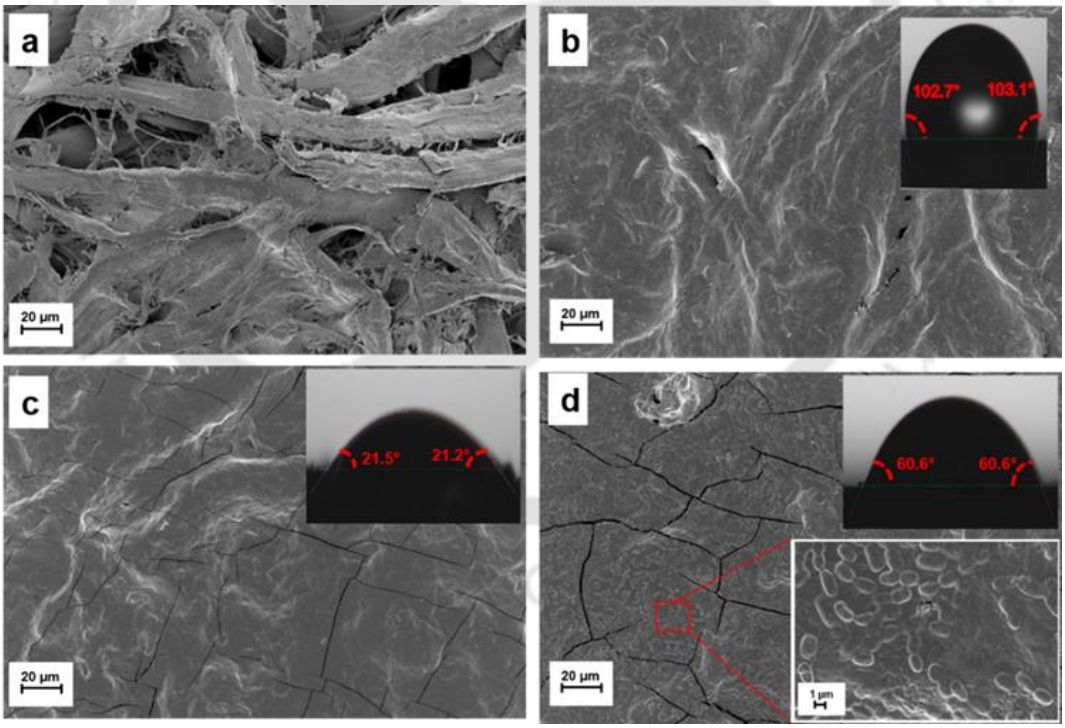


**Figure 4.13:** FESEM images of p-PMFC at different fabrications steps (a) Whatman® chromatography Paper No.1, (b) paper coated with conductive GNP based paint, (c) layering of the nano-biocomposite matrix over the GNP based paint and (d) immobilized cyanobacteria cells onto the matrix (bottom inset exploded view). Top Insets b-d depicts the contact angles of the respective surfaces with water.

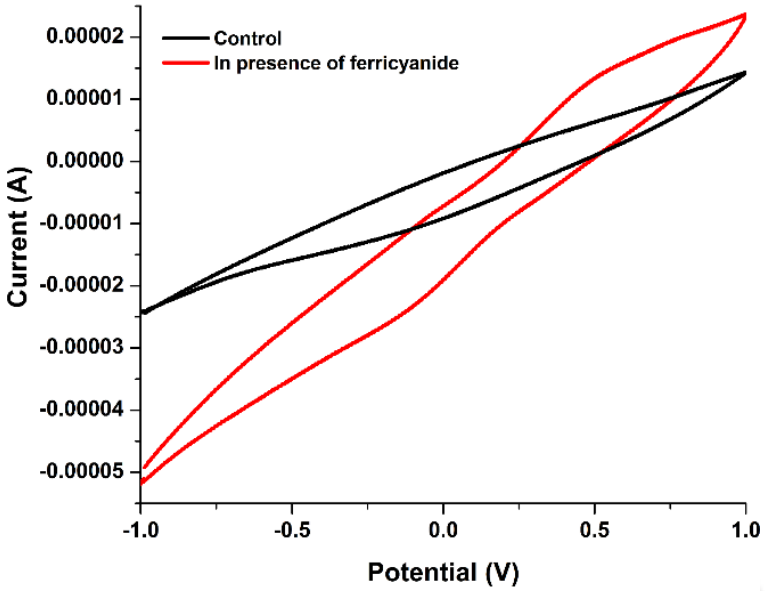


**Figure 4.14:** CV of GNP based painted paper at a scan rate of 100 mV/ s.

The magnitude of the contact angles implies that the hydrophobic GNP based paint surface (> 90 °) was transformed to a hydrophilic surface when the nano-biocomposite matrix was layered over it, which facilitated the adsorption of cyanobacterial cells over the matrix. The immobilized cyanobacteria with a contact angle of 60.6° represents a physically stable cell layer (Please refer chapter II), as the biocompatible nano-biocomposite matrix supports the native structure and activity of the cells, surged the photosystems with adequate light and minimized electrochemical potential losses (please refer chapter III). This enabled generation of a stable baseline and repeatability. Notably, the immobilized materials govern the efficiency of the bio-electrodes in terms of electron transfer kinetics, mass transport, stability, and reproducibility (Yang *et al*., 2012). When alcohol (10 %) was dropped onto the immobilized cell layer, the contact angles were changed from 60.6° to 52.8° and 57.5° for ethanol and methanol, respectively (Figure 4.15). This suggests an increase in the liquid adsorption in the order of EtOH > MeOH by the immobilized cells in the p-PFMC (Fletcher, 1983). According to Traube's rule, the addition of a new $CH_2$ group to methanol (which gives ethanol) leads to a decrease in the surface tension promoting strong interactions with the membranes. Ethanol, owing to its lower polarity than methanol ($\in_r$ = 24.5 for ethanol and $\in_r$ = 32.7 for methanol) has a greater effect on the fluidity and permeability of the membrane at a shorter time scale (Patra *et al*., 2006).

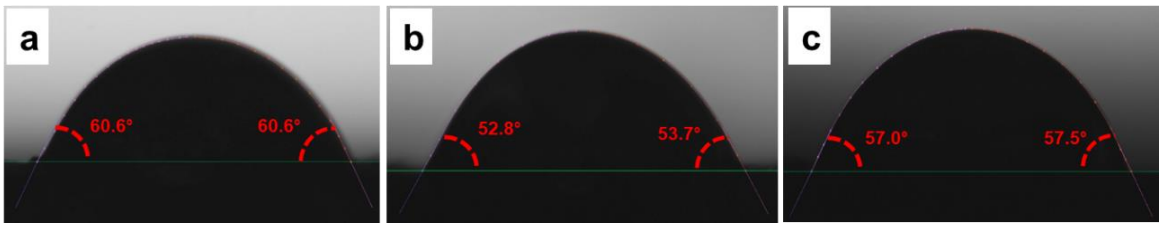


**Figure 4.15:** Contact angles of the cyanobacterial cells layered over the anode of p-PFMC with (a) water, (b) EtOH and (c) MeOH.

The p-PMFC exhibited a stable open circuit potential (OCP) in the range of ~ 0.28 – 0.35 V within 20 min of activation (Figure 4.16). The OCP response (without load) of the p-PMFC at different concentrations of alcohols was investigated and found that methanol at a lower concentration of < 0.5 % did not elicit any tangible OCP response. Both the alcohols however, did not generate a reproducible response beyond their concentration of 10 %. Hence, only ethanol up to a maximum concentration of 10 % was considered for generating the calibration curve (Figure 4.17 A). The response characteristics of ethanol are shown in Table 4.2 and Figure 4.18 a-d. A stark decrease in start-up and response time as well as improved LOD, on converting the design from the lab scale to the paper format is encouraging, as most of the MFC biosensors developed so far to detect BOD, toxicity, and monitoring anaerobic digestions exhibit long response time (2 – 4 h) (Schneider *et al*., 2016a). The electron transfer mediator-less system adapted here rendered to overcome the mass transport limitation (McCormick *et al*., 2011). Further, this open-air p-PMFC design was not prone to cross-over of the anode and cathode reactants at the optimized volume of activating buffer and not limited by the depletion of the gases for the cells and electrodes due to the surface exposure of the electrode to the air. The benefit of direct electron transfer based principle to avert the overpotential losses is well documented (Das *et al*., 2014).

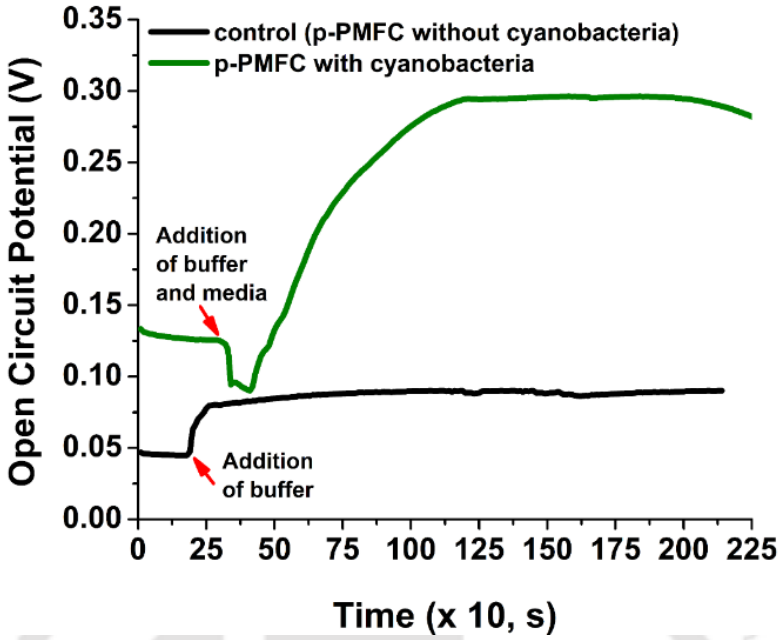


**Figure 4.16:** Stability of OCP after activation of the p-PFMC device with buffer and ASN III media.

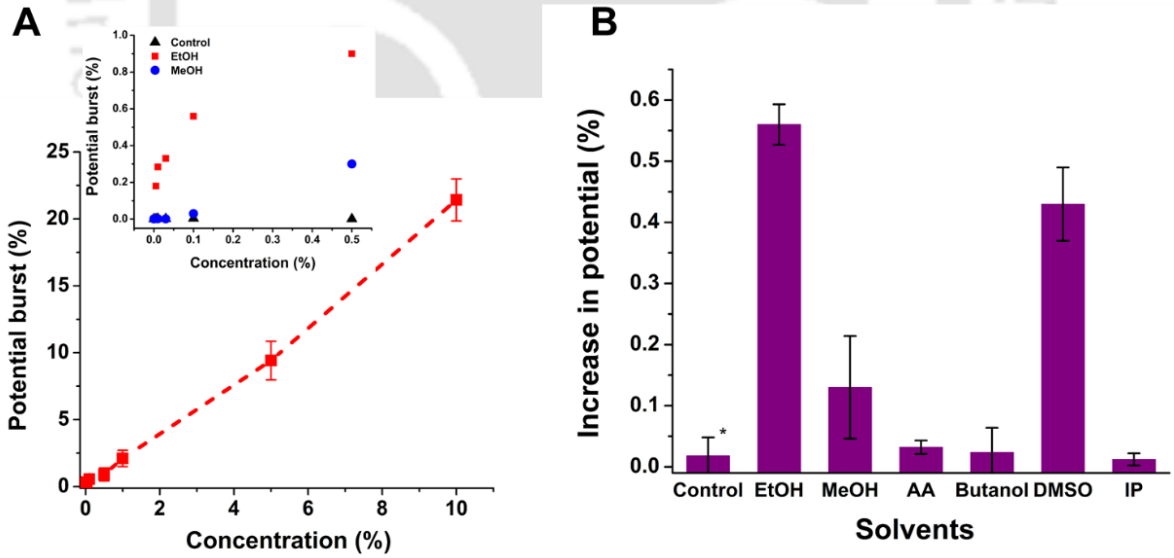


**Figure 4.17:** (A) Potential burst (%) vs concentration (%) of ethanol in p-PMFC. Inset graph is an enlarged segment of response data at lower concentration (< 0.5 %) of alcohols. (B) Effect of different solvents (2 mM) on the response of the p-PMFC. Each datum is the mean (N = 3) ± SD.

**Table 4.2:** Comparison of the developed cyanobacteria based PMFC biosensors for ethanol detection. The response data for methanol are shown in the parentheses.

| Mode of detection | Response time, $t_R$ | Linearity ($R^2$) | Limit of detection (LOD) | Linear range |
|---|---|---|---|---|
| **PMFC** | ~ 60 s | 0.96 (0.93) | 0.13 % (0.20 %) | 0.001 – 20 % (0.01 – 20 %) |
| **p-PFMC** | ~ 10 s | 0.99 | 0.02% | 0.005 – 10 % |

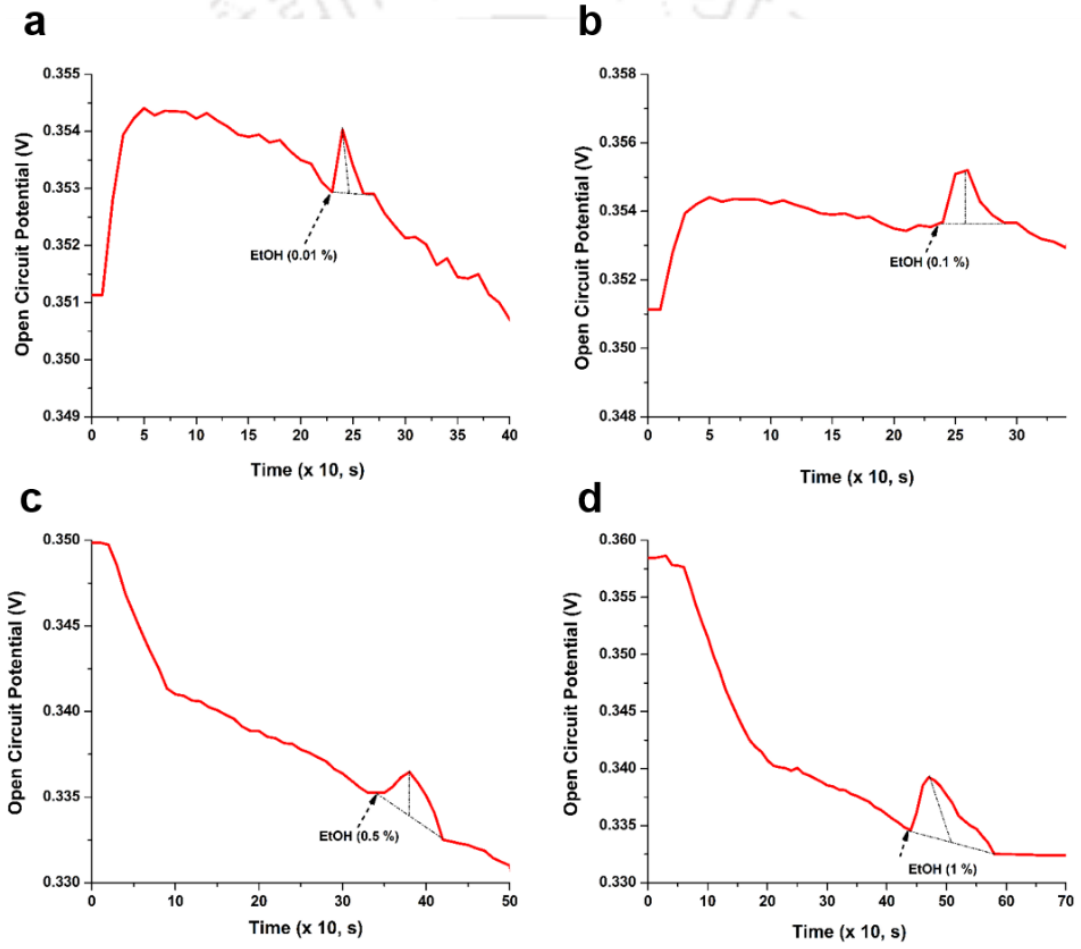


**Figure 4.18:** The OCP profile of the p-PMFC under different concentration of EtOH (a) 0.01 %, (b) 0.1 %, (c) 0.5 % and (d) 1 %.

A p-PMFC without immobilized cells on the anodic zone served as the control, which did not produce any significant signal following the ethanol addition. The effect of some common solvents relevant to the context of alcohol detection in fermentation and fuel

industries on the potential response was evaluated by exposing the biosensor to each of the solvents in 0.1 M phosphate buffer at pH 7.0. DMSO was evaluated because it is frequently used as a solvent and extractant for chemical, biochemical and cell biological work. The burst potential increase (%) for the solvents except DMSO and methanol was not significant (Figure 4.17 B). The signal to noise ratio for acetic acid (0.05), butanol (0.04), DMSO (0.76), methanol (0.23) and isopropanol (0.01) are shown in the parentheses considering the signal for ethanol as one. It is likely, that DMSO also has a detrimental effect on the cell membrane as alcohols. The inhibitory activity of DMSO (< 10 %) paralleled to alcohols on some common bacterial species is known (Wadhwani *et al*., 2009). The biosensor retained 85 % of its initial activity after 90-day of storage at 4 °C in dark. The longer lifetime is attributed to the native environment of the bioelectrode supported by the nano-biocomposite matrix on the paper substrate that offered an excellent biocompatible microenvironment for the autotrophic cells to survive and maintain its physiological activity during the day and night (McCormick *et al*., 2015). Further, p-PMFC promoted rapid adsorption of the bacteria into the electrode surface thus, reducing the start-up time to 20 min from 48 h in lab scale format. It may be mentioned that MFCs could detect low levels (1 mg $L^{-1}$) of heavy metals and pesticides but these studies did not document concentration-response relationship for these targets. Further, the enrichment of such devices including inoculation, immobilization and stabilization took a long time and reported a measurement time of minimum 10 min (Kim *et al*., 2007). A miniaturized MFC with *G. sulfurreducens* as a biocatalyst could detect formaldehyde (detection limit 0.1 %) within 3 min but clarity in calibration, the upper limit of detection and drop in voltage with varying concentration range were missing (Dávila *et al*., 2011). MFCs were also proposed for detection of microbial activity in the extra-terrestrial zone with a measurement time of 72 h (Abrevaya *et al*., 2015). Microbial biosensors for alcohol detection have been previously reported (Wen *et al*., 2014; Thungon *et al*., 2017). Bio-assays for detection of both methanol and ethanol using pH-sensitive field effect transistors were developed using the mutant methylotrophic yeast cells. The developed sensor did not demonstrate cross-sensitivity to other alcohols namely, butanols, propanols and pentanols. However, the sensor exhibited a long response time of 25 min and responded to formaldehyde (Korpan *et al*., 1993). Electrochemical detection of ethanol based on the fungus *A. niger* was also developed (Subrahmanyam *et al*., 2001). The current

responses (μA) of the sensor for ethanol (660), methanol (15), propanol (50), glycerol (10), and formic acid (10) are shown in the parentheses. Reshetilov *et al*. used *P. methanolica* to design a paper-based sensor with a Clark type oxygen electrode to detect alcohol. Of all the substrates tested (ethanol, methanol, glucose, citrate, xylitol, acetate, isopropanol, xylose, glycerol, arabinose, arabitol and pyruvate), the sensor had a higher selectivity towards ethanol and methanol (Reshetilov *et al*., 2001). In another study, amperometric-based ethanol sensing was conducted using *G. oxydans* cell on ferricyanide mediated glassy carbon electrode. The ethanol to glucose sensitivity ratio was improved by a factor of 58.2 with the aid of the size exclusion effect of a cellulose acetate membrane. The sensitivity of the sensor was 3.5 μA $mM^{-1}$ (Tkac *et al*., 2003). A potentiometric oxygen electrode was successfully used to produce a microbial alcohol biosensor based on immobilised *S. ellipsoideus* cells. The selectivity (100 % relative response) of the biosensor for ethanol was impressive as it did not respond to methanol, propanol, and acetic acid. However, the biosensor exhibited a significant response (30 %) towards glucose (Rotariu *et al*., 2004). Valach et al. also constructed an amperometric-based microbial (*G. oxydans*) biosensor for measurement of ethanol in flow injection analysis (FIA) system. Ethanol to glucose selectivity ratio of 6.8 was achieved by the system (Valach *et al*., 2009).

## 4.4 Conclusion

This work reports a novel strategy to detect alcohol selectively, sensitively and quantitatively using a low-cost p-PMFC as the sensor device. The sensor relies on the signal generated rapidly in the form a potential burst upon injection of the target alcohols on the anodic surface immobilized with a layer of *Synechococcus* sp. cells. Contrary to the conventional principle of substrate – biocatalysts interaction or metabolic inhibition based detection of the target, the membrane properties of the bacterial cells that succumb to degradation under solvation with selective hydrophobic target molecules have been exploited here. The alcohol led degradation of the membrane has been confirmed by various methods and techniques. The degradation of the cell membrane increases the exposure of the electron transfer proteins leading to the instantaneous surging of the bioanode that manifested in the form of a potential burst. Injection of alcohol also sparked the microbial respiration, which was independent to the cellular growth. A report on alcohol triggered

elevation of NADH level is also available (Manzo-Avalos and Saavedra-Molina, 2010); the exact mechanism on this impute for the case of cyanobacteria, is however not yet known. Nevertheless, the microbial respiration is known to link to the level of NADH, which furnishes electrons and protons to generate the emf and pmf, respectively across the cell membrane. The electrons are channelized through the electron carrier membrane-bound redox proteins under a potential gradient caused by the terminal electron acceptor, which is oxygen for a wide range of microorganisms. In MFC, the anode behaves as the electron acceptor even when the anoxic condition is not maintained as validated for the p-PMFC developed through this investigation. Thus the linkage of the potential burst with the enhanced respiration and the membrane depolarization and degradation of the cyanobacteria cells could be logically drawn in the present case.

The concept was initially investigated in a lab scale PMFC to understand the precise performance behavior of the sensor. When translated to a paper-based format, a majority of the performance factors for ethanol were improved such as, long shelf life, improved LOD, selective towards ethanol with an absolute selectivity at the low concentration < 0.5 % range and short response time. The decrease in response time has been attributed to the diminishing diffusional barrier for the alcohol substrate due to its direct interaction with the cells immobilized over the paper surface. The probable reason for the constricted dynamic range is the reduction of the catalytic cell concentrations while scaling down the PMFC from lab scale to chip size. The fundamental relation between the biocatalyst concentration and dynamic range is widely known (Wen *et al*., 2014). Hence, optimization study on the loading of the bacterial cells on the paper surface may expand the range for screening a wide concentration range of samples. The novel design is not prone to reactant cross-over between the electrode chambers at the optimized sample volume and easy to operate as it is free from an external mediator. The self-sustaining phototrophic growth of cyanobacterial cells endorses their long shelf life. Overall, the developed p-PMFC and the novel rapid response signal forms for sensitive and selective detection of ethanol has a great application potential in various fields.

# Overall Conclusion and Scope for Future Research

# Overall Conclusion and Scope for Future Research

## Overall conclusion

The major goal defined for the present investigation was to develop an efficient PMFC using a cyanobacteria strain, *Synechococcus* sp. as anodic catalyst. A further objective was to explore the utility of the developed PMFC as small, disposable alcohol biosensor. As a maiden step, we conducted a study on the creation of cyanobacteria biofilm on solid supports with an aim of extrapolating the spawn concept to a solid electrode surface of the PMFC. Different polymer thin-films were examined for their capability to support rapid biofilm growth of *Synechococcus* sp. We demonstrated for the first time that the natural polymers, silk and chitosan blended silk thin films strongly support rapid biofilm growth not only for the *Synechococcus* sp. but also for the other two bacterial strains of industrial significance, namely, *E. coli* and *L. plantarum*. The hydrophobic property of silk fibroin played a critical role in accelerating the biofilm growth. As a whole, the interplay of two physico-chemical properties namely, hydrophobicity and surface charge of cells and thin films were found to be responsible for facile adhesion of bacterial cells on the film that prelude to the massive biofilm formation. We confirmed that the biofilm growth was accelerated by the biomaterial films not only on the commonly employed solid supports, namely, glass and polystyrene but also on graphite material, which is otherwise unreceptive to microbial growth. The concept conceived through this investigation on developing microbial biofilm in a short timescale was then implemented in a newly constructed dual chambered (partitioned by Nafion membrane) PMFC assembled with a ferricyanide based abiotic cathode and a modified graphite electrode as anode using acetate as feed to the anodic chamber. In this second phase of work, the silk-film was however, modified by rationally doping CdTe QD and GNP in the silk fibroin to generate a novel silk-based nano-biocomposite matrix endowed with biocompatible, optoelectronic and electroactive properties apt for the bioanode fabrication. The nano-biocomposite matrix, when cast on graphite anode, promoted rapid biofilm growth of *Synechococcus* sp., supported FRET to surge the photosystems of the underneath bacteria in the biofilm and provided an electroactive surface for relaying metabolic electrons from the cells to the electrode through

DET during operation of the PMFC. The cumulative action of these properties not only enhanced the power density but also stabilized the power during the dark phase of the PMFC operation. Each of these functions of the nano-biocomposite matrix was adequately evaluated to validate their evolved properties in the hybrid state. We envision that our approach will be a big step forward, not only to improve the overall current density in a PMFC, but also to sustain its power at low light operating conditions, due to FRET guided surging of the photosystems of the cyanobacteria. The next phase of the work involved the study of performance behaviour of the lab scale PMFC in presence of different concentrations of alcohol in the anodic chamber. We succeeded in generating a novel signal form that relied upon the potential burst following injection of the target alcohols on the *Synechococcus* sp. biofilm-based bioanode chamber of the PMFC. A series of experiments were conducted to understand the effect of alcohol on the integrity of the bacterial cells and the observed potential burst. Contrary to the conventional principle of substrate – biocatalysts interaction or metabolic inhibition based detection of the target, the membrane properties of the bacterial cells that succumb to degrade under solvation with selective hydrophobic target molecules was exploited here. The degradation of the cell membrane increases the exposure of the electron transfer proteins leading to the instantaneous surging of the bioanode that manifested in the form of a potential burst. The involvement of the DET mechanism in generating current in this PMFC was validated by the appearance of clear redox peaks of the cell membrane-bound redox proteins in the cyclic voltammograms. The other reason that prompted us to conclude the involvement of DET mechanism was that no external electron transfer mediator was used to operate the system. Notably, no nanowire kind of external filament on the cell surface of the tested cyanobacteria could be detected from the high resolution microscopic studies; which therefore, negated the involvement of nanowire-based mechanism for channelizing cellular electrons to the anode. The PMFC could detect the presence of ethanol within ~ 60 s with a LOD of 0.13 %. It was observed that the injection of alcohol sparked the respiration of the cyanobacteria cells. Interestingly, the alcohol led increased respiration was independent to the cellular growth of this micro-organism. Thus the linkage of the alcohol triggered potential burst with the enhanced respiration, membrane depolarization, degradation of the cell membrane and enhanced exposure of the redox membrane proteins to the anode could be logically drawn in the

present case. In our final phase of the work, we successfully reproduced the PMFC from lab scale to a chip-based portable format using paper as the support substrate. When translated to a paper format, many of the performance factors for the ethanol detection were improved as revealed from the increased shelf life, improved LOD (0.02 %), increased selectivity towards ethanol with an absolute selectivity at the low concentration < 0.5 % range and reduced response time (~ 10 s). The decrease in response time was attributed to the diminishing diffusional barrier for the alcohol substrate due to its direct interaction with the cells immobilized over the paper surface. The probable reason for the constricted dynamic range is the reduction of the catalytic cell concentrations while scaling down the PMFC from lab scale to chip size. The novel design is not prone to reactant cross-over between the electrode chambers at the optimized sample volume and easy to operate as it is free from an external mediator. Interestingly, in this paper based PMFC (p-PMFC), the DET based bio-electrocatalytic function of the bioanode was not hampered by the open oxygenic condition of operation. Hence, this biofilm-based bioanode developed through the novel concept made the p-PMFC device technically simple that obviated the need of creating anoxic anodic compartment to prevent interference from the electron scavenging effect of oxygen. Overall, the developed p-PMFC with the novel signal form for sensitive, selective and rapid detection of ethanol has a great potential for developing this device of practical use.

## Scope for future research

The results of the work included in this thesis demonstrated an enormous possibility of using cyanobacteria *Synechococcus* sp. as the anodic catalyst for developing small-scale MFC sensors for practical applications. On a critical evaluation note, we would like to forward the following points on the present work that need to be properly addressed for further augmenting the work:

(i) The biochemical and molecular biological basis on the rapid development of biofilm on the selected biomaterials needs to be elucidated. The knowledge may be useful in developing a rational approach for inducing biofilm rapidly on material surfaces for various applications.

(ii) The exact molecular bio-electrochemistry on channelizing the cellular electrons to the electrode in PMFC should be identified. The finding may be

useful to develop a strategy for reducing the activation overpotential, which in turn may help in enhancing the power efficiency of the PMFC.

(iii) A suitable strategy needs to be explored for expanding the linear dynamic range for detecting alcohol in the p-PMFC. A pertinent solution is that the active bio-electrocatalytic surface area on the anode should be increased for which, an optimization study on the loading of the immobilized cells on the anodic paper surface may be performed. For better reproducibility and commercial perspectives, the bioelectrode fabrication should be performed by using screen printing technology following the optimization study.

(iv) The portable p-PMFC device needs to be integrated to a suitable processor unit that can convert the signal to a digital form for quantitative analysis of alcohol in real samples from fuel and fermentation industries.

(v) The developed p-PMFC may be further tested with other potential interfering agents including solvents and amphipathic compounds to understand the level of selectivity being delivered by the system.

(vi) The performance of the portable p-MFC may be investigated by using commonly available bacterial strains such as, *E. coli* and *Pseudomonas* sp. as anodic catalysts for a comparative analysis and understanding of the proposed sensing mechanism.

# Bibliography


**Abrevaya, X.C., Sacco, N.J., Bonetto, M.C., Hilding-Ohlsson, A., Cortón, E.** Analytical applications of microbial fuel cells. Part II: toxicity, microbial activity and quantification, single analyte detection and other uses. Biosens. Bioelectron. 63, 591–601 (2015).

**Akhairi, M.A.F., Kamarudin, S.K.** Catalysts in direct ethanol fuel cell (DEFC): An overview. Int. J. Hydrogen Energy 41, 4214–4228 (2016).

**Akyilmaz, E., Dinçkaya, E.** An amperometric microbial biosensor development based on *Candida tropicalis* yeast cells for sensitive determination of ethanol. Biosens. Bioelectron. 20, 1263–1269 (2005).

**Andrade, C., Danielly, M., Faulin, T., Hering, V., Parra Abdall, D.S.** Biosensors for detection of low-density lipoprotein and its modified forms, Biosensors for Health, Environment and Biosecurity. InTech, UK. 215–219 (2011).

**Antal, T.K., Kukarskikh, G.P., Volgusheva, A.A., Krendeleva, T.E., Tyystjärvi, E., Rubin, A.B.** Hydrogen photoproduction by immobilized S-deprived *Chlamydomonas reinhardtii* : Effect of light intensity and spectrum, and initial medium pH. Algal Res. 17, 38–45 (2016).

**Asakura, T., Miller, T.** Biotechnology of Silk. Springer Netherlands (2013).

**Asha, S., Sangappa, Y., Sanjeev, G.** Optical properties of electron irradiated *Bombyx mori* silk fibroin films. J. Opt. 45, 66–72 (2016).

**Azeredo, J., Visser, J., Oliveira, R.** Exopolymers in bacterial adhesion: interpretation in terms of DLVO and XDLVO theories. Colloids Surfaces B Biointerfaces 14, 141–148 (1999).

**Azevedo, A., Prazeres, D., Cabral, J., Fonseca, L.** Ethanol biosensors based on alcohol oxidase. Biosens. Bioelectron. 21, 235–247 (2005).

**Badger, M.R.** $CO_2$ concentrating mechanisms in cyanobacteria: molecular components, their diversity and evolution. J. Exp. Bot. 54, 609–622 (2003).

**Baranitharan, E., Khan, M.R., Prasad, D.M.R., Teo, W.F.A., Tan, G.Y.A., Jose, R.** Effect of biofilm formation on the performance of microbial fuel cell for the treatment of palm oil mill effluent. Bioprocess Biosyst. Eng. 38, 15–24 (2015).

**Baudler, A., Schmidt, I., Langner, M., Greiner, A., Schröder, U.** Does it have to be carbon? Metal anodes in microbial fuel cells and related bioelectrochemical systems. Energy Environ. Sci. 8, 2048–2055 (2015).

**Bayoudh, S., Othmane, A., Ponsonnet, L., Ben Ouada, H.** Electrical detection and characterization of bacterial adhesion using electrochemical impedance spectroscopy-based flow chamber. Colloids Surfaces A Physicochem. Eng. Asp. 318, 291–300 (2008).

**Bazaka, K., Jacob, M. V., Crawford, R.J., Ivanova, E.P.** Efficient surface modification of biomaterial to prevent biofilm formation and the attachment of microorganisms. Appl. Microbiol. Biotechnol. 95, 299–311 (2012).

**Behera, B.K., Balasundaram, R., Gadgil, K., Sharma, D.K.** Photobiological production of hydrogen from *Spirulina* for fueling fuel cells. Energy Sources, Part A Recover. Util. Environ. Eff. 29, 761–767 (2007).

**Bell, P.D., Xin, Y., Blankenship, R.E.** Purification and characterization of cytochrome $c_6$ from *Acaryochloris marina*. Photosynth. Res. 102, 43–51 (2009).

**Bernroitner, M., Tangl, D., Lucini, C., Furtmüller, P.G., Peschek, G.A., Obinger, C.** Cyanobacterial cytochrome $c_M$: Probing its role as electron donor for CuA of cytochrome *c* oxidase. Biochim. Biophys. Acta - Bioenerg. 1787, 135–143 (2009).

**Blankenship, R.E., Tiede, D.M., Barber, J., Brudvig, G.W., Fleming, G., Ghirardi, M., Gunner, M.R., Junge, W., Kramer, D.M., Melis, A., Moore, T. a, Moser, C.C., Nocera, D.G., Nozik, A.J., Ort, D.R., Parson, W.W., Prince, R.C., Sayre, R.T.,** Comparing photosynthetic and photovoltaic efficiencies and recognizing the potential for improvement. Science. 332, 805–809 (2011).

**Bombelli, P., Bradley, R.W., Scott, A.M., Philips, A.J., McCormick, A.J., Cruz, S.M., Anderson, A., Yunus, K., Bendall, D.S., Cameron, P.J., Davies, J.M., Smith, A.G., Howe, C.J., Fisher, A.C.** Quantitative analysis of the factors limiting solar power transduction by *Synechocystis sp*. PCC 6803 in biological photovoltaic devices. Energy Environ. Sci. 4, 4690 (2011).

**Bombelli, P., Müller, T., Herling, T.W., Howe, C.J., Knowles, T.P.J.** A high power-density, mediator-free, microfluidic biophotovoltaic device for cyanobacterial cells. Adv. Energy Mater. 5, 1401299 (2015).

**Bombelli, P., Zarrouati, M., Thorne, R.J., Schneider, K., Rowden, S.J.L., Ali, A., Yunus, K., Cameron, P.J., Fisher, A.C., Ian Wilson, D., Howe, C.J., McCormick, A.J.** Surface morphology and surface energy of anode materials influence power outputs in a multi-channel mediatorless bio-photovoltaic (BPV) system. Phys. Chem. Chem. Phys. 14, 12221 (2012).

**Bond, D.R., Lovley, D.R.** Electricity production by *Geobacter sulfurreducens* attached to electrodes. Appl. Environ. Microbiol. 69, 1548–1555 (2003).

**Bradley, R.W., Bombelli, P., Lea-Smith, D.J., Howe, C.J.** Terminal oxidase mutants of the cyanobacterium *Synechocystis sp.* PCC 6803 show increased electrogenic activity in biological photo-voltaic systems. Phys. Chem. Chem. Phys. 15, 13611 (2013).

**Bruno, L., Di Pippo, F., Antonaroli, S., Gismondi, A., Valentini, C., Albertano, P.** Characterization of biofilm-forming cyanobacteria for biomass and lipid production. J. Appl. Microbiol. 113, 1052–1064 (2012).

**Cartwright, C.P., Juroszek, J.-R., Beavan, M.J., Ruby, F.M.S., De Morais, S.M.F., Rose, A.H.** Ethanol dissipates the proton-motive force across the plasma membrane of *Saccharomyces cerevisiae*. Microbiology 132, 369–377 (1986).

**Cereda, A., Hitchcock, A., Symes, M.D., Cronin, L., Bibby, T.S., Jones, A.K.** A bioelectrochemical approach to characterize extracellular electron transfer by *Synechocystis sp.* PCC6803. PLoS One 9, e91484 (2014).

**Checchetto, V., Segalla, A., Allorent, G., La Rocca, N., Leanza, L., Giacometti, G.M., Uozumi, N., Finazzi, G., Bergantino, E., Szabo, I.** Thylakoid potassium channel is required for efficient photosynthesis in cyanobacteria. Proc. Natl. Acad. Sci. 109, 11043–11048 (2012).

**Chen, M., Li, J., Zhang, L., Chang, S., Liu, C., Wang, J., Li, S.** Auto-flotation of heterocyst enables the efficient production of renewable energy in cyanobacteria. Sci. Rep. 4, 3998 (2015a).

**Chen, X.F., Wang, X.S., Liao, K.T., Zeng, L.Z., Xing, L.D., Zhou, X.W., Zheng, X.W., Li, W.S.** Improved power output by incorporating polyvinyl alcohol into the anode of a microbial fuel cell. J. Mater. Chem. A 3, 19402–19409 (2015b).

**Chern, C.S., Lee, C.K., Ho, C.C.** Colloidal stability of chitosan-modified poly(methyl methacrylate) latex particles. Colloid Polym. Sci. 277, 507–512 (1999).

**Chinnadayyala, S.R., Kakoti, A., Santhosh, M., Goswami, P.** A novel amperometric alcohol biosensor developed in a 3rd generation bioelectrode platform using peroxidase coupled ferrocene activated alcohol oxidase as biorecognition system. Biosens. Bioelectron. 55, 120–126 (2014).

**Choi, J.S., Lee, H.K., An, S.J.** Synthesis of a graphene oxide/sodium silicate nanocomposite using sodium silicate solution. RSC Adv. 5, 38742–38747 (2015).

**Choi, S.** Microscale microbial fuel cells: advances and challenges. Biosens. Bioelectron. 69, 8–25 (2015).

**Chu, Y.F., Hsu, C.H., Soma, P.K., Lo, Y.M.** Immobilization of bioluminescent *Escherichia coli* cells using natural and artificial fibers treated with polyethyleneimine. Bioresour. Technol. 100, 3167–3174 (2009).

**Churski, K., Ruszczak, A., Jakiela, S., Garstecki, P.** Droplet microfluidic technique for the study of fermentation. micromachines 6, 1514–1525 (2015).

**Clapp, A.R., Medintz, I.L., Mauro, J.M., Fisher, B.R., Bawendi, M.G., Mattoussi, H.** Fluorescence resonance energy transfer between quantum dot donors and dye-labeled protein acceptors. J. Am. Chem. Soc. 126, 301–310 (2004).

**Clementi, E.A., Marks, L.R., Roche-Håkansson, H., Håkansson, A.P.** Monitoring Changes in membrane polarity, membrane monitoring changes in membrane polarity, membrane integrity, and intracellular ion concentrations in *Streptococcus pneumoniae* using fluorescent dyes. J. Vis. Exp. 84, 1–8 (2014).

**Croisier, F., Jérôme, C.** Chitosan-based biomaterials for tissue engineering. Eur. Polym. J. 49, 780–792 (2013).

**Darus, L., Sadakane, T., Ledezma, P., Tsujimura, S., Osadebe, I., Leech, D., Gorton, L., Freguia, S.** Redox-polymers enable uninterrupted day/night photo-driven electricity generation in biophotovoltaic devices. J. Electrochem. Soc. 164, H3037–H3040 (2017).

**Das, M., Barbora, L., Das, P., Goswami, P.** Biofuel cell for generating power from methanol substrate using alcohol oxidase bioanode and air-breathed laccase biocathode. Biosens. Bioelectron. 59, 184–191 (2014).

**Dávila, D., Esquivel, J.P., Sabaté, N., Mas, J.** Silicon-based microfabricated microbial fuel cell toxicity sensor. Biosens. Bioelectron. 26, 2426–2430 (2011).

**Dawar, S., Behera, B.K., Mohanty, P.** Development of a low-cost oxy-hydrogen bio-fuel cell for generation of electricity using *Nostoc* as a source of hydrogen. Int. J. Energy Res. 22, 1019–1028 (1998).

**Deere, D.** Evaluation of the suitability of bis-(1,3-dibutylbarbituric acid) trimethine oxonol, (diBA-C4(3) −), for the flow cytometric assessment of bacterial viability. FEMS Microbiol. Lett. 130, 165–169 (1995).

**Diaz-Herraiz, M., Jurado, V., Cuezva, S., Laiz, L., Pallecchi, P., Tiano, P., Sanchez-Moral, S., Saiz-Jimenez, C.** The actinobacterial colonization of etruscan paintings. Sci. Rep. 3, 1440 (2013).

**Dittrich, M., Sibler, S.** Cell surface groups of two picocyanobacteria strains studied by zeta potential investigations, potentiometric titration, and infrared spectroscopy. J. Colloid Interface Sci. 286, 487–495 (2005).

**Dombek, K.M., Ingram, L.O.** Effects of ethanol on the *Escherichia coli* plasma membrane. J. Bacteriol. 157, 233–239 (1984).

**Du, Z., Li, H., Gu, T.** A state of the art review on microbial fuel cells: A promising technology for wastewater treatment and bioenergy. Biotechnol. Adv. 25, 464–482 (2007).

**ElMekawy, A., Hegab, H.M., Pant, D., Saint, C.P.** Bio-analytical applications of microbial fuel cell-based biosensors for onsite water quality monitoring. J. Appl. Microbiol. 124, 302–313 (2018).

**ElMekawy, A., Hegab, H.M., Vanbroekhoven, K., Pant, D.** Techno-productive potential of photosynthetic microbial fuel cells through different configurations. Renew. Sustain. Energy Rev. 39, 617–627 (2014).

**Enning, D., Garrelfs, J.**. Corrosion of iron by sulfate-reducing bacteria: new views of an old problem. Appl. Environ. Microbiol. 80, 1226–1236 (2014).

**Esteve-Núñez, A., Sosnik, J., Visconti, P., Lovley, D.R.** Fluorescent properties of *c*-type cytochromes reveal their potential role as an extracytoplasmic electron sink in *Geobacter sulfurreducens.* Environ. Microbiol. 10, 497–505 (2008).

**Fan, J., Shi, Z., Ge, Y., Wang, J., Wang, Y., Yin, J.** Gum arabic assisted exfoliation and fabrication of Ag–graphene-based hybrids. J. Mater. Chem. 22, 13764 (2012).

**Farris, S., Introzzi, L., Biagioni, P., Holz, T., Schiraldi, A., Piergiovanni, L.** Wetting of biopolymer coatings: contact angle kinetics and image analysis investigation. Langmuir 27, 7563–7574 (2011).

**Fattom, A., Shilo, M.** Hydrophobicity as an adhesion mechanism of benthic cyanobacteria. Appl. Environ. Microbiol. 47, 135–43 (1984).

**Faulkner, C.J., Lees, S., Ciesielski, P.N., Cliffel, D.E., Jennings, G.K.** Rapid assembly of photosystem I monolayers on gold electrodes. Langmuir 24, 8409–8412 (2008).

**Flemming, H.C., Wingender, J.** The biofilm matrix. Nat. Rev. Microbiol. 8, 623–633 (2010).

**Fletcher, M.** The effects of methanol, ethanol, propanol and butanol on bacterial attachment to surfaces. Microbiology 129, 633–641 (1983).

**Fraiwan, A., Choi, S.** Bacteria-powered battery on paper. Phys. Chem. Chem. Phys. 16, 26288–26293 (2014).

**Fraiwan, A., Kwan, L., Choi, S.** A disposable power source in resource-limited environments: A paper-based biobattery generating electricity from wastewater. Biosens. Bioelectron. 85, 190–197 (2016).

**Fu, C.C., Hung, T.C., Wu, W.T., Wen, T.C., Su, C.H.** Current and voltage responses in instant photosynthetic microbial cells with *Spirulina platensis*. Biochem. Eng. J. 52, 175–180 (2010).

**Gabdulkhakov, A.G., Dontsova, M. V.** Structural studies on photosystem II of cyanobacteria. Biochem. 78, 1524–1538 (2013).

**Gademann, K.** Cyanobacterial natural products for the inhibition of biofilm formation and biofouling. Chim. Int. J. Chem. 61, 373–377 (2007).

**Gill, R.T., Katsoulakis, E., Schmitt, W., Taroncher-Oldenburg, G., Misra, J., Stephanopoulos, G.** Genome-wide dynamic transcriptional profiling of the light-to-dark transition in *Synechocystis sp.* Strain PCC 6803. J. Bacteriol. 184, 3671–3681 (2002).

**Golbeck, J.H.** Photosystem I in Cyanobacteria, in: Bryant, D.A. (Ed.), The Molecular Biology of Cyanobacteria. Springer Netherlands, Dordrecht, 319–360 (1994).

**Gómez-Anquela, C., García-Mendiola, T., Abad, J.M., Pita, M., Pariente, F., Lorenzo, E.** Scaffold electrodes based on thioctic acid-capped gold nanoparticles coordinated Alcohol Dehydrogenase and Azure A films for high performance biosensor. Bioelectrochemistry 106, 335–342 (2015).

**Gorby, Y.A., Yanina, S., McLean, J.S., Rosso, K.M., Moyles, D., Dohnalkova, A., Beveridge, T.J., Chang, I.S., Kim, B.H., Kim, K.S., Culley, D.E., Reed, S.B., Romine, M.F., Saffarini, D.A., Hill, E.A., Shi, L., Elias, D.A., Kennedy, D.W., Pinchuk, G., Watanabe, K., Ishii, S., Logan, B., Nealson, K.H., Fredrickson, J.K.** Electrically conductive bacterial nanowires produced by *Shewanella oneidensis* strain MR-1 and other microorganisms. Proc. Natl. Acad. Sci. 103, 11358–11363 (2006).

**Grabolle, M., Spieles, M., Lesnyak, V., Gaponik, N., Eychmüller, A., Resch-Genger, U.** Determination of the fluorescence quantum yield of quantum dots: suitable procedures and achievable uncertainties. Anal. Chem. 81, 6285–6294 (2009).

**Guo, K., Freguia, S., Dennis, P.G., Chen, X., Donose, B.C., Keller, J., Gooding, J.J., Rabaey, K.** Effects of surface charge and hydrophobicity on anodic biofilm formation, community composition, and current generation in bioelectrochemical systems. Environ. Sci. Technol. 47, 7563–7570 (2013).

**Hall, D.O., Markov, S.A., Watanabe, Y., Krishna Rao, K.** The potential applications of cyanobacterial photosynthesis for clean technologies. Photosynth. Res. 46, 159–167 (1995).

**Hancock, V., Witsø, I.L., Klemm, P.** Biofilm formation as a function of adhesin, growth medium, substratum and strain type. Int. J. Med. Microbiol. 301, 570–576 (2011).

**Hasan, K., Bekir Yildiz, H., Sperling, E., Ó Conghaile, P., Packer, M. a, Leech, D., Hägerhäll, C., Gorton, L.** Photo-electrochemical communication between cyanobacteria (*Leptolyngbia sp.*) and osmium redox polymer modified electrodes. Phys. Chem. Chem. Phys. 16, 24676–24680 (2014).

**He, Z., Kan, J., Mansfeld, F., Angenent, L.T., Nealson, K.H.** Self-sustained phototrophic microbial fuel cells based on the synergistic cooperation between photosynthetic microorganisms and heterotrophic bacteria. Environ. Sci. Technol. 43, 1648–1654 (2009).

**Hicks, D.B., Yocum, C.F.** Properties of the cyanobacterial coupling factor ATPase from *Spirulina platensis*. Arch. Biochem. Biophys. 245, 220–229 (1986).

**Hink, M.A., Visser, N. V., Borst, J.W., van Hoek, A., Visser, A.J.W.G.** Practical use of corrected fluorescence excitation and emission spectra of fluorescent proteins in förster resonance energy transfer (FRET) studies. J. Fluoresc. 13, 185–188 (2003).

**Horcas, I., Fernández, R., Gómez-Rodríguez, J.M., Colchero, J., Gómez-Herrero, J., Baro, A.M.** WSXM: A software for scanning probe microscopy and a tool for nanotechnology. Rev. Sci. Instrum. 78, 013705 (2007).

**Huang, H., Xiao, X., Ghadouani, A., Wu, J., Nie, Z., Peng, C., Xu, X., Shi, J.,**. Effects of natural flavonoids on photosynthetic activity and cell integrity in *Microcystis aeruginosa*. Toxins (Basel). 7, 66–80 (2015).

**Huang, L., Li, C., Yuan, W., Shi, G.** Strong composite films with layered structures prepared by casting silk fibroin–graphene oxide hydrogels. Nanoscale 5, 3780 (2013).

**Ikeda, T., Kato, K., Maeda, M., Tatsumi, H., Kano, K., Matsushita, K.** Electrocatalytic properties of *Acetobacter aceti* cells immobilized on electrodes for the quinone-mediated oxidation of ethanol. J. Electroanal. Chem. 430, 197–204 (1997).

**Inglesby, A.E., Beatty, D. A., Fisher, A.C.** *Rhodopseudomonas palustris* purple bacteria fed *Arthrospira maxima* cyanobacteria: demonstration of application in microbial fuel cells. RSC Adv. 2, 4829 (2012).

**Inglesby, A.E., Yunus, K., Fisher, A.C.** In situ fluorescence and electrochemical monitoring of a photosynthetic microbial fuel cell. Phys. Chem. Chem. Phys. 15, 6903 (2013).

**Inoue, S., Parra, E. A., Higa, A., Jiang, Y., Wang, P., Buie, C.R., Coates, J.D., Lin, L.** Structural optimization of contact electrodes in microbial fuel cells for current density enhancements. Sensors Actuators A Phys. 177, 30–36 (2012).

**Kakoti, A., Siddiqui, M.F., Goswami, P.** A low cost design and fabrication method for developing a leak proof paper based microfluidic device with customized test zone. Biomicrofluidics 9, 026502 (2015).

**Kalathil, S., Khan, M.M., Lee, J., Cho, M.H.** Production of bioelectricity, bio-hydrogen, high value chemicals and bioinspired nanomaterials by electrochemically active biofilms. Biotechnol. Adv. 31, 915–924 (2013).

**Kaplan, A., Reinhold, L.** $CO_2$ concentrating mechanisms in photosynthetic microorganisms. Annu. Rev. Plant Physiol. Plant Mol. Biol. 50, 539–570 (1999).

**Karatan, E., Watnick, P.** Signals, regulatory networks, and materials that build and break bacterial biofilms. Microbiol. Mol. Biol. Rev. 73, 310–347 (2009).

**Katuri, K.P., Rengaraj, S., Kavanagh, P., O'Flaherty, V., Leech, D.,**. Charge transport through *Geobacter sulfurreducens* biofilms grown on graphite rods. Langmuir 28, 7904–7913 (2012).

**Kim, M., Sik Hyun, M., Gadd, G.M., Joo Kim, H.** A novel biomonitoring system using microbial fuel cells. J. Environ. Monit. 9, 1323 (2007).

**Komenda, J., Sobotka, R., Nixon, P.J.** Assembling and maintaining the photosystem II complex in chloroplasts and cyanobacteria. Curr. Opin. Plant Biol. 15, 245-251 (2012).

**Korpan, Y.I., Soldatkin, A.P., Starodub, N.F., El'skaya, A.V., Gonchar, M.V., Sibirny, A.A., Shul'ga, A.A.** Methylotrophic yeast microbiosensor based on ion-sensitive field effect transistors for methanol and ethanol determination. Anal. Chim. Acta 271, 203-

208 (1993).

**Kost, T.A., Condreay, J.P., Jarvis, D. L.** Baculovirus as versatile vectors for protein expression in insect and mammalian cells. Nat. Biotechnol. 23, 567–575 (2005).

**Kothe, T., Pöller, S., Zhao, F., Fortgang, P., Rögner, M., Schuhmann, W., Plumeré, N.** Engineered electron-transfer chain in photosystem I based photocathodes outperforms electron-transfer rates in natural photosynthesis. Chemistry 20, 11029-34 (2014).

**Kraushaar, H., Hager, S., Wastyn, M., Peschek, G.A.** Immunologically cross-reactive and redox-competent cytochrome b6/f-complexes in the chlorophyll-free plasma membrane of cyanobacteria. FEBS Lett. 273, 227–231 (1990).

**Krishnaraj R, N., R, K., Berchmans, S., Chandran, S., Pal, P.** Functionalization of electrochemically deposited chitosan films with alginate and Prussian blue for enhanced performance of microbial fuel cells. Electrochim. Acta 112, 465–472 (2013).

**Lam, K.B., Irwin, E.F., Healy, K.E., Lin, L.** Bioelectrocatalytic self-assembled thylakoids for micro-power and sensing applications. Sensors Actuators B Chem. 117, 480–487 (2006).

**Larom, S., Kallmann, D., Saper, G., Pinhassi, R., Rothschild, A., Dotan, H., Ankonina, G., Schuster, G., Adir, N.** The photosystem II D1-K238E mutation enhances electrical current production using cyanobacterial thylakoid membranes in a bio-photoelectrochemical cell. Photosynth. Res. 126, 161–169 (2015).

**Lee, H., Choi, S.** A micro-sized bio-solar cell for self-sustaining power generation. Lab Chip 15, 391–398 (2015).

**Leonat, L., Sbarcea, G., Branzoi, I.V.** Cyclic voltammetry for energy levels estimation of organic materials. UPB Sci. Bull. Ser. B Chem. Mater. Sci. 75 (2013).

**Li, B., Zhou, J., Zhou, X., Wang, X., Li, B., Santoro, C., Grattieri, M., Babanova, S., Artyushkova, K., Atanassov, P., Schuler, A.J.** Surface modification of microbial fuel cells anodes: approaches to practical design. Electrochim. Acta 134, 116–126 (2014).

**Li, J., Song, L.** Applicability of the MTT assay for measuring viability of cyanobacteria and algae, specifically for *Microcystis aeruginosa* (Chroococcales, Cyanobacteria). Phycologia 46, 593–599 (2007).

**Li, M., Lv, K., Wu, S., Chen, S.** Immobilization of anodophilic biofilms for use in aerotolerant bioanodes of microbial fuel cells. ACS Appl. Mater. Interfaces 8, 34985–34990 (2016).

**Li, X.G., Wu, L.Y., Huang, M.R., Shao, H.L., Hu, X.C.** Conformational transition and liquid crystalline state of regenerated silk fibroin in water. Biopolymers 89, 497–505 (2008).

**Li, Y., Scales, N., Blankenship, R.E., Willows, R.D., Chen, M.** Extinction coefficient for red-shifted chlorophylls: chlorophyll *d* and chlorophyll *f*. Biochim. Biophys. Acta -

Bioenerg. 1817, 1292–1298 (2012).

**Lim, J.W., Ha, D., Lee, J., Lee, S.K., Kim, T.** Review of micro/nanotechnologies for microbial biosensors. Front. Bioeng. Biotechnol. 3, 1–13 (2015).

**Lin, C.C., Wei, C.H., Chen, C.I., Shieh, C.J., Liu, Y.C.** Characteristics of the photosynthesis microbial fuel cell with a *Spirulina platensis* biofilm. Bioresour. Technol. 135, 640–643 (2013).

**Liu, L., Choi, S.** Self-sustainable, high-power-density bio-solar cells for lab-on-a-chip applications. Lab Chip 17, 3817–3825 (2017a).

**Liu, L., Choi, S.** Self-sustaining, solar-driven bioelectricity generation in micro-sized microbial fuel cell using co-culture of heterotrophic and photosynthetic bacteria. J. Power Sources 348, 138–144 (2017b).

**Liu, X., Zhang, K.** Oligomerization of chemical and biological compounds. InTech, UK (2014).

**Liu, Y., Yang, S.F., Li, Y., Xu, H., Qin, L., Tay, J.H.** The influence of cell and substratum surface hydrophobicities on microbial attachment. J. Biotechnol. 110, 251–256 (2004).

**Logan, B.E.** Exoelectrogenic bacteria that power microbial fuel cells. Nat. Rev. Microbiol. 7, 375–381 (2009).

**Logan, B.E., Hamelers, B., Rozendal, R., Schröder, U., Keller, J., Freguia, S., Aelterman, P., Verstraete, W., Rabaey, K.** Microbial fuel cells: methodology and technology. Environ. Sci. Technol. 40, 5181–5192 (2006).

**Logan, B.E., Regan, J.M.** Electricity-producing bacterial communities in microbial fuel cells. Trends Microbiol. 14, 512–518 (2006).

**Lubberding, H.J., Zimmer, G., Walraven, H., Schrickx, J., Kraayenhof, R.** Isolation, purification and characterization of the ATPase complex from the thermophilic cyanobacterium *Synechococcus* 6716. Eur. J. Biochem. 137, 95–99 (1983).

**Lv, Z., Chen, Y., Wei, H., Li, F., Hu, Y., Wei, C., Feng, C.** One-step electrosynthesis of polypyrrole/graphene oxide composites for microbial fuel cell application. Electrochim. Acta 111, 366–373 (2013).

**Madeira, A., Leitão, L., Soveral, G., Dias, P., Prista, C., Moura, T., Loureiro-Dias, M.C.** Effect of ethanol on fluxes of water and protons across the plasma membrane of *Saccharomyces cerevisiae*. FEMS Yeast Res. 10, 252–258 (2010).

**Madiraju, K.S., Lyew, D., Kok, R., Raghavan, V.** Carbon neutral electricity production by *Synechocystis sp*. PCC6803 in a microbial fuel cell. Bioresour. Technol. 110, 214–218 (2012).

**Malvankar, N.S., Tuominen, M.T., Lovley, D.R.** Biofilm conductivity is a decisive variable for high-current-density *Geobacter sulfurreducens* microbial fuel cells. Energy

Environ. Sci. 5, 5790 (2012).

**Manzo-Avalos, S., Saavedra-Molina, A.** Cellular and mitochondrial effects of alcohol consumption. Int. J. Environ. Res. Public Health 7, 4281–4304 (2010).

**Mao, L., Verwoerd, W.S.** Selection of organisms for systems biology study of microbial electricity generation: a review. Int. J. Energy Environ. Eng. 4, 17 (2013).

**Martinez, A.W., Phillips, S.T., Whitesides, G.M., Carrilho, E.** Diagnostics for the developing world: microfluidic paper-based analytical devices. Anal. Chem. 82, 3–10 (2010).

**Matos, C.T., Lopes da Silva, T.** Using multi-parameter flow cytometry as a novel approach for physiological characterization of bacteria in microbial fuel cells. Process Biochem. 48, 49–57 (2013).

**Matsumoto, S., Ohtaki, A., Hori, K.** Carbon fiber as an excellent support material for wastewater treatment biofilms. Environ. Sci. Technol. 46, 10175-10181 (2012).

**Matthews, B.W.** Hydrophobic interactions in proteins, encyclopedia of life sciences. John Wiley & Sons, Ltd, Chichester, UK (2001).

**McCormick, A.J., Bombelli, P., Bradley, R.W., Thorne, R., Wenzel, T., Howe, C.J.** Biophotovoltaics: oxygenic photosynthetic organisms in the world of bioelectrochemical systems. Energy Environ. Sci. 8, 1092–1109 (2015).

**McCormick, A.J., Bombelli, P., Scott, A.M., Philips, A.J., Smith, A.G., Fisher, A.C., Howe, C.J.** Photosynthetic biofilms in pure culture harness solar energy in a mediatorless bio-photovoltaic cell (BPV) system. Energy Environ. Sci. 4, 4699 (2011).

**McNally, J.G., Karpova, T., Cooper, J., Conchello, J.A.** Three-dimensional imaging by deconvolution microscopy. Methods 19, 373–385 (1999).

**Minak-Bernero, V., Bare, R.E., Haith, C.E., Grossman, M.J.** Detection of alkanes, alcohols, and aldehydes using bioluminescence. Biotechnol. Bioeng. 87, 170–177 (2004).

**Mohan, V. S., Veer Raghavulu, S., Sarma, P.N.** Influence of anodic biofilm growth on bioelectricity production in single chambered mediatorless microbial fuel cell using mixed anaerobic consortia. Biosens. Bioelectron. 24, 41–47 (2008).

**Mohan, V. S., Velvizhi, G., Annie Modestra, J., Srikanth, S.** Microbial fuel cell: Critical factors regulating bio-catalyzed electrochemical process and recent advancements. Renew. Sustain. Energy Rev. 40, 779–797 (2014).

**Moraes, M.A. de, Nogueira, G.M., Weska, R.F., Beppu, M.M.** Preparation and characterization of insoluble silk fibroin/chitosan blend films. Polymers (Basel). 2, 719–727 (2010).

**Morand, L.Z., Frame, M.K., Colvert, K.K., Johnson, D.A., Krogmann, D.W., Davis,**

**D.J.** Plastocyanin cytochrome *f* interaction. Biochemistry 28, 8039–8047 (1989).

**Moriuchi, T., Sumida, S., Furuya, A., Morishima, K., Furukawa, Y.** Development of a flexible direct photosynthetic/metabolic biofuel cell for mobile use. Int. J. Precis. Eng. Manuf. 10, 75–78 (2009).

**Mullineaux, C.W.** Electron transport and light-harvesting switches in cyanobacteria. Front. Plant Sci. 5, 1–6 (2014).

**Mustakeem.** Electrode materials for microbial fuel cells: nanomaterial approach. Mater. Renew. Sustain. Energy 4, 22 (2015).

**Nguyen, P.Q., Botyanszki, Z., Tay, P.K.R., Joshi, N.S.** Programmable biofilm-based materials from engineered curli nanofibres. Nat. Commun. 5, 4945 (2014).

**Nicholls, P., Obinger, C., Niederhauser, H., Peschek, G.A.** Cytochrome oxidase in *Anacystis nidulans*: stoichiometries and possible functions in the cytoplasmic and thylakoid membranes. Biochim. Biophys. Acta-Bioenerg. 1098, 184–190 (1992).

**Notley, S.M., Pettersson, B., Wågberg, L.** Direct measurement of attractive Van Der Waals' forces between regenerated cellulose surfaces in an aqueous environment. J. Am. Chem. Soc. 126, 13930–13931 (2004).

**Nucleo, E., Steffanoni, L., Fugazza, G., Migliavacca, R., Giacobone, E., Navarra, A., Pagani, L., Landini, P.** Growth in glucose-based medium and exposure to subinhibitory concentrations of imipenem induce biofilm formation in a multidrug-resistant clinical isolate of *Acinetobacter baumannii*. BMC Microbiol. 9, 270 (2009).

**O'Toole, G. A,**. Microtiter dish biofilm formation assay. J. Vis. Exp. 47, 10–11 (2011).

**Osman, M.H., Shah, A.A., Walsh, F.C.** Recent progress and continuing challenges in bio-fuel cells. Part I: Enzymatic cells. Biosens. Bioelectron. 26, 3087–3102 (2011).

**Ozkan, A., Berberoglu, H.** Physico-chemical surface properties of microalgae. Colloids Surfaces B Biointerfaces 112, 287–293 (2013a).

**Ozkan, A., Berberoglu, H.** Cell to substratum and cell to cell interactions of microalgae. Colloids Surfaces B Biointerfaces 112, 302–309 (2013b).

**Pankratova, G., Gorton, L.** Electrochemical communication between living cells and conductive surfaces. Curr. Opin. Electrochem. 5, 193–202 (2017).

**Parlak, O., Seshadri, P., Lundström, I., Turner, A.P.F., Tiwari, A.** Two-dimensional gold-tungsten disulphide bio-interface for high-throughput electrocatalytic nano-bioreactors. Adv. Mater. Interfaces 1, 1400136 (2014).

**Parnasa, R., Nagar, E., Sendersky, E., Reich, Z., Simkovsky, R., Golden, S., Schwarz, R.** Small secreted proteins enable biofilm development in the cyanobacterium *Synechococcus elongatus*. Sci. Rep. 6, 32209 (2016).

**Patra, M., Salonen, E., Terama, E., Vattulainen, I., Faller, R., Lee, B.W., Holopainen,**

**J., Karttunen, M.** Under the influence of alcohol: the effect of ethanol and methanol on lipid bilayers. Biophys. J. 90, 1121–1135 (2006).

**Paul, H.** Chemical and biochemical means to detect alcohol determination of ethanol concentration in fermented beer samples and distilled products. Biotek 1–6 (2012).

**Paumann, M., Regelsberger, G., Obinger, C., Peschek, G.A.** The bioenergetic role of dioxygen and the terminal oxidase(s) in cyanobacteria. Biochim. Biophys. Acta - Bioenerg. 1707, 231–253 (2005).

**Perozzo, R., Folkers, G., Scapozza, L.** Thermodynamics of protein–ligand interactions: history, presence, and future aspects. J. Recept. Signal Transduct. 24, 1–52 (2004).

**Pisciotta, J.M., Zou, Y., Baskakov, I. V.** Light-dependent electrogenic activity of cyanobacteria. PLoS One. 5, e10821 (2010).

**Pisciotta, J.M., Zou, Y., Baskakov, I. V.** Role of the photosynthetic electron transfer chain in electrogenic activity of cyanobacteria. Appl. Microbiol. Biotechnol. 91, 377–385 (2011).

**Poderys, V., Matulionyte, M., Selskis, A., Rotomskis, R.** Interaction of water-soluble CdTe quantum dots with bovine serum albumin. Nanoscale Res. Lett. 6, 1–6 (2010).

**Qiao, Y., Bao, S.J., Li, C.M.** Electrocatalysis in microbial fuel cells-from electrode material to direct electrochemistry. Energy Environ. Sci. 3, 544 (2010).

**Rabaey, K., Boon, N., Siciliano, S.D., Verhaege, M., Verstraete, W.** Biofuel cells select for microbial consortia that self-mediate electron transfer. Appl. Environ. Microbiol. 70, 5373–5382 (2004).

**Raghukumar, C., Vipparty, V., David, J. J., Chandramohan, D.** Degradation of crude oil by marine cyanobacteria. Appl. Microbiol. Biotechnol. 57, 433–436 (2001).

**Rajbanshi, B., Sarkar, S., Sarkar, P.** Band gap engineering of graphene-CdTe quantum dot hybrid nanostructures. J. Mater. Chem. C. 2, 8967–8975 (2014).

**Rasmussen, M., Minteer, S.D.** Photobioelectrochemistry: solar energy conversion and biofuel production with photosynthetic catalysts. J. Electrochem. Soc. 161, H647–H655 (2014).

**Rasmussen, M., Wingersky, A., Minteer, S.D.** Improved performance of a thylakoid bio-solar cell by incorporation of carbon quantum dots. ECS Electrochem. Lett. 3, H1–H3 (2013).

**Reguera, G., Nevin, K.P., Nicoll, J.S., Covalla, S.F., Woodard, T.L., Lovley, D.R.** Biofilm and nanowire production leads to increased current in *Geobacter sulfurreducens* fuel cells. Appl. Environ. Microbiol. 72, 7345–7348 (2006).

**Ren, L., Ahn, Y., Hou, H., Zhang, F., Logan, B.E.** Electrochemical study of multi-electrode microbial fuel cells under fed-batch and continuous flow conditions. J. Power

Sources 257, 454–460 (2014).

**Reshetilov, A.N., Trotsenko, J.A., Morozova, N.O., Iliasov, P. V., Ashin, V. V.** Characteristics of *Gluconobacter oxydans* B-1280 and *Pichia methanolica* MN4 cell based biosensors for detection of ethanol. Process Biochem. 36, 1015–1020 (2001).

**Rijnaarts, H.H., Norde, W., Bouwer, E.J., Lyklema, J., Zehnder, A.J.** Bacterial adhesion under static and dynamic conditions. Appl. Environ. Microbiol. 59, 3255–65 (1993).

**Rijnaarts, H.H.M., Norde, W., Lyklema, J., Zehnder, A.J.B.** DLVO and steric contributions to bacterial deposition in media of different ionic strengths. Colloids Surfaces B Biointerfaces 14, 179–195 (1999).

**Rockwood, D.N., Preda, R.C., Yücel, T., Wang, X., Lovett, M.L., Kaplan, D.L.** Materials fabrication from *Bombyx mori* silk fibroin. Nat. Protoc. 6, 1612–1631 (2011).

**Rosenbaum, M., He, Z., Angenent, L.T.** Light energy to bioelectricity: photosynthetic microbial fuel cells. Curr. Opin. Biotechnol. 21, 259–264 (2010).

**Rossi, F., De Philippis, R.** Role of cyanobacterial exopolysaccharides in phototrophic biofilms and in complex microbial mats. Life 5, 1218–1238 (2015).

**Rotariu, L., Bala, C.** New type of ethanol microbial biosensor based on a highly sensitive amperometric oxygen electrode and yeast cells. Anal. Lett. 36, 2459–2471 (2003).

**Rotariu, L., Bala, C., Magearu, V.** New potentiometric microbial biosensor for ethanol determination in alcoholic beverages. Anal. Chim. Acta 513, 119–123 (2004).

**Safi, J., Awad, Y., El-Nahhal, Y.** Bioremediation of diuron in soil environment: influence of cyanobacterial mat. Am. J. Plant Sci. 05, 1081–1089 (2014).

**Santhosh, M., Chinnadayyala, S.R., Singh, N.K., Goswami, P.** Human serum albumin-stabilized gold nanoclusters act as an electron transfer bridge supporting specific electrocatalysis of bilirubin useful for biosensing applications. Bioelectrochemistry 111, 7–14 (2016).

**Santoro, C., Arbizzani, C., Erable, B., Ieropoulos, I.** Microbial fuel cells: From fundamentals to applications. A review. J. Power Sources 356, 225–244 (2017).

**Sawa, M., Fantuzzi, A., Bombelli, P., Howe, C.J., Hellgardt, K., Nixon, P.J.** Electricity generation from digitally printed cyanobacteria. Nat. Commun. 8, 1327 (2017).

**Schneider, G., Kovács, T., Rákhely, G., Czeller, M.** Biosensoric potential of microbial fuel cells. Appl. Microbiol. Biotechnol. 100, 7001–7009 (2016a).

**Schneider, K., Thorne, R.J., Cameron, P.J.** An investigation of anode and cathode materials in photomicrobial fuel cells. Philos. Trans. R. Soc. A Math. Phys. Eng. Sci. 374, 20150080 (2016b).

**Schulze, K., López, D. a, Tillich, U.M., Frohme, M.** A simple viability analysis for unicellular cyanobacteria using a new autofluorescence assay, automated microscopy,

and ImageJ. BMC Biotechnol. 11, 118 (2011).

**Sekar, N., Ramasamy, R.P.** Photosynthetic energy conversion: recent advances and future perspective. Interface Mag. 24, 67–73 (2015).

**Sekar, N., Umasankar, Y., Ramasamy, R.P.** Photocurrent generation by immobilized cyanobacteria via direct electron transport in photo-bioelectrochemical cells. Phys. Chem. Chem. Phys. 16, 7862 (2014).

**Sekretaryova, A.N., Eriksson, M., Turner, A.P.F.** Bioelectrocatalytic systems for health applications. Biotechnol. Adv. 34, 177–197 (2016).

**Serban, B., Costea, S., Buiu, O., Cobianu, C., Diaconu, C.** Pyrene-1-butyric acid-doped polyaniline for fluorescence quenching-based oxygen sensing, in: CAS 2012 (International Semiconductor Conference). IEEE, pp. 265–268 (2012).

**Serebryakova, E. V., Darmov, I. V, Medvedev, N.P., Alekseev, S.M., Rybak, S.I.** Evaluation of the hydrophobicity of bacterial cells. Microbiology 71, 202–204 (2002).

**Shao, C.Y., Howe, C.J., Porter, A.J.R., Glover, L.A.** Novel cyanobacterial biosensor for detection of herbicides. Appl. Environ. Microbiol. 68, 5026–5033 (2002).

**Sommer, F., Drepper, F., Haehnel, W., Hippler, M.** The hydrophobic recognition site formed by residues PsaA-Trp$^{651}$ and PsaB-Trp$^{627}$ of photosystem I in *Chlamydomonas reinhardtii* confers distinct selectivity for binding of plastocyanin and cytochrome $c_6$. J. Biol. Chem. 279, 20009–20017 (2004).

**Steinhauser, D., Fernie, A.R., Araújo, W.L.** Unusual cyanobacterial TCA cycles: not broken just different. Trends Plant Sci. 17, 503–509 (2012).

**Su, L., Jia, W., Hou, C., Lei, Y.** Microbial biosensors: A review. Biosens. Bioelectron. 26, 1788–1799 (2011).

**Subrahmanyam, S., Shanmugam, K., Subramanian, T. V., Murugesan, M., Madhav, V.M., Jeyakumar, D.** Development of electrochemical microbial biosensor for ethanol based on *Aspergillus niger*. Electroanalysis 13, 944–948 (2001).

**Sullivan, E.M., Oh, Y.J., Gerhardt, R.A., Wang, B., Kalaitzidou, K.** Understanding the effect of polymer crystallinity on the electrical conductivity of exfoliated graphite nanoplatelet/polylactic acid composite films. J. Polym. Res. 21, 563 (2014).

**Süss, K.H., Schmidt, O.** Evidence for an $\alpha_3$, $\beta_3$, $\gamma$, $\delta$, I, II, $\varepsilon$, $III_5$ subunit stoichiometry of chloroplast ATP synthetase complex ($CF_1 - CF_0$ ). FEBS Lett. 144, 213–218 (1982).

**Svensater, G., Bergenholtz, G.** Biofilms in endodontic infections. Endod. Top. 9, 27–36 (2004).

**Takahashi, H., Uchimiya, H., Hihara, Y.** Difference in metabolite levels between photoautotrophic and photomixotrophic cultures of *Synechocystis sp.* PCC 6803 examined by capillary electrophoresis electrospray ionization mass spectrometry. J.

Exp. Bot. 59, 3009–3018 (2008).

**Tanaka, K., Tamamushi, R., Ogawa, T.** Bioelectrochemical fuel-cells operated by the cyanobacterium, *Anabaena variabilis*. J. Chem. Technol. Biotechnol. Biotechnol. 35, 191–197 (1985).

**Thungon, P.D., Kakoti, A., Ngashangva, L., Goswami, P.** Advances in developing rapid, reliable and portable detection systems for alcohol. Biosens. Bioelectron. 97, 83–99 (2017).

**Tkac, J., Vostiar, I., Gorton, L., Gemeiner, P., Sturdik, E.** Improved selectivity of microbial biosensor using membrane coating. Application to the analysis of ethanol during fermentation. Biosens. Bioelectron. 18, 1125–1134 (2003).

**Torimura, M., Miki, A., Wadano, A., Kano, K., Ikeda, T.** Electrochemical investigation of cyanobacteria *Synechococcus sp.* PCC7942-catalyzed photoreduction of exogenous quinones and photoelectrochemical oxidation of water. J. Electroanal. Chem. 496, 21–28 (2001).

**Toyofuku, M., Inaba, T., Kiyokawa, T., Obana, N., Yawata, Y., Nomura, N.** Environmental factors that shape biofilm formation. Biosci. Biotechnol. Biochem. 80, 7–12 (2016).

**Trammell, S.A., Wang, L., Zullo, J.M., Shashidhar, R., Lebedev, N.** Orientated binding of photosynthetic reaction centers on gold using Ni-NTA self-assembled monolayers. Biosens. Bioelectron. 19, 1649–1655 (2004).

**Tsiotis, G., Nitschke, W., Haase, W., Michel, H.** Purification and crystallization of photosystem I complex from a phycobilisome-less mutant of the cyanobacterium *Synechococcus* PCC 7002. Photosynth. Res. 35, 285–297 (1993).

**Tsujimura, S., Wadano, A., Kano, K., Ikeda, T.** Photosynthetic bioelectrochemical cell utilizing cyanobacteria and water-generating oxidase. Enzyme Microb. Technol. 29, 225–231 (2001).

**Umeda, H., Aiba, H., Mizuno, T.** *somA*, a novel gene that encodes a major outer-membrane protein of *Synechococcus sp*. PCC 7942. Microbiology 142, 2121–2128 (1996).

**Ursell, T., Chau, R.M.W., Wisen, S., Bhaya, D., Huang, K.C.** Motility enhancement through surface modification is sufficient for cyanobacterial community organization during phototaxis. PLoS Comput. Biol. 9, e1003205 (2013).

**Valach, M., Katrlík, J., Šturdík, E., Gemeiner, P.** Ethanol *Gluconobacter* biosensor designed for flow injection analysis. Sensors Actuators B Chem. 138, 581–586 (2009).

**Van Der Mei, H., Van De Belt-Gritter, B., Pouwels, P., Martinez, B., Busscher, H.** Cell surface hydrophobicity is conveyed by S-layer proteins - a study in recombinant lactobacilli. Colloids Surfaces B Biointerfaces 28, 127–134 (2003).

**Van Der Plas, J., De Groot, R., Woortman, M., Cremers, F., Borrias, M., Van Arkel, G., Weisbeek, P.** Genes encoding ferredoxins from *Anabaena sp.* PCC 7937 and *Synechococcus sp.* PCC 7942: structure and regulation. Photosynth. Res. 18, 179–204 (1988).

**Vermaas, W.F.** Photosynthesis and Respiration in Cyanobacteria, Encyclopedia of Life Sciences. John Wiley & Sons, Ltd, Chichester, USA (2001).

**Vijayakumar, S.** Potential Applications of cyanobacteria in industrial effluents-a review. J. Bioremediation Biodegrad. 03 (2012).

**Voronova, E.A., Iliasov, P. V., Reshetilov, A.N.** Development, investigation of parameters and estimation of possibility of adaptation of *Pichia angusta* based microbial sensor for ethanol detection. Anal. Lett. 41, 377–391 (2008).

**Wadhwani, T., Desai, K., Patel, D., Lawani, D., Bahaley, P., Joshi, P., Kothari, V.** Effect of various solvents on bacterial growth in context of determining MIC of various antimicrobials. Internet J. Microbiol. 7, 1–8 (2009).

**Walter, S.A.** Phycobilisome and phycobiliprotein structures, in: Bryant, D.A. (Ed.), the molecular biology of cyanobacteria, advances in photosynthesis and respiration. Springer Netherlands, Dordrecht, 139–216 (2004).

**Wang, L., Tian, L., Deng, X., Zhang, M., Sun, S., Zhang, W., Zhao, L.** Photosensitizers from *Spirulina* for solar cell. J. Chem. 2014, 1–5 (2014a).

**Wang, L., Lu, C., Zhang, B., Zhao, B., Wu, F., Guan, S.** Fabrication and characterization of flexible silk fibroin films reinforced with graphene oxide for biomedical applications. RSC Adv. 4, 40312–40320 (2014b).

**Wei, J., Liang, P., Huang, X.** Recent progress in electrodes for microbial fuel cells. Bioresour. Technol. 102, 9335–44 (2011).

**Wei, X., Lee, H., Choi, S.** Biopower generation in a microfluidic bio-solar panel. Sensors Actuators, B Chem. 228, 151–155 (2016).

**Wen, G., Wen, X., Shuang, S., Choi, M.M.F.** Whole-cell biosensor for determination of methanol. Sensors Actuators B Chem. 201, 586–591 (2014).

**Whitelegge, J.P., Zhang, H., Aguilera, R., Taylor, R.M., Cramer, W.A.** Full subunit coverage liquid chromatography electrospray ionization mass spectrometry (LCMS+) of an oligomeric membrane protein : cytochrome $b_6f$ complex from spinach and the cyanobacterium *Mastigocladus Laminosus* . Mol. Cell. Proteomics 1, 816–827 (2002).

**Whitmore, L., Wallace, B.A.** Protein secondary structure analyses from circular dichroism spectroscopy: methods and reference databases. Biopolymers 89, 392–400 (2008).

**Wilderer, P.A., Arnz, P., Arnold, E.** Application of biofilms and biofilm support materials as a temporary sink and source. Water. Air. Soil Pollut. 123, 147–158 (2000).

**Wong, L.S., Lee, Y.H., Surif, S.** Performance of a cyanobacteria whole cell-based fluorescence biosensor for heavy metal and pesticide detection. Sensors 13, 6394–6404 (2013).

**Xu, S., Jangir, Y., El-Naggar, M.Y.** Disentangling the roles of free and cytochrome-bound flavins in extracellular electron transport from *Shewanella oneidensis* MR-1. Electrochim. Acta 198, 49–55 (2016).

**Yagishita, T., Horigome, T., Tanaka, K.** Effects of light, $CO_2$ and inhibitors on the current output of biofuel cells containing the photosynthetic organism *Synechococcus sp.* J. Chem. Technol. Biotechnol. 56, 393–399 (2007).

**Yagishita, T., Sawayama, S., Tsukahara, K., Ogi, T.** Effects of glucose addition and light on current outputs in photosynthetic electrochemical cells using *Synechocystis sp*. PCC6714. J. Biosci. Bioeng. 88, 210–214 (1999).

**Yang, J.T., Wu, C.S.C., Martinez, H.M.** Calculation of protein conformation from circular dichroism, in: Methods Enzymology. 208–269 (1986).

**Yang, X.-Y., Tian, G., Jiang, N., Su, B.-L.** Immobilization technology: A sustainable solution for biofuel cell design. Energy Environ. Sci. 5, 5540–5563 (2012).

**Yang, Y., Shao, Z., Chen, X., Zhou, P.** optical spectroscopy to investigate the structure of regenerated *Bombyx mori* silk fibroin in solution. Biomacromolecules 5, 773–779 (2004).

**Yang, Y., Sun, G., Xu, M.** Microbial fuel cells come of age. J. Chem. Technol. Biotechnol. 86, 625–632 (2011).

**Yang, Y., Wu, Y., Hu, Y., Cao, Y., Poh, C.L., Cao, B., Song, H.** Engineering electrode-attached microbial consortia for high-performance xylose-fed microbial fuel cell. ACS Catal. 5, 6937–6945 (2015).

**Ye, C., Li, M., Luo, J., Chen, L., Tang, Z., Pei, J., Jiang, L., Song, Y., Zhu, D.** Photo-induced amplification of readout contrast in nanoscale data storage. J. Mater. Chem. 22, 4299 (2012).

**Yehezkeli, O., Tel-Vered, R., Wasserman, J., Trifonov, A., Michaeli, D., Nechushtai, R., Willner, I.** Integrated photosystem II-based photo-bioelectrochemical cells. Nat. Commun. 3, 742 (2012).

**Yi, H., Nevin, K.P., Kim, B.C., Franks, A.E., Klimes, A., Tender, L.M., Lovley, D.R.** Selection of a variant of *Geobacter sulfurreducens* with enhanced capacity for current production in microbial fuel cells. Biosens. Bioelectron. 24, 3498–3503 (2009).

**Yong, Y.C., Yu, Y.Y., Zhang, X., Song, H.** Highly active bidirectional electron transfer by a self-assembled electroactive reduced-graphene-oxide-hybridized biofilm. Angew. Chemie Int. Ed. 53, 4480–4483 (2014).

**You, J., Walter, X.A., Greenman, J., Melhuish, C., Ieropoulos, I.** Stability and reliability

of anodic biofilms under different feedstock conditions: towards microbial fuel cell sensors. Sens. Bio-Sensing Res. 6, 43–50 (2015).

**Yu, F., Wang, C., Ma, J.** Capacitance-enhanced 3D graphene anode for microbial fuel cell with long-time electricity generation stability. Electrochim. Acta 259, 1059–1067 (2018).

**Yu, F., Wang, C., Ma, J.** Applications of graphene-modified electrodes in microbial fuel cells. Materials (Basel). 9, 807 (2016).

Z**hang, A., Mu, H., Zhang, W., Cui, G., Zhu, J., Duan, J.** Chitosan coupling makes microbial biofilms susceptible to antibiotics. Sci. Rep. 3, 3364 (2013).

**Zhang, J.Z., Bombelli, P., Sokol, K.P., Fantuzzi, A., Rutherford, A.W., Howe, C.J., Reisner, E.** Photoelectrochemistry of photosystem II in vitro vs in vivo. J. Am. Chem. Soc. 140, 6–9 (2018).

**Zhang, S., Bryant, D. A.** The tricarboxylic acid cycle in cyanobacteria. Science 334, 1551–3 (2011).

**Zhang, X., Jiang, Z., Li, M., Zhang, X., Wang, G., Chou, A., Chen, L., Yan, H., Zuo, Y.Y.** Rapid spectrophotometric method for determining surface free energy of microalgal cells. Anal. Chem. 86, 8751–8756 (2014).

**Zhao, C., Li, H., Zheng, J., Chen, L., Li, F., Yang, S., Dong, C., Choi, M.M.F.** Isolation of a *Methylobacterium organophilium* strain, and its application to a methanol biosensor. Microchim. Acta 167, 67–73 (2009a).

**Zhao, F., Slade, R.C.T., Varcoe, J.R.** Techniques for the study and development of microbial fuel cells: an electrochemical perspective. Chem. Soc. Rev. 38, 1926 (2009b).

**Zhou, M., Chi, M., Luo, J., He, H., Jin, T.** An overview of electrode materials in microbial fuel cells. J. Power Sources 196, 4427–4435 (2011).

**Zou, Y., Pisciotta, J., Billmyre, R.B., Baskakov, I. V.** Photosynthetic microbial fuel cells with positive light response. Biotechnol. Bioeng. 104, 939–946 (2009).

# List of Publications

## Publications in refereed journals

1. Mrinal K. Sarma, **Sharbani Kaushik*** and Pranab Goswami, 2016. "Cyanobacteria: A metabolic power house for harvesting solar energy to produce bio-electricity and biofuels". ***Biomass and Bioenergy*** 90, 187–201. ***equal first author contribution**. (This publication is a part of chapter I).

2. **Sharbani Kaushik**, Mrinal K. Sarma, P.D. Thungon, M. Santhosh and Pranab Goswami, 2016. "Thin films of silk fibroin and its blend with chitosan strongly promote biofilm growth of Synechococcus sp. BDU 140432". ***Journal of Colloid and Interface Science*** 479, 251–259. (This publication is a part of chapter II).

3. **Sharbani Kaushik,** Mrinal K. Sarma and Pranab Goswami, 2017. "FRET-guided surging of cyanobacterial photosystems improves and stabilizes current in photosynthetic microbial fuel cell". ***Journal of Materials Chemistry A*** 5, 7885–7895. (This publication is a part of chapter III).

4. **Sharbani Kaushik** and Pranab Goswami, 2018. "Bacterial Membrane Depolarization-Linked Fuel Cell Potential Burst as Signal for Selective Detection of Alcohol". ***ACS Applied Materials and Interfaces***, 10 (22), 18630–18640. (Special highlight by THE HINDU newspaper dated 27/05/2018 and SERB in social platform). (This publication is a part of chapter IV).

5. Mrinal Kumar Sarma, Mohammed Ghulam Abdul Quadir, Rupam Bhaduri, **Sharbani Kaushik**, Pranab Goswami, 2018. "Composite polymer coated magnetic nanoparticles based anode enhances dye degradation and power production in microbial fuel cells". ***Biosensors and Bioelectronics*** 119, 94–102.

## Abstracts Published in Conferences

1. **Sharbani Kaushik** and Pranab Goswami – "Paper-based photosynthetic microbial fuel cell chip as portable power source and alcohol sensing device", ICRC-NISTADS Northeast Energy Conclave organized jointly by Interdisciplinary Climate Research Center, Cotton University and CSIR-National Institute of Science, Technology and Development Studies, Delhi held at Cotton University, Guwahati, Assam, India, on June 6-7, 2018.

2. **Sharbani Kaushik**, Priyanki Das, Pranab Goswami - "Paper based biofuel cell with photosynthetic microbial anode and air breathing enzymatic cathode". Oral OP 10, pp. 193. Fourth International Symposium on Advances in Sustainable Polymers (ASP-17) organized by CoE-SusPol, Chemical Engineering, IIT Guwahati held, during January 8-11, 2018.

3. **Sharbani Kaushik**, Pranab Goswami - "Quantum dots and Graphene Nanoplatelets in a Silk film matrix stimulates cyanobacterial photosystems to generate steady current in a PMFC, 5th International Conference on Advanced Nanomaterial and Nanotechnology (ICANN 2017), organized by Centre for Nanotechnology, IIT Guwahati, held during December 18-21, 2017.

4. **Sharbani Kaushik** and Pranab Goswami - "FRET-guided surging of cyanobacterial photosystems improves and stabilizes current in photosynthetic microbial fuel cell", Young scientists Colloquium 2017 (YSC 2017) organised by Materials Research Society of India (MRSI), Kolkata Chapter, IIEST, Shibpur, held during October 11, 2017.

5. **Sharbani Kaushik**, Pranab Goswami - "Optically and electronically active hybrid nano-biocomposite for cyanobacteria based photosynthetic microbial fuel cell". PP9, pp. 70, International conference on sophisticated instruments in Modern Research (ICSIMR 2017), Organized by CIF, IIT Guwahati, held during June 30 - July 1, 2017.

6. **Sharbani Kaushik** and Pranab Goswami - "CdTe-Silk fibroin -Graphene based hybrid materials support FRET to cyanobacterial photosystems and improve light to current conversion efficiency in a fuel cell setup through direct electron transfer mechanism", ACS Symposium, IIT Guwahati, held during January 2017.

7. **Sharbani Kaushik**, Pranab Goswami – "CdTe quantum dots decorated silk fibroin with graphene blend enhances light to current conversion efficiency of *Synechococcus* sp. biofilm grown on graphite anode in photo-microbial fuel cell". Oral. ABS-110-ICYRAM, on behalf of International Union of Materials Research Society, Materials Research Society of India, International Conference of Young Researchers on Advanced Materials (IUMRS-ICYRAM 2016), IISc Bangalore, held during December 11-15, 2016.

8. **Sharbani Kaushik**, Pranab Goswami – "Development of cyanobacterial biofilm for biofuel cell applications using chitosan as biofilm inducing biomaterial". Oral BI-119, pp. 157, 68th Annual Session of Indian Institutes of Chemical Engineering (CHEMCON), CHEMCON 2015, IIT Guwahati, held during December 27-30, 2015.

# Awards and Achievements

1. **MRSI Young Scientist Award 2017** for creditable contribution to advanced materials research, awarded by **Materials Research Society of India** (MRSI), Kolkata Chapter, held in IIEST, Shibpur, during October 11, 2017.

2. **Best Poster award (1st prize)** in the **ICRC-NISTADS Northeast Energy Conclave** organized jointly by Interdisciplinary Climate Research Center, Cotton University and CSIR-National Institute of Science, Technology and Development Studies, Delhi held at Cotton University, Guwahati, Assam, India, during June 6-7, 2018.

3. **Special Highlight** in **THE HINDU** newspaper for the research work on portable, selective alcohol biosensor dated May 27, 2018.

4. **Third Prize** in **RedStart**- the **Startup challenge** sponsored by **Numaligarh Refinery Limited** Guwahati, Research Conclave 2018, IIT Guwahati, held during February 8-11. 2018.

5. **Best Oral presentation (1st prize)** in the 4th **International Symposium on Advances in Sustainable Polymers** (ASP 17) organized by Center of Excellence for Sustainable Polymers (Dept. of Chemical Engineering), IIT Guwahati, India and Polymer Processing Academy, India, held during January 8-11, 2018.

6. **Best Poster award** in the 5th **International Conference on Advanced Nanomaterial and Nanotechnology** (ICANN 2017), organized by Centre for Nanotechnology, IIT Guwahati, held during December 18-21, 2017.

# Front Page of the Papers Published in International Journals

Biomass and Bioenergy 90 (2016) 187–201

Contents lists available at ScienceDirect

Biomass and Bioenergy

journal homepage: http://www.elsevier.com/locate/biombioe

Review

# Cyanobacteria: A metabolic power house for harvesting solar energy to produce bio-electricity and biofuels

Mrinal Kumar Sarma [a], Sharbani Kaushik [a, 1], Pranab Goswami [b, *]

[a] Center for Energy, Indian Institute of Technology Guwahati, Guwahati 781039, Assam, India
[b] Department of Biosciences and Bioengineering, Indian Institute of Technology Guwahati, Guwahati 781039, Assam, India

ARTICLE INFO

*Article history:*
Received 13 September 2015
Received in revised form
7 March 2016
Accepted 8 March 2016

*Keywords:*
Cyanobacteria
Photosynthesis
Bioelectricity
Biofuel
Biofuel cell

ABSTRACT

Cyanobacteria are a group of light harvesting prokaryotic microorganisms displaying a vast diversity in terms of their morphology, physiology, and metabolic capabilities, which appear to be important factors for their survival in diverse ecological niches. The metabolism of cyanobacteria does not fit well into a linear understanding of generalized photosynthetic microorganisms. In addition to the water oxidizing photosynthesis accomplished by coupling photosystem I and photosystem II activities, they also possess intersecting photosynthetic and respiratory electron transport chains in thylakoid membranes which help them to adjust electron flow in the membranes and linked energy metabolism as per the need or demand of the situation. The cyanobacteria have an incomplete tricarboxylic acid (TCA) cycle as they lack 2-oxoglutarate dehydrogenase. However, the enzymes, 2-oxoglutarate decarboxylase and succinic semialdehyde dehydrogenase encoded by their genes convert 2-oxoglutarate to succinate, and thereby use this shunt pathway not only to support the cells to maintain production of reducing equivalents (NADPH), but also to provide unique flexibility to its metabolic system that manifested in their various functions some of which are being progressively understood. The existence of unusual TCA cycle shunt in cyanobacteria opens up a new research avenue for engineering cyanobacteria for biotechnological applications including production of various biofuels of high commercial interest. The unique respiratory metabolisms could also be exploited to generate electrogenic cyanobacterial cells for production of bioelectricity in a fuelcell setup.



**Contents**



## 1. Introduction

Cyanobacteria are one of the oldest known living phyla with fossil remnants of more than 3.5 billion years [1]. The phylum of the cyanobacteria has been divided into *Gloeobacterales, Synechococcales, Spirulinales, Chroococcales, Pleurocapsales, Oscillatoriales,*

* Corresponding author.
*E-mail address:* pgoswami@iitg.ernet.in (P. Goswami).
[1] Equal first author contribution.

http://dx.doi.org/10.1016/j.biombioe.2016.03.043
0961-9534/

Journal of Colloid and Interface Science 479 (2016) 251–259

Contents lists available at ScienceDirect

Journal of Colloid and Interface Science

journal homepage: www.elsevier.com/locate/jcis

Regular Article

# Thin films of silk fibroin and its blend with chitosan strongly promote biofilm growth of *Synechococcus* sp. BDU 140432

Sharbani Kaushik [a], Mrinal K. Sarma [a], Phurpa Dema Thungon [b], Mallesh Santhosh [b], Pranab Goswami [a,b,*]

[a] Centre for Energy, Indian Institute of Technology Guwahati, Guwahati 781039, Assam, India
[b] Department of Biosciences and Bioengineering, Indian Institute of Technology Guwahati, Guwahati 781039, Assam, India

## GRAPHICAL ABSTRACT

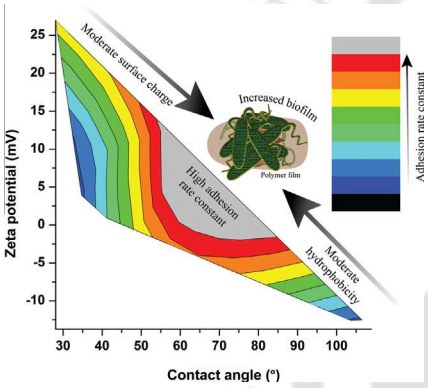


## ARTICLE INFO

*Article history:*
Received 17 May 2016
Revised 27 June 2016
Accepted 27 June 2016
Available online 28 June 2016

*Keywords:*
Biofilm
*Synechococcus* sp.
Silk
Chitosan
Hydrophobicity
Surface charge

## ABSTRACT

The activating role of different polymer thin films coated over polystyrene support on the *Synechococcus* sp. biofilm growth was examined concurrently by measuring biofilm florescence using a dye and by measuring cell density in the isolated biofilm. Compared to blank (no coating), the increase in biofilm formation (%) on silk, chitosan, silk-chitosan (3:2) blend, polyaniline, osmium, and Nafion films were 27.73 (31.16), 21.55 (23.74), 37.21 (38.34), 5.35 (8.96), 6.70 (6.55) and (nil), respectively with corresponding cell density (%) shown in the parentheses. This trend of biofilm formation on the films did not significantly vary for *Escherichia coli* and *Lactobacillus plantarum* strains. The films of 20 residues long each of glycine-alanine repeat peptide, which mimics a silk fibroin motif, and a hydrophobic glycine-valine repeat peptide, increased the biofilm growth by 13.53 % and 26.08 %, respectively. Silk and blend films showed highest adhesion unit (0.48–0.49), adhesion rate ($(4.2–4.8) \times 10^{-6}$, m/s) and Gibbs energy of adhesion (−8.5 to −8.6 *kT*) with *Synechococcus* sp. The results confirmed interplay of electrostatic and hydrophobic interaction between cell-surface and polymer films for promoting rapid biofilm growth. This study established that the thin films of silk and the blend (3:2) promote rapid biofilm growth for all the tested microorganisms.



## 1. Introduction

Biofilms are microbial communities growing on solid surfaces and frequently embedded in a matrix of extracellular polymeric substances (EPS) [1]. The major driving forces for biofilm research

* Corresponding author at: Department of Biosciences and Bioengineering, Indian Institute of Technology Guwahati, Guwahati 781039, Assam, India.
*E-mail address:* pgoswami@iitg.ernet.in (P. Goswami).

http://dx.doi.org/10.1016/j.jcis.2016.06.065
0021-9797/

Journal of Materials Chemistry A

PAPER



Cite this: J. Mater. Chem. A, 2017, 5, 7885

# FRET-guided surging of cyanobacterial photosystems improves and stabilizes current in photosynthetic microbial fuel cell†

Sharbani Kaushik,[a] Mrinal K. Sarma[a] and Pranab Goswami *[ab]

Received 6th February 2017
Accepted 24th March 2017

DOI: 10.1039/c7ta01137g

rsc.li/materials-a

Improving power generation under low light conditions and efficiently capturing electrons from the photosynthetic bacteria on the electrode are critical issues for developing a viable photosynthetic microbial fuel cell (PMFC). To address these issues, an anode was developed for a dual-chambered PMFC with an abiotic cathode, *via* casting a nanocomposite matrix comprising CdTe quantum dots (QD), graphene nanoplatelets (GNP) and silk-fibroin (SF) on a graphite electrode. The nanocomposite matrix supported biofilm growth of the photo-catalyst *Synechococcus* sp., surged the bacterial photosystems (PS I and PS II) with appropriate light ($\lambda_{650-750\ nm}$) at a broad excitation spectrum ($\lambda_{350-644\ nm}$) through fluorescence resonance energy transfer and facilitated the metabolic electron relay through direct electron transfer (DET) to the anode. The maximum current density of the PMFC obtained with the nanocomposite bioanode (1.89 A $m^{-2}$) was ~5.7 fold higher than that of the corresponding blank graphite anode. The positive effect of QD was further confirmed from the fading reversal of polarity during the circadian cycle, leading to sustained current generation in the PMFC. The GNP reduced the band gap of the nanocomposite to 2.9 eV and decreased the charge transfer resistance by ~9 fold, thus enabling DET on the electrode, as is evident from a pair of redox peaks of the bioanode with the formal potential of −156 mV. Structural studies demonstrated the rational interactions of the hydrophobic β-sheet of the SF with the nanomaterials. An unprecedented light conversion efficiency of 4.01% for the cyanobacteria was achieved with the nanocomposite bioanode-based PMFC.

## 1. Introduction

The interest in cyanobacteria as fuel cell catalysts is sharply increasing, owing to many advantages being identified on their use in these electrical power generating devices.[1] These photosynthetic microorganisms are widespread in nature and can grow heterotrophically as well as photo-autotrophically in a self-sustainable manner following the carbon concentrating mechanism. The application potential of these microorganisms for combined power generation and waste treatment through photosynthetic microbial fuel cell (PMFC) technology is vast due to their inherent survival capacity at high salt concentrations, in the presence of organic contaminants and under adverse environmental conditions. However, to develop an efficient, practical PMFC, a few critical issues need to be addressed first, among which the harvesting of adequate light energy to boost the photosynthetic machinery of the cells under low light conditions and the approach for capturing the metabolic electrons efficiently on the electrode surface are to be reckoned first. It must be mentioned that the theoretical maximal light energy conversion efficiency (LCE) of photosynthesis in cyanobacteria is ~11%, as only ~50% of the incident solar energy can be assessed.[2,3] The mechanisms that are relied upon for capturing the metabolic electrons are mostly limited to direct electron transfer (DET) and mediating electron transfer (MET) processes, while a third approach involving bacterial nanowires for transferring the metabolic electrons to the electrode is in a nascent stage.[4] When the PMFC is destined for deployment in an open environment situation, the design approach for developing the electrode may be focused on adopting the DET mechanism, as the complementary MET based approach is often snagged with gradual leaching of the chemical mediators, which are largely hazardous in nature and are thus unwanted from the ecological perspective.[4,5] To implement the concept of DET in a microbial fuel cell for the steady generation of electric current, a naturally sustained close contact between the bacterial cells and the conductive electrode is a desired condition. To meet this condition, the creation of a natural bacterial biofilm over the electrode surface has been evolved as the method of choice for generating stable current from the cellular electrons in the fuel cell setup.[6] However,

[a]Centre for Energy, Indian Institute of Technology Guwahati, Guwahati 781039, Assam, India. E-mail: pgoswami@iitg.ernet.in; Fax: +91 361 2582249; Tel: +91 361 2582202

[b]Department of Biosciences and Bioengineering, Indian Institute of Technology Guwahati, Guwahati 781039, Assam, India

† Electronic supplementary information (ESI) available. See DOI: 10.1039/c7ta01137g

ACS APPLIED MATERIALS & INTERFACES

Research Article

Cite This: ACS Appl. Mater. Interfaces 2018, 10, 18630−18640

www.acsami.org

# Bacterial Membrane Depolarization-Linked Fuel Cell Potential Burst as Signal for Selective Detection of Alcohol

Sharbani Kaushik[†] and Pranab Goswami*[,†,‡]

[†]Centre for Energy and [‡]Department of Biosciences and Bioengineering, Indian Institute of Technology Guwahati, Guwahati 781039, Assam, India

Supporting Information

**ABSTRACT:** The biosensing application of microbial fuel cell (MFC) is hampered by its long response time, poor selectivity, and technical difficulty in developing portable devices. Herein, a novel signal form for rapid detection of ethanol was generated in a photosynthetic MFC (PMFC). First, a dual chambered (100 mL each) PMFC was fabricated by using cyanobacteria-based anode and abiotic cathode, and its performance was examined for detection of alcohols. A graphene-based nano-biocomposite matrix was layered over graphite anode to support cyanobacterial biofilm growth and to facilitate electron transfer. Injection of alcohols into the anodic chamber caused a transient potential burst of the PMFC within 60 s (load 1000 Ω), and the magnitude of potential could be correlated to the ethanol concentrations in the range 0.001−20% with a limit of detection (LOD) of 0.13% ($R^2$ = 0.96). The device exhibited higher selectivity toward ethanol than methanol as discerned from the corresponding cell−alcohol interaction constant ($K_i$) of 780 and 1250 mM. The concept was then translated to a paper-based PMFC (p-PMFC) (size ∼20 $cm^2$) wherein, the cells were merely immobilized over the anode. The device with a shelf life of ∼3 months detected ethanol within 10 s with a dynamic range of 0.005−10% and LOD of 0.02% ($R^2$ = 0.99). The fast response time was attributed to the higher wettability of ethanol on the immobilized cell surface as validated by the contact angle data. Alcohols degraded the cell membrane on the order of ethanol > methanol, enhanced the redox current of the membrane-bound electron carrier proteins, and pushed the anodic band gap toward more negative value. The consequence was the potential burst, the magnitude of which was correlated to the ethanol concentrations. This novel approach has a great application potential for selective, sensitive, rapid, and portable detection of ethanol.

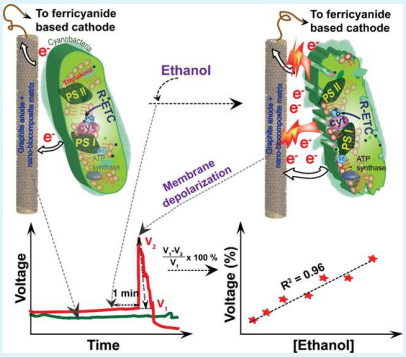


**KEYWORDS:** *photosynthetic microbial fuel cell, cyanobacteria, alcohol, biosensors, potential burst, paper-based photosynthetic microbial fuel cell*

## INTRODUCTION

The search for novel biosensing techniques is becoming an integral research and development activity in various sectors including environmental monitoring, diagnostics, fuel, food, and pharmaceutical industries. This is owing to certain distinct advantages of biosensors such as, higher selectivity, sensitivity, and better scope for improving the properties of the biorecognition elements over the conventional chemical and physical recognition-based sensors.[1] Among the different biorecognition elements used in biosensor applications, whole-cell-based recognition elements find special interest in the fields where information related to toxicology, pharmacology, and cell physiology of a sample is to be gathered, which is normally difficult to achieve by using the molecule-based recognition elements in the biosensor platforms. Additionally, the cell-based recognition systems offer better stability under the ambient conditions as compared to their free biomolecular counterparts. Microbial biosensors with different transduction principles have been explored among which microbial fuel cell (MFC) sensors have received increasing attention over the last few years because of their fabrication simplicity, feasibility to operate in external environments in a self-sustained manner, low cost of operation, and sensitive signal transduction mechanism.[2] However, most of these MFC-based biosensors are snagged with long response time as the response acquired from the interaction of the target species with the catalytic cells in the MFC is usually governed by the metabolism and growth of the organisms on the electrode surface. This long response time and poor selectivity of the MFC-based biosensors discourage their applications in the fields where rapid and specific detection of the targets is an ardent task. The requirement of cellular growth of the biocatalysts in the MFC-based sensors is another constrain that impedes the development of small-scale and chip-based MFC biosensors. Hence, a strategy to impasse the aforesaid challenges needs to be explored to develop MFC-based biosensors with a fast response time, specific detection capability, low cost, and

Received: February 1, 2018
Accepted: May 14, 2018
Published: May 14, 2018







DOI: 10.1021/acsami.8b01838
ACS Appl. Mater. Interfaces 2018, 10, 18630−18640